GIS-BASED APPROACHES TO SLOPE STABILITY ANALYSIS AND EARTHQUAKE-INDUCED LANDSLIDE HAZARD ZONATION

A

THESIS

Presented to the Faculty

of the University of Alaska Fairbanks

in Partial Fulfillment of the Requirements

for the Degree of

DOCTOR OF PHILOSOPHY

By

Huayang Luo, B.S., M.S.

Fairbanks, Alaska

May 2006

GIS-BASED APPROACHES TO SLOPE STABILITY ANALYSIS AND EARTHQUAKE-INDUCED LANDSLIDE HAZARD ZONATION

By

Huayang Luo

RECOMMENDED: _____

_____

_____

_____

Advisory Committee Chair

_____

Chair, Department of Mining and Geological Engineering

APPROVED: _____

Dean, College of Engineering and Mines

_____

Dean of the Graduate School

April 26, 2006

Date

Abstract

This dissertation presents newly developed GIS-based deterministic and probabilistic approaches for slope stability analysis and earthquake-induced landslide hazard zonation. The described approaches combine numerical slope stability analysis with GIS spatial analysis to evaluate earthquake-induced slope failures, both shallow and deep-seated. The study has four major research components.

The first component is a GIS-based procedure which was developed based on one-, two-, and three-dimensional (1D, 2D, and 3D) deterministic approaches to slope stability analysis and landslide hazard zonation. Slope stability methods in the GIS-based procedure included the infinite slope model, the block sliding model, the ordinary method of slices, the Bishop simplified method, and the Hovland's column method.

The second component focuses on causative factors analysis of earthquake-induced landslide hazards. This component also discusses the determination of peak ground acceleration for slope stability analysis.

The third component consists of an evaluation of the topographic effect of ground motion and the seismic response in the Balsamo Ridge area in Nueva San Salvador.

The fourth component is concerned with the regional and site-specific landslide hazard zonation, using newly developed models for landslide hazard assessment in Nueva San Salvador. The slope stability and landslide susceptibility were mapped in terms of slope stability index (factor of safety, critical acceleration, Newmark displacement, failure probability, and reliability index).

The landslides triggered by an earthquake on January 13, 2001 in El Salvador provide a setting for the calibration of results from GIS-based approaches. The procedures developed in this research proved to be feasible and cost-effective for slope stability analysis and earthquake-induced landslide hazard zonation.

Table of Contents

List of Figures

Page

List of Tables

Acknowledgments

My sincerest gratitude goes to my advisory committee chair, Dr. Wei Zhou, Assistant Professor of Geological Engineering, University of Alaska Fairbanks (UAF), for her advice, support, and encouragement as I carried out this research which integrated my knowledge of GIS in geohazard assessment.

I also want to express my highest appreciation to Dr. Scott L. Huang, Professor of Geological Engineering, UAF, for his thoughtful and critical review of my dissertation and his advice on research methods and the usage of the GIS process for slope stability analysis.

I wish to thank Dr. Gang Chen, Professor of Mining Engineering, for his attentive review of this research and his helpful advice on slope stability analysis methods, especially with regard to the probability analysis.

My thanks also goes to Dr. Anupma Prakash, Associate Professor of Geology and Remote Sensing, UAF, for her advice on the usage of GIS and remote sensing and for giving me a myriad of helpful suggestions and support.

This research was supported by a research fellowship grant from the Graduate School of the University of Alaska Fairbanks, which I gratefully acknowledge.

I am indebted to the many people who volunteered their time and effort to help me collect data, both in Alaska and in El Salvador. In particular, I would like to express my gratitude to Mr. Steve Huang, Mr. Walter Hernandez, and Mr. Roberto Flores, all of San Salvador in El Salvador, for guiding me in the field and for providing me with valuable GIS data. I also would like to thank Mr. Jose M. Cepeda at the University of Central America (Universidad Centroamericana) in San Salvador, El Salvador. Mr. Cepeda has generously made available to me a valuable seismic dataset.

Finally, I would like to express sincere appreciation to my wife Lin, my son Derek, and my parents for their support and encouragement.

Chapter 1 Introduction

1.1 Introduction

A landslide is a downslope mass movement of soil and/or rock and is one of the major natural hazards in the world. In recent years, population growth and the expansion of settlements and life-lines over hazardous areas are increasing the impact of natural disasters in both the developed and developing countries (Rosenfeld, 1994). Much of the damage and sometimes a considerable proportion of the fatalities occurring during earthquakes and intense storms are due to landslides (Varnes, 1984).

Landslides within the United States constitute a major geologic hazard, occurring in all 50 states, causing on average 25 to 50 fatalities and damage of approximately $1 billion to $3 billion each year (Spiker and Gori, 2000). China also frequently suffers from landslides. In 1998, about 180,000 geological hazards such as avalanches, landslides, and debris flows on different scales occurred in China, resulting in 1,573 deaths, more than 10,000 people injured and 500,000 houses destroyed. From 1998 to 2004, landslides within China caused on average 974 fatalities with up to $3 billion direct economic losses each year (CIGEM, 2004).

Landslides can be triggered by many factors including heavy rainfall, earthquakes, volcanic eruptions, groundwater change, river erosion, glaciers, ocean waves, and human activity. In an earthquake prone area, seismic shaking is often a major cause of widespread landslides. Structural damage and/or fatalities from earthquake-triggered landslides and other ground failures sometimes exceed the damage directly related to strong shaking and fault rupture during the earthquake (Keefer, 1984). In the United States, annualized losses from earthquakes have been estimated at an amount ranging from $4.1 billion (direct damage only) to $10 billion (including indirect losses) (NRC, 1985, Schuster and Highland, 2001). Some deadly earthquake-induced landslides in recent centuries have killed a huge number of people. Table 1.1 lists major earthquakes worldwide that triggered catastrophic landslides in the 20th and 21st centuries. Such

earthquakes and induced landslides had a tremendous impact on the society and environment in which they occurred. For example, on December 16, 1920, Haiyuan Earthquake in Northwest China (M_w=8.7) triggered thousands of slope failures and landslides that killed over 100,000 people and affected an area of more than 4,000 km^2 (Close and McCormick, 1922). On March 27, 1964, the Alaska Earthquake (M_w=9.2) devastated the Turnagain Heights residential development and many downtown areas in Anchorage. It has been estimated that 56% of the total cost of damage in Alaska was caused by earthquake-induced landslides (Youd, 1978, Wilson and Keefer, 1985).

In May 1970, an earthquake in Peru took about 70,000 lives, and about 20,000 people perished in the avalanche of debris from the north peak of Nevado Huascaran (Varnes, 1984). In Japan, more than half of all deaths in large earthquakes (M > 6.9) between 1964 and 1980 were caused by landslides (Kobayshi, 1981). In southern California, the Northridge Earthquake in 1994 with a magnitude of 6.7 triggered more than 11,000 landslides—the vast majority were highly disrupted, shallow falls, and slides of rock and debris occurring over wide areas (Harp and Jibson, 1995).

In early 2001, two earthquakes (January 13 with M7.6 and February 13 with M6.6) struck El Salvador. Both earthquakes triggered thousands of landslides that caused most of the damage and fatalities in the southern half of El Salvador. One destructive landslide, the Las Colinas Landslide, caused 585 fatalities when it slid off the north slope of Balsamo Ridge (Jibson et al., 2004).

Although earthquakes can hardly be predicted, the susceptibility to earthquake-induced landslides of a certain area can be assessed on the basis of potential ground motion, geological, geotechnical, and geomorphologic conditions. The identification and map portrayal of areas highly susceptible to damaging landslides is the first necessary step toward loss reduction (Zeizel, 1988). Slope instability recognition, analysis, and hazard zonation are some of the most important challenges facing earthquake engineers, geotechnical engineers, researchers, and land use planners.

Table 1.1 Major earthquakes that triggered catastrophic landslides in the world

Name and Date	Location	Magnitude	Deaths	Comments
Haiyuan earthquake, 12/16/1920	Ningxia, China	8.5	234,117	Widespread landslides destroying many villages
Diexi earthquake, 08/25/1933	Shichuan, China	7.5	20,000	Blockage of Minjiang River by landslides
Alaska earthquake, 03/27/1964	Alaska, USA	9.2	131	Many earthquake-induced landslides and liquefaction
Anchas earthquake, 05/31/1970	Peru	7.7	70,000	Avalanches of rock and snow buried two towns
Guatemala earthquake, 02/04/1976	Guatemala	7.5	22,000	More than 10,000 landslides
San Salvador earthquake, 10/10/1986	El Salvador	5.4	200	Many landslides around San Salvador area
Ecuador earthquake, 03/05/1987	Ecuador	6.1 and 6.9	2,000	Mass wasting and flooding
Tajikistan earthquake, 01/23/1988	Tajikistan	5.5	230	Landslides and debris flow
Loma Prieta earthquake 10/17/1989	California	7.1	42	2,000~4,000 rock, earth and debris falls
Manjil earthquake, 06/21/1990	Iran	7.3	50,000	Landslides, rockfalls
Luzon earthquake, 07/16/1990	Philippines	7.8	1,621	Landslides, subsidence
Hokkaido Nansei-Oki earthquake, 07/12/1993	Hokkaido, Japan	7.8	230	Landslides and tsunami, Okushiri-Port slide with 30 fatalities
Northridge earthquake, 01/17/1994	California, USA	6.7	57	Rock falls, landslides, and severe structure damages
Paez earthquake, 06/06/1994	Colombia	6.4	>1,000	Landslides and debris flows
Hyogo-Ken Nanbu earthquake, 01/171995	Kobe, Japan	6.9	5,300	Widespread liquefaction, landslides, and damage to subway
ChiChi earthquake, 09/21/1999	Taiwan	7.6	2,375	Landslides, severe structural damage
El Salvador earthquake, 01/13/2001	Off-shore, El Salvador	7.6	844	Widespread landslides in the southern part of the country
El Salvador earthquake, 02/13/2001	San Salvador, El Salvador	6.6	315	Many landslides in San Salvador area
Peru earthquake, 06/23/2001	Peru	7.9	118	Landslides and house collapses
Sources: Schuaster and Flemming (1986), Kramer (1996), USGS website, Sassa (1999), Wieczorek (1999), and Jibson et al. (2004)				

1.2 GIS Applications in Landslide Hazard Zonation

According to a description by the Southern California Earthquake Center (SCEC, 2002), the zones of earthquake-induced landslide hazards are areas known to have experienced earthquake-induced slope failures during historical earthquakes, or areas identified as having past landslide movement including both landslide deposits and source areas, or areas where the geological materials are susceptible to earthquake-induced slope failure. Zonation refers to the division of the land surface into areas and the ranking of these areas according to the degree of actual or potential hazard from landslides or other mass movements on slopes (Varnes, 1984). The goal of earthquake-induced landslide hazard zonation is to evaluate the location of landslide susceptibility zones where landslides could be induced by future strong earthquake shaking. The procedure of slope stability analysis and hazard zonation requires an evaluation of spatially varying terrain, geological and hydrological conditions, and spatial distribution of existing landslides.

The Geographic Information System (GIS) has been described as "a powerful set of tools for collecting, storing, retrieving at will, transforming and displaying spatial data from the real world for a particular set of purposes" (Burrough, 1986). Over the past three decades, GIS has attracted great attention in the assessment of natural disasters. Government agencies and research institutions have expended great effort in landslide hazard mapping. A large amount of research on landslide hazard zonation has been done in recent years. Overviews of various landslide hazard zonation techniques can be found in publications by Varnes (1984), Hartlen and Viberg (1988), Guzzetti et al. (1999), and Van Westen (2000). Many scientists and engineers have attempted to assess landslide hazards and their spatial and temporal distributions. The literature on this subject is voluminous.

From the literature reviews on GIS application to slope stability analysis and landslide hazard zonation, it appears that most of the studies focused on using statistical methods to assess and predict the landslide susceptibility (Carrara, 1983, Chung and

Fabbri, 1999, Carrara et al., 1991), and the remainder focused on integrating the GIS technique with a deterministic model for slope stability analysis (Van Westen, 1993 & 2000, Jibson, 1998, Xie et al., 2003[1], 2003[2], Zhou et al., 2003). For seismic-induced landslide hazard assessment, there are two components which are commonly used: pseudo-static slope stability analysis and Newmark displacement method. For deterministic and probabilistic approaches, most research employs the infinite slope model, Newmark displacement, and Monte-Carlo simulation to estimate the factor of safety and displacement, or failure probability (Jibson and Harp, 1998, Christian and Urzua, 1998, Luzi et al., 2000, Refice et al., 2002, Khazai and Sitar, 2002).

In the last two decades, research has proven that GIS provides an excellent tool for landslide hazard zonation. However, seismic-induced landslide susceptibility assessment inherits complex uncertainties of terrain, seismic, and geotechnical parameters. Most existing GIS-based analysis models can only assess approximate landslide hazards. For deterministic analysis of slope stability, the assumption of current analysis models such as the infinite slope model, are only applicable for shallow slope sliding prediction. In fact, circular slope failure and deep slope sliding occur more commonly than otherwise in earthquake prone areas and these types of landslides usually are the major cause of property damage and fatalities. More accurate analysis and better techniques are needed to improve the mapping of landslide hazards and the prediction of seismic-induced slope instability. It is essential to develop a reliable analysis model that considers failure modes, geotechnical parameters, and uncertainties to achieve the accuracy needed for seismic-induced landslide hazard zonation.

1.3 Objective and Scope

The overall objective of this research is to develop reliable deterministic and probabilistic models for slope stability analysis and earthquake-induced landslide hazard zonation. These models combine a slope stability analysis model with GIS-based techniques for mapping landslide hazards and for evaluating shallow and deep slope

failures. The primary goal of this research is to develop one-dimensional (1D), two-dimensional (2D), and three-dimensional (3D) deterministic and probabilistic analysis models for earthquake-induced landslide hazard zonation. The city of Nueva San Salvador, El Salvador, and its vicinity were selected as the study area.

The other main tasks of the study are:

(1) to characterize causative factors based on the available data in the study area to determine peak ground acceleration for slope stability analysis in El Salvador, and to analyze the influence of causative factors on slope stability;

(2) to evaluate the topographic effect of ground motion and seismic response in the Balsamo Ridge area where the most damaging landslide destroyed the neighborhood of Nueva San Salvador;

(3) to use terrain and hydrology analysis with manual correction to determine mapping units (slope profiles for 2D analysis and slope units for 3D analysis), which are related to geomorphology, geological conditions, and rock/soil properties;

(4) to use ArcObjects to perform the slope stability analysis inside a GIS platform (1D model) and to write a VBA program for slope stability analysis outside of the GIS environment (2D and 3D model); and

(5) to perform regional and site-specific landslide hazard zonation for Nueva San Salvador, El Salvador using the developed analysis models. The landslides triggered by the January 13, 2001 earthquake provide a reference setting to calibrate the modeling results and to predict seismic-induced landslide hazards in the Balsamo Ridge mountain area.

Slope stability analysis methods employed in this study include the infinite slope model, the block sliding model, the ordinary method of slices, the Bishop simplified method, and the Hovland's column method. Both pseudo-static and Newmark displacement methods are adopted in seismic slope stability analysis. A large portion of this research is concentrated on developing GIS-based analysis models of slope stability and GIS process.

In probabilistic analysis, in order to simplify the problem solving process, the Monte-Carlo simulation is used to simulate the uncertainty of geotechnical parameters (soil friction angle, cohesion, and unit weight) and groundwater depth. Both the Monte-Carlo simulation and the first order reliability analysis (Hasofer-Lind method) are employed in the slope failure probability analysis.

In the 2D model, a number of slope profiles are selected based on the characteristics of the terrain. The dataset of each profile is sampled and exported to external slope stability analysis models for computation calculation. The results of stability analysis are imported to the GIS environment for display and for performance of landslide hazard zonation according to the degree of slope stability. In the 3D model, the slope units are sampled and exported to an external 3D slope stability analysis model. Similar to the 2D model, the analyzed data are processed in GIS for landslide susceptibility mapping.

Slope stability and earthquake-induced landslide hazard zonation is a process of integrating analytical techniques with practical decision-making. Figure 1.1 shows the framework of the GIS-based deterministic and probabilistic methods developed in this study. The GIS approach developed here is based on the spatial analysis of the raster dataset which models the slope as an aggregate of grids (or cells). The first step, shown in Figure 1.1, is data collection. All the available datasets related to slope stability analysis are to be collected. The second step is data preparation in which parameter data layers for GIS-based slope stability analysis are generated. At this stage, effective data management, spatial analysis, and information generation, such as interoperable geodatabases, is integrated into the GIS process. The third step is the application of 1D, 2D, or 3D models to regional or site-specific slope stability analysis. Using various analyses and modeling tools with diverse data sources in combination, the slope stability maps are produced. In the final step, landslide hazard zonation maps are obtained through reclassification of the slope stability indexes.

Evaluation of landslide hazards is a complex, multicriteria decision making problem, which requires experience and expertise pertaining to the geosciences, terrain

analysis, GIS spatial analysis, and slope stability analysis. The resulting interpretation and validation involve comparisons of historic landslide occurrence and the judgment of an expert. However, in this framework, deterministic and probabilistic analysis can supply more accurate slope stability and landslide hazard information. The ultimate goal of earthquake-induced landslide hazard zonation is to predict where and in what seismic conditions slope failure will most likely occur with a threshold earthquake magnitude and horizontal acceleration.

The analytical models are tested in the study area. The landslide susceptible areas and the hazard levels are estimated through slope stability analysis and regional and site-specific landslide hazard zonation.

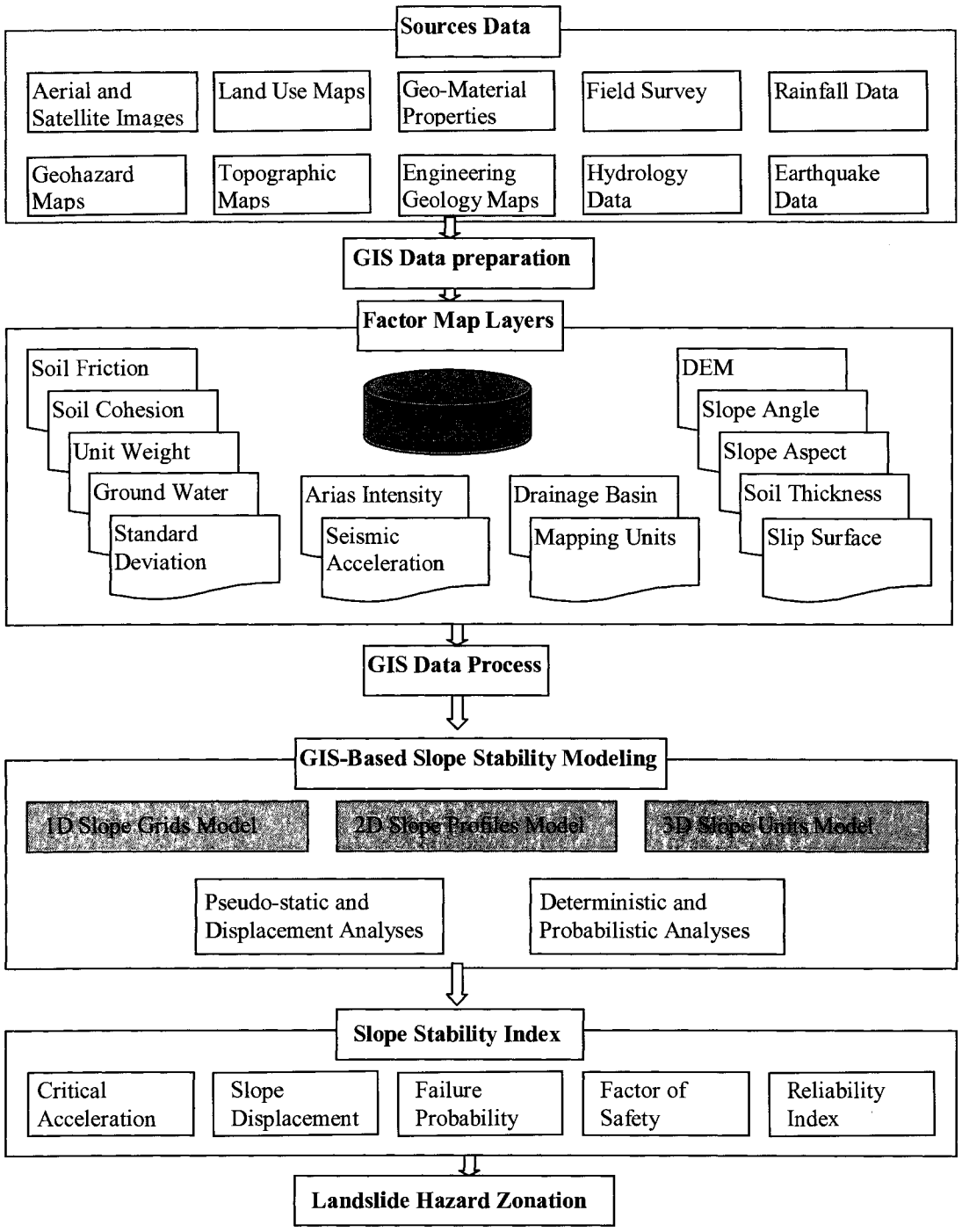

Figure 1.1 Framework of GIS-based slope stability analysis and landslide hazard zonation applied in the study. The procedures of the analysis include source data collection, data preparation for each analysis model, data integration for regional or site-specific slope stability analysis, and landslide hazard zonation.

Chapter 2 Earthquake-Induced Landslides and Analysis Methods

2.1 Characteristics of Earthquake-Induced Landslides

Earthquakes have triggered landslides in many different topographic and geological settings. Keefer (1984) studied 40 earthquakes worldwide to determine the characteristics, geological environments, and hazards caused by seismic events. Fourteen types of landslides were identified, the most abundant of which were rock falls, disrupted soil flows, and rock slides. Different types of slope movement and shaking threshold values for rock and soil slope sliding are listed in Tables 2.1 and 2.2. For rock slopes (Table 2.1), the earthquake-induced slope moment is often divided into falls and slides. For soil slopes (Table 2.2), there can also be earthquake-induced falls and slides. In addition, the slope can be subjected to a flow slide or lateral spreading (Keefer, 1984, Day, 2002). In the tables, the minimum slope inclination refers to the minimum slope angle that is usually required to initiate a specific type of earthquake-induced slope movement. The shaking threshold value refers to the minimum local magnitude (also known as Richter magnitude scale) required to produce earthquake-induced slope movement.

Earthquake-induced landslides can be divided into three main categories: disrupted slides and falls, coherent slides, and lateral spreads and flows. Keefer (1984) and Kramer (1996) have identified characteristics of earthquake-induced slope failures:

- Disrupted slides and falls include rock falls, rock slides, rock avalanches, soil falls, disrupted soil slides, and soil avalanches. The earth materials involved in such failures are sheared, broken, and disturbed into a nearly random order. These types of failures, usually found in steep terrain, can produce extremely rapid movements and devastating damage; rock avalanches and rock falls have historically been among the leading causes of death from earthquake-induced landslides.

- Coherent slides, such as rock and soil slumps, rock and soil blocks slides, and slow earth flows, generally consist of a few coherent blocks that translate or rotate on somewhat deeper failure surfaces in moderate to steeply sloping terrain. Most coherent slides occur at lower velocities than that of disrupted slides and falls.
- Lateral spreads and flows generally involve liquefiable soils, although sensitive clays can produce landslides with very similar characteristics as well. Due to the low residual strength of these materials, sliding can occur on remarkably flat slopes and produce very high velocities.

Different types of earthquake-induced landslides occur with different frequencies. Historically, rock falls, disrupted soil slides, and rock slides have been most common. Subaqueous landslides, slow earth flows, rock block slides, and rock avalanches are least common, although the difficulty of observing subaqueous slides might have contributed to their apparent rarity.

Keefer (1984) studied the effect of earthquake magnitude and epicentral distance on the occurrence of earthquake induced landslides. The study was based on 300 U.S. earthquakes between 1958 and 1977, and showed that for local magnitudes less than 4.0, landslides rarely occur. The smallest earthquake that produced landslides had a local magnitude of about 4.0. The minimum magnitudes for different types of landslides were estimated as shown in Tables 2.1 and 2.2. The threshold values needed to produce liquefaction-related landslides (flow slides, subaqueous flows, and lateral spreading) are at peak ground acceleration (a_{max}) of about 0.1g and the local magnitude M_L of about 5.0. In general, the most abundant types of slope failure during earthquakes tend to have the lowest threshold value of earthquake magnitude. For example, rockfalls and rock slides have low threshold values (M_L=4.0). When earthquake magnitude reaches 7.0, it can cause landslides as far as 200 km from epicenter. Keefer (1984) also observed that earthquakes of moderate to high magnitude can cause landslides over an area as large as 500,000 km^2.

Table 2.1 Types of earthquake-induced slope movement in rock

Name	Type of Movement	Material Type	Min. Slope Inclination	Threshold Value	Depth
Rock falls	Bounding, rolling, free fall	Rock weakly cemented, intensely fractured, or weathered; containing conspicuous planes of weakness dipping out of slope or containing boulders in a weak matrix.	40° (1.2:1)	M_L=4.0	Shallow
Rock slides	Translational sliding on basal shear surface		35° (1.4:1)	M_L=4.0	Shallow
Rock avalan-ches	Complex, involving sliding and/or flow, as stream of rock fragments	Rock intensely cemented and exhibiting one of the following properties: significant weathering, planes of weakness dipping out of slope, weak cementation, or evidence of previous landsliding.	25° (2.1:1)	M_L=6.0	Deep
Rock slumps	Sliding on basal shear surface with component of headward rotation	Intensely fractured rocks, pre-existing rock slump deposits, shale, and other rocks containing layers of weakly cemented or intensely weathered material.	15° (3.7:1)	M_L=5.0	Deep
Block slides	Translational sliding on basal shear surface	Rocks having conspicuous bedding planes or similar planes of weakness dipping out of slopes.	15° (3.7:1)	M_L=5.0	Deep

Source: Keefer (1984), Division of Mines and Geology, CA (1997), and Day (2002).
Velocity: extremely slow (<0.6 m/yr), very slow (0.6~1.5 m/yr), slow (1.5 m/yr~1.5 m/month), moderate (1.5 m/month~1.5 m/day), rapid (1.5 m/day~0.3 m/min), very rapid (0.3 m/min~3 m/sec), extremely rapid (>3 m/sec).
Depth: shallow (thickness generally <3 m) and deep (thickness generally > 3 m)

Table 2.2 Types of earthquake-induced slope movement in soil

Name	Type of Movement	Material Type	Min. Slope Inclination	Threshold Value	Depth
Soil falls	Bounding, rolling, free fall	Granular soils with slight cementation or containing clay binder	40° (1.2:1)	M_L=4.0	Shallow
Soil avalanches	Translational sliding with subsidiary flow	Loose, unsaturated sand	25° (2.1:1)	M_L=6.5	Shallow
Disrupted soil slides	Translational sliding on basal shear surface or zone of weakened, sensitive clay	Loose, unsaturated sand	15° (3.7:1)	M_L=4.0	Shallow
Soil slumps	Sliding on basal shear surface with component of headward rotation	Loose, partly to completely saturated sand or silt	10° (5.7:1)	M_L=4.5	Deep
Soil block sliding	Translational sliding on basal shear surface	Loose, partly to completely saturated sand or silt	5° (11:1)	M_L=4.5	Deep
Slow earth flows	Translational sliding on basal shear surface with minor internal flow	Stiff, partly to completely saturated clay, flow deposits	10° (5.7:1)	M_L=5.0	Shallow or deep
Flow slides	Flow	Saturated sand or sandy silt; loose, saturated granular soils	2.3° (25:1)	M_L=5.0 a_{max}=0.1g	Shallow
Subaqueous flows	Complex, involving lateral spreading or flow, slumping	Loose, saturated granular soils	0.5° (110:1)		Variable
Lateral spreading	Translational on basal zone of liquefied sand, silt, or weakened sensitive clay	Loose, partly to completely saturated silt or sand, artificial fill composed of sand	0.3° (190:1)		Variable

Source: Keefer (1984), Division of Mines and Geology, CA (1997), and Day (2002). Definition of velocity and depth same as in Table 2.1.

2.2 Seismic Slope Stability Analysis

2.2.1 General Methods

Earthquake-induced landslides usually occur in marginally or moderately stable slopes where earthquake inertial forces may be sufficient to trigger a failure. In the case of weak materials, repeated ground shaking may cause loss of strength of the soil materials (e.g. liquefaction) and subsequent slope failure. The evaluation of slope stability is a process that requires the collection of detailed information on geology, geomorphology, hydrogeology, and the soil/rock properties of a site. Slope stability analysis can yield sufficiently accurate results when the above data are evaluated carefully and the appropriate parameters are used in a slope stability calculation.

Seismic slope stability analyses are further complicated by two additional factors: (1) earthquake-induced dynamic stresses, and (2) the effect of dynamic stresses on the stress-stain behavior and strength of slope materials. Depending on the behavior of soil/rock materials during seismic shaking, seismic instability analyses may be grouped into two general categories: inertial slope stability analysis and weakening slope stability analysis (Day, 2002).

Weakening slope stability analysis is preferred for those materials that will experience a significant reduction in shear strength during earthquake. This analysis is usually confined to slope failure caused by soil liquefaction, such as mass flow sliding and liquefaction-induced lateral spreading caused by the shear strength reduction of strain-softening soil such as slow earthquake flows.

Inertial slope stability analysis is preferred for those materials that retain their shear strength during an earthquake. Slope instability can occur due to an inertia force from the earthquake.

There are numerous analytical techniques that deal with slope in the above two categories and these are either based on limit equilibrium or stress-deformation analyses. The most commonly used approaches for inertial slope stability analysis are the pseudo-

static and Newmark displacement (Newmark, 1965) methods. They are commonly applied in GIS-based landslide hazard zonation. Other numerical methods, such as stress-deformation analysis carried out by the dynamic finite element method, are rarely used in GIS-based landslide hazard zonation because they are too complicated to allow efficient data processing.

2.2.2 Pseudo-Static Analysis

Since 1920s engineers have used the pseudo-static approach to analyze the seismic stability of earth structures. This analysis ignores the cyclic nature of the earthquake and treats it as if it applies an additional static force on the slope. Pseudo-static analysis represents the effects of earthquake shaking by pseudo-static acceleration that produces inertial earthquake force, which acts through the centroid of sliding mass. The magnitudes of the inertial earthquake force are given by:

$$F_h = ma_h = \frac{a_h W}{g} = k_h W \qquad (2.1)$$

$$F_v = ma_v = \frac{a_v W}{g} = k_v W \qquad (2.2)$$

where: F_h and F_v are horizontal and vertical pseudo-static earthquake forces (kN), respectively; m is total mass of sliding materials (kg); a_h and a_v are horizontal and vertical earthquake accelerations (m/s^2); W is total weight of sliding materials (kN); k_h ($=a_h/g$) and k_v ($=a_v/g$) are dimensionless horizontal and vertical pseudo-static seismic coefficients; and g is gravity acceleration (or gravitational constant, g=9.81 m/s^2).

An earthquake could subject the sliding mass to both vertical and horizontal pseudo-static forces. However, the vertical earthquake force, F_v, is usually ignored in the standard pseudo-static analysis because it has a much less effect on the stability of a slope than does horizontal acceleration. In addition, in most cases a_v is less than a_h, and hence k_v is smaller than k_h (Day, 2002). If not specified, the seismic coefficient, k, usually refers to k_h.

The unit of the seismic coefficient has been defined loosely. In some literature, it is presented with a dimension of gravity acceleration (e.g., 0.2 g). The seismic coefficient should not be confused with the particle acceleration generated by an earthquake (Cornforth, 2005). In some practices, engineers mistakenly refer to the seismic coefficient, *k,* as a substitute for ground acceleration, *a.* In pseudo-static analysis, the coefficient *k* is an arbitrary number used to aid analysis of nonliquefying soils.

The limit equilibrium method in slope stability analysis is the most commonly used method for static and pseudo-static slope stability analysis. This method postulates that the slope might fail due to a soil mass sliding on a failure surface. The shear strength of the soil is normally given by the Mohr-Coulomb failure criterion, in which the shear stress at failure is expressed as follows:

$$\tau = c' + (\sigma - p)\tan\phi' \qquad (2.3)$$

where: τ is the shear stress at failure, kPa; c ' is the cohesion with respect to effective stresses, kPa; σ is total applied normal stress, kPa; ϕ' is the angle of effective internal friction; and p is the pore-water pressure, kPa.

Figure 2.1 illustrates the simplest type of slope failure. The failure mass has a planar slip surface inclining at an angle α to the horizontal.

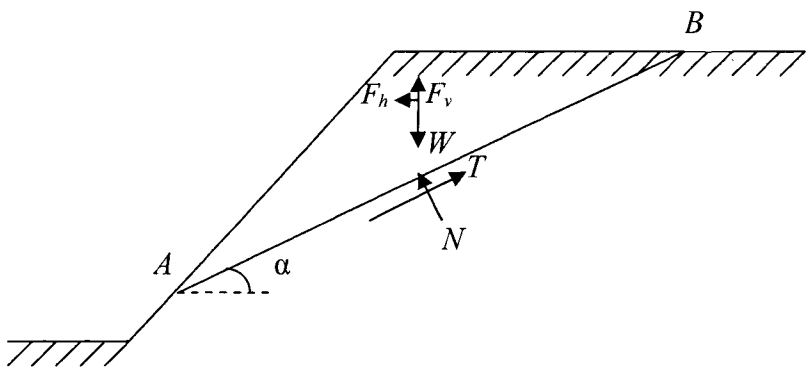

Figure 2.1 Plane failure with forces acting on the sliding mass for pseudo-static slope stability analysis (N is normal reaction force, T is shear strength)

For a plane failure (Figure 2.1), assuming that the sliding mass will move in the same direction as the slip surface, the factor of safety of the slope can be derived by summing forces along the sliding direction. Ignoring the vertical earthquake forces, the factor of safety of the slope is defined as follows:

$$FS = \frac{resisting\ forces}{driving\ forces} = \frac{cL + N\tan\phi}{W\sin\alpha + F_h\cos\alpha} = \frac{cL + (W\cos\alpha - F_h\sin\alpha)\tan\phi}{W\sin\alpha + F_h\cos\alpha} \quad (2.4)$$

where: N is the normal force acting at the slip surface, kN; L is length of slip surface (length of AB, see Figure 2.1), m; c is cohesion of sliding material along slip surface, kPa; and ϕ is friction angle of the slip surface.

Theoretically, in the equilibrium analysis, an FS of unity is a critical condition and would indicate an imminent failure, an FS greater than 1.0 indicates a stable condition, and an FS less than one indicates a failure condition.

Many methods have been developed for slope stability analysis based on the limit equilibrium concept. The common methods of 2D and 3D slope stability analysis are listed in Tables 2.3 and 2.4. Usually, the Bishop modified, Janbu simplified, and Spencer's methods are used in slope engineering design.

The failure surface to be analyzed for slope stability consists of a combination of linear and/or circular traces that result in the lowest factor of safety. The typical circular sliding surface in homogenous soil is shown in Figure 2.2. In 2D slope stability analysis, it is essential to perform a thorough search for the slip surface, which has a minimum factor of safety.

The pseudo-static method is inherently conservative because the cyclic earthquake force is replaced by a constant force equal to the maximum transient force. The degree of conservativeness in pseudo-static analysis critically depends on the value of a horizontal seismic coefficient. Thus, the selection of a proper seismic coefficient to be used for design purposes is quite important. However, it is also one of the most difficult issues facing engineers.

Table 2.3 Common methods for 2D limit equilibrium analysis in geotechnical engineering (after Duncan, 1996)

Method	Date	Equilibrium Conditions Satisfied	Shape of Slip Surface	Assumptions
Infinite slope (Skempton)	1957	Force equilibrium	Plane	Slip surface is parallel to the ground surface
Ordinary method of slices (Fellenuis)	1927	Moment equilibrium of entire mass	Circular	Normal force on base of slice is Wcosα and shear force is Wsinα. No interslice forces (W: weight of slice; α: angle of slip surface)
Method of slices (Fellennuis)	1910	Force equilibrium of each slice		
Bishop modified method	1955	Vertical equilibrium and overall moment equilibrium	Circular	Side forces are horizontal.
Friction circle method (Taylor)	1937	Moment equilibrium	Circular	Resultant force is tangent to friction circle
Janbu's simplified method	1968	Force equilibrium	Any shape	Side forces are horizontal
Modified Swedish method (U.S. army corps of engineers method)	1970	Force equilibrium	Any shape	Side force inclinations are parallel to the slope
Lowe and Karafiath's method	1960	Vertical and horizontal force equilibrium	Any shape	Side force inclinations are average of slope surface and slip surface (varies from slice to slice)
Janbu's generalized method	1968	All conditions of equilibrium	Any shape	Assumes heights of side forces above the base vary from slice to slice
Spencer's method	1967	All conditions of equilibrium	Any shape	Inclinations of side forces are the same for every slice; side force inclinations is calculated in the process for solution
Morgenstern and Price's method	1965	All conditions of equilibrium	Any shape	Inclinations of side force follow a prescribed pattern; side forces can vary from slice to slice
Sarma's method	1973	All conditions of equilibrium	Any shape	Magnitudes of vertical side forces follow prescribed patterns

Table 2.4 Common methods of 3D slope stability analysis in geotechnical engineering (after Duncan, 1996). Most 3D methods are an extension of 2D methods.

Authors	Method	Geometry of slope/Slip Surface	Result comparison with 2D method
Hovland (1977)	Extended ordinary method of slices	Unrestricted/ unrestricted	$F_{3D} < F_{2D}$ for some cases
Hungr (1987)	Extended Bishop method	Unrestricted/ surface of revolution	$F_{3D} > F_{2D}$
Gens et al. (1988)	Extended Swedish circle	Simple slope/surface of revolution	$F_{3D} > F_{2D}$
Leshchinsky and Huang (1992)	Limit equilibrium and variational analysis	Unrestricted/ unrestricted	$F_{3D} > F_{2D}$
Note: F_{2D} and F_{3D} are 2D and 3D factor of safety, respectively.			

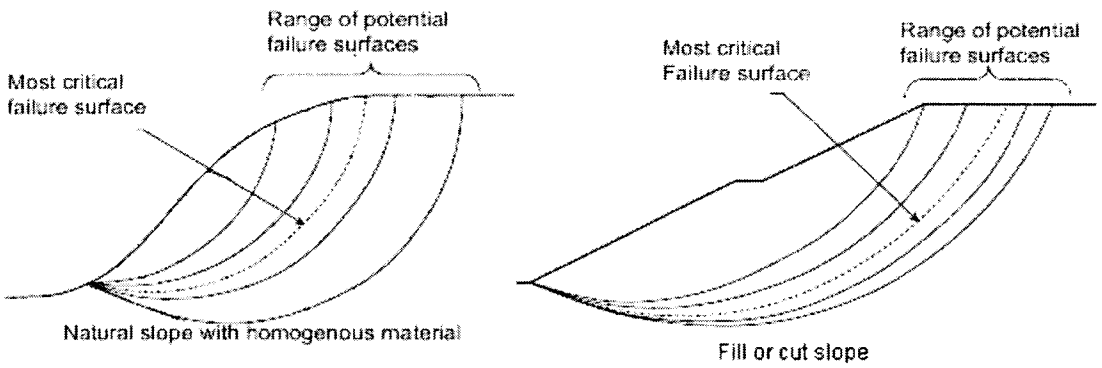

Figure 2.2 Slope geometry of circular failure surfaces in homogenous soil (after SCEC, 2002). The slope usually fails along the most critical failure surface, which has the lowest factor of safety.

The general concept for selection of a seismic coefficient is that a higher value of k should be used if the site experienced or will probably experience a higher peak ground acceleration, a larger earthquake, or a longer shaking period. Note that the k should never be greater than a_{max}/g. The seismic coefficient k is usually one-half or less than the maximum ground acceleration, a_{max}/g. The typical practice in the U.S. uses k values ranging from 0.10 to 0.15. In Japan, the earth dam code specifies values between 0.15

and 0.25. For slope, dam, and embankment stability analysis, the selected horizontal seismic coefficients usually are from 0.15 to $0.5a_{max}/g$. Typical seismic coefficients and factors of safety used in practice today are given in Table 2.5.

Table 2.5 The selection of horizontal seismic coefficients (k) in slope and embankment stability analysis

Authors	Seismic coefficient, k	Conditions
Terzaghi, 1950	0.10	Severe earthquake
	0.20	Violent and destructive earthquake
	0.50	Catastrophic earthquake
Seed, 1979	0.10	Near fault site, M=6.5, acceptable $FS \geq 1.15$
	0.15	Near fault site, M=8.25, acceptable $FS \geq 1.15$
Marcuson, 1981	$0.33a_{max}/g$ to $0.50a_{max}/g$	Dam engineering, k including amplification and deamplification effect
Krinitzsky et al. 1993, Tanguchi and Sasaki, 1986	$0.65a_{max}/g$	Intermediate slide mass. This constant 0.65 is used in the liquefaction analysis.
Hynes-Griffin and Franklin, 1984	$0.50a_{max}/g$	Earth dam, $FS \geq 1.0$; earth dam will not develop "dangerously large deformation"
Division of Mines and Geology, California, 1997	≥ 0.15	California
SCEC, 2002	0.15	LA county, $FS \geq 1.10$
Japan earth dam code	0.12~0.25	Japan

Hynes-Griffith and Franklin (1984), based on a study of the earthquake records from 354 accelerograms, use a horizontal earthquake coefficient equal to $0.5a_{max}/g$ for earth dam analysis. By using this coefficient and having a pseudo-static factor of safety greater than 1.0, they concluded that earth dams will not be subjected to "dangerously large" deformations. Seed (1979) recommended a k value based on a study of earth dams constructed of ductile soils with crest accelerations less than 0.75 g. Ductile soils are those which do not generate additional pore water pressure and which show no more than 15% loss of strength upon cyclic loading. In those cases, deformations would be

acceptably small if the earthquake coefficients are 0.10 (M=6.5) to 0.15 (M=8.25) and factors of safety are at least 1.15.

Although the pseudo-static approach to stability analysis is relatively simple, it suffers from many limitations as it sometimes cannot realistically simulate the complex dynamic effects of earthquake shaking with a seismic coefficient. These limitations were clearly recognized by many researchers including Terzaghi (1950), Seed et al. (1969), etc. More specifically, in the case of soils that build up large pore water pressures or have strength degradation of more than 15% due to earthquake shaking, the analysis can become unreliable. As a case in point, the upper and lower San Fernando Dams (k=0.15) and the Sheffield Dam (k=0.1) failed due to earthquake shaking even when the calculated factors of safety by the pseudo-static method were well above 1.0 (Seed, 1979, Kramer, 1996). Due to the limitations of the pseudo-static approach, in the last two decades researchers have increasingly used methods based on the assessment of Newmark earthquake-induced displacement.

2.2.3 Newmark Displacement Method

The purpose of the Newmark method (1965) is to estimate the cumulative displacement of earth dams and slopes in response to earthquake shaking. It is based on the concept of a rigid frictional block resting on an inclined plane that is subjected to a sinusoidal wave. The method calculates the acceleration, a_y, needed to exceed the static equilibrium (Figure 2.3). When the ground acceleration of seismic wave exceeds a_y, the slope moves. When this occurs, the blocks are no longer stable, and they will be accelerated down the slope. To simplify the calculations, areas in the same general direction as the slope face are used. The acceleration plots above the zero line in the time history of the acceleration curve (Figure 2.4) are thus considered in the analysis.

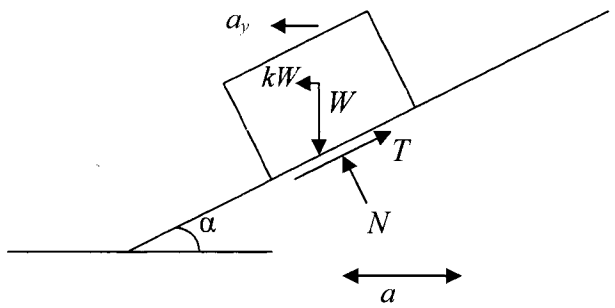

Figure 2.3 Sliding block analogy of Newmark analysis (N is normal reaction force; T is shear strength; W is weight of the block; k is horizontal seismic coefficient). When $k > a_y$, the factor of safety < 1, block moves. a_y is critical acceleration (yield acceleration).

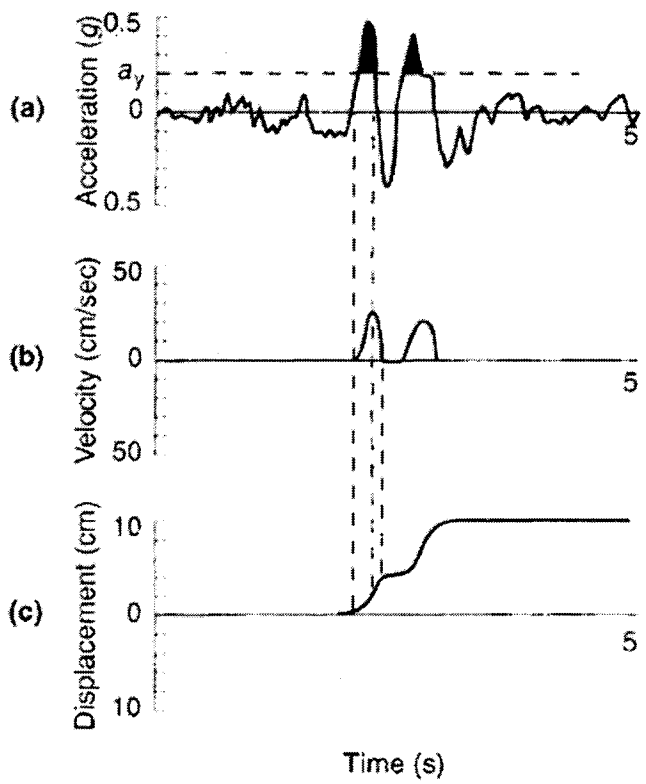

Figure 2.4 Diagram illustrating the Newmark method (*a*) acceleration versus time; (*b*) velocity versus time for the darkened portions of the acceleration pulses; (*c*) the corresponding downslope displacement versus time in response to the velocity pulses (after Wilson and Keefer, 1985; and Day, 2002).

In slope stability analysis, the Newmark method further assumes that the slope will deform only during those periods of earthquake shaking when the out-of-slope earthquake forces cause the pseudo-static factor of safety to drop to below 1.0. Figure 2.4 can be used to illustrate the basic premise of the Newmark method. The darkened portions of the acceleration pulses will cause permanent lateral movement of the slope. Total displacement during an earthquake can be calculated via integration and by examining significant representative cycles of ground motion. The Newmark method does not apply to soils that liquefy or experience a significant reduction in shear strength during an earthquake. The magnitude of slope displacement depends on horizontal yield acceleration (critical acceleration), a_y, peak ground acceleration, a_{max} (or PGA), duration of earthquake (time), and number of acceleration pulses (frequency). Many different equations have been developed utilizing the basic Newmark (1965) method (discussed in Section 6.4).

Newmark displacement analysis requires a prior knowledge of the static factor of safety, slope angle, and the earthquake strong-motion record. Interpretation of the results of Newmark analysis and determination of tolerable Newmark displacement of a slope is more complicated. The allowable displacement for a slope depends on the relationship between shear strength and shear strain of the material along the failure surface, and the slope's geometry, material properties, and seismic characteristics. The allowable displacement could be estimated from the measurement in slope displacement monitoring programs or damage in structures associated with slope displacement. Unfortunately, such data are very limited, and hence there is currently no rational basis for selecting allowable displacements. However, several observations of seismic-induced displacement are available and they can be use to understand the relationship between the slope failure and displacement. Those displacement data were obtained after the Loma Prieta earthquake (M7.1) which struck the San Francisco Bay area on October 17, 1987. Engineers and geoscientists performed a reconnaissance of landslide damage caused by the earthquake. These observations were summarized by the California Division of Mines and Geology (Manson et al., 1992). Shortly after the earthquake, about 50 landslides

were documented and seismic-induced displacements were estimated based on ground features at the headscarp for each slide. Among them, 12 landslides were active prior to the earthquake. According to the observation, two landslides had displacements over 90cm. The other landslides had displacements ranging from about 5 to 60 cm where the corresponding epicenter distance ranged from 5 km to 35 km. These observations provided information on the likely range of movement at a particular distance from the epicenter (Cornforth, 2005).

Due to these constraints, allowable displacements are often established based on observations of landslide movement and engineering judgment. The judgment from SCEC (2002) is that "if the critical slip surface from slope stability analysis daylights within a structure that is likely to be occupied by people during an earthquake, the median displacement should be maintained at less than 5 cm". Wang et al. (2001) applied Jibson's (1993) model to calculate the Newmark displacement and factor of safety using an infinite slope model in seismic hazard assessment of Benton County, Oregon, and used the following range of displacement (u) and factor of safety (FS) to categorize the seismic-induced hazard: low hazard (u<10 cm, FS>3.0); moderate (u=10~100 cm, FS=1.25~3.0); and high (u>100 cm, FS<1.25). Wieczorek et al. (1985) used 5 cm as the critical displacement for ground cracking and slope failure assessment in San Mateo County, California; Keefer and Wilson (1989) used 10 cm as the critical displacement for coherent landslides in southern California, and Jibson and Keefer (1993) used a range of 5 to 10cm as critical displacement for landslides in the Mississippi Valley.

In seismic slope stability analysis, the pseudo-static and permanent deformation methods may be combined into a single, unified method. First, a pseudo-static analysis is performed using a suitable value of the seismic coefficient. If the pseudo-static analysis results in an unacceptable factor of safety, a permanent seismic deformation analysis is then performed (Munfakh, 1998).

2.3 Review of GIS-based Approaches to Landslide Hazard Zonation

2.3.1 Landslide Susceptibility and Hazard Mapping

The generally accepted terminology related to landslide hazard mapping were defined by Varnes (1984), National Research Council (NRC) of the National Academies (2004), and Spiker and Gori (2000). Several important terms, such as "landslide hazard", "susceptibility", "zonation", and "vulnerability" were defined as follows:

(1) Landslide hazard refers to the potential for occurrence of a damaging landslide within a given area and in a give period of time. Such damage could include loss of life or injury, property damage, social and economic disruption, or environmental degradation.

(2) Landslide susceptibility refers to the likelihood of a landslide occurrence in an area on the basis of local terrain conditions. Susceptibility does not consider the probability of occurrence, which depends also on recurrence of triggering factors such as rainfall and seismicity. The terms of hazard and susceptibility are frequently used incorrectly as synonymous terms.

(3) Landslide vulnerability reflects extent of potential loss to a given element (or a set of elements) within an area affected by the hazard, expressed on a scale of 0 (no loss) and 1 (total loss). Vulnerability is influenced by physical, social, economic, and environmental conditions.

(4) Landslide hazard zonation refers to division of the land into homogenous areas or domains and the ranking of the area according to their degrees of actual or potential hazard or susceptibility to landslides.

(5) A landslide susceptibility map ranks slope stability of an area into categories ranging from stable to unstable. Susceptibility maps show where landslides may form. Many susceptibility maps use a color scheme that relates warm colors (red, orange, and yellow) to unstable and marginally unstable areas and cool colors (blue and green) to more stable areas.

The landslide zonation maps can be constructed at various scales including regional, neighborhood, and site-specific landslide hazard zonation maps. The definitions are as follows (NRC, 2004):

(1) National zonation maps provide a general inventory of landslide problem areas for the nation with a low level of detail. These maps are useful to national policy makers and the general public.

(2) Regional zonation maps provide engineers and planners an overview of potential impacts on large projects or regional developments during initial planning phases. The areas investigated are quite large and the required map detail is low.

(3) Neighborhood zonation maps identify landsliding zones for large engineering structures, roads, and urban areas. The investigations may cover quite large areas; yet a considerably higher level of detail is required. Slopes adjacent to landslides should be evaluated separately and may be assigned different hazard scores depending on their characteristics.

(4) Site-specific zonation maps are used during site investigations to provide absolute hazard classes and variable safety factors as a function of slope conditions and the influence of specific triggering factors.

There is no consensus on the map scale of landslide hazard zonation. The working scale is determined by the purpose of assessment, and extent of the study area, and the availability of data. The following map scale, which is used by the International Association of Engineering Geology (1976) for engineering geology mapping, may be used as a guideline for landslide hazard zonation mapping: national scale at <1:1,000,000; regional scale at 1:100, 000 to 1: 500,000; medium scale (neighborhood zonation) at 1:25,000 to 1: 50,000; and large scale (site-specific zonation) at 1:5,000 to 1: 15,000.

Landslide hazard zonation is commonly portrayed on maps using GIS techniques. Preparation of these maps requires an in-depth knowledge of the mass movement processes and an understanding of the causative factors that may lead to an occurrence of

potentially damaging landslides. Therefore, this is a task that should be undertaken by geoscientists (NRC, 2004).

2.3.2 General Methodology

The Geographic Information System contains a set of procedures which facilitate data input, storage, manipulation and analysis, and which output both spatial and attribute data to support decision-making activities (Grimshaw, 1994). It provides an excellent tool for landslide hazard zonation. The first application of GIS to landslide hazard zonation took place in the late 1970s (Newman et al., 1978). In the 1980s, the application of GIS to landslide mapping increased rapidly because of fast developing computer technology and commercial GIS software packages. Over the past three decades, geoscientists have developed several approaches to landslide hazard analysis. The methods presented in the literature can be broadly classified into five basic approaches: direct mapping, heuristic approach (geomorphic analysis), statistical analysis, deterministic analysis, and probabilistic analysis.

Despite a lack of agreement on methods and the scope of research, all of the methods are founded upon a basic concept (Carrara et al., 1995) which includes the following aspects: mapping of landslides over a target region; identification and mapping of a set of causative factors which are correlated with slope instability; estimation of the relative contribution of these factors in generating slope-failures; and classification of the land surface into domains of different degrees of hazard by different analysis methods. Most of the current hazard mapping aims to predict where failures are most likely to occur instead of when they are likely to take place.

Landslide hazard mapping and assessment requires a preliminary selection of a suitable mapping unit that refers to a portion of the land surface which has a set of ground conditions that differ from adjacent units across definable boundaries (Hansen, 1984). Various methods have been proposed to partition terrain into mapping units for the purpose of landslide hazard zonation (Carrara et al., 1995). The commonly used mapping

units can be classified into five groups: grid cells, terrain units, unique-condition units, slope units, and geomorphic units.

Guzzetti et al. (1999) summarized the definition of each mapping unit. Grid cell, or pixel, is preferred by raster-based GIS users. The area is divided into regular squares of a predefined size which become the mapping unit of reference. Each grid is assigned a value for a particular factor (terrain parameters, geological, and land use, etc.). A stack of raster map layers, each representing a single factor of slope instability, is obtained for the grid based landslide hazard assessment. The grid format offers many advantages due to the simplicity of operation through matrix algebra, and has been widely used by many researchers in heuristic, statistical, and deterministic analysis. Different analysis models have been developed to perform landslide hazard assessment based on the factor map layers.

Terrain units, which are traditionally preferred by geomorphologists, can be described as natural divisions of the terrain that can be distinguished on aerial photographs: for example, bottom and summit areas, relative flatness and steepness in slope, convergent and divergent areas. Terrain units are the basis of the land-system or land-unit classification approach, which has found wide application in many land resources investigations (Meijerink, 1988).

Unique condition units are constructed by the overlay of different categorical maps, so each map unit is defined by a unique combination of attributes. It implies the classification of each slope-instability factor into a few significant classes, which are stored in a single map or layer. By sequentially overlaying all layers, homogeneous domains (Chung et al., 1995) are singled out whose number, size and nature are strictly dependent on the criteria used in classifying the input factors.

Slope units can be obtained by partitioning the terrain into hydrological regions between drainage and divides (Carrara, 1988). It can be considered as the left or right side of a sub-basin of any order into which a watershed can be partitioned. It can be automatically derived from a high resolution Digital Elevation Model (DEM). According to the prevailing slope failure mode and size, slope units can be resized by partitioning a

river basin into nested subdivisions, coarser for larger landslides and finer for smaller slope failures (Montgomery and Dietrich, 1994). Slope units can be further subdivided into geomorphic units.

Methods for landslide hazard assessment and zonation can be qualitative or quantitative, and direct or indirect. Qualitative methods are subjective in defining landslide hazard using descriptive terms. Quantitative methods produce numeric estimations such as factor of safety or failure probability. Van Westen (1993, 2000), Van Westen et al. (1996, 1997), and Soeters and Van Westen (1999) discussed the main approaches in landslide hazard zonation and the scales of mapping. The main methods and their characteristics in landslide hazard analysis are listed in Table 2.6.

Table 2.6 The main methods used in landslide hazard zonation (after Van Westen, 1993 , 2000)

Methods	Main Characteristics
Direct mapping	Direct mapping of mass movement for those sites where landslides have occurred in the past. This method usually involves aerial and satellite image interpretation and field work.
Heuristic approach (geomorphic analysis)	Direct or semi-direct methods in which the geomorphological map is derived into a landslide hazard map by terrain analysis, direct mapping of data analysis, or by combining several maps into one using subjective decision rules based on the experience of the earth scientist.
Statistical analysis	Indirect methods in which statistical analyses are used to obtain predictions of the mass movement hazard from a number of parameter maps. Usually, the bivariate, multivariate, and fuzzy logic approaches are used.
Deterministic analysis	Indirect methods in which parameter maps are combined in calculations including slope stability analysis by geotechnical engineering methods and Newmark displacement analysis for seismic-induced slope stability assessment.
Probability analysis	Indirect methods in which the uncertainties in geotechnical parameters are considered in slope stability analysis by a probabilistic method such as Monte-Carlo simulation and the first order second moment approach. The failure probability or reliability index is used in landslide hazard assessment.

Geomorphic analysis is generally used for very large areas such as national hazard maps. The scale of such maps can be on the order of 1:100,000 to 1:250,000. This kind of

mapping is mostly used by large regional or national planning. The statistical analysis has the most flexibility in scale and in data type. It can also be used for medium scale mapping with scale of 1: 25,000 to 1:50,000. This scale of mapping can be used for infrastructure and transportation route planning. The deterministic and probabilistic analyses are used generally for local, regional, and site-specified hazard analyses such as land use planning for large engineering projects like dams, nuclear power plants, highways, and slopes of open pit mines and spoils. The scales for local regional hazard assessment can be at 1:15,000 to 1:25,000. For detailed engineering study, the scale of hazard mapping can be at 1:5,000 to 1:15,000. Such large scale mapping needs large scale digital topographic maps and geological maps, and/or high resolution aerial or satellite images (e.g. 1 to 4 m in spatial resolution).

2.3.3 Direct Mapping

Direct mapping is the most straightforward approach to landslide hazard zonation. It relies on visual analysis of aerial photographs, satellite images, topographic and geologic maps, field observations, and the database of historical landslide occurrence of a study area. Direct mapping creates interpretative maps of the extent and relative activity of landslide features. Such landslide maps are a basic data source for other landslide hazard mapping projects. Four major classes of maps can be produced by direct mapping approach: landslide inventory maps (Wieczorek, 1984), landslide density maps, landslide activity maps, and qualitative combination maps.

The direct interpretation of high resolution aerial and satellite images can lead directly to the identification of the large landslides and scarps. For identification of small scales of mass movement, a knowledge of characteristics of landslides and image features such as color, tone, shape, and texture is necessary. The landslide information extracted from images is related to terrain, vegetation, and hydrological conditions. Landslides disrupt the vegetation cover and expose the basal soil/rock and hence alter their spectral characteristics; therefore, vegetation cover and high moisture content in the debris along

with their shapes and locations are used as a key in demarcating the slide area (Sarkar and Kanungo, 2001).

2.3.4 Heuristic Approach (Geomorphic Analyses)

The heuristic qualitative approach combines the directly mapped landslides with their geomorphic setting to generate hazard maps. This approach is based on the direct relationship between the occurrence of slope failure and the causative terrain parameters. Causative factors are ranked and weighted according to their assumed or expected importance in causing slope failure (Guzzetti et al., 1999). Causative factors can be determined by the analysis of historic landslides and their terrain conditions. This method is subjective and relies on the professional experience of the expert and the rule of decision making, especially for the causative factor extraction and its weight assignment. Usually, the decision rules are difficult to formulate because they vary from place to place. Therefore, a good knowledge on the causes of landslide is essential in the decision making process. For hazard zonation, the historic databases of landslide and terrain parameters are of the utmost importance. This method can be applied at all map scales. The application of this approach is common in some European countries where sufficient experience in the determination of the relationship of terrain parameters and landslide hazards distribution exists (Varnes, 1984).

2.3.5 Statistical Methods

The statistical approach is based on the observed relationship between each factor and the past and present landslide distribution. All possible causative terrain parameters are weighted and integrated using GIS for landslide susceptibility analysis. The strength of this functional approach is also directly dependent on the quality and quantity of data collected. Bivariate, multivariate statistic, probability, and favorability functions are used

to analyze the parameters of instability (Carrara et al., 1991, Van Westen, 1993, Chung and Fabbri, 1999, Fabbri et al., 2003, Santacana et al., 2003).

A statistical approach assesses hazard by assuming that the past events are guides to the future. The basic assumption for this method is that the factors which caused slope failure in a region in the past are the same factors that will generate landslides in the future.

Results of a statistically based analysis usually are indices indicating the degrees of hazard. The analysis methods applied in statistical analysis are listed in Table 2.7.

Table 2.7 The statistical methods in GIS-based landslide hazard assessment (after Van Westen, 1993, 2000)

Statistical Model	Analysis Methods	Evaluation Parameters	Authors
Bivariate statistical methods	Susceptibility analysis	Landslide density	Brabb, 1984, Van Weston, 1992, 1993
	Information value method	Information value	Yin and Yan, 1988
	Weights of evidence modeling	Landslide occurrences	Spiegelhalter, 1986
Multivariate statistical methods	Multiple regression	Percentage of a terrain unit covered by landslides	Carrara, 1983, Carrara et al., 1991, 1995
	Discriminate analysis	Pixels with mass movements	
Probability and favorability function	Likelihood ratio function	Favorability index	Chung and Fabbri, 1993 , 1999
	Membership function (fuzzy set)	Membership	
	Dempster-Shafer belief function	Belief and plausible function	

In the bivariate statistical model, the role of individual factors or combinations related to slope failure is evaluated. The weight or contribution of a causative factor to the landslide hazard is determined on the basis of landslide density in each individual class. The GIS procedures for bivariate analysis usually are: (1) the division of each parameter map into a number of relevant classes; (2) the overlaying of the landslide map with each parameter map; (3) the determination of landslide density and weighting the value of each parameter class; (4) the assignment of weighting values to the various

parameters maps; (5) the final overlay mapping using a decision rule and determination of susceptibility threshold values; and (6) the classification of the resulting score in a few landslide hazard classes.

In many cases, the principal causative factors for rain- or earthquake-induced landslides are found to be slope steepness. Other parameters may be taken into account in bivariate models include soil type, slope aspect, slope height, land use, distance to a river, drainage density, etc. Medium scale maps are most appropriate for this type of analysis. Large scale maps do not supply sufficient detail for this type of analysis.

Van Westen (1993) applied density functions to determine weights of causative factor classes. Yin and Yan (1988) developed an information value method for landslide hazard assessment, which can be applied on a pixel-base as well as rock units. The landslide hazard information of each unit can be calculated, and the degree of hazard for a unit is calculated by the total information value. The hazard zonation map is generated by reclassifying the total information value map.

Bivariate statistical methods have a serious drawback because of the assumption of conditional independence, in which the different parameter maps are independent with respect to the probability for the occurrence of a landslide. This assumption is generally invalid. The problem can be avoided if the user evaluates the data and makes a new parameter map by combining the dependent maps (Van Westen et al., 1997).

Multivariate statistical models were developed for landslide hazard zonation by Carrara (1983) and Carrara et al. (1991, 1995). In their applications, the grids or morphometric units are reclassified into landslide hazard classes. The analysis is based on the presence and absence of mass movement phenomena. For each of the sample units, the presence or absence of landslides is determined. The resulting matrix is analyzed by multiple regression methods. A statistical model of slope instability in hazard is assessed through correlation of past landslides with several influential factors. The general linear model assumes the form as:

$$L = \beta_0 + \beta_1 X_1 + \beta_2 X_2 + \beta_3 X_3 + \cdots \beta_n X_n + \varepsilon \qquad (2.5)$$

where: L is the presence/absence (or area percentage) of landslide in each mapping unit. The X_n's are input predictor variables (or instability factors) measured or observed for each mapping unit. The β_n's are coefficients estimated from the data through techniques, which are dependent on the statistical tool selected (multiple regression, discriminant analysis, and neural networks, etc.), and ε represents the residual error of the model.

The procedure in multivariate analysis involves several preliminary steps, which can be described as follows: (1) the determination of a list of factors which will be included in the analysis; (2) the partition of the study area into mapping units such as grid cells, terrain units, unique condition units, or slope units etc.; (3) the identification of the percentage of landslide affected area in each mapping unit; (4) the creation of various classes of parameters/factors map; (5) the creation of presence/absence values for each mapping unit by overlaying the parameter maps with the mapping unit map, and the creation of a large matrix; (6) the combination of the mapping units map with the mass movement map via map overlay and the division of mapping units into stable and unstable units; (7) the exportation of the matrix to a statistical package for subsequent analysis; (8) the importation of the results per mapping unit into the GIS and recoding of the land units; (9) the verification of the frequency distribution of classified stable and unstable units for proper separation; and (9) the classification of the map into a few hazard classes.

Two types of multivariate analyses have been conducted extensively: multiple regression and discriminant analysis (Carrara, 1983, Carrara et al., 1991). Both methods are often employed in parallel in the same project. It is preferable to apply discriminant analysis with continuous variables, while the regression analysis can be used with normal variables.

Chung and Fabbri (1993, 1999) developed a prediction model to produce a thematic map showing the area likely to be affected by future landslides and thematic classes indicating the degree of uncertainties associated with the prediction. This prediction model is also referred to as the favorability function approach, which is based on two assumptions: (1) past landslides of a given type can be characterized by sets of

layers of supporting spatial data, and (2) landslides of the same type will occur in the future under similar circumstances (Chung and Fabbri, 1999).

The basic assumption for statistical analysis is that the future landslides will take place under the conditions which led to past and present slope instability (Varnes, 1984). This assumption could be true for static factors such as geology, structure, and geomorphology. For factors which vary with time such as groundwater conditions, slope inclination, and seismic activities, the assumption might not be applicable. Earthquake shaking that triggers slope movements in one earthquake may differ from the shaking of another earthquake in the same region at a different time, and the instability factors determined for a particular earthquake-induced landslide event may vary greatly in response to changes in the ground motion characteristics (Khazai, 2004). Thus, for earthquake-induced landslide hazard assessment, attention should be given to the dynamic instability factors analysis.

Although multivariate techniques can be applied at different scales, their use becomes quite restricted at the regional scale, where an accurate input map of landslide occurrences may not be available and most of the important parameters cannot be collected with satisfactory accuracy. At large scales, different factors will have to be used (such as groundwater depth, soil sequences and thickness). These data are very difficult to obtain even for relatively small areas. Therefore, the medium scale is considered most appropriate for multivariate analysis.

In statistical analysis, the accuracy of the final hazard maps might be tested by comparison with the historic landslides in the area, and through an iterative process of analysis and classification, an optimalization of the model can be established.

2.3.6 Deterministic Methods

Heuristic and statistical approaches give no information on the stability of a slope as expressed in terms of its factor of safety or reliability. In order to obtain this information, it is necessary to use the deterministic slope stability method. This analysis

model is based on the failure mechanism that is used in geotechnical engineering. The advantage of these 'white box' models is that they can obtain quantitative values of slope stability through stability analysis. Usually, the limit equilibrium method is employed in GIS-based stability analysis and landslide hazard zonation. The results, such as factor of safety and/or displacement can be used directly by land developers and geotechnical engineers in stability prediction, engineering design, and geohazard management (Van Westen, 1996, 2000, Capolongo et al., 2002, Xie, et al., 2003, Zhou, et al., 2003).

The deterministic approach includes the pseudo-static analysis and Newmark displacement model. A pseudo-static analysis combines a traditional static slope stability analysis with the addition of a horizontal force component that models the effects of earthquake-induced ground motions. The pseudo-static analysis yields a factor of safety against seismic slope failure. This effectively provides a simple binary index of whether a slope is expected to fail or not at a given level of seismic acceleration.

Many deterministic methods for assessing earthquake-induced landslide susceptibility have been developed on the basis of Newmark's block sliding model. Permanent displacement techniques provide information regarding actual slope performance through calculation of some indices of relative or actual displacement based on commonly accepted characterizations of earthquake-shaking severity. Permanent displacement analysis is often chosen because of its higher information content, better modeling of ground motion, and increasing acceptance in the earthquake engineering community over static slope stability analysis. In recent years, many researchers have integrated GIS and various deterministic models for slope failure zonation. Wilson and Keefer (1985) developed a deterministic method for evaluating landslide susceptibility in terms of exceedance of significant threshold value of Arias Intensity and permanent displacement for different types of landslides. Wieczorek et al. (1985) predicted the spatial distribution of unstable slopes using a displacement method.

Deterministic models are increasingly being used in seismic-induced landslide hazard analysis, especially with the aid of GIS techniques which can perform a large number of calculations of pseudo-static safety factors or seismic-induced displacement

over large areas. Deterministic methods are applicable when the geomorphic and geologic conditions are fairly uniform over the entire study area and the landslide type is simple. The analysis models that can be used in the deterministic method are listed in Table 2.8.

Table 2.8 The deterministic methods of slope stability analysis used in GIS-based landslide hazard assessment

Methods	Analysis Model	Evaluation Parameters
Pseudo-static analysis	Infinite slope model	Factor of safety, critical acceleration
	2D analysis of slices: Ordinary method of slice, Bishop Method, Janbu's generalized method, Spencer's method	
	3D analysis of columns: Hovland's column method, Hungr's Method	
Displacement analysis	Newmark displacement: Integration from ground motion time-history, Ambraseys and Menu's (1988) equation, Jibson's (1993) and Jibson et al. (1998) equation, Yegian et al. (1991) equation	Earthquake-induced slope displacement

For application of the GIS-based deterministic model, the 1D, 2D, and 3D approaches can be used. The 2D and 3D slope stability methods are complex, and need to sample data at pre-defined slope profiles or slope units and export these data to an external 3D slope stability model. This is only applicable to small areas where detailed terrain and material data are available. A common deterministic method, usually applied to translational slides, is the infinite slope model. Wieczorek (1985) first applied the infinite slope model and simplified displacement method to produce seismic landslide susceptibility map for a study area in San Mateo County, California. This method has been widely used in GIS-based landslide susceptibility mapping and has become a popular slope stability analysis tool because it is simple and applicable to many shallow landslides. The infinite slope model is appropriate for failure analysis of a soil mass that overlies a sloping drainage barrier, such as a bedrock or a less permeable and well

compacted soil layer (Hammond el al., 1992). However, the infinite slope model does not adequately predict deep-seated, rotational failure. In recent research on GIS slope stability analysis, the 3D limit equilibrium analysis method was employed by several researchers (Xie et al., 2003, 2005). In the 3D method, the entire study area is divided into slope units by terrain analysis tools. Taking each slope unit as a study object, the 3D factor of safety can be obtained and the landslide hazard distribution can be then mapped for the entire study area.

The advantage of these models is that they are based on deterministic slope stability models, allowing the calculation of quantitative values of stability (safety factors, displacement, or critical acceleration). The main problem with these methods, however, is the degree of simplification, which is constrained by the assumptions. Another problem is that the data requirements for the deterministic model can be difficult to achieve in order to make the model effective.

2.3.7 Probabilistic Methods

Obviously, all input data for the deterministic calculation of a factor of safety inherit uncertainties. In recent years, considerable research has been directed towards applying probabilistic methods to site-specific stability analysis (Varne 1984). Because the parameters in slope stability analysis are inherently uncertain, a probability of failure should be estimated. Some parameters that are highly variable in space and time, including soil/rock strength, depth of potential sliding mass, saturated depth, and unit weight, can be considered as random variables. Probabilistic methods might be a more efficient approach to earthquake-induced landslide hazard analysis because they allow for spatial variability and uncertainties in all the parameters including earthquake occurrence, ground motion parameters, and material and slope features.

The probability methods applied in GIS-based landslide hazard zonation include three approaches. The first is to apply the reliability or probability analysis method, which is used in slope engineering design. This approach uses the limit equilibrium

model and probability method to consider the randomness of input parameters. The result is a map showing the average safety factor or failure probability for a given groundwater depth and horizontal seismic acceleration in conjunction with the return period of triggering events. The factor of safety or failure probability can be used to test different scenarios of slip surfaces and groundwater depths. The landslide susceptibility of a study area can be determined by the relative magnitude of calculated results. Many articles are available concerning this approach to slope stability analysis (Low and Tang, 1997, Low et al., 1998, Christian and Urzua, 1998, Malkawi et al., 2000, El-Ramly et al., 2002). Many approaches to reliability analysis can be applied to slope stability estimation. Among them, the Monte-Carlo simulation and the first order second moment approach are commonly used in probability analysis. The probabilistic methods used in GIS-based landslide assessment are listed in Table 2.9.

Table 2.9 The probabilistic methods used in GIS-based landslide hazard assessment

Stability Analysis Methods	Probabilistic Analysis Methods	Evaluation Parameters
Pseudo-static analysis	Monte-Carlo simulation	Failure probability, reliability index, mean factor of safety
	First order second moment method	
	Point estimate method	
	Hasofer-Lind approach	
Displacement and critical acceleration analysis	Probability function method	Failure probability
	Monte-Carlo simulation	

The second approach to probabilistic analysis is based on displacement analysis. The displacement in an area is compared with the inventory of seismic triggered landslides to construct a probability curve relating predicted displacement to failure probability. A probability function is applied to predict and to map the spatial variation in failure probability under earthquake conditions (Jibson and Harp, 1998, Capolongo et al., 2002). In displacement methods, the landslide hazard also can be predicted by probability of Newmark displacement exceeding the threshold value (Del Gaudio et al., 2003).

Threshold values of 5 cm or 10 cm are usually used for displacement based probabilistic analysis.

The third probabilistic method is based on the critical acceleration exceedance probability for a given seismic shaking threshold value. The critical acceleration, a_y, of each earthquake represents the minimum shear resistance required for the slope to remain stable under such seismic shaking. In order to estimate whether the slope has a significant probability of failure under future seismic shaking, the spatial distribution of calculated critical acceleration can be compared with the actual acceleration value of a slope (Del Gaudio et al., 2003). This procedure is a simplified method of characterizing the earthquake-induced landslide hazards.

Chapter 3 Study Area: Nueva San Salvador, El Salvador

3.1 Introduction

El Salvador is a small and densely populated country in Central America. It extends about 21,040 km^2 over a flat erosion surface 650 to 750 m above sea level. The surface slopes to the east and is cut by numerous, deeply incised streams and rivers. In the south, it is bordered by the coastal cordillera (Cadena Del Balsamo with maximum altitude 1,100 m) and Cerro San Jacinto (1,154 m), in the west by Boqueron volcano (1,967 m), and in the north by the relatively subdued Cerros de Mariona (798 m). To the east is the steep slope towards Lake Ilpango (438 m of water level) (Schmidt-Thome, 1975). Figure 3.1 shows the map of El Salvador.

Figure 3.1 Map of El Salvador (after Baum et al., 2001)

The population, estimated at about 6.4 million (2001), is very unevenly distributed throughout the country. Well over half of the population is concentrated in the southwest, the zone of the highest seismic hazard, in which at least twelve destructive

earthquakes have occurred during the 20th century alone (Bommer et al., 1998, 2002). Landslides are a common occurrence in El Salvador.

On January 13, 2001, a destructive earthquake of M7.6 struck El Salvador, which centered off the coast at 13.049°N, 88.660°W in the subduction zone occurring in the lower Cocos plate with a focal depth of 60 km. This earthquake was followed by numerous aftershocks of the same origin (Jibson et al., 2004). One month later, on February 13, 2001, a second major inland earthquake of M6.6 occurred which centered at 13.64°N, 88.94°W with a shallower depth of 10 to 15 km. The February 13 earthquake was caused by a strong, shallow intraplate strike-slip fault, which likely occurred in response to the complicated stresses in the Caribbean plate as it overrides the Cocos plate (USGS, 2001). Figure 3.2 shows the distribution of recorded historic landslides in El Salvador during the 1986 and 2001 earthquakes.

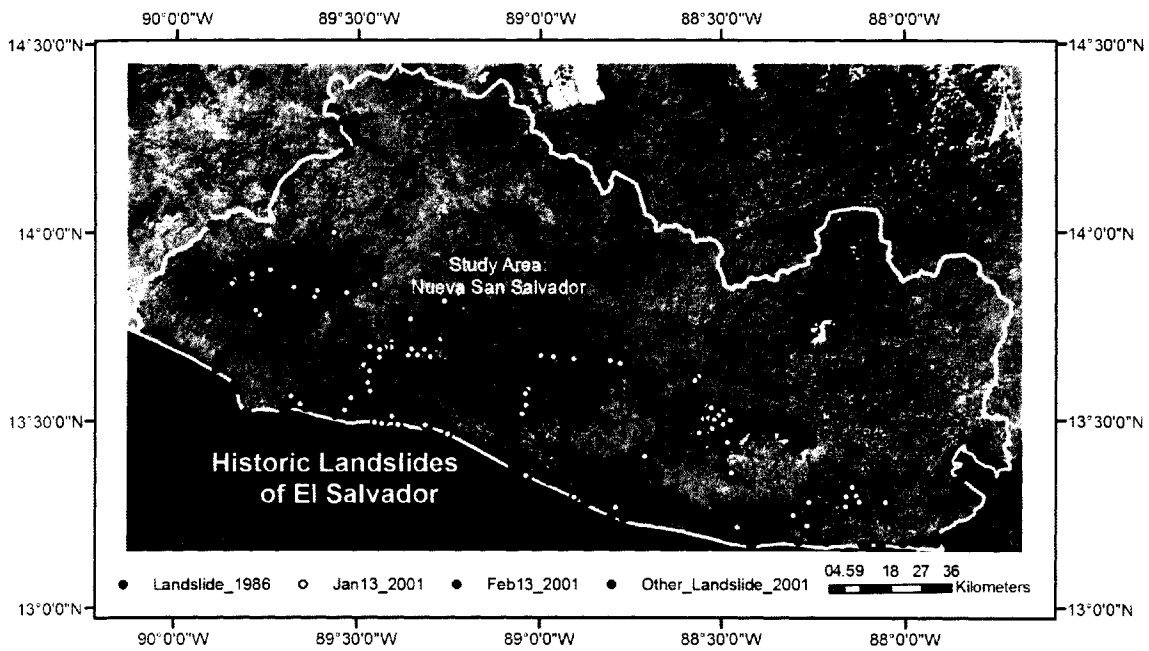

Figure 3.2 The distribution of historic landslides in El Salvador. The background image is the Landsat satellite image. Data source: SNET (National Services of Territorial Studies, El Salvador)

The January 13, 2001 earthquake triggered widespread destructive landslides in many parts of the country. Most of the southern two-thirds of the country had experienced ground acceleration of at least 0.1 g, and several strong-motion stations in South Central El Salvador recorded peak accelerations of 0.4 g or greater. The strong earthquake shaking of the January 13, 2001 earthquake affected a large part of El Salvador. Most of the triggered landslides were relatively shallow falls and slides in rock and debris primarily within young volcanic pyroclastic deposits (Jibson and Crone, 2001). The most significant concentration of landslides occurred on slopes around the periphery of San Salvador, in the Cordillera Balsamo region west and south of San Salvador, in the area around Lake Ilopango and Lake Coatepeque, and on steep flank of some volcanoes in the southern part of the country (Jibson et al, 2004).

3.2 Study Area: Nueva San Salvador

The study area, Nueva San Salvador, formally known as Santa Tecla is located west of San Salvador. The city of Nueva San Salvador is at the southern foothills of the San Salvador Volcano. Situated on the Pan-American Highway, the city is in an area with coffee plantations, livestock farms, and many large estates. In 1992, the population of the area was 116,575.

Geographically, the study area is located in the Cordillera Balsamo region. There was a highly seismic landslide occurrence area during the January 13 and February 13, 2001 earthquakes which caused a great loss of life in this area. In view of this tragedy, there is great public concern about the slope stability above Nueva San Salvador along the Balsamo Ridge. The public's concerns include whether and how potential landslides could be triggered and how slopes might respond to future large earthquakes similar to those of January 13 and February 13, 2001 (Jibson and Crone, 2001).

After a preliminary search of the target sites during a field trip in Nueva San Salvador area in June 2003, the author and his professors identified the Balsamo Ridge area around the City of Nueva San Salvador as a prime study area. Regional earthquake-

induced landslide hazard assessment was performed in Nueva San Salvador and its vicinity. Furthermore, the Balsamo Ridge area, which is a critical seismic hazard prone area, was selected for site-specific landslide hazard zonation study. As shown in Figure 3.3, the areas for regional landslide hazard zonation cover over 200 km^2. The site-specific area inside the study area, a part of Balsamo Ridge, was selected for the 2D and 3D slope stability analysis.

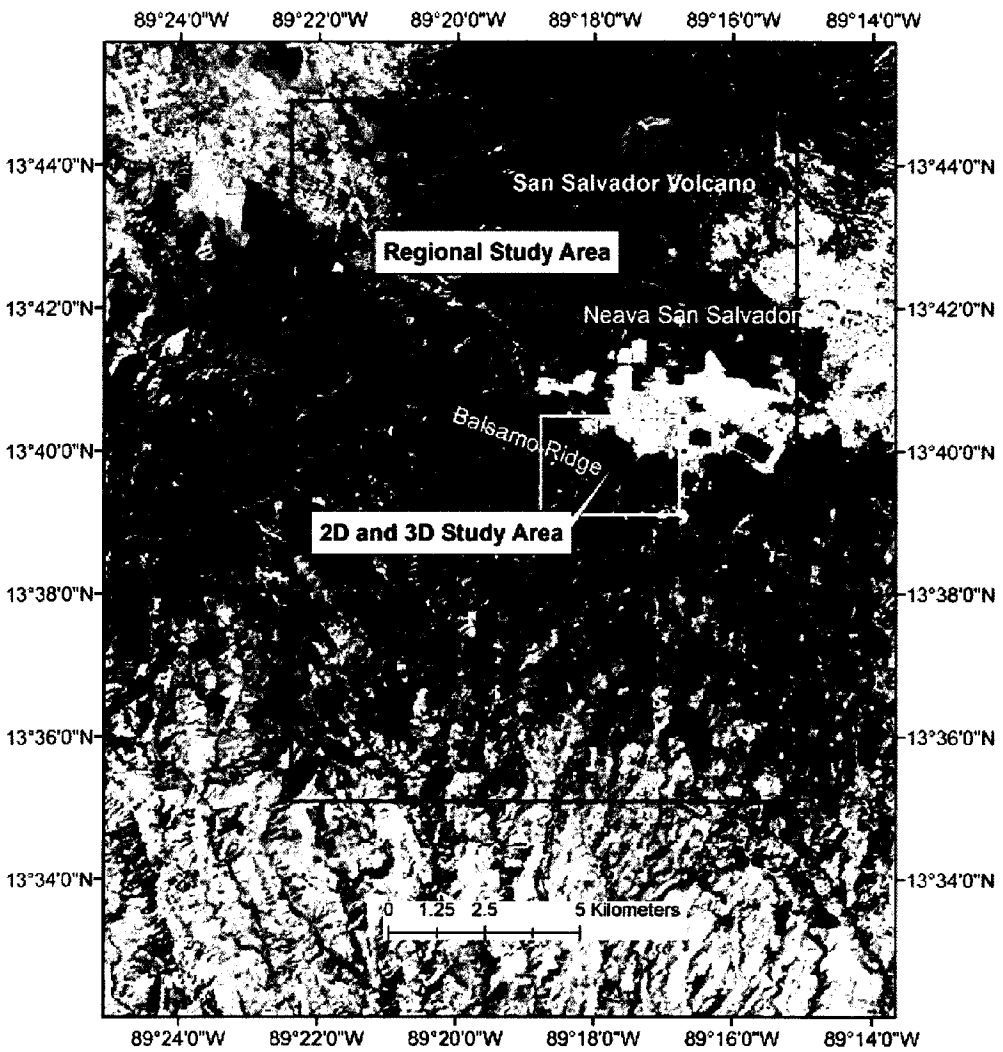

Figure 3.3 The study area for the regional and site-specific (2D and 3D) landslide hazard zonation. The boundaries of study areas are overlaid on a Landsat satellite image. The area is 200 km^2 for regional landslide hazard zonation, and about 5 km^2 for site-specific zonation.

The study of seismic-induced landslide hazard zonation was carried out using GIS-based deterministic and probabilistic models developed in this study. The study includes: (1) characterizing the landslides that occurred in natural terrain in Nueva San Salvador; (2) determining the statistical correlations between landslide occurrence and terrain parameters; (3) determining seismic parameters according to the original ground motion records during earthquake; (4) performing slope stability analysis using the developed GIS-based deterministic and probabilistic methodologies, including seismic-induced displacement analysis, 1D, 2D, and 3D slope stability calculations; and (5) performing landslide hazard zonation based on the degree of seismic-induced slope stability.

Various types of data are available and can be used to predict the level of landslide hazard susceptibility of slopes during earthquakes. In this study, the information integrated into the predictive model includes geology, in-situ material properties, dynamic properties of soil and rock, hydrologic conditions, topographic data, peak ground motion, and derivative information from satellite images. The GIS-based analysis model is applied to perform earthquake-induced slope stability analysis and landslide hazard zonation, which aims to alleviate the public concerns and supply landslide susceptibility information for hazard mitigation, future infrastructure planning, and earthquake response decision-making by the government of El Salvador.

3.3 Geology

3.3.1 Geological Setting of El Salvador

El Salvador sits atop the western part of the Caribbean plate, where it is overriding the Cocos plate. The Cocos plate is subducting beneath the Caribbean plate from the Middle American trench at a relatively high rate of 92 mm/year with a deep subducting angle. Figure 3.4 shows the tectonic setting of Central America.

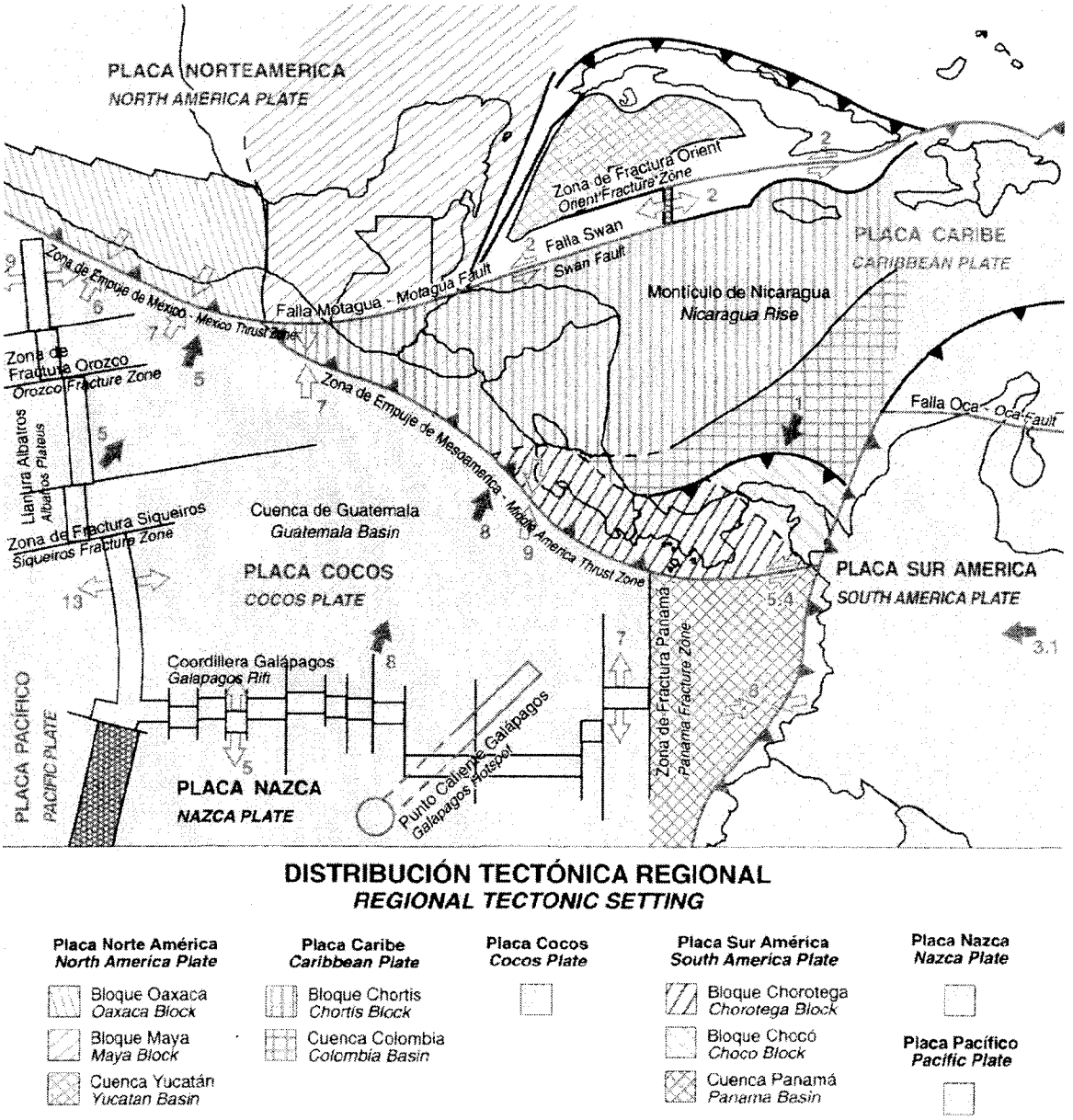

DISTRIBUCIÓN TECTÓNICA REGIONAL
REGIONAL TECTONIC SETTING

Placa Norte América *North America Plate*	Placa Caribe *Caribbean Plate*	Placa Cocos *Cocos Plate*	Placa Sur América *South America Plate*	Placa Nazca *Nazca Plate*
Bloque Oaxaca *Oaxaca Block*	Bloque Chortis *Chortis Block*		Bloque Chorotega *Chorotega Block*	
Bloque Maya *Maya Block*	Cuenca Colombia *Colombia Basin*		Bloque Chocó *Choco Block*	Placa Pacífico *Pacific Plate*
Cuenca Yucatán *Yucatan Basin*			Cuenca Panamá *Panama Basin*	

Figure 3.4 Tectonic setting of Central America (Baxter, S., 2001). The solid and open arrows in the figure indicate direction of relative plate and fault motion, respectively; and the labels of value indicate relative motion (cm/year).

Subduction zones are geologically complex and produce numerous earthquakes from multiple sources. The country is crossed from west to east by a chain of Quaternary volcanoes as a result of the subduction process. Earthquakes in this region can be divided into two types: shallow intraplate earthquakes and deep intraplate earthquakes. Shallow intraplate (crustal) earthquakes occur within the crust of the overriding Caribbean plate. They have been mostly produced by right-lateral faults running parallel to the volcanic range as a result of oblique convergence of the Cocos plate relative to the Caribbean plate. The February 13, 2001 (M6.5) earthquake was caused by this type of faulting. Deeper intraplate earthquakes occur within the shear zone of subducting Cocos plate. The January 13, 2001 earthquake (M7.6) is an example of this type of earthquake (JSCE, 2001).

3.3.2 Geology of Nueva San Salvador and Vicinity

The surface geology of Nueva San Salvador is dominated by the primary and reworked products of Upper Tertiary to Holocene volcanism. All rocks cropping out in the study area are volcanic and consist of intercalated primary and reworked Upper Tertiary to Holocene deposits. The stratigraphic sequence in the area consists, from oldest to youngest, of the Balsamo Formation (B1 –B3), Cuscatlan Formation (C1-C3), and San Salvador Formations (S1, S2, S3A-S3C, S4, S5A-S5C, and Qf) that are largely composed of pyroclastic deposits and associated volcaniclastics. Table 3.1 shows the stratigraphic sequence of Nueva San Salvador and its surrounding area (listed from top to bottom).

South of the older rocks, the Miocene to Pliocene Balsamo Formation (B1-B3) covers a large part of El Salvador. It is comprised of intermediate to basic volcanic rocks and reworked material from these rocks (i.e. volcanic epiclastic rocks).

The Balsamo Formation forms the coastal mountains of El Salvador. The belt of volcanoes of this formation has a maximum width of 90 km. In Plio-Pleistocene, local but widespread eruptions of acid extrusive rocks occurred in the central part of El Salvador.

Table 3.1 Stratigraphy of volcanic materials in the vicinity of Nueva San Salvador (listed from top to bottom)

Formation	Age	Stratigraphic Groups	
San Salvador	Pleisto-Holocene	Qf	Alluvium including artificially reworked material, up to 20 m
		S5	Basaltic extrusive rocks, volcanic ash and tuff deposit
		S4	White acidic pumice ash (Tierra Blanca) up to 50 m, produced when the Lake Ilopango depression formed
		S3	Brown pyroclastic and volcanic epiclastic deposits (Tobas Color Café) up to 25 m
		S2 S1	Andesitic and basaltic extrusive rocks, locally scoria, from La Laguna crater partly interbeded in S3
Cuscatlan	Plio-Pleistocene	C3	Acidic to intermediate-acidic extrusive rocks, partly of the same age as C2.
		C2 C1	Acidic pyroclastic and volcanic epiclastic rocks, up to 80 m. Locally ignimbritic and welded tuff deposit, up to 25 m
Balsamo	Mio-Pliocene	B3	Andesite basaltic extrusive rocks, up to 30 m
		B2 B1	Volcanic epiclastic and basic pyroclastic rocks with intercalation of andesitic lava flows (up to 10 m), up to 100 m
After Evans and Bent (2004), Weber (1978), and Schmidt-Thome (1975)			

The rocks of lower Cuscatlan Formation (C1, C2) were deposited in and around Ahuachapan, and the Lake Ilopango area. In the Balsamo Ridge, ignimbrite of the Cuscatlan Formation overlies rocks of Balsamo Formation.

The upper Cuscatlan Formation (C3, Pleistocene) and the acidic volcanism of the San Salvador Formation (S1-S5, Holocene) overlie the older formation to the north. The coastal mountains consist mostly of the Balsamo Formation (B_1 and B_2, Mio-Pliocene) to the south.

The San Salvador Formation is present mainly in the northern part of the study area. The formation starts, in general, with acidic, brown and yellowish, more or less consolidated, medium to fine-grained pyroclastic and epiclastic rocks (known as Tobas Color Café or TCC) with thickness up to 25 m. The stability of TCC depends mainly on the degree of consolidation. In the case of heavy rainfall, exposed TCC is rapidly eroded down to considerable depth and over large areas. The youngest part of the San Salvador

Formation, which is rather widely distributed, consists of white acidic pyroclastic and epiclastic rocks (known as Tierra Blanca or TB). They were produced by a center within the Lake Ilopango depression. The TB consists of light-grey to white, fine-grained dacitic pumice ash. The thickness varies from a few meters, or even a few centimeters up to 50 m. TB is relatively well-consolidated and is stable only in places where it is thick. However, in most of the area, TB is poorly consolidated and can be easily eroded (Schmidt-Thome, 1975)

Two sets of fault systems with strike directions of northwest-southeast and east-west cross each other in the study area. The individual faults probably were formed at different times but were repeatedly reactivated. Ring-like structures formed by volcanotectonic subsidence are also present in the study area around volcano craters. The geologic map of the study area (Nueva San Salvador) is shown in Figure 3.5. The lithologic units were converted into a GIS map layer, which is shown in Figure 3.6.

3.4 Historic Destructive Earthquakes

The area of San Salvador is situated in a zone of frequent and sometimes disastrous earthquakes. In general, about 20 earthquakes of medium intensity are perceivable annually (Schmidt-Thome, 1975). El Salvador was hit by at least 14 destructive earthquakes of intensity up to X (modified Mercalli intensity scale) between 1915 and 2001. The information on triggered landslides is available for the most recent events (the 2001 earthquakes). The main parameters for these earthquakes are summarized in Table 3.2.

3.5 Landslides in Nueva San Salvador Area

Major earthquakes with magnitudes greater than 5.4 have caused widespread landsliding in San Salvador and its vicinity. Table 3.3 shows the major events and landslide damages since 1982. The locations of earthquake-induced landslides during 1986 and 2001 are shown in Figure 3.2.

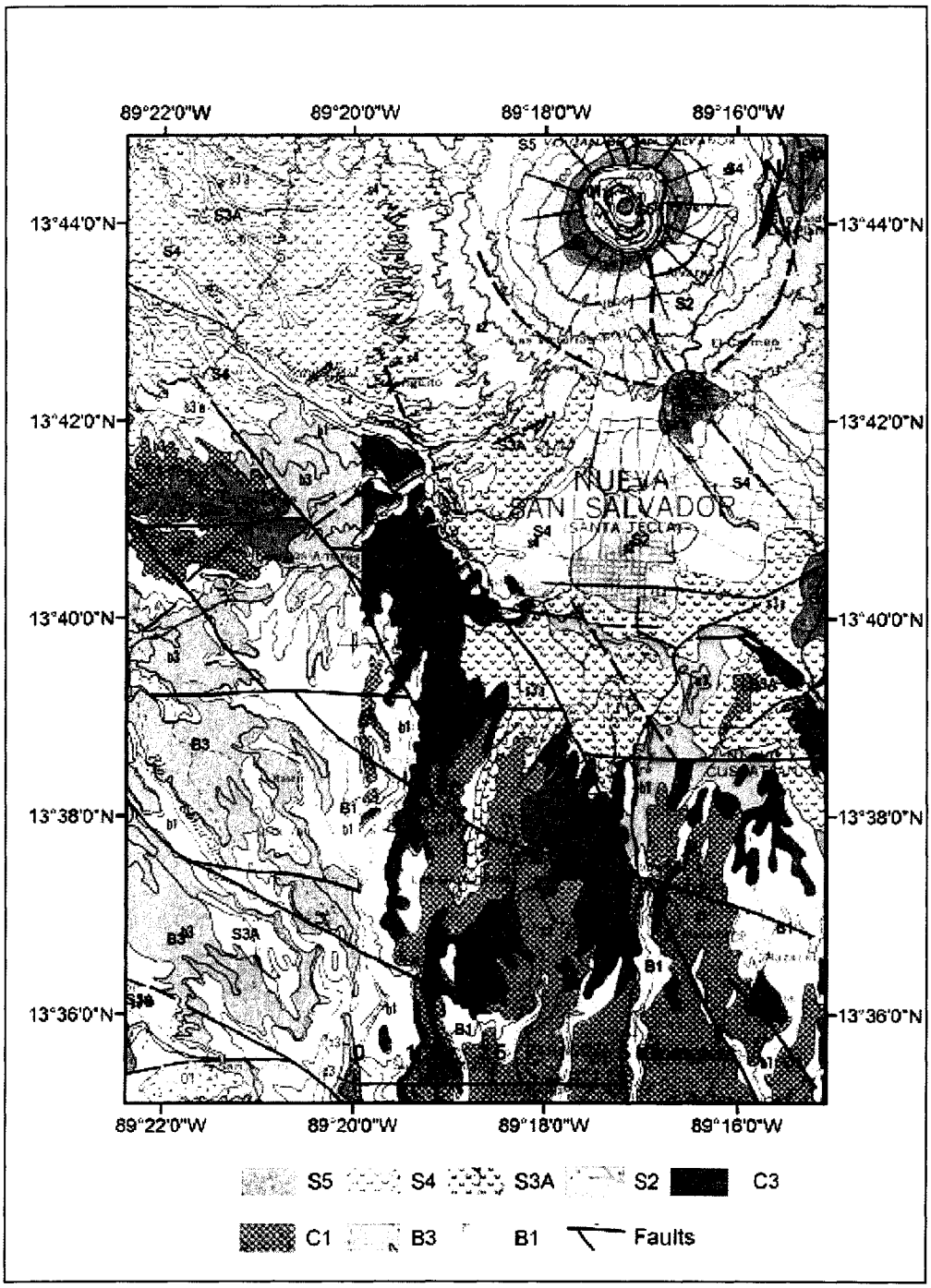

Figure 3.5 The geologic map of Nueva San Salvador (Scanned from 1:100,000 geology map of El Salvador). The legend of lithology is listed in Table 3.1.

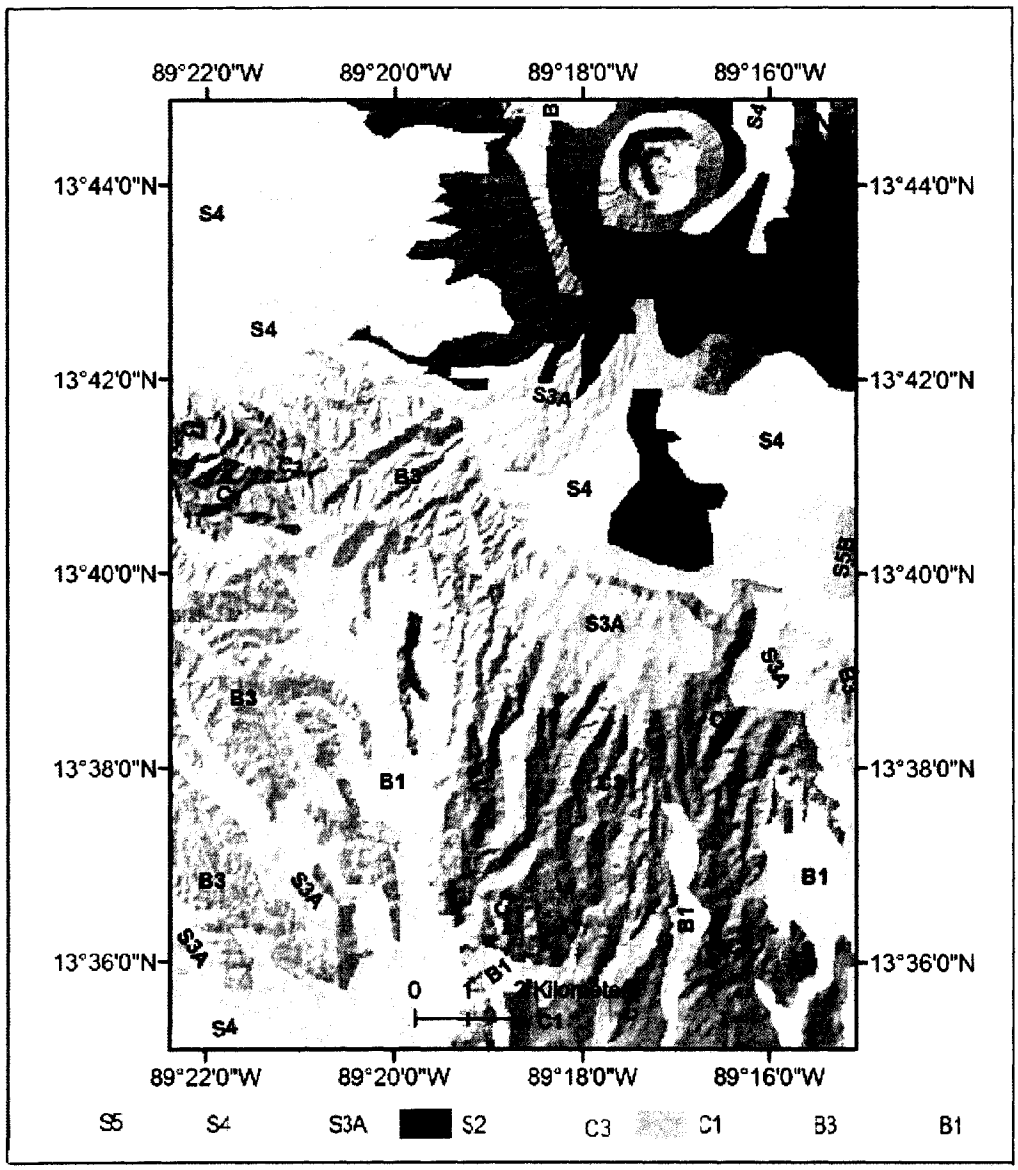

Figure 3.6 GIS map layers for lithology of Nueva San Salvador (digitized from 1:100,000 geology map of El Salvador)

Table 3.2 Source parameters of some of the destructive earthquakes in El Salvador in the past century (Benito et al., 2004)

Year/Month/Day /Hours/Minutes	Latitude (°)	Longitude (°)	M_s	Depth (km)	Intensity (MM)	Source
1915/09/07/01:20	13.90	-89.60	7.7	60	IX	Subduction
1917/06/08/00:51	13.83	-89.31	6.7	10	VIII	Local
1917/06/08/01:30	13.77	-89.50	5.4	10	VIII	Local
1919/04/28/06:45	13.69	-89.19	5.9	10	X	Local
1930/07/14/22:40	14.12	-90.25	6.9	30	VII	Local
1932/05/21/10:12	12.80	-88.00	7.1	150	VIII	Subduction
1936/12/20/02:45	13.72	-88.93	6.1	10	VIII	Local
1937/12/27/00:43	13.93	-89.78	5.9	10	VII-IX	Local
1951/05/06/23:03	13.52	-88.40	5.9	10	VIII	Local
1965/05/03/10:01	13.70	-89.17	6.3	15	VIII	Local
1982/06/19/06:21	13.30	-89.40	7.3	80	VII	Subduction
1986/10/10/17:49	13.67	-89.18	5.4	10	VIII-IX	Local
2001/01/13/17:33	13.05	-88.66	7.8	60	VIII	Subduction
2001/02/13/14:22	13.67	-88.94	6.5	10	VIII	Local

M_s: Surface wave magnitude scale.
Intensity (MM): Modified Mercalli Intensity Scale (I to XII).

Table 3.3 Major events and landslide damages in El Salvador since 1982

Date	Damages
September, 1982 Heavy rainfall	Triggered debris flow. Originated on the steep eastern flanks of San Salvador volcano. Struck the Montebello area on the northern side of San Salvador. Killed over 500 people.
October 10, 1986 San Salvador Earthquake (M5.4)	Landslides were largely confined to the Tierra Blanca deposits of San Salvador Formation. The main type of landslides was debris flow. Killed over 200 people.
January 13, 2001 Earthquake (M7.6)	Triggered thousands of landslides. The most devastating landslide occurred in the Las Colinas area of Nueva San Salvador. Killed over 900 people
February 13, 2001 Earthquake (M6.6)	Triggered thousands of landslides. Killed over 300 people.

The January 13, 2001 earthquake triggered widespread landslides in Cordillera Balsamo. The Balsamo Ridge defines the northern boundary of the Cordillera Balsamo. The major types of landslides triggered by the earthquake were relatively small (tens to

hundreds of cubic meters), shallow falls and slides (depth < 5 m) in surface rock and debris within young volcanic pyroclastic deposits (Jibson et al., 2004). However, it also triggered a few large, deep, and destructive landslides.

The field investigation of landslides had been carried out by National Services of Territorial Studies, El Salvador (SNET), U.S. Geological Survey (USGS), and other organizations. According to the landslide data provided by SNET, the occurrence of the landslides triggered by the January 13 and February 13, 2001 earthquakes was correlated with lithology and terrain parameters including lithological unit, slope angle, slope aspect, land use, and water drainage.

The geologic units most affected by landslides include the Balsamo Formation, and the younger pyroclastic units that overlie the Balsamo Formation. Among these overlying materials, the San Salvador Formation, especially S4 (TB), is particularly prone to slope failure. The Cordillera Balsamo region at the south of Nueva San Salvador city was most affected by the January 13, 2001 earthquake. The most damaging landslide was the Las Colinas landslide, which buried a middle-class Las Colinas neighborhood in Nueva San Salvador. The landslide, which was off the steep northern flank of the Balsamo Ridge, originated at an elevation of about 1,040 to 1,070 m and traveled northward for a distance of about 800 m. The vertical drop from the ridge to the neighborhood was about 160 m. The volume of the landslide material was about 250,000 m^3 (Jibson and Crone, 2001). Figure 3.7 is an IKONOS satellite image (March 16, 2001) showing the Balsamo Ridge and Las Colinas areas. The large scale landslides such as the Las Colinas landslide can be directly identified from the image. Figure 3.8 shows some slope failures along the Pan-American Highway on the west of Nueva San Salvador. Figure 3.9 shows slope failures along the Balsamo Ridge investigated by a team from the Japan Society of Civil Engineers. Figure 3.10 is an oblique aerial view of the Las Colinas landslide that buried the southern portion of the community. Figure 3.11 shows a cross-section of the Las Colinas landslide. In 2003, the slide mass of the Las Colinas landslide was moved and the unstable area was mitigated. Figure 3.12 shows a typical profile of volcanic deposit at the site of the Las Colinas landslide.

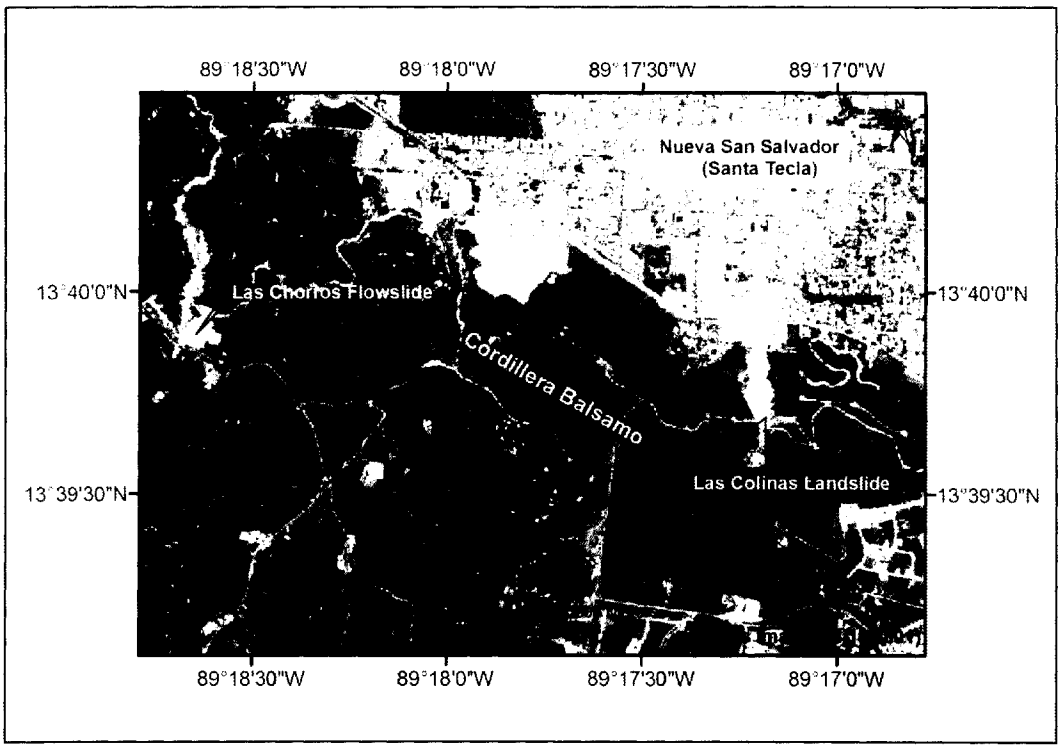

Figure 3.7 The Las Colinas landslide and the Las Chorios flowslide in the Balsamo Ridge area (IKONOS satellite image, March 16, 2001)

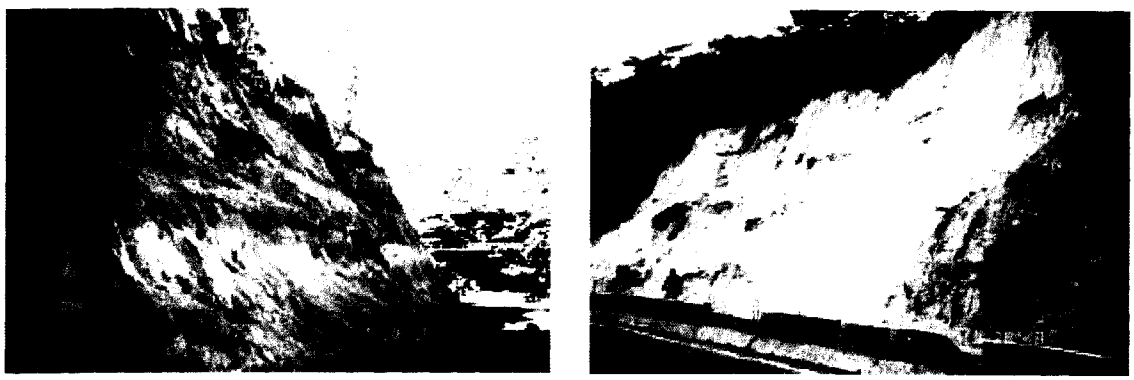

Figure 3.8 The slope failures along the Pan-American Highway (JSCE, 2001)

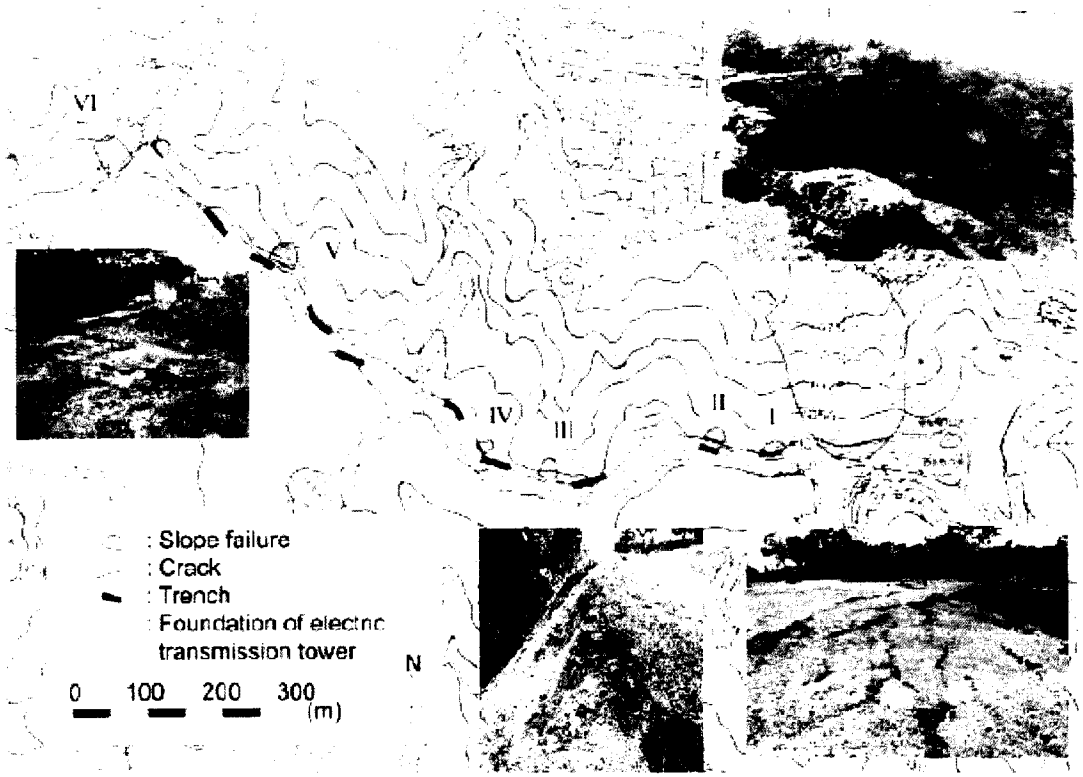

Figure 3.9 Slope failures along the Balsamo Ridge (after JSCE, 2001, Jibson and Crone, 2001 topographical map: Ministerio de Obras Públicas, 1970)

Figure 3.10 Oblique aerial views of the Las Colinas landslide (slope towards north) that buried a middle class neighborhood of Nueva San Salvador (Photograph by Edwin L. Harp, U.S. Geological Survey, 2001)

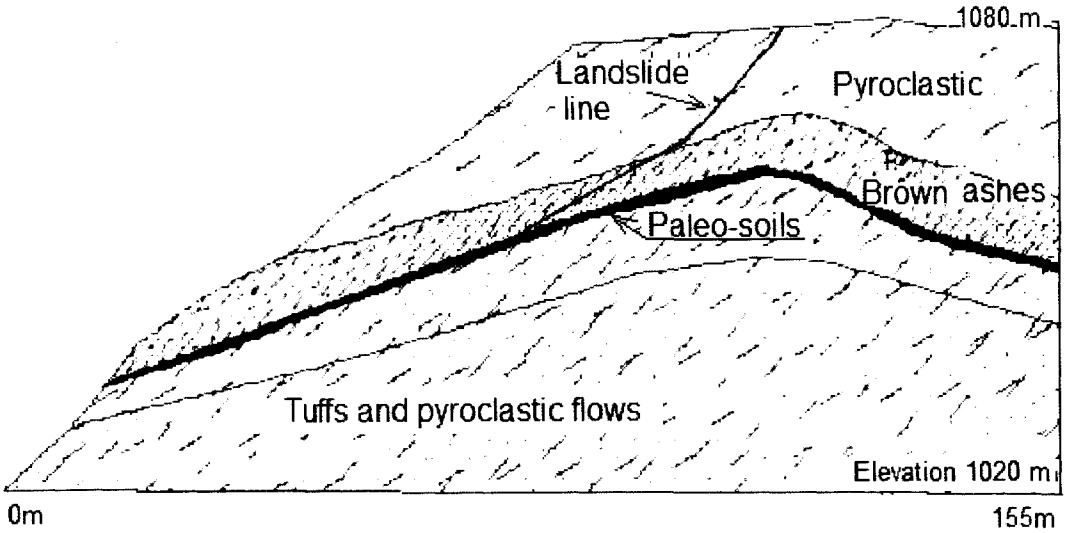

Figure 3.11 Cross-section of the Las Colinas landslide showing four generalized geological strata (after Lotti C. & Association, 2001).

Figure 3.12 A photograph showing the soil profile where excavation for slope mitigation at the top of the Las Colinas landslide was conducted (photograph by S. L. Huang, 2003)

Chapter 4 Causative Factor Analysis and GIS Data Processing

4.1 Introduction

The factors that affect slope stability are numerous and the occurrence of landslides in general is a function of the interaction of natural phenomena such as unfavorable geological conditions. The main complex contributing factors are geological materials, geomorphologic features, groundwater, hydrologic conditions, land use, rainfall, earthquakes, and human activities. Generally, these factors can be categorized into three major classes: (1) geology, (2) geomorphology, and (3) external triggering factors. A landside can be trigged by an earthquake or by other natural causes such as heavy rainfall, volcanic eruptions, or river erosion. The three classes and their subdivisions are listed in Table 4.1. Detailed descriptions of these factors can be found in the literature (Varnes, 1984, Khazai, 2004). In this chapter, geology, geomorphology, earthquakes, and vegetation of the study area are discussed. The GIS source data were processed for landslide hazard zonation. The ground motion, which is the major external triggering factor for an earthquake-induced landslide, will be discussed in Chapter 5.

4.2 Geology

4.2.1 Lithology

The geological units in an area may be grouped by lithology. Lithologic features such as material composition and structure influence mechanical behaviors of rock and soil. The type of slope failure is also related to the material types. Tables 2.1 and 2.2 (see Chapter 2) show the material types for different types of slope movement. In the study area, the young pyroclastic Tierra Blanca deposits occur within the upper part of the San Salvador Formation and blanket the surface of the area. These deposits were produced by

a crater within Lake Ilopango (which occupies Ilopango Caldera) and reach up to 50m in thickness.

Table 4.1 The factors controlling slope stability and landslides

Factor Classification	Factor	Subdivision	Description
Geology (Slope material)	Lithology	Lithologic unit	Control slope stability and failure mode
		Geotechnical parameters	
	Structure	Geological discontinuities	Control failure mode
	Hydrogeology	Groundwater	Change shear strength
		Drainage network	
Geomorphology (Slope geometry)	Slope Geometry	Slope angle	Affect slope stability as the boundary condition of slope
		Slope height	
		Profile shape	
	Slope Direction	Aspect	Influence soil moisture and seismic force
External Triggering Factors	Earthquake	Earthquake magnitude	Change stress condition, decrease shear strength and increase pore water pressure
		Ground motion	
		Earthquake duration	
	Climate	Rainfall	Change groundwater table, strength and pore pressure
		Rain duration	
	Weathering	Weathering depth	Change strength
	Land Use	Agriculture	Change slope geometry and/or vegetation
		Engineering activity	
Other factors	Vegetation	Vegetation type	Change slope material property
		Vegetation index	

In the past 75,000 years, Ilopango Caldera has been the source of four exceptionally large and violent explosive Tierra Blanca eruptions that produced widespread tephra layers and ignimbrites (Rolo et al., 2004). There are at least four Tierra Blanca (TB) pyroclastic sequences, each separated from the others by a brown to reddish-brown paleo-soil several meters thick. These sequences are informally called TB4, TB3, TB2 and TBJ (Tierra Blanca Joven), from oldest to youngest.

The geotechnical properties of Tierra Blanca have been investigated by several researchers and consulting companies (e.g. Bommer et al., 1998, 2002, Lotti C. &

Association, 2001, Rolo et al., 2004). The main engineering problem caused by the Tierra Blanca deposits is their susceptibility to landslides during heavy rainfall and earthquake ground shaking (Rolo et al., 2004). Tierra Blanca material has also been observed to be susceptible to liquefaction, but this hazard is limited because of the deep groundwater table in most of the area. Some liquefaction-related damage was observed on the shores of Lake Ilopango (Bommer et al., 2002).

According to the particle size distribution, Tierra Blanca can be classified as sandy silt or silty sand. The index properties of Tierra Blanca are summarized in Table 4.2 (after Rolo et al., 2004). The samples of the first three rows in Table 4.2 were extracted from a depth of 1.5~2.0 m under an undisturbed condition with natural moisture content during the later part of the dry season in El Salvador (October to April). The soil typically has a moisture content that varies from 7.5 to 29.5% and with a degree of saturation from 21.8 to 82.5%. The specific gravity, Gs, usually varies between 2.25 to 2.5, with moist unit weight, γ, ranging from 11 to 15 kN/m^3.

Table 4.2 Index properties of Tierra Blanca (After Rolo et al., 2004)

References	Moisture Content	Specific Gravity	Porosity	Degree of Saturation	Unit Weight
	W (%)	G_s	n (%)	S_r(%)	γ (kN/m^3)
Berdousis , 2001	7.95	2.44	46.1	22.63	13.91
Mavrommati , 2000	9.92	2.50	51.7	23.44	13.02
Rolo, 1998	7.63	-	49.2	21.80	13.70
Amaya Dubon and Hayem Breve, 2000	20.88	2.26	44.0	59.81	14.98
	29.48	2.29	53.0	60.11	13.70
Guzman Urbina and Melara, 1996, Min. and Max. value	16.70	2.43	47.5	43.0	10.80
	28.10	2.50	62.3	82.5	12.9

The shear strength of Tierra Blanca was determined from direct shear and triaxial compression tests conducted by several authors (Lotti C. & Association, 2001, Rolo et al., 2004). Table 4.3 shows shear strength of undisturbed and remolded samples at natural moisture content. In Table 4.3, the soil friction angle of undisturbed samples varies from

30 to 39°, corresponding to soil cohesion of 1.2 to 30 kPa. The geotechnical parameters of pyroclastic deposits at Balsamo Ridge are listed in Table 4.4. In the Las Colinas landslide area, the range of tested cohesion is between 5 and 80 kPa for the samples of paleo-soils.

Table 4.3 Strength parameters of Tierra Blanca by direct shearing test (after Rolo et al., 2004)

Reference	Friction Angle	Cohesion	Condition/Sample Location
	ϕ, °	c, kPa	
Mavrommati, 2000 Berdousis, 2001	39	30	Undisturbed, natural moisture
	34	0	Undisturbed, saturated
	36	10	Remold, natural moisture
	35	0	Remold, saturated
Amaya Dubon, Hayem Breve, 2000	35	6	Undisturbed, natural moisture/ San Antonio
	30	1.2	Undisturbed, natural moisture/ Cumbres de Cuscatlan,
Bernal Riosalido, 2002	34	70~90	Undisturbed, natural moisture

Table 4.4 Soil properties of Balsamo Ridge at Las Colinas landslide (by Lotti C. & Association, 2001, and Loria, 2003)

Strata		Average Thickness	SPT	Density	Shear Wave Velocity	Dry Unit Weight	Friction Angle
		m	N	kg/m^3	Vs,m/s	kN/m^3	ϕ, °
1	Pyroclasts	15~25	10~40	1500	90~145	11	30~35
2	Brown ashes	20~80	10~40	1530	390~750	11	30~33
3	Paleo~soils	1.5	8~10	1760	390~750	11	20~24
4	Pyroclasts	N/A	Refusal	1900	660~1100	18	35~38

Table 4.4 (Continued)

Strata		Cohesion	Young's Modulus	Poisson's Ratio	Shear Modulus	Max. Shear Modulus
		c, kPa	E, kPa	ν	G, kPa	G_{max}, kPa
1	Pyroclasts	60~80	6.0×10^4	0.43	2.0×10^4	$1.2\times10^4 \sim 3.2\times10^4$
2	Brown ashes	30~40	3.6×10^5	0.33	1.5×10^5	$2.3\times10^5 \sim 8.6\times10^5$
3	Paleo~soils	5~10	3.6×10^5	0.33	1.5×10^5	$2.7\times10^5 \sim 9.9\times10^5$
4	Pyroclasts	200	3.8×10^6	0.26	1.7×10^6	$8.3\times10^5 \sim 2.3\times10^6$

The shear strength is particularly influenced by the negative pore water pressures and the presence of weak cementation. Negative pore-water pressure increases the effective stress and makes a positive contribution to the shear strength. The cementation provides an additional strength and stiffness to the soil mass. However, the weak cementation of volcanic soil is easily broken when the soil is subjected to a small strain. Both factors play an important role in the stability of slopes and these types of deposits show a tendency to fail during heavy rainfall and seismic activity (Rolo et al., 2004).

4.2.2 Geotechnical Parameters

Laboratory test data and field engineering measurements are limited for this study area. Most of the historic landslides occurred in TB4 units (Tierra Blanca). The friction angles are in the range of 30~39° and cohesions are in the range of 30~90kPa. Because laboratory and field measurements are lacking, it is difficult to determine the geotechnical parameters of other lithologic units. However, it is probably true that the other units should have higher shear strengths than the TB4 unit (i.e., the Cuscaltan and Balsamo formation would have higher friction angle and cohesion). All of the soils or rocks near the ground surface have been weathered and their strengths decrease under the influence of weathering and groundwater. The strength parameters of these near-surface materials should be much lower than those of the unweathered bedrock. For the GIS-based slope stability analysis, the average value and range of the geotechnical parameters assigned to each lithologic unit based on the above analogy are shown in Table 4.5.

4.2.3 Groundwater

Besides soil strength parameters, groundwater also plays a vital role in stability of slopes, especially for slopes consisting of loosened volcanic soil. The effects of groundwater on slope stability include increasing pore water pressure and decreasing shear strength of soil. Both effects are clearly causative factors of slope failure. The direct

influence of pore water pressure on slope stability is illustrated in Figure 4.1. The estimation of the effect of groundwater condition on slope stability analysis usually includes evaluation of the depth of the groundwater table or the soil saturation ratio. In order to illustrate the influence of groundwater conditions on the factor of safety, factors of safety were calculated by using the FLAC/Slope 5.0 program at the condition of homogenous soil, slope angle=50°, $\phi = 36°$, and c=35 kPa. Figure 4.1 shows the relationship between the factor of safety and the soil saturation ratio (in here, saturation ratio is H_w/H, see Figure 4.1) for a slope. Both slopes (H=15 m and 30 m) failed at full saturation ($H_w/H=1$). In dry soil conditions, slopes were stable with factors of safety over 1.5.

Table 4.5 Geotechnical parameters of lithologic units

Formation	Units	Friction, ϕ (°)		Cohesion, c (kPa)		Dry Unit Weight, γ (kN/m^3)	
		Average	Range	Average	Range	Average	Range
San Salvador	S5	39	35~43	75	60~90	15	13~17
	S4	35	32~38	35	20~50	12	11~13
	S3	36	33~39	50	40~60	13	11~15
	S2	38	35~41	65	50~80	13	12~14
Cuscatlan	C3	39	35~43	80	60~100	15	13~17
	C1	40	36~44	85	65~105	15	13~17
Balsamo	B3	41	36~46	110	90~130	17	15~19
	B1	42	37~47	120	90~150	17	15~19

The direct evaluation of groundwater conditions in the study area was not carried out due to lacking of drill-hole data. However, groundwater was involved in some slope failures (for example, debris flows). For simplification, the analysis often assumes completely dry or fully saturated condition. A drained slope could be a valid assumption for the earthquake-induced slope stability analysis, such as those for the 2001 El Salvador earthquakes, because they occurred during a long dry season. Otherwise, groundwater distribution should be determined according to field investigation of the hydrogeological conditions in a study area.

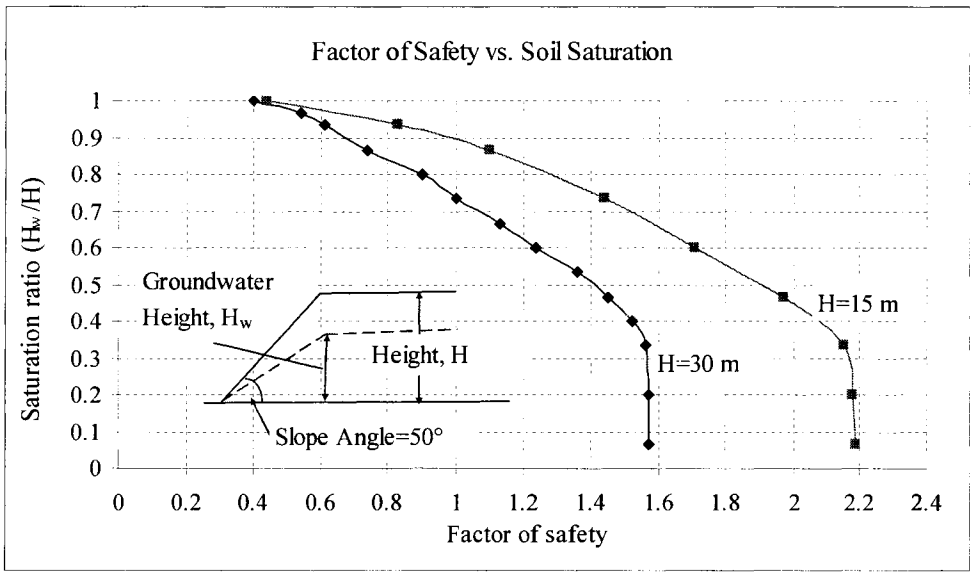

Figure 4.1 Factor of safety vs. soil saturation ratio (H_w/H) under homogenous soil condition (slope angle=50°, ϕ=36°, c=35 kPa). The factor of safety drops rapidly after the saturation ratio is greater than 0.3. Both slopes (H=15 and 30m) will fail under a fully saturated condition (H_w/H=1).

4.3 Geomorphology

4.3.1 Slope Angle and Height

Slope angle is one of the most important causative factors affecting slope stability. Estimating the critical slope angle is one of the goals of conventional slope stability analysis. The characteristics of earthquake-induced landslides have shown strong relationships among slope inclination, failure mode, and mechanism. Rock falls and rock slides generally occur on steep slopes, usually greater than 35° (Keefer, 1984). In landslide hazard assessment, a statistical relationship between slope angle and historic landslide occurrence can be used to evaluate potential landslide activity.

In the study area, in dry conditions volcanic soil such as Tierra Blanca (TB) is able to stand in deep, near-vertical slopes. A numerical analysis of slope stability for a simple slope was performed using FLAC/Slope 5.0 (Itasca, 2005). Figure 4.2 shows the relationship between the factor of safety and slope angle for homogenous volcanic soil

under a static and dry soil condition ($\phi = 36°$, c=35 kPa). Under these conditions, slopes can withstand heights up to 15m with a nearly vertical slope but the factor of safety decreases steeply with increasing slope angles.

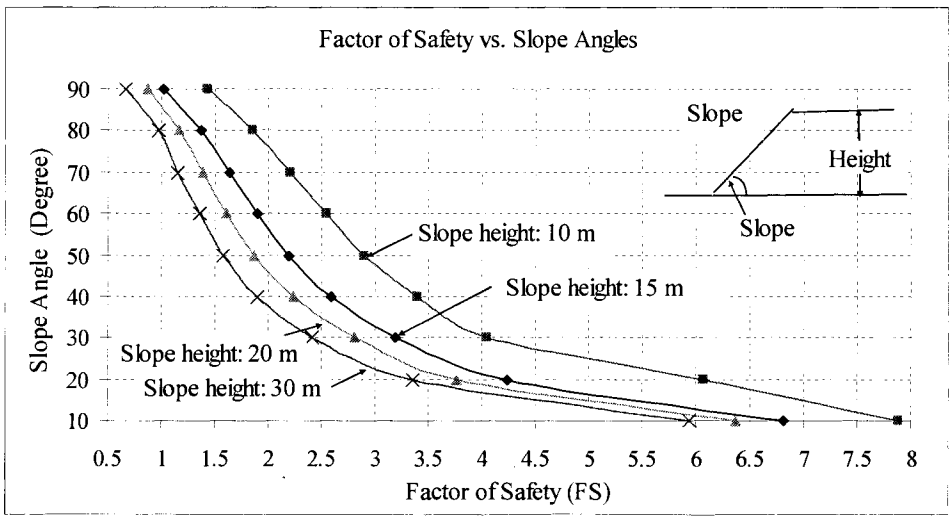

Figure 4.2 Relationship between factor of safety and slope angle under a static and dry soil conditions for homogenous volcanic soil ($\phi = 36°$, c=35 kPa).

In El Salvador, according to the statistics of historic landslides during the 1986 and 2001 earthquakes, the records of 139 landslides indicate an increase in failure frequency as the slope angle approached 30~50°. Beyond that, a sharp decrease follows. However, landslide frequency increases again when the slope angle is greater than 80° (Figure 4.3a). Many steep road cuts likely contributed to sliding of steep slopes during these earthquakes.

The engineering activity of road cutting strongly influences slope stability. In El Salvador, around 20% of the triggered landslides occurred in steep slopes with slope angles greater than 70°, and most of them were initiated by road cuts along highways. High population density resulting from residential development close to such steep, unprotected slopes in the San Salvador area has compounded the problem (Bommer et al., 1998).

4.3.2 Slope Aspect

Slope aspect (i.e. dip direction of slope surface) and curvature may also influence slope stability. Soil moisture, vegetation, and the orientation of geological structures may be reflected by slope aspect, which in turn may influence soil strength and susceptibility to landslides. Figure 4.3b shows the correlation between landslide frequency and slope aspect in volcanic material during the 2001 earthquakes. The NE (45°~90°) direction shows the highest landslide frequency.

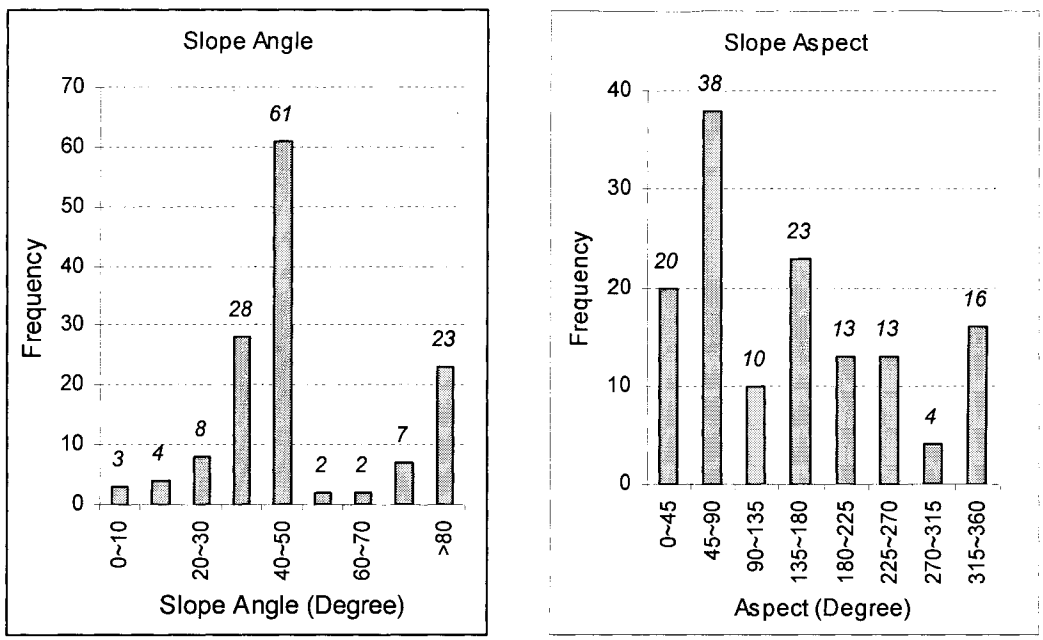

(a) Slope angle (b) Slope aspect

Figure 4.3 Histogram of landslide frequency (number of landslides) vs. slope angle and slope aspect. In the El Salvador area, landslide frequency increased as the slope angle approached 30~50°.

4.3.3 Depth and Dimension of Slope Failure

The slope failures triggered by the 2001 earthquakes was relatively shallow. The histogram of 137 landslides' frequency vs. corresponding failure depth shows that the

failure depth for 56% of the landslides was 2 to 4m, and a further 20% of landslides had 4~6 m failure depths (Figure 4.4a). Around 10% of landslides had failure depths over 20 m. The Las Colinas landslide, which had a failure depth of 35 m, was one of the deepest, most massive slides and had devastating consequences.

Figure 4.4b shows the dimensions (length of slides in source area) of seismic-induced landslides. According to the statistics of 44 landslides with size measurements, 52% of landslides were less than 50 m in length. Few landslides had dimensions greater than 500 m, which might have included the runoff distance of debris flow. The Las Chorros flowslide traveled 1300 m downslope, and Las Colinas landslide had a runoff distance of 700~800 m.

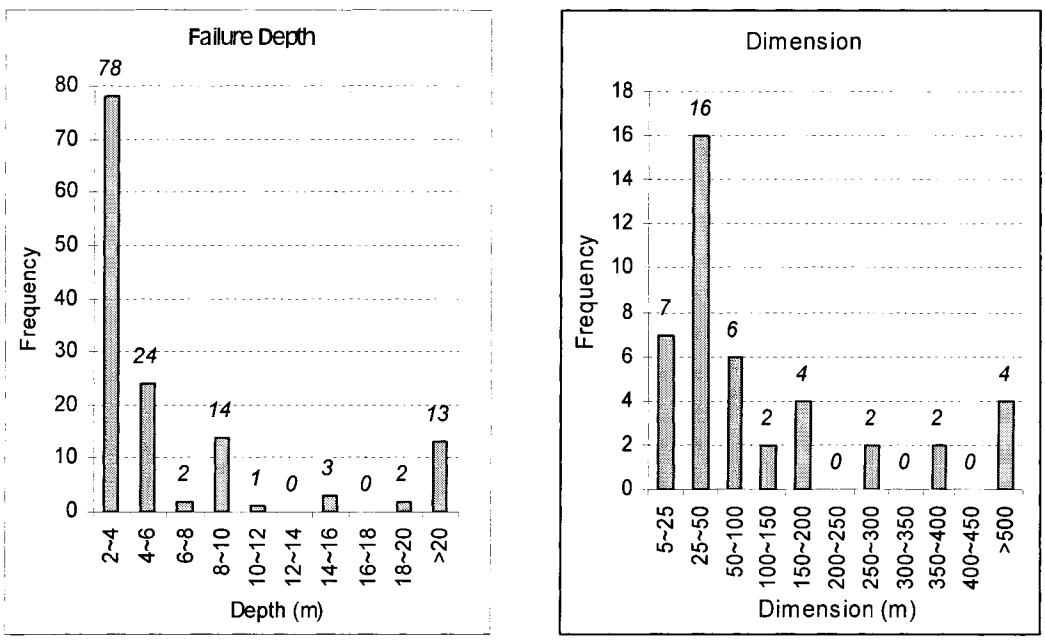

(a) Depth (b) Dimension

Figure 4.4 Histogram of landslide frequency (number of landslides) vs. failure depth and the dimension of sliding mass (137 landslides in statistic of failure depth and 43 in failure dimension). The failure depth for 56% of the landslides was within 4 m, and 20% of landslides had 4~6m failure depths. Slightly over half (52%) of landslides are less than 50 m in length.

4.4 Earthquakes

Slopes frequently become unstable during earthquakes or heavy rainfall. A sensitivity analysis was carried out for volcanic soil under dry conditions and different horizontal accelerations using the Bishop Circular Surface method and the RSS slope stability program (U.S Department of Transportation, 1996). Figure 4.5 shows the curves of factor of safety vs. horizontal acceleration and slope height under dry soil conditions (slope angle=50°, $\phi = 36°$, c=35 kPa). At same slope angle, the factor of safety drops sharply with the increase of horizontal acceleration and slope height. As the slope height increases from 15 m to 80 m, the critical horizontal acceleration decreases from 0.6 g to 0.08 g. The influence of ground motion on slope stability will be discussed in detail in Chapter 5.

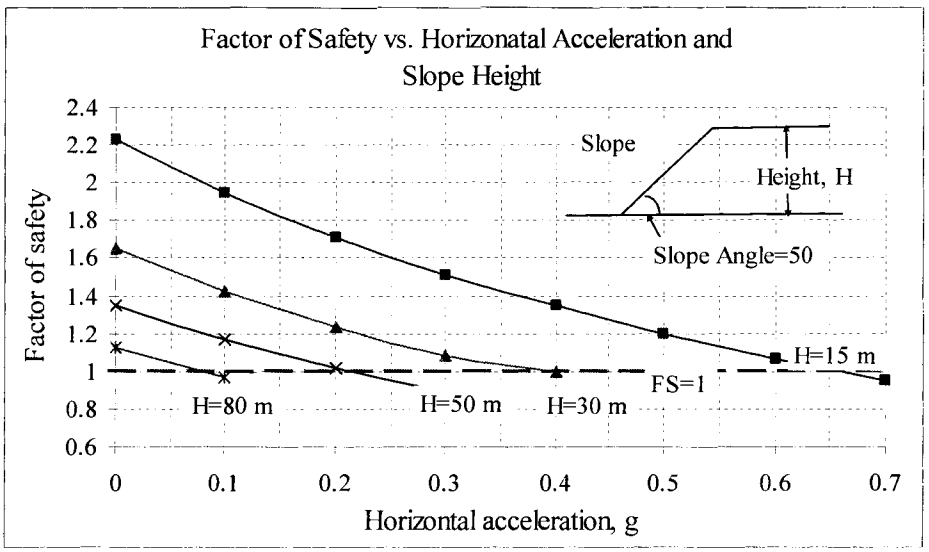

Figure 4.5 The factors of safety vs. horizontal acceleration and slope height at a dry soil condition (slope angle=50°, $\phi = 36°$, c=35 kPa). At the same slope angle, the factors of safety drop sharply with an increase in horizontal acceleration and slope height.

4.5 Vegetation

4.5.1 Root Strength

Some research shows that vegetation cover can improve the stability of slopes because root systems provide additional shear strength to the soil mass (Gray and Leiser, 1982, Greenway, 1987).

Vegetation influences slope stability in two ways: through hydrological effects and through mechanical effects (Chok et al., 2004). Hydrological effects involve removal of soil water by evapotranspiration through vegetation, which leads to an increase in soil suction or a reduction in porewater pressure, and hence an increase in the effective shear strength of the soil. The shear strength of the soil is also increased through the mechanical effects of the plant root matrix system which provides a laterally reinforcing surface layer that acts as a membrane to hold the underlying soil in place (O'Loughlin and Ziemer, 1982) and by anchoring an unstable soil mantle to stable subsoils or rocks where the roots penetrate a potential failure surface. The density of the roots within a soil mass and the roots' tensile strength contribute to the ability of the soil to resist shear stress. The effects of soil suction and root reinforcement have been quantified as an increase in apparent soil cohesion.

In the slope stability analysis (infinite slope and block sliding models), the two parameters, root strength and tree surcharge, can be considered. Root strength is expressed as root cohesion and tree surcharge as the tree weight per unit area. Tables 4.6 and 4.7 list the root strength and surcharge values cited in literature.

4.5.2 Vegetation Index

In the study area, the density of the vegetation cover can be determined through digital processing of remote sensing images. Identification of vegetation is based on differences in spectral characteristics between vegetation and soil. These differences are

particularly distinct in the red (around 0.675 μm) and near-infrared (0.8 to 1.0 μm) channels. Many researchers have developed various 'vegetation indices' based on certain combinations of the intensities of these channels. These indices are used to identify and monitor the temporal variation of vegetation cover.

Table 4.6 The root strength value cited in the literature

Soil Type	Vegetation Type	Root Strength, kPa	Investigators
Nursery loam	Sugi	1.8~5.7	Tsukamto and Minematsu, 1987
SM (ϕ'=30°)	Hemlock	5.6~12.6	Wu, 1984
	Sitka Spruce	3.7~7.0	
	Yellow cedar	5.4	
SM (ϕ'=35~37°)	Mixed Sitka Spruce & hemlock	4.2~5.5	Wu et al., 1979
Tyee S. S. (SM)	Coastal Oregon Douglas-fir	11.5~22.7	Burroughs and Thomas, 1977
	Douglas-fir	4.2~14.0	

Table 4.7 Tree surcharge values reported in the literature

Tree Species	Tree Surcharge, kPa	Investigators
Unspecified, 30~80m high	0.48~1.91	Greenway, 1987
Sitka spruce, Alaska	2.51 (average)	Sidle, 1984
Sitka spruce, 30~60m high	2.39	Wu et al., 1979

The most commonly used index is the Normalized Difference Vegetation Index (*NDVI*). It is defined by the following general equation:

$$NDVI = \frac{NIR - R}{NIR + R} \qquad (4.1)$$

Where: *NIR* is the reflection in the near infrared band; *R* is the reflection in the red band. For Landsat TM and IKONOS satellite images, band 3 is for red, and band 4 is for *NIR*.

In general, vegetation yields high positive *NDVI* values. Clouds, water, and snow yield negative values due to larger red reflectance than *NIR*. The *NDVI* value for rock and bare soil areas are near zero due to their similar reflectance in both bands. Therefore, in an *NDVI* image the lighter tone areas are associated with dense coverage with healthy vegetation. Figure 4.6 shows the classification of vegetation in the Nueva San Salvador area into 4 classes: heavy vegetation, moderate vegetation, scattered trees, and grass and bare land.

4.6 GIS Data Preparation and Processing

All of the data sets which were needed to conduct a detailed seismic-induced landslide hazard zonation were digitized and rasterized at a 30m grid spacing for the entire regional analysis and at a 10 m grid spacing for site-specified analysis (2D and 3D analysis) in the ArcGIS platform. Figure 4.7 shows the data layers used in seismic-induced slope stability analysis in the study area. The GIS source data obtained from the study area for seismic-induced landslide hazard zonation are as follows:

(1) 1:25,000 topographic maps and digitized vector topographic data with a 10m contour interval in the study area (Nueva San Salvador HOJA-2357III-SE, Zaragoza HOJA-2356IV-NE). This map can be transformed into a digital elevation model (DEM) or ESRI grid, which is elevation expressed as a 3D digital surface;

(2) Geological map of El Salvador at 1:100,000 scale, which is used to define the lithology;

(3) Digital strong ground motion records from the 2001 El Salvador earthquakes and the published seismic hazard map;

(4) Historic landslides occurrence during 1986 and 2001 earthquakes in El Salvador;

(5) Landsat TM images with 30 m resolution and IKONOS images with 4 m resolution; and

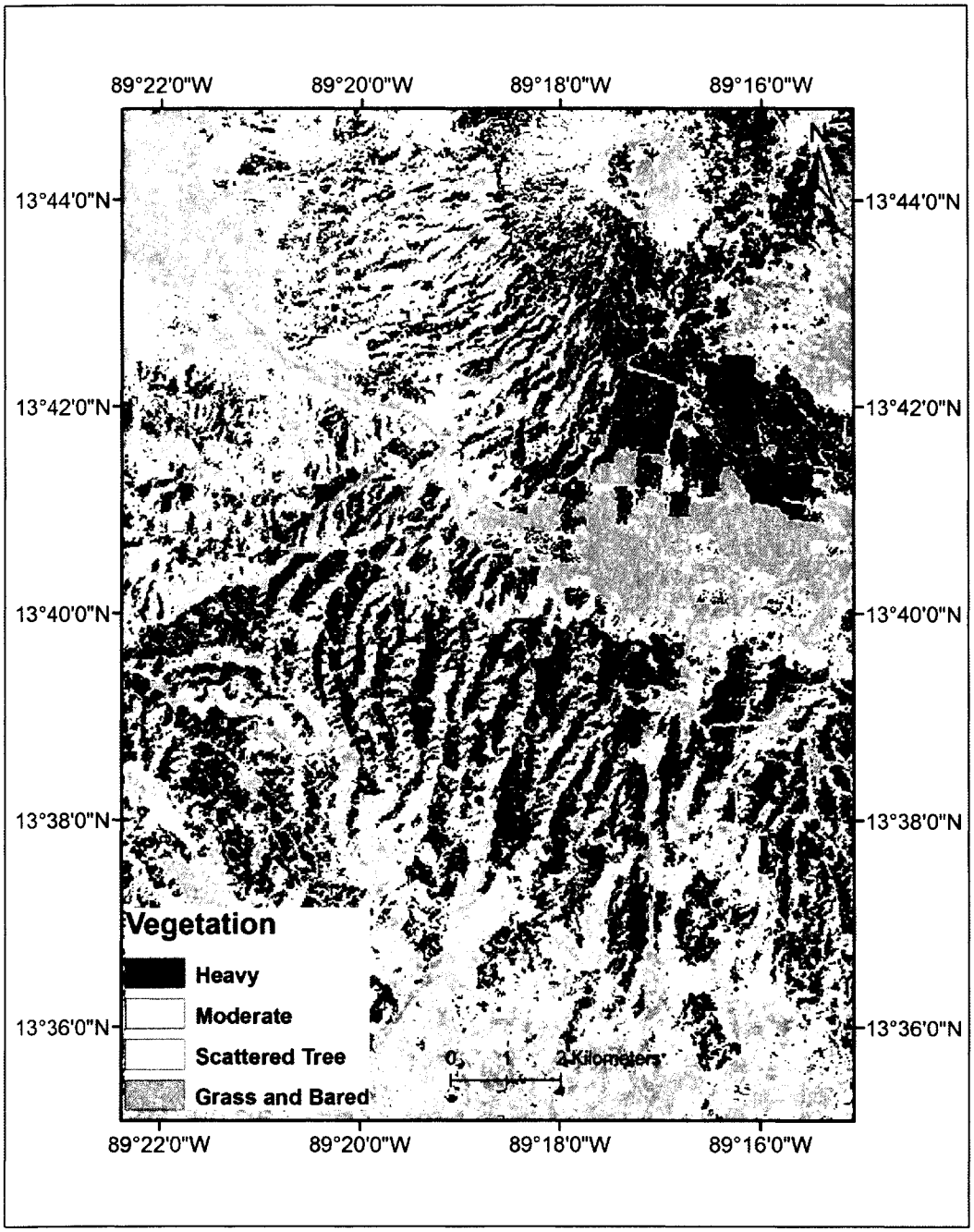

Figure 4.6 The vegetation classification in the study area using vegetation index. The vegetation was classified into 4 groups: heavy, moderate vegetation area, scattered trees, and grass and bared land.

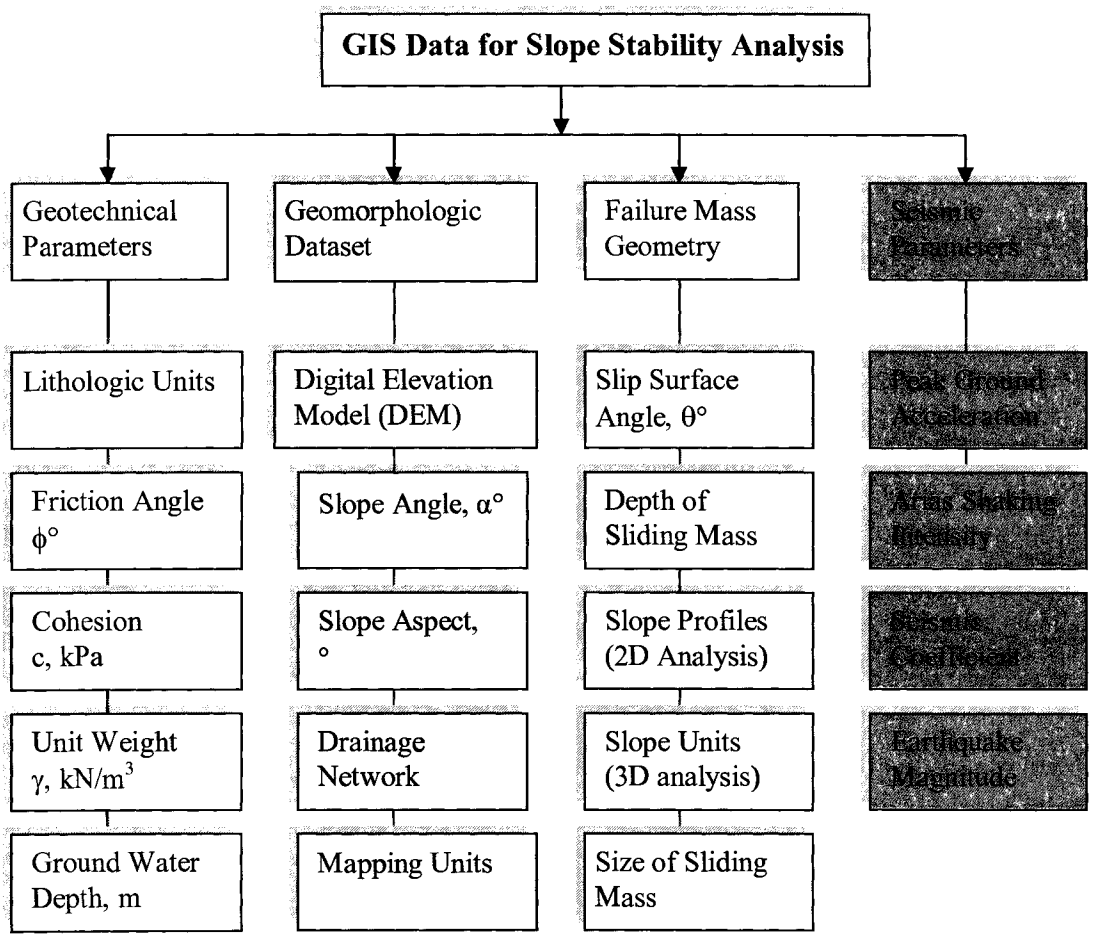

Figure 4.7 GIS datasets for seismic-induced slope stability analysis in the study area

(6) Research papers and reports of investigations of the 2001 earthquakes by USGS, the Japan Society of Civil Engineers, and Lotti C. & Association, and literature related to seismic hazard study and volcanic soil in El Salvador.

The GIS data preparation for the above mentioned factors can be described as follows.

(1) Surface Model Creation

An ArcGIS TIN (Triangulated Irregular Network) was created using a 1:25,000 vector digital topographic map. It was then converted into a digital elevation model (DEM or Grid). The ArcGIS Spatial Analyst was used to do the terrain surface analysis.

Figure 4.8 shows the hillshade map of the study area with stream networks. Figures 4.9 and 4.10 show the slope angle and slope aspect of the study area.

(2) Geotechnical Parameters

Geotechnical parameters have been collected on a site-specific basis. The values of strength properties vary spatially throughout the terrain. Distribution of geomaterials is shown as lithologic layers based on the geological map (polygon shapefile). The geotechnical strength parameters were assigned according to Table 4.5. The polygon file (including attributes of friction angle, cohesion, unit weight of soil materials) was converted into friction, cohesion and unit weight grid files. The friction angle of surface lithology in the study area is shown in Figure 4.11. The soil cohesion and unit weights on the surface soil map were produced the same way as the friction angle.

(3) Depth of the Potential Sliding Surface

The depth of the potential sliding surface also varies spatially throughout the area. With information from the historic landslide database, the depth at unsampled points was done in ArcGIS through interpolation using the Kriging method. The prediction map of soil depths was converted into grid map layers. The predicted map of the depth of the potential sliding mass is shown in Figure 4.12.

(4) Groundwater Condition

Due to the lack of data for the groundwater table distribution, the model considered three scenarios: a dry condition, 5~7 m depth of the groundwater table, and a fully saturated condition during the factor of safety analysis. For the fully saturated condition, it was assumed that the groundwater table coincided with the ground surface.

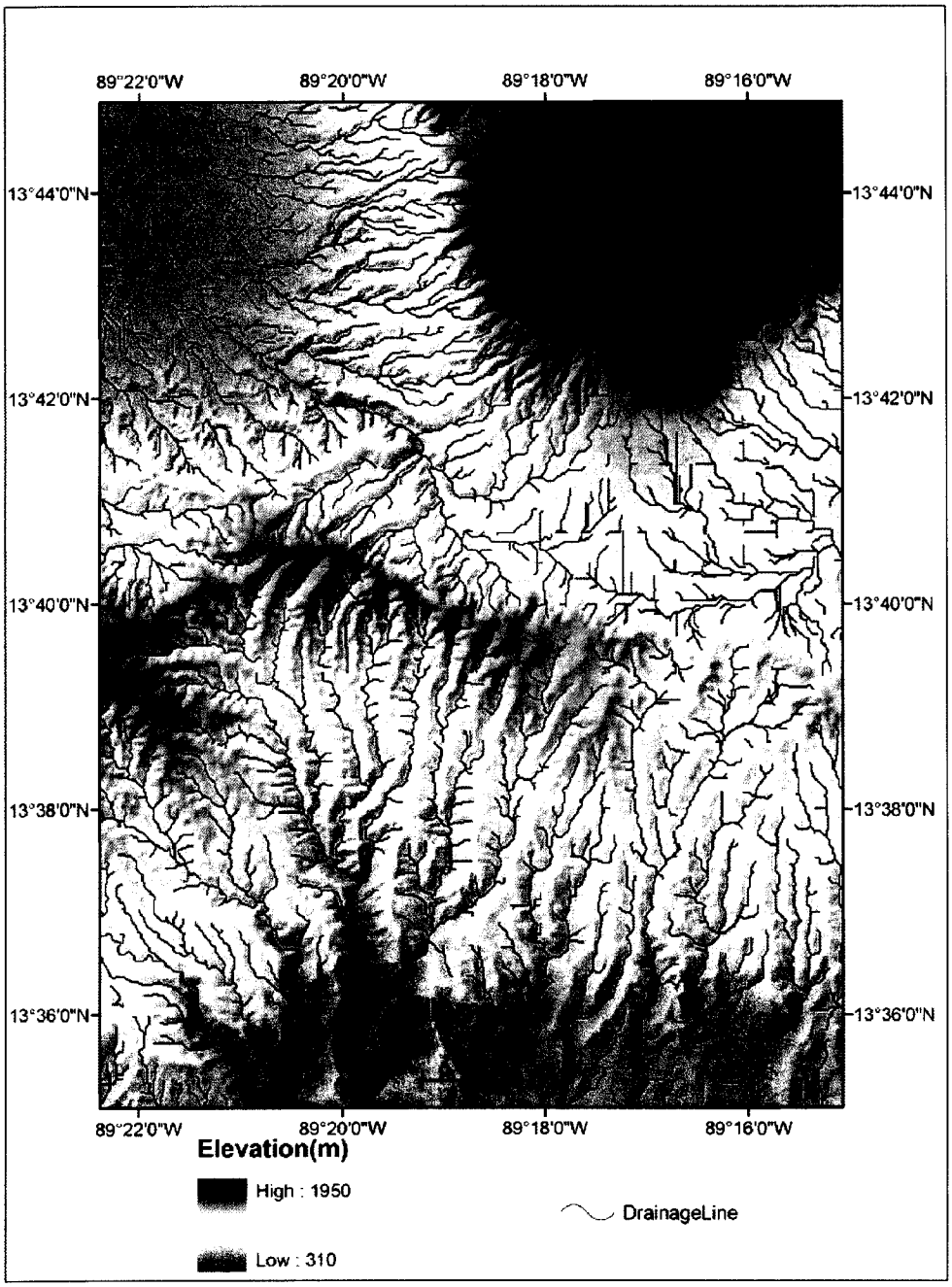

Figure 4.8 The hillshade map of the study area with stream network. The map was produced using ArcGIS with ArcHydro tools. The San Salvador Volcano is in the north, and the ridge in the middle of the map is known as the Balsamo Ridge.

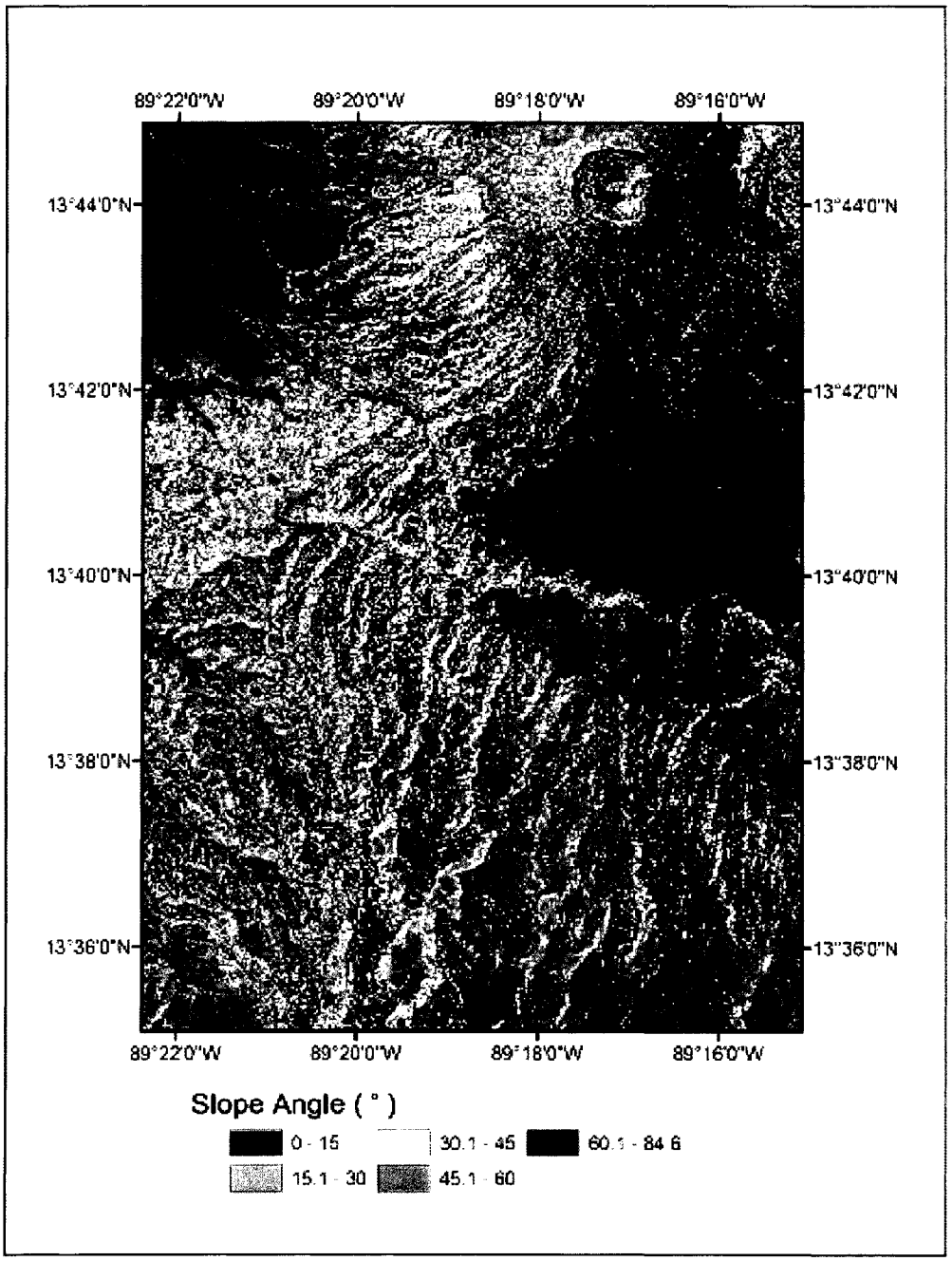

Figure 4.9 Slope angle variation in the study area. The map is produced from a digital topographic map (1:25000). The grid size is 30×30 m^2.

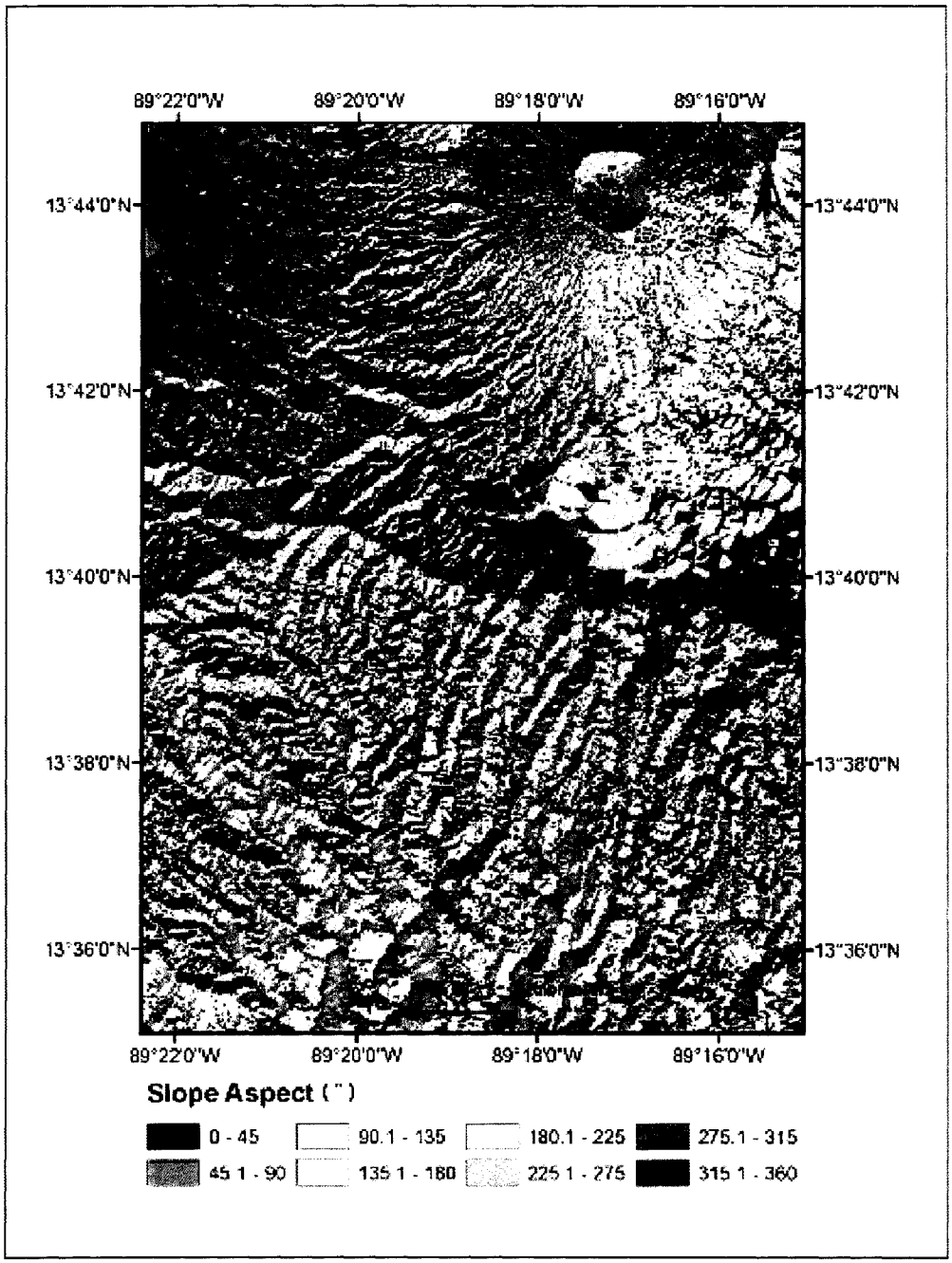

Figure 4.10 Slope aspect map (dip direction of ground surface) of the study area. The map is produced from a digital topographic map (1:25000).

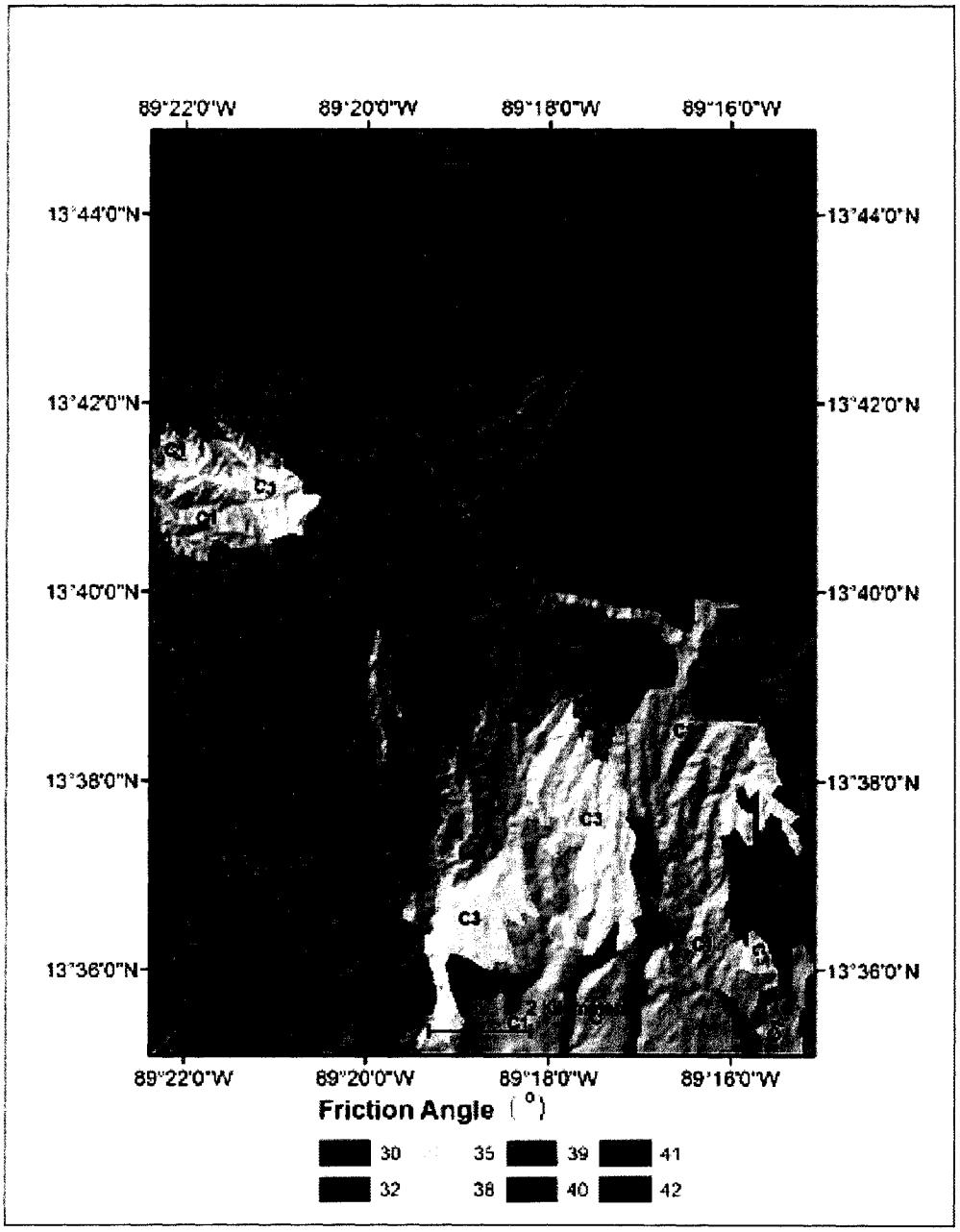

Figure 4.11 Average friction angle of the surface lithology in the study area. The map is reproduced from the geological map of El Salvador and the strength parameter values were assigned according to Table 4.6.

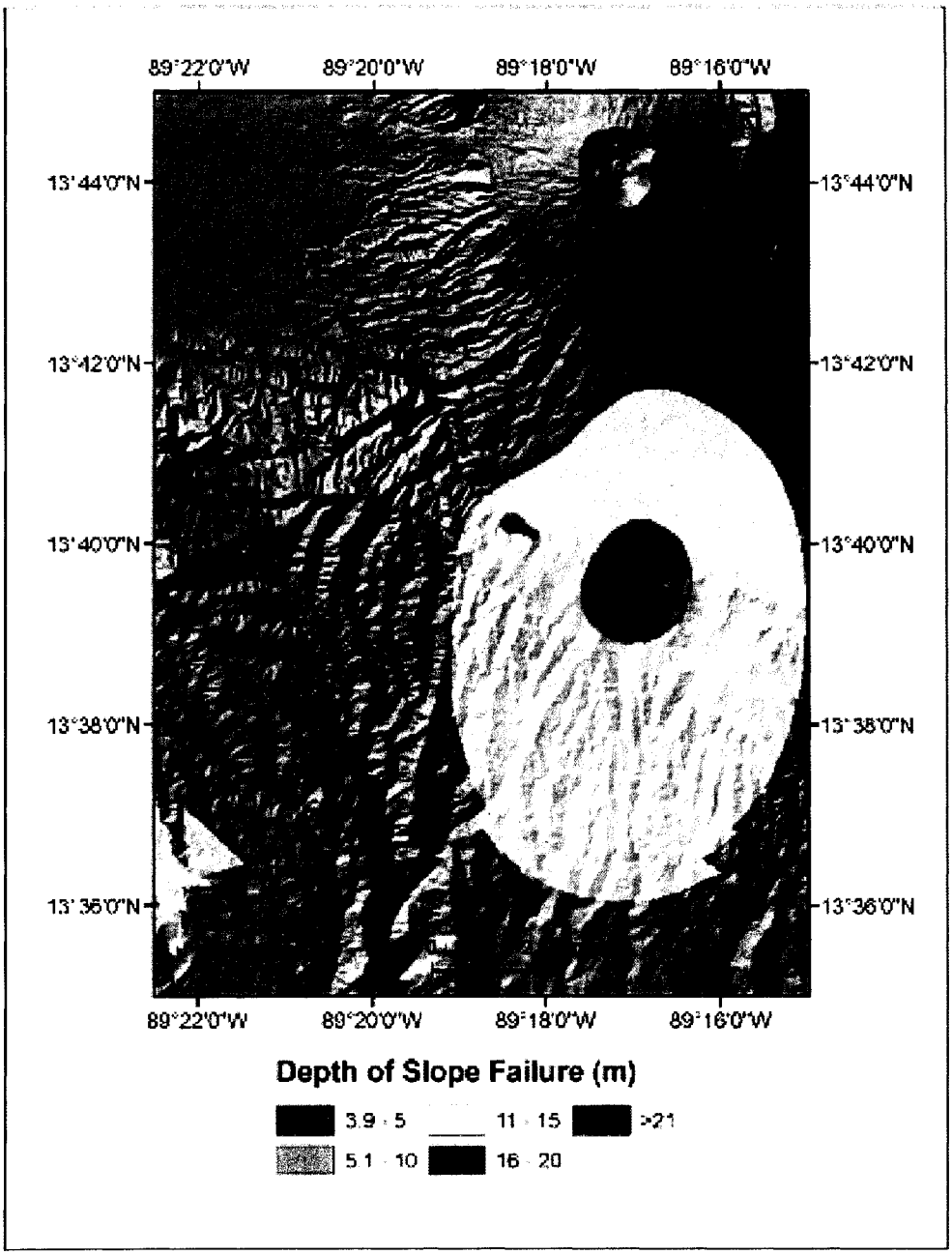

Figure 4.12 The estimated depth of the sliding surface by the ordinary kriging method. The spatial distribution of the historic landslides during the 1986 and 2001 earthquake was used for this statistical analysis.

Chapter 5 Ground Motion and Topographic Effect

5.1 Introduction

Ground motion was found to be the primary factor in earthquake-induced slope failure. Seismic-induced ground motion is often sufficient to trigger landslides in slopes that have low to moderate stability in static conditions. The minimum ground acceleration or earthquake magnitude to trigger landslides depends on the earthquake duration, terrain characteristics, and geotechnical parameters of the potential sliding mass.

In January and February of 2001, El Salvador experienced two major earthquakes that caused widespread damage and fatalities throughout much of the country. The earthquake of January 13 had a magnitude, M_w, of 7.6, and the epicenter was located 40 km off the coast of El Salvador beneath the Pacific Ocean (13.049°N, 88.660°W) at an estimated focal depth of 60 km. The focal mechanism indicates normal faulting in the overriding Caribbean plate (Jibson et al., 2004).

In the city of Nueva San Salvador, a nearby seismograph recorded base motion with a maximum horizontal acceleration of 587.7 cm/s^2 (0.6 g) along the north–south direction (Santa Tecla station). In order to estimate the seismic hazards in the study area, this chapter discussed ground motion characteristics, seismic response, and slope stability in the Las Colinas landslide area.

5.2 Strong Ground Motion

The ground motion produced by earthquakes can be recorded by a seismograph. The actual record of ground shaking from the seismograph, known as a seismogram, can provide information about the characteristics of earthquake. For engineering purposes, the earthquake amplitude, frequency, and duration have primary significance. Strong ground motion can be described by various ground motion parameters. Among them, the earthquake magnitude, peak ground acceleration (*PGA*), and Arias Intensity (I_a) are

widely used in landslide hazard estimation. A typical ground motion record, including acceleration, velocity, and displacement histories during the January 13, 2001 earthquake, is shown in Figure 5.1.

Tables 5.1 and 5.2 list the characteristics of the strong-motion stations and instruments in El Salvador (Cepeda et al., 2004). Each station was assigned a National Earthquake Hazard Reduction Program (NEHRP) site class (Dobry et al., 2000), which is listed in the last column of Table 5.1.

The NEHRP site class was originally calculated as the average shear wave velocity within the top 30 m. B sites (rock sites) have average velocities of 760 m/s to 1500 m/s. C sites are very dense soils or soft rocks with average velocities of 360 m/s to 760 m/s. D sites are defined as stiff soils with average velocities of 180 m/s to 360 m/s. The definitions of NEHRP site classes are listed in Table 5.3.

Figure 5.2 shows the distribution of recorded horizontal acceleration in El Salvador during the January 13, 2001 earthquake. Contour lines of horizontal acceleration were generated using the ordinary kriging method based on the seismograms at the stations listed in Tables 5.1 and 5.2. Southern El Salvador experienced strong earthquake shaking with horizontal earthquake acceleration reaching 0.3~0.8 g. Horizontal acceleration close to the coastline was greater than 0.8 g. In northern El Salvador, horizontal acceleration decreased to 0.1~0.3 g.

Nueva San Salvador experienced an acceleration of 0.3~0.8 g. The records from the Hospital San Rafael (TE) and Santa Tecla (ST) accelerograph stations in the Nueva San Salvador recorded peak horizontal accelerations (N-S component) of 0.46 g and 0.6 g, respectively. Such high earthquake shaking would be strong enough to trigger landslides, rock falls, or soil cracks in the study area.

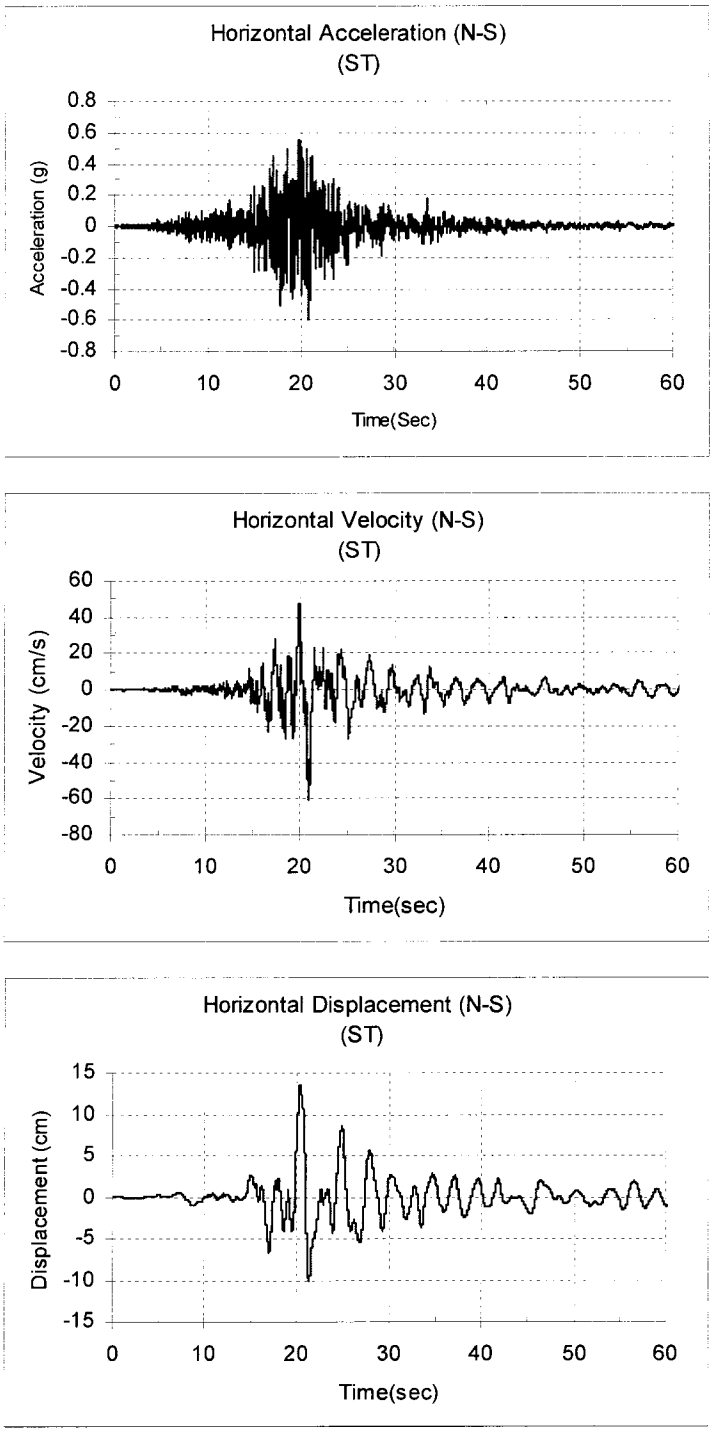

Figure 5.1 Horizontal acceleration, velocity, and displacement (N-S) component during the January 13, 2001 El Salvador earthquake recorded at ST station located at Santa Tecla (Nueva San Salvador). Sources: corrected accelerogram from the USGS website.

Table 5.1 Characteristics of strong motion recording stations (after Cepeda et al., 2004)

Code	Description	Owner	Instrument	Latitude (°N)	Longitude (°W)	Geology	NEHRP Site
AH	Ahuachapán	CIG	SMA-1	13.925	89.805	S3	D
AR	Armenia	UCA	SSA-2	13.744	89.501	S3	D
BA	San Bartolo	UCA	SSA-2	13.704	89.106	S4	D
BE	Berlin	GESAL	SSA-2	13.497	88.529	S2	D
CA	CEPA, Acajutla	CIG	SMA-1	13.567	89.833	B1	Rock
CI	Centro de Investigaciones Geotécnicas, San Salvador	CIG	SMA-1	13.698	89.173	S5'A	Rock
CM	CESSA, Metapán	CIG	SMA-1	14.333	89.450	Q'F	Rock
CU	Cutuco	CIG	SMA-1	13.333	87.817	C3	Rock
DB	Ciudadela Don Bosco, Soyapango	CIG	SMA-1	13.733	89.150	S4	D
EX	Externado, San Salvador	UCA	SSA-2	13.707	89.207	S4	D
LI	La Libertad	UCA	SSA-2	13.486	89.327	Q'F	C
MG	San Miguel	CIG	SMA-1	13.475	88.183	S3	C
NO	San Pedro Nonualco	UCA	SSA-2	13.602	88.927	C1	D
OB	Observatorio, San Salvador	CIG	SMA-1	13.681	89.198	S4	D
PA	Panchimalco	UCA	SSA-2	13.614	89.179	C1	Rock
QC	"15 de septiembre" dam (zero level)	CIG	SMA-1	13.616	88.550	B3	Rock
RF	Relaciones Exteriores (bottom of borehole)	CIG	SMA-1	13.692	89.250	S3'A	C
RS	Relaciones Exteriores (ground level)	CIG	SMA-1	13.692	89.250	S3'A	D
SA	Santa Ana	CIG	SMA-1	13.992	89.550	S3	D
SE	Sensuntepeque	CIG	SMA-1	13.867	88.663	B1	Rock
SM	Santiago de María	CIG	SMA-1	13.486	88.471	S3	D
SS	Seminario "San José de La Montaña" (ground level)	CIG	SMA-1	13.705	89.225	S4	D
ST	Santa Tecla	CIG	SMA-1	13.675	89.300	S3	D
TE	Hospital San Rafael, Santa Tecla	UCA	SSA-2	13.671	89.279	S2	C
TO	Tonacatepeque	UCA	SSA-2	13.778	89.114	C1	D
TR	Planta Boca Pozo, Berlín	GESAL	SSA-2	13.520	88.512	S2	D
UC	Universidad Centroamericana, Antiguo Cuscatlán	CIG	SMA-1	13.677	89.236	S3'A	D
VF	Viveros de DUA (bottom of borehole), San Salvador	CIG	SMA-1	13.737	89.209	S4	C
VI	San Vicente	UCA	SSA-2	13.642	88.784	S4	D
VS	Viveros de DUA (ground level), San Salvador	CIG	SMA-1	13.737	89.209	S4	D
ZA	Zacatecoluca	UCA	SSA-2	13.517	88.869	B1	Rock

Table 5.2 Records for the January 13, 2001 earthquake, peak acceleration, peak velocity and pseudo spectral accelerations for 0.3s and 1.0s. Stations ordered with increasing rupture distance (after Cepeda et al., 2004)

Code	Rupture Distance (km)	*PGA* (cm/s^2)	PGV (cm/s)	PSA T=0.3 s (cm/s^2)	PSA T= 1 s (cm/s^2)	*PGA* (cm/s^2)	PGV (cm/s)	*PGA* (cm/s^2)	PGV (cm/s)	PSA T=0.3 s (cm/s^2)	PSA T= 1 s (cm/s^2)
		North-South				Vertical		East-West			
LI	61.3	1092	53.2	1290	285	604	15.9	564	35.5	958	237
ZA	72.0	255	12.3	362	140	247	8.6	305	19.1	410	229
PA	75.4	173	9.2	223	174	87	7.3	151	9.4	182	111
SM	77.7	864	27.8	1607	350	432	16.1	702	40.4	2011	415
NO	78.9	569	37.5	1063	402	430	18.2	479	26.4	1789	319
TE	79.2	486	57.0	1103	385	239	18.5	477	34.2	1112	389
TR	79.4	453	18.6	1017	163	235	18.0	364	24.2	1279	220
ST	79.4	588	60.5	1119	514	464	21.6	761	43.3	2570	343
RF	81.0	204	19.5	476	233	184	13.9	205	16.6	470	251
RS	81.0	317	27.6	1207	280	323	15.3	298	22.9	1026	268
OB	81.4	420	38.4	1096	555	301	13.0	372	26.2	1052	507
SS	83.2	267	15.0	544	211	157	11.3	247	20.3	656	330
EX	83.7	295	25.4	962	441	151	11.9	273	17.4	584	394
BA	85.2	154	25.2	615	491	163	15.2	195	31.2	485	454
CA	86.5	106	18.6	209	282	49	4.2	96	14.6	226	183
VS	86.5	301	21.9	N/A	N/A	207	12.5	306	37.3	N/A	N/A
DB	87.1	221	23.2	473	523	157	11.3	245	19.2	502	183
QC	87.2	149	23.5	365	209	120	10.2	183	16.0	574	163
AR	87.3	589	49.6	751	1050	219	19.6	445	53.3	1183	657
MG	91.9	118	12.1	215	252	88	6.0	133	12.8	204	225
TO	92.0	258	23.1	594	424	201	9.8	230	23.2	611	208
SE	108.7	81	8.5	213	115	57	6.2	60	9.1	190	71
SA	112.1	133	19.5	373	407	50	6.2	84	13.6	169	175
CU	113.6	76	13.8	205	100	62	4.0	78	8.6	179	149
AH	114.8	210	16.6	335	335	121	10.8	143	14.9	318	324
CM	144.1	14	1.7	23	18	N/A	N/A	12	2.2	21	25

Notes: Rupture distance = distance to plane of rupture; *PGA* = horizontal peak ground acceleration; PGV = horizontal peak ground velocity; PSA = pseudo spectral acceleration; T = period; N/A = No data.

Table 5.3 Definition of NEHRP site classes by shear velocity V_s and blowcount N (Dobry et al., 2000)

Site Class	Shear Velocity Range, m/s	SPT Blowcount, N	Description
A	$V \geq 1500$	Not applicable	Hard rock
B	$760 \leq V < 1500$	$N > 100$	Rock
C	$360 \leq V < 760$	$50 \leq N < 100$	Dense soil or soft rock
D	$180 \leq V < 360$	$15 \leq N < 50$	Stiff soil
E	$V < 180$	$N < 15$	Stiff soil

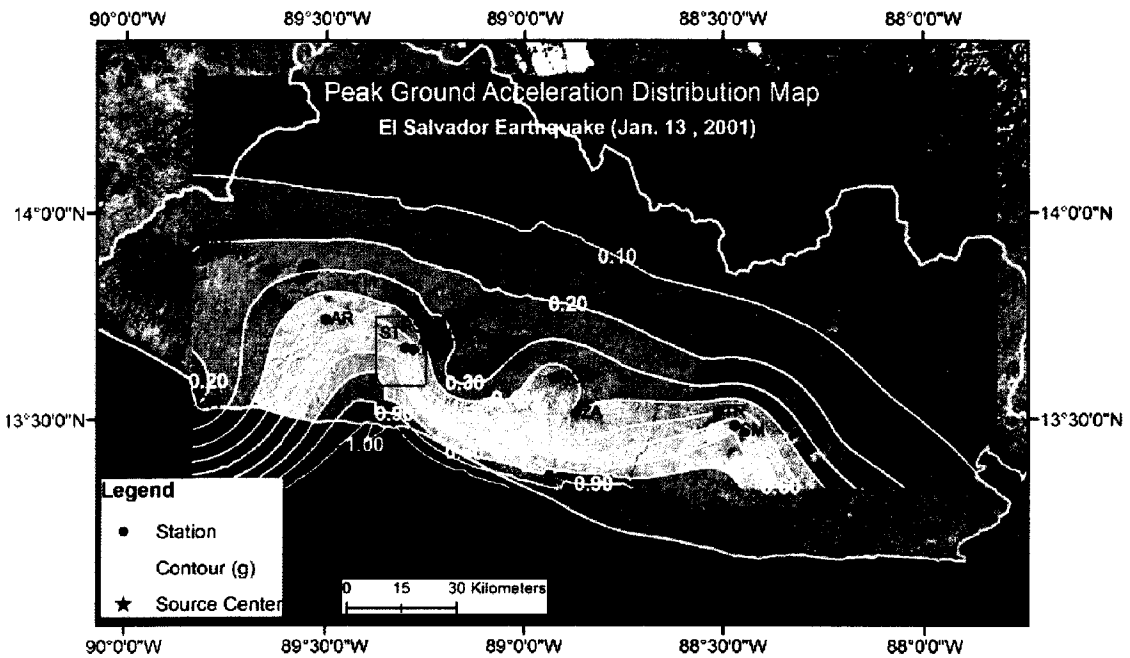

Figure 5.2 Peak ground acceleration of the January 13, 2001 El Salvador earthquake. The contour map was obtained by using the ordinary kriging. The Southern part of El Salvador experienced strong earthquake shaking. The horizontal earthquake acceleration reached 0.35~0.8g and increased to 1.0g near the coastline.

5.3 Regional Ground Motion Estimation

5.3.1 Estimation Methods

The ground motion caused by the earthquake is generally characterized in terms of ground surface displacement, velocity, and acceleration. Geotechnical engineers have traditionally used acceleration because it is directly related to the dynamic force that earthquake induces in soil mass.

Peak ground acceleration (*PGA*, or a_{max}) is the most commonly used ground motion parameter in seismic hazard assessment and Newmark displacement calculation. For earthquake engineering analysis, *PGA* is one of the most difficult parameters to determine. It represents an acceleration that will be induced sometime in the future. Since it is not possible to predict an earthquake, the peak ground acceleration must be based on prior earthquakes and fault studies (Day, 2002).

Engineering geologists can determine *PGA* at a site based on fault structure, seismicity, and attenuation relationships. Some of the commonly used methods to determine *PGA* at site are as follows (Day, 2002):

(1) Historic earthquake: past seismic activities, more recent earthquakes, and data from seismographs can be used in determination of *PGA*. The *PGA* determined from an earthquake history study should be compared with other methods because the time frame of recorded earthquake history is usually too small.

(2) Code or other regulatory requirements: there may be local building code or other regulatory requirements that specify the design value of *PGA*.

(3) Maximum credible earthquake: the maximum credible earthquake is often considered to be the largest earthquake that can reasonably be expected to occur based on known geologic and seismologic data. It is also considered to be the maximum earthquake that an active fault can produce. The method used to determine maximum credible earthquake is referred to as the deterministic seismic hazard analysis (DSHA) method. Ground motion is estimated from a given set of seismological parameters, such

as earthquake magnitude and the distance from the earthquake rupture zone to the site of interest.

(4) Maximum probable earthquake: a commonly used definition of maximum probable earthquake as the largest earthquake that a fault is capable of generating within a specified time period, such as 50 years or the design life of a project.

(5) Seismic hazard map: another method for determining the peak ground acceleration is to determine the a_{max} that has a certain probability of being exceeded in a specific number of years. Basic ground acceleration can be determined through site-specific seismic hazard analysis, or from a hazard map produced by a government agency, for example, USGS seismic hazard maps. Usually, seismic hazard maps show *PGA* with a 10% probability of exceedance in 50 years. The method used to determine *PGA*, based on the concept of acceptable risk, is referred to as probabilistic seismic hazard analysis (PSHA) method. Ground motion is estimated statistically using all possible earthquake locations and magnitudes together with their expected probabilities of occurrence.

5.3.2 Seismic Hazard and Attenuation Relationship

Seismic hazard is the likelihood, or probability, of experiencing a specified intensity of any damaging phenomenon at particular site, or over a region, in some period of interest (Tenhaus and Campbell, 2003). Seismic hazard analysis involves the quantitative estimation of ground-shaking hazard at a particular site.

Probability values that are commonly used and cited in probabilistic seismic hazard analysis (PSHA) are ground motions that have a 10% probability of being exceeded in a 50-year exposure period of engineering interest. The return period of ground motion, x, is defined as (Tenhaus and Campbell, 2003):

$$R_x(x) = \frac{1}{\lambda[X \geq x]} = \frac{-t}{\ln(1 - P[X \geq x])} \qquad (5.1)$$

where $\lambda[X \geq x]$ is the annual frequency that ground motion at a site exceeds the chosen level $X = x$. $P[X \geq x]$ is the conditional probability that the chosen ground motion level is

exceeded for a given magnitude and distance. Based on Equation 5.1, the return period for ground motions having a 10% probability of being exceeded in a 50-year exposure period will be 475 years.

Seismic design codes exist in the form of zonation maps, which show, explicitly or through generalized zones, the distribution and level of hazard in terms of peak ground acceleration, usually with a return period of 475 years.

Ground motion estimation is usually done using a ground motion relation, or an attenuation relation. A number of empirical equations of the attenuation relationship for different geographic and tectonic environments were developed.

Strong ground motion can be estimated from the attenuation relationship of the common logarithmic form (Campbell, 2003):

$$\log Y = b_1 + b_2 M - b_3 \log R - b_4 R + b_5 F + b_6 S + \varepsilon \qquad (5.2)$$

where the distance term R is given by one of the alternative expressions:

$$R = \begin{cases} r + b_7 \exp(b_8 M) \\ or \\ \sqrt{r^2 + [b_7 + \exp(b_8 M)]^2} \end{cases} \qquad (5.3)$$

where Y is strong ground motion of interest, usually, PGA in g; M is earthquake magnitude (M_w); R is distance from the earthquake sources to the site (km); ε is a random error term with a mean of zero and a standard deviation equal to the standard error of estimate of σ_{logY}; r is a measure of the shortest distance from the site to the source of the earthquake; b_3, b_6, and b_7 are defined in terms of M and R; and b_1, b_2, b_4, b_5 and b_8 are parameters dependent on the tectonic environment.

Several attenuation relations commonly used to estimate PGA for engineering evaluation are listed in Table 5.4.

Table 5.4 Attenuation relations used to estimate *PGA* (after Campbell, 2003)

Region	Tectonic Environment	Attenuation Relation
Western North America	Shallow active crust	Abrahamson and Silva, 1977 Boore et al., 1997
Eastern North America	Shallow stable crust	Atkinson and Boore, 1995, 1997, 2003 Toro et al., 1997
Europe	Shallow active crust Shallow stable crust	Ambraseys et al., 1996 Dahle et al., 1990
Japan	All types undivided	Molas and Yamazaki, 1995, 1996
Worldwide	Shallow extended crust Subduction interface Subduction intraslab Subduction undivided	Spudich et al., 1999 Youngs et al., 1997 Youngs et al., 1997 Crouse, 1991

5.3.3 Seismic Hazard in El Salvador

The frequency of destructive earthquakes in El Salvador demonstrates that it is a country with very high seismic hazard. The historic earthquakes in El Salvador from 1915 to 2001 are shown in Table 3.2 (Chapter 3). Four earthquakes of magnitude 7.1 or larger impacted the Nueva San Salvador area. The largest historic earthquake from 1915 to 2001 was the January 13, 2001 earthquake. In Nueva San Salvador, the interpolated *PGA* based on recorded peak ground accelerations of January 13, 2001 was 0.35 to 0.8g (Figure 5.2).

Various researchers and organizations have estimated the seismic hazard in El Salvador. Since the San Salvador earthquake of 1986, three seismic hazard studies have been carried out for El Salvador and another for Central America as a whole (Bommer et al., 1996, Lopez et al., 2004). The first study for El Salvador was conducted by the U.S. Geological Survey (Algermissen et al., 1988). The second was conducted by Stanford University (Alfaro et al., 1990), and the third was conducted by the Universidad Nacional Autónoma de México (Singh et al., 1993).

The attenuation relationship for peak ground acceleration has been derived in many hazard studies in Central America and El Salvador.

Bommer et al. (1996), using records from Central America subduction earthquakes and the model of Crouse et al. (1988), obtained a prediction equation for *PGA* as:

$$\ln(PGA) = -1.47 + 0.608M - 1.181\ln(R) + 0.0089H$$
$$\sigma_{\ln(PGA)} = 0.54 \qquad (5.4)$$

where M is earthquake magnitude; R is hypocentral distance; and H is focal depth, both in kilometers; $\sigma_{ln(PGA)}$ is the standard deviation.

Alfaro et al. (1990) separately studied crustal and subduction data because crustal and subduction earthquakes have different travel paths and stress conditions. For the near-field events (events within one source dimension of the epicenter, where source refers to the width or length of faulting, whichever is shorter), a dataset of 20 records obtained at epicentral distances between 1 and 27 km from 12 earthquakes in Guatemala, Nicaragua, and El Salvador with magnitudes in the range of 4.1 to 7.5, were used. The equation obtained for *PGA* (g), using the larger horizontal component, is:

$$\log(PGA) = -1.116 + 0.312M_s - \log(R^2 + 7.9^2)^{1/2} \qquad (5.5)$$

where R is the epicentral distance in km; standard deviation of *PGA* is $\sigma = 0.21$. For far-field events (beyond near-field), a dataset for San Salvador was comprised of 20 single recordings of earthquakes with magnitudes from 4.2 to 7.2, depths between 36 and 94 km, and epicentral distances from 31 to 298 km. The equation obtained from the regression on this dataset is:

$$\log(PGA) = -1.638 + 0.438M_s - 1.181\log(R^2 + 70.0^2)^{1/2} \qquad (5.6)$$

with the same standard deviation as Equation 5.5.

Since the above attenuation relations did not consider events after 1990, they tend to predict smaller *PGA* values because the large earthquakes in 2001 would have an influence on the relation.

Figure 5.3 shows hazard maps from each of these three studies, which show *PGA* levels with a 10% probability of exceedance in 50 years. A revised regional hazard assessment presented by Lindholm et al. (1995) is also illustrated in Figure 5.3. There is considerable disagreement amongst the four maps both in terms of the geographical

distribution of hazard and of the expected levels of acceleration. Singh et al. (1993) gives the highest acceleration of 0.7~1.02 g for El Salvador. Lindhom et al. (1995) gives the lowest acceleration of 0.25~0.35 g. The 475-year *PGA* values for San Salvador were 0.5 g, 0.8 g, and 1.0 g in the maps of Algermissen et al. (1988), Alfaro et al. (1990) and Singh et al. (1993), respectively.

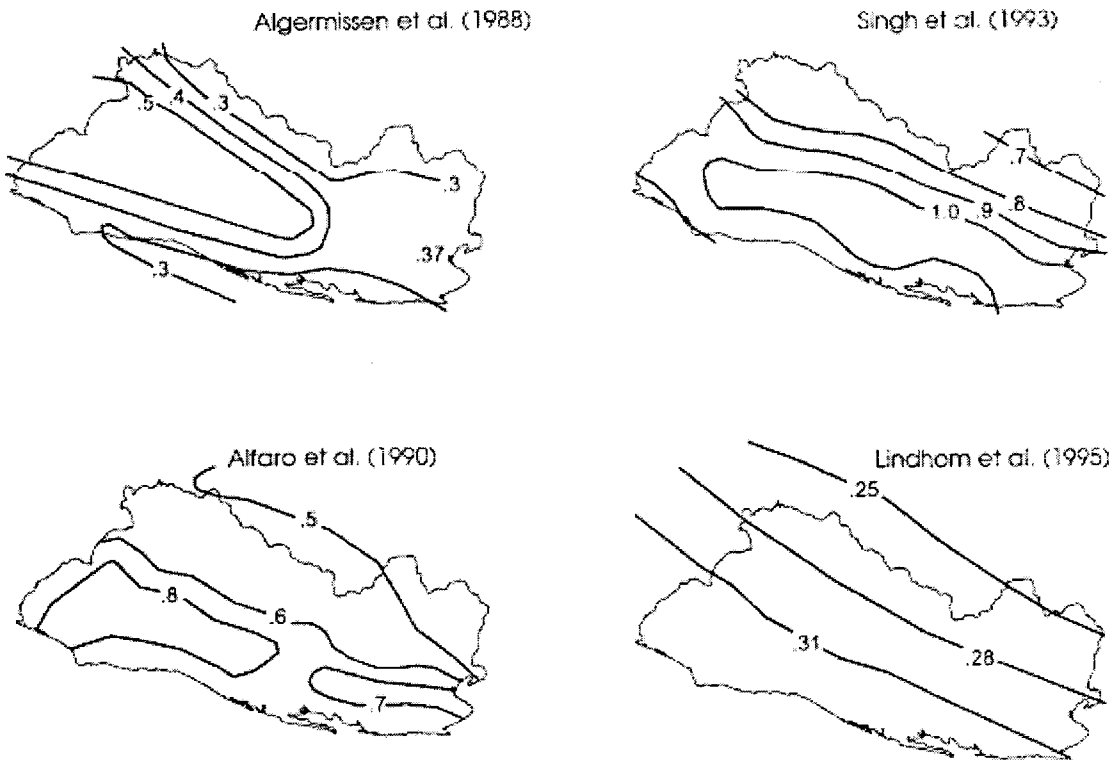

Figure 5.3 Seismic hazard maps for El Salvador, showing 475-year return period (10% probability of exceedance in 50 years) accelerations (g) proposed by different studies (Bommer et al., 1997).

The average *PGA* with a 10% probability of exceedance in 50 years presented in each of the hazard studies for San Salvador are summarized in Table 5.5.

The possible maximum earthquake magnitude in each source zone in El Salvador was treated differently in each of the studies (Bommer et al., 1996). The maximum earthquakes in El Salvador predicted by the different methods and studies are listed in

Table 5.5. The January 13, 2001 earthquake represented the largest subduction zone earthquake and February 13, 2001 earthquake represented the largest volcanic chain (intraplate) earthquake in El Salvador.

Table 5.5 Summary of *PGA* value from seismic hazard maps and maximum earthquake in El Salvador predicted by different methods and studies.

Hazard Study	*PGA* (g)		Maximum Earthquake Magnitude (M)	
	San Salvador	Study Area	Subduction Zone	Volcanic Chain
2001 El Salvador Earthquake (M7.6)	0.42[1] (01/13/2001)	0.6[2] (01/13/2001)	7.6 (01/13/2001)	6.6 (02/13/2001)
Algermissen et al., 1988	0.50	0.45~0.5	7.3	6.6
Alfaro et al., 1990	0.8	0.80	7.8~8.2	6.5~6.6
Lindhom et al., 1993	0.30	0.31	-	-
Singh et al., 1993	1.00	0.8~1.00	8.0~8.2	7.7
Rojas et al., 1993	0.75	-	7.5~8.0	7.0
Notes: [1] and [2] are recorded ground acceleration obtained at OB and ST stations, respectively.				

The El Salvador government released three seismic hazard maps for seismic design codes in 1966, 1989, and 1994. The country was divided into two parts, Zone I and Zone II. Zone I is a higher hazard area containing all of the Great Interior Valley and the coast mountain ranges and coastal plains. The design values of *PGA* from the current regulations (released in 1994) are 0.4 g and 0.3 g in Zones I and II, respectively. The study area, Nueva San Salvador is located in Zone I.

There is a considerable variation in *PGA* as shown above from a low of 0.3 g to a high of 1.0 g. For earthquake-induced landslide hazard assessment, the selection of an appropriate range of *PGA* should be based on a combination of risk analysis and the experience of earthquake engineers and engineering geologists. In the Nueva San Salvador area, due to the high population density, the slope around the city must be able to resist the largest maximum earthquake for planning purposes. Thus, for this study 0.5 to 0.8 g was chosen as the appropriate value of peak ground acceleration a_{max}.

5.3.4 Arias Intensity

One of the most commonly used earthquake shaking intensities in seismic hazard analysis is Arias Intensity (Arias, 1970), which is defined as:

$$I_a = \frac{\pi}{2g}\int_0^{\infty}[a(t)]^2 dt \qquad (5.7)$$

where I_a is the Arias Intensity in units of velocity, m/s; $a(t)$ is the acceleration-time history in units of g; t is the duration time, sec; and g is the acceleration of gravity.

This earthquake shaking intensity is directly proportional to the integral of the square of an entire acceleration time-history of an earthquake, which is simply the area enclosed by the time-domain strong-motion record. An earthquake does not have an Arias Intensity, but rather an earthquake strong-motion record has an Arias Intensity, because I_a is measured directly from a given acceleration time-history (Jibson, 1987). Arias Intensity has been shown to correlate well with earthquake damage, and it is a fairly reliable parameter to describe earthquake shaking necessary to trigger landslides (Wilson and Keefer, 1983, 1985, Jibson, 1987, Jibson and Harp, 1998).

Wilson and Keefer (1985) suggested a relationship between Arias Intensity, earthquake magnitude, and depth-corrected source distance as:

$$\log(I_a) = M - 2\log R - 4.1 \qquad (5.8)$$

where M is the moment magnitude of a design earthquake and R is the earthquake source-to-site distance in km.

Jibson (1987) used the same dataset as Wilson and Keefer (1986), but included the strong-motion record from the 1978 Tabas, Iran, earthquake that added a large value of Arias Intensity to the dataset. The multiple regression analysis yielded the following equation:

$$\log(I_a) = 0.98M - 1.35\log(R) - 4.90 \qquad (5.9)$$

This model yields a correlation coefficient (r) of 0. 84, and is thus well fitted to the data.

Figure 5.4 illustrates the correlation between Arias Intensity and peak ground acceleration, using the same dataset as Wilson and Keefer (1986), Jibson (1987), and

additional records from 1986 San Salvador earthquake (Hotel Camino Real station) and January 13, 2001 El Salvador earthquake (ST and OB stations). The regression equation is shown below:

$$I_a = 0.0336e^{9.0692(GPA)} \quad (5.10)$$

or $$\ln I_a = 9.0692(PGA) - 3.393 \quad (5.11)$$

In Equation 5.11, I_a is Arias Intensity in m/s; PGA is peak ground acceleration in g. This equation yields a correlation coefficient (R-square) of 0.79, and is also well fitted to the data.

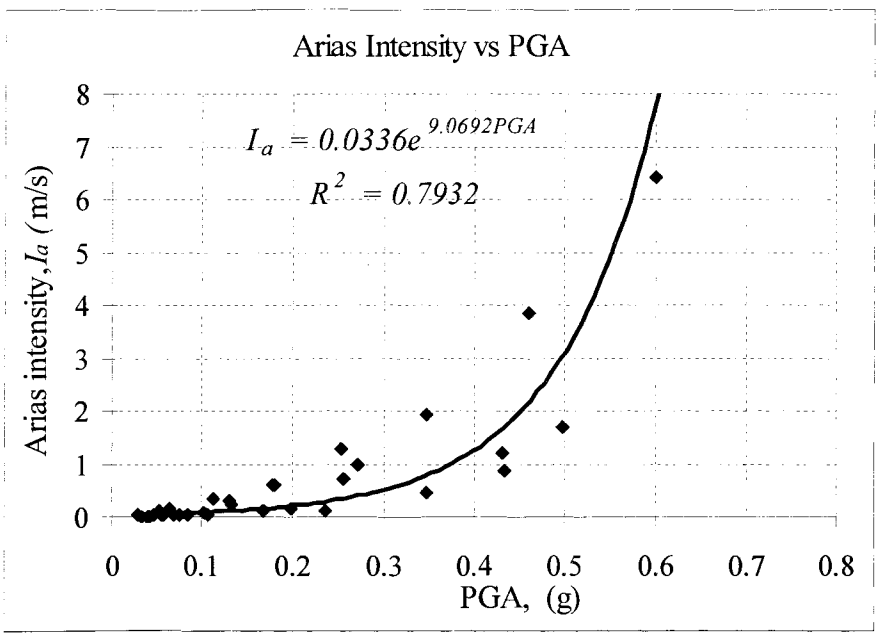

Figure 5.4 The correlation between Arias Intensity and peak ground acceleration (Data sources: Wilson and Keefer (1986), Jibson (1987), and 1986, 2001 El Salvador earthquakes)

Use of Arias Intensity as a measure of earthquake shaking is preferred over the use of peak ground acceleration, typically in slope-stability studies, because I_a depends not only on the ground acceleration, which may have a peak value of very high frequency and short duration that will not affect many slopes, but also on the duration of strong shaking (Jibson, 1987).

Harp and Wilson (1995) found a minimum Arias Intensity of 0.11 m/s for the initiation of rock falls and disrupted soil slides. The same authors reported a minimum Arias Intensity of 0.32 m/s required for the initiation of coherent deep-seated slumps.

5.4 Topographic Effect of Peak Ground Acceleration

Amplification of seismic waves caused by surface topography is an important site effect and is often advocated as one of the possible causes of concentration of damage during earthquakes.

Faccioli (1991) shows a simplified model of a valley and crest effect (Figure 5.5). At the vertex of the crest, the displacement of shear waves traveling parallel to the ridge axis is amplified by a factor $2\pi/\varphi$, where φ is the vertex angle of the crest.

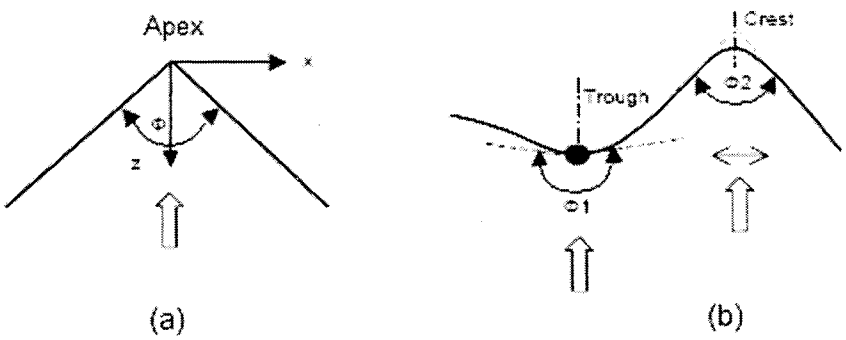

Figure 5.5 An infinite wedge subjected to vertically propagated shear wave (with particle motion parallel to its axis): (a) a triangular infinite wedge; (b) an approximation of ground surface at trough and crest (after Faccioli, 1991, Kramer, 1996)

Paolucci (2002) obtained a topographic amplification factor (the ratio of acceleration response spectra of output vs. input motion) from case studies, using 2D and 3D numerical simulation. In the 'extreme' case of internal wedge angle $\varphi=\pi/2$, the resulting topographic amplification would be 2 at the apex.

PWRI (Public Works Research Institute of the Ministry of Construction, Japan) located at Tsukuba Science City, Japan, carried out a model test of topographic amplification of seismic shaking in the Matsuzaki slope. The slope is located on a long ridge having a gently sloping (less than 10°) upper part and a steep sloping (15-25°) face. Station #1 is located where the ridge abruptly steepens. Stations #2 to #5 are spaced along the steep lower part of the ridge face and extend to the base of the ridge. Peak ground accelerations from strong motion records from five earthquakes were recorded. Figure 5.6 shows the ratio of the *PGA* recorded at each station to the *PGA* recorded at station #5 plotted versus the elevations of the stations above the ground surface at station #5. The ratios increased significantly from the bottom to the ridge crest. The results show that the average peak crest acceleration was about 2.8 times the average base acceleration (Jibson, 1987).

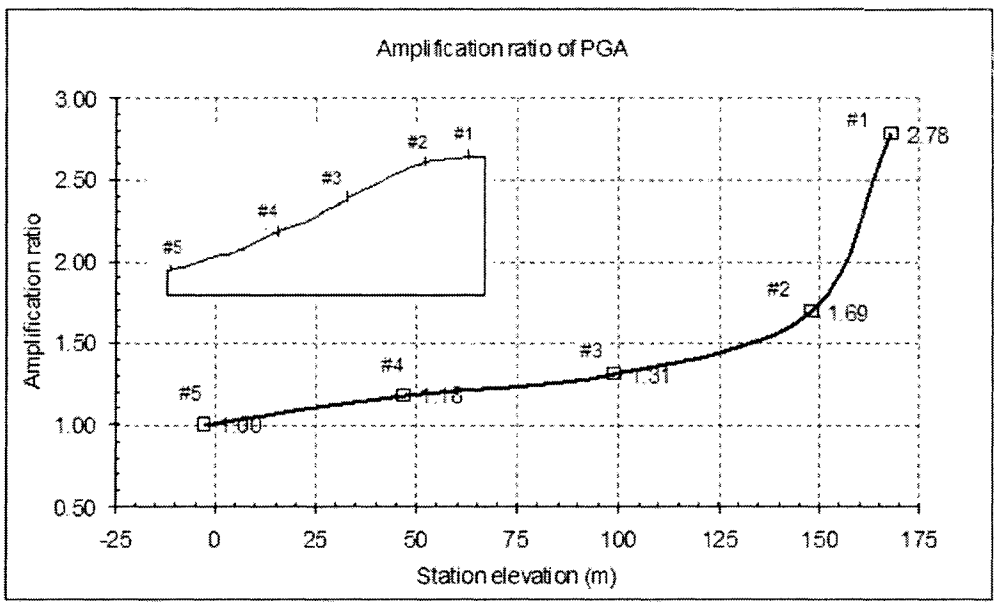

Figure 5.6 Average topographic amplification ratio of *PGA* at the slope surface in Matsuzaki, Japan. The amplification ratio is relative to the *PGA* of station #5. The ratio at the top station, #1, was 2.78 (Data source: Jibson, 1987).

Eurocode 8 (CEN European Committee for Standardization, 1994) provides amplification factors ranging from 1.2 to 1.4, as a function of the slope angle and the topographic feature. Usually, for slope angles <15° the topographic effects can be neglected. The highest values apply to places near the top of ridge with a crest width significantly less than the base width and average slope angles >30°. The amplification factor can be assumed to linearly decrease towards the base, where it becomes unity (Paolucci, 2002).

Amplification phenomena were observed and were significant in the Balsamo Ridge areas during the 2001 El Salvador earthquakes. Field observations revealed that hilltop towns suffered considerably more damage than their lower-elevation counterparts in the Cordillera del Balsamo region (Bent and Evans, 2004). Additional evidence for this conclusion was provided by the significant cracking which was observed in the ridgetops from Santa Tecla to Comasagua. At Balsamo Ridge, the evidence includes trees that were snapped off, boulders that were thrown from their sockets, and deep fissures along the edge of the ridge (Jibson and Crone, 2001). The recorded *PGA* near ST station was more than 0.6g, but shaking on the ridge top appears to have been even greater. This effect may play a significant role in the activation of landslides and rockslides during earthquakes, which in many cases are one of the major causes of devastation. The Las Colinas Landslide that caused hundreds of casualties during the January 13, 2001 El Salvador earthquake is evidence of this effect (Paolucci, 2002). Many observations of the intensive damage related to the surface topographic effects on earthquake ground shaking can be found in the literature (Bard and Riepl-Thomas, 1999).

Generally, local horizontal acceleration depends on the ground seismic response to a local topographic and soil/rock condition. In order to determine topographic influence on the acceleration, a seismic response analysis was performed using the dynamic finite element method and the Fast Lagrangian Analysis of Continua (FLAC) for the Las Colinas landslide.

5.5 Ground Response Analysis

5.5.1 Dynamic Model

The evaluation of ground response is one of the most important and most widely encountered problems in geotechnical earthquake engineering (Kramer, 1996). In slope stability and earthquake-induced landslide hazard estimation, ground response analysis can be used to predict ground surface motion, to evaluate dynamic stresses and strains, and to determine earthquake-induced forces in a slope. Two and three-dimensional dynamic response problems are most commonly solved using dynamic finite element analysis and finite difference analysis. The ground response analysis of Balsamo Ridge at the site of the Las Colinas landslide was carried out using FLAC5.0 (Itasca, 2005).

FLAC is a computer software package for engineering mechanics computation. FLAC5.0 is a two-dimensional explicit finite difference program. This program simulates the behavior of structures built of soil, rock or other materials that may undergo plastic flow when their yield limits are reached. Materials are represented by elements, or zones, which form a grid that is adjusted by the user to fit the shape of the slope to be modeled. Each element behaves according to a prescribed linear or nonlinear stress/strain law in response to the applied forces or boundary restraints. Although FLAC was originally developed for geotechnical and mining engineers, the program offers a wide range of capabilities to solve complex problems in mechanics (Itasca, 2005).

Dynamic analysis is often very complicated and a considerable amount of judgment is required to interpret it correctly. Dynamic modeling with FLAC involves several stages, which include (1) model building, including material assignment and boundary conditions; (2) initial equilibrium analysis; (3) ground motion input and dynamic boundary setup; and (4) dynamic analysis. Since dynamic analysis is a complex procedure, a complete description of dynamic modeling can be found in the User's Manuals for FLAC5.0.

Under the initial conditions, gravity acceleration was applied to the model. First, the static equilibrium condition must be satisfied. Then, displacement and velocity must be redefined to zero to remove kinetic energy so that it does not affect the dynamic calculation.

The initial horizontal stress coefficient, k_0, is:

$$k_0 = \sigma'_x / \sigma'_y = \frac{\nu}{1-\nu} \tag{5.12}$$

where σ'_x, σ'_y are horizontal stress and vertical stress, kPa, respectively; ν is Poisson's ratio.

Rayleigh damping was used to represent energy dissipation through the material. The damping matrix for each grid, C, is formulated using the assemblage of element damping matrices, which are constructed using the Rayleigh formation:

$$C = \alpha \cdot M + \beta \cdot K \tag{5.13}$$

where α is mass-proportional damping constant; β is stiffness-proportional damping constant.

For a multiple degree-of-freedom system, the critical damping ratio, ξ_i, at any angular frequency of the system, ω_i, can be found from:

$$\alpha + \beta\omega_i^2 = 2\omega_i\xi_i \tag{5.14}$$

$$\xi_i = \frac{1}{2}\left(\frac{\alpha}{\omega_i} + \beta\omega_i\right) \tag{5.15}$$

The critical damping ratio, ξ_i, is also known as the fraction of critical damping for mode i with angular frequency ω_i. In FLAC, Rayleigh damping is specified as minimum critical damping, ξ_{min}, and center frequency, f_{min} in Hz (Itasca, 2005).

Geological materials normally present a critical damping ratio in the range of 2% to 5% (Hart, 1991). In a plasticity constitutive model (such as Mohr-Coulomb material), a considerable amount of energy dissipation can occur during plastic flow. For many dynamic analyses that involve large-strain, only a minimal percentage of damping (e.g. 0.5%) may be required (Itasca, 2005).

5.5.2 Material Models and FLAC Grid

As shown in Figure 5.7, a slope profile crossing the ridgetop of the Las Colinas landslide along the sliding direction was selected for the slope stability and dynamic analysis. The height and width of the section are 185m and 750 m, respectively. The material constitutive model was assumed as elastic in initial gravity stress analysis and as Mohr-Coulomb material during dynamic analysis. To simplify problem solving, the study considered three layers of Mohr-Coulomb materials. Underground water was not considered in the seismic response analysis. Table 5.6 summarized the properties used in the model.

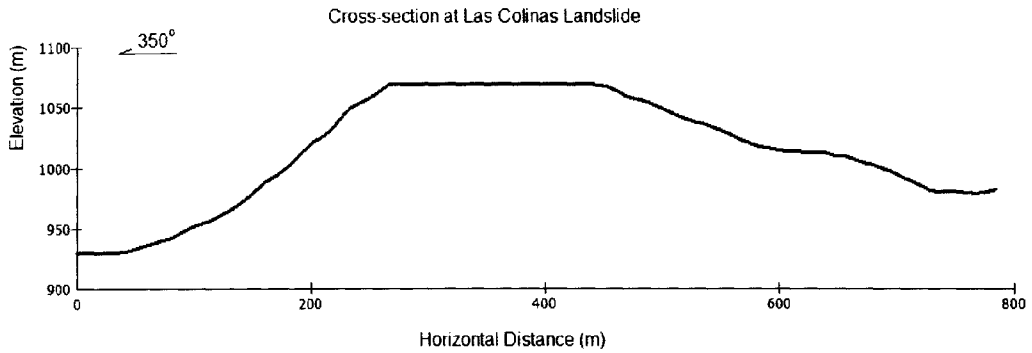

Figure 5.7 The slope profile crossing the ridgetop of the Las Colinas landslide (Generated by ArcGIS based on 10m resolution DEM)

Table 5.6 The geotechnical parameters in dynamic analysis

Strata		Density	Young's Modulus	Poisson's Ratio	Shear Modulus	Shear Wave Velocity	Friction Angle	Cohesion
		kg/m^3	E, kPa	v	G, kPa	V_s, m/s	$\phi°$	c, kPa
1	Pyroclasts	1500	6.0×10^4	0.43	2.0×10^4	120	30	60
2	Brown ashes paleosoil	1540	3.6×10^5	0.33	1.5×10^5	570	35	100
3	Tuffs and pyroclastic flows	1900	3.78×10^6	0.26	1.7×10^6	1100	39	200

In dynamic analysis, the frequency of the input motion and the velocities of wave propagation influence the accuracy of numerical solution. In the FLAC model, the maximum grid size, Δl, must be smaller than one-tenth to one-eighth of the shear wavelength, λ:

$$\Delta l = \frac{\lambda}{10} = \frac{V_s}{10f} \approx 8(m) \qquad (5.16)$$

where V_s is the velocity of shear wave in m/s; and f is the highest frequency component in Hz. The parameters considered in this analysis are 500 m/s and 6 Hz, respectively. The grid size in this analysis is around 4×4 m^2. The grids for dynamic analysis are shown in Figure 5.8.

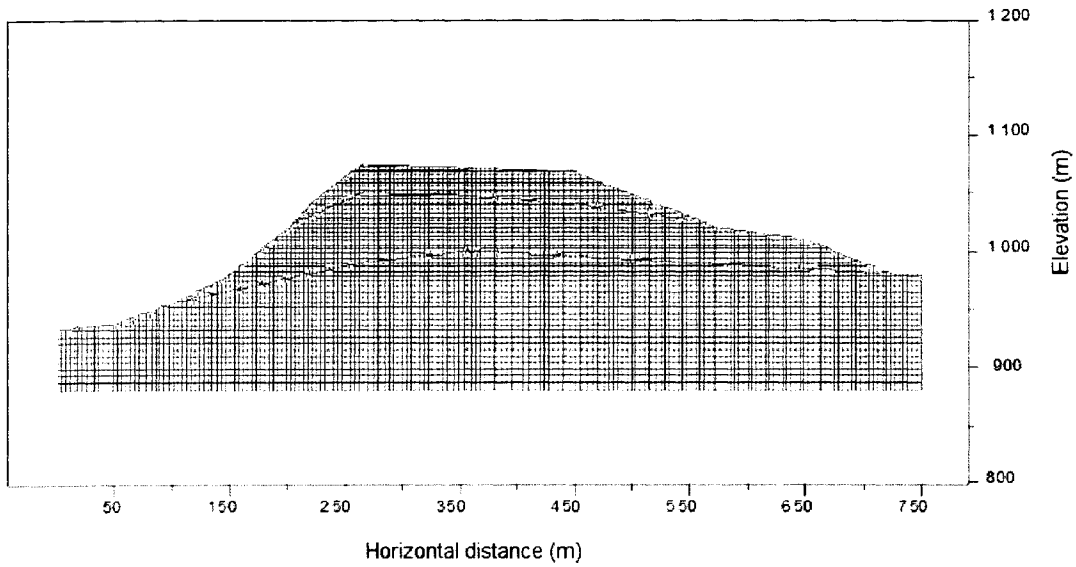

Figure 5.8 Grids in the dynamic analysis model. The average grid size is 4×4m. Three types of materials are considered in the dynamic analysis.

5.5.3 Boundary Conditions

The seismic analysis requires an adequate representation of the propagation of elastic waves over the unbounded half plane. The outwardly propagating wave must be transmitted (or absorbed) by the artificial boundaries (without boundary reflection). In the initial static condition, the base boundary is fixed in the vertical direction, and the lateral

boundaries are fixed in the horizontal direction. At the stage of dynamic analysis, the free-field boundaries are assigned to the lateral sides to account for free-field motion.

5.5.4 Input Acceleration and Damping Ratio

In this calculation, the horizontal accelerogram generated during the January 13, 2001, earthquake was selected as the input horizontal base acceleration. The seismic load was applied to the base of the model. The acceleration time-history from ST station was used for the dynamic analysis (*PGA*=0.6 g). In order to avoid numerical distortions, frequencies above 6.0Hz were filtered by applying the Fourier Transformation. The dynamic damping in the model was provided by the Rayleigh damping option in FLAC. A damping ratio of 5% was used, which is a typical value for geological materials. A damping frequency of 3.3 Hz was used for this model.

5.5.5 Results

The topographic characteristics of the hill increased the magnitude of ground vibration. Peak ground acceleration and displacement at the ridge top were significantly amplified. The shaking-induced displacements are shown in Figure 5.9. The northern slope near the crest had a horizontal displacement up to 105 cm and vertical displacement about 30 cm. Movement of the south slope was minimal (25 cm). This simulation is an agreement with the actual failure area of Las Colinas landslide during the January 13, 2001 earthquake. The analysis indicates that the slope near the crest on the north side is the critical area in which the slope is most likely to fail.

Figure 5.10 shows ground motion and displacement time-history monitoring points in the seismic response analysis. Figure 5.11 shows the horizontal time-history at the crest point (#8), and slope point near the crest (#7), respectively. The maximum horizontal displacements are 50 cm at #8, and 105cm at #7 (the largest displacement point on the slope surface). The displacement at point #6 reduces to 30 cm.

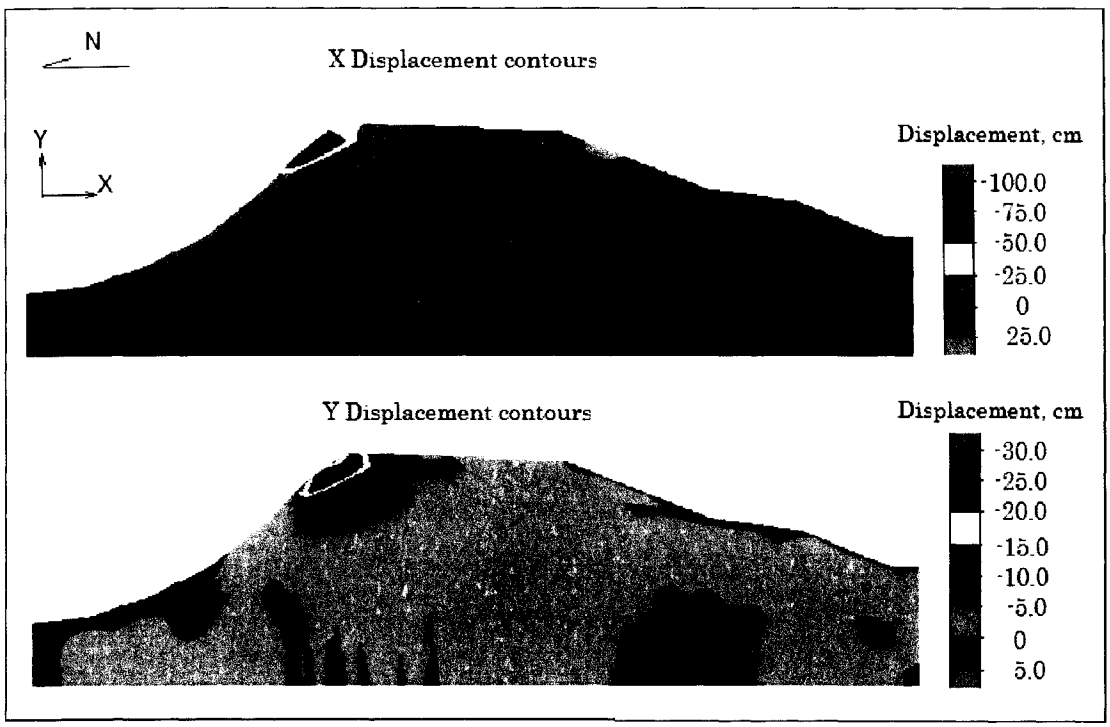

Figure 5.9 Contour map of seismic-induced displacement. The maximum displacement occurred at the north side of the ridge near the crest. The maximum horizontal displacement (X) is 100 cm, and the maximum vertical displacement (Y) is 30 cm.

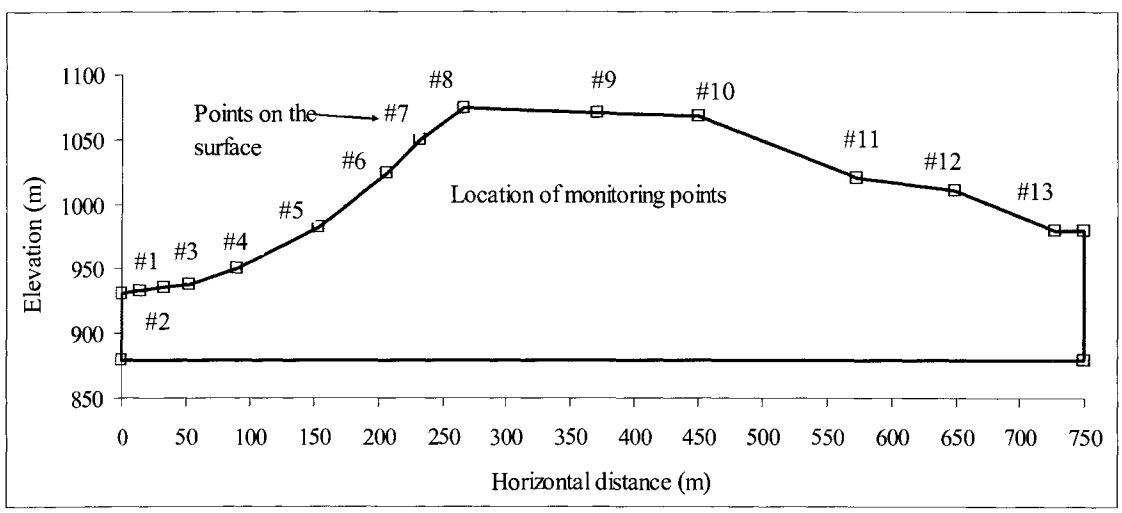

Figure 5.10 Ground motion monitoring points on the slope surface for the seismic response analysis.

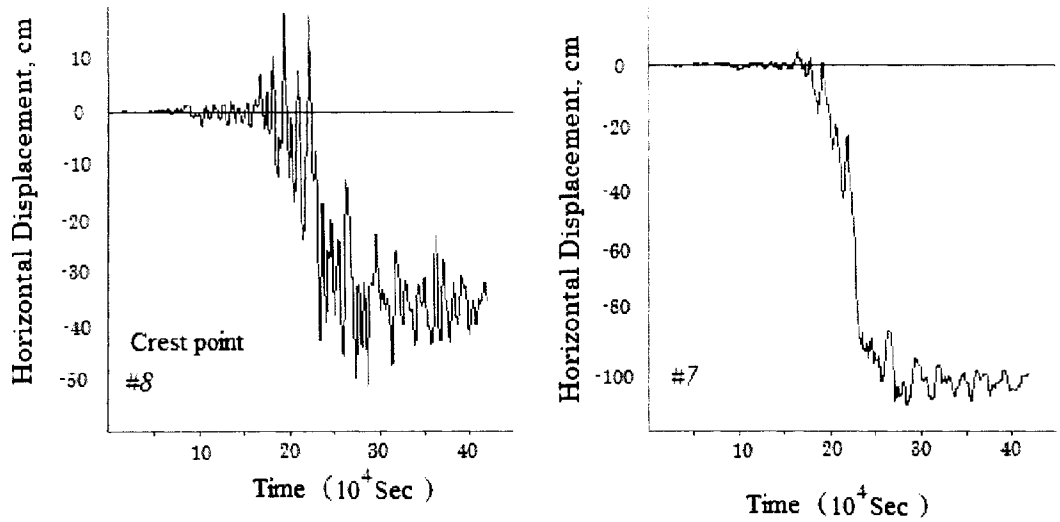

Figure 5.11 Horizontal displacement time-history at the crest point (#8 and #7). The maximum downhill displacement is over 50 cm at #8 and 105 cm at #7.

Figure 5.12 shows the *PGA* and *PGA* amplification ratio at different locations (monitoring points) along the surface of the ridge. The *PGA* is obtained from the horizontal acceleration time-history, and the *PGA* amplification ratio is the value of the *PGA* at each point over the *PGA* of point #1 (the foot of the slope). The *PGA* at points #1 and #2 is about 0.6 g. With increasing elevation along the slope, *PGA* increases and reaches 1.56 g at point #8 (the crest). At the top of the ridge, *PGA* remained above 1.43 g (#9), and reached 1.5 g (#10) on the south crest. At the bottom of the southern slope, *PGA* drops to 0.71 g (#12). The equivalent amplification ratios at the northern and southern crests reached 2.6 and 2.5, respectively. This result is consistent with the results of field monitoring in Japan (Figure 5.6).

5.6 Slope Stability of the Las Colinas Landslide

The pseudo-static method is applied in the slope stability analysis of the Las Colinas landslide. In the pseudo-static slope stability analysis, a constant horizontal acceleration was used to represent an earthquake event. A force equal to the product of the acceleration and the soil mass is applied to the slope. Figure 5.13 shows a circular

failure surface determined using the Bishop simplified method under the static condition. The slope was stable with FS=1.78. A numerical analysis using FLAC/Slope was also performed to determine critical sliding surface, and obtained a similar sliding surface and the factor of safety. Under the conditions of seismic coefficient k=0.3 and average shear strength, the results are shown in Figures 5.14 and 5.15. The results indicate that the factor of safety is 1.04 with the groundwater level below sliding surface and 0.90 with the groundwater level slightly above sliding surface. The sensitivity analysis of the effect of horizontal earthquake acceleration on the stability of the Las Colinas slope is illustrated in Figure 5.16. The safety factor calculated by the Bishop circle method shows that the critical horizontal acceleration triggering the landslide was 0.24~0.38 g.

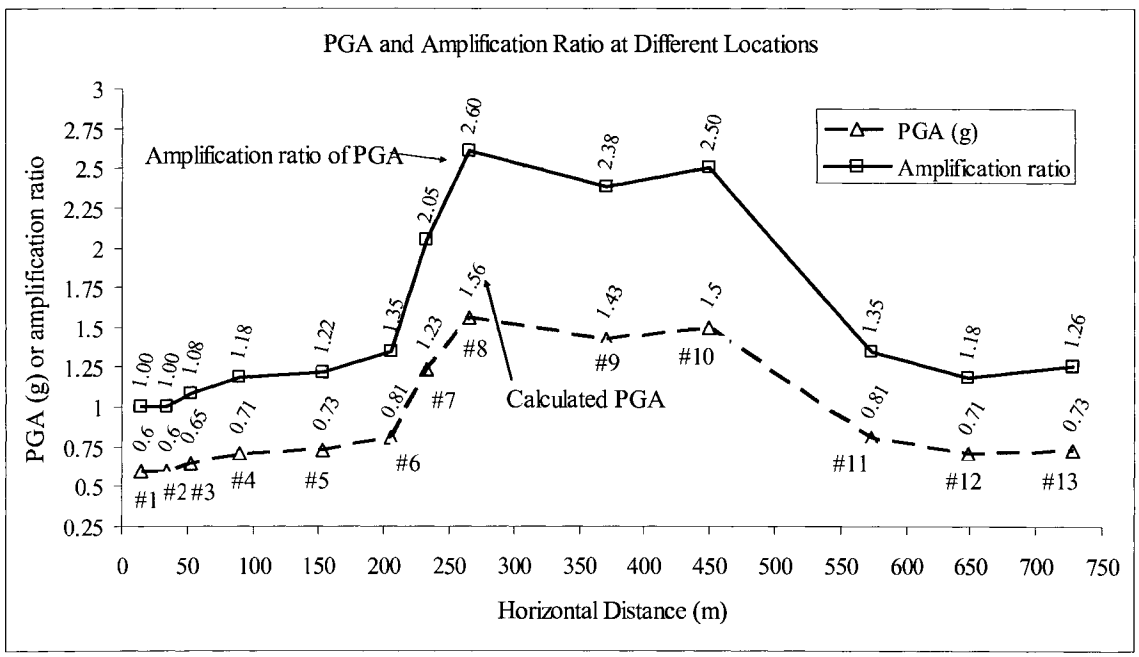

Figure 5.12 Horizontal peak ground acceleration and their amplification ratios at different surface points along the profile. Amplification ratio is the ratio of *PGA* at the local points over the input *PGA* of acceleration time-history at the base. The location of the monitoring points (such as #2) can be found in Figure 5.10.

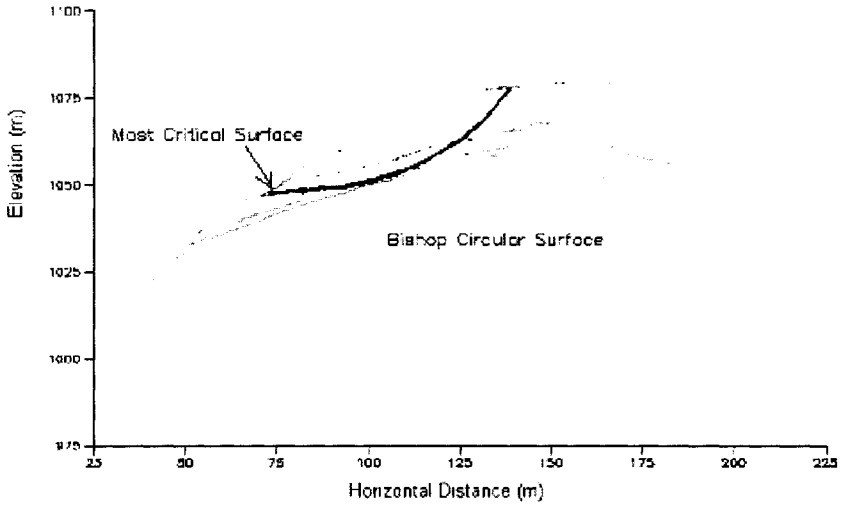

Figure 5.13 Most critical slip surface determined using the Bishop circular method at the static condition (without earthquake). The slope is stable with FS=1.78.

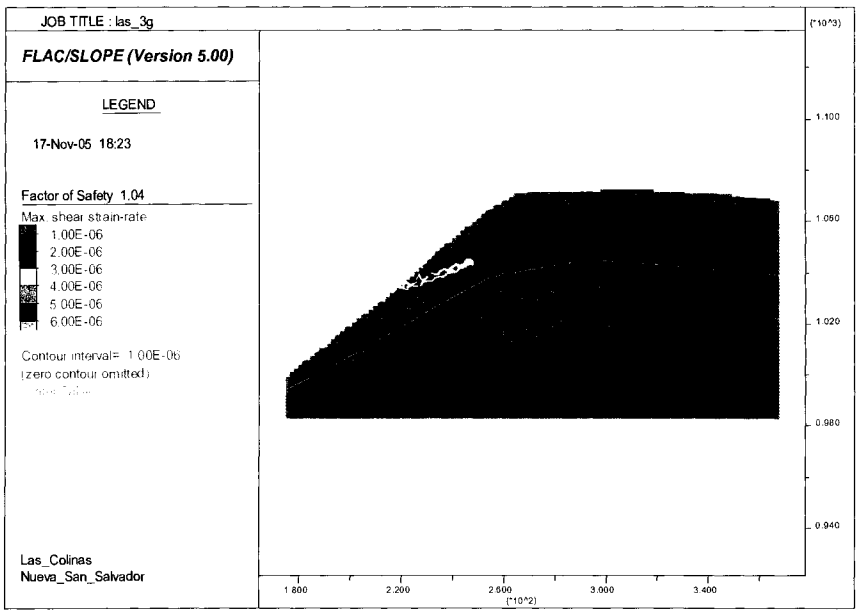

Figure 5.14 The most critical slip surface determined using the strength reduction method under the condition of seismic coefficient k=0.3. The area of higher shear strain rate forms the sliding surface. The groundwater level is below the sliding surface. Under this condition, the factor of safety is 1.04.

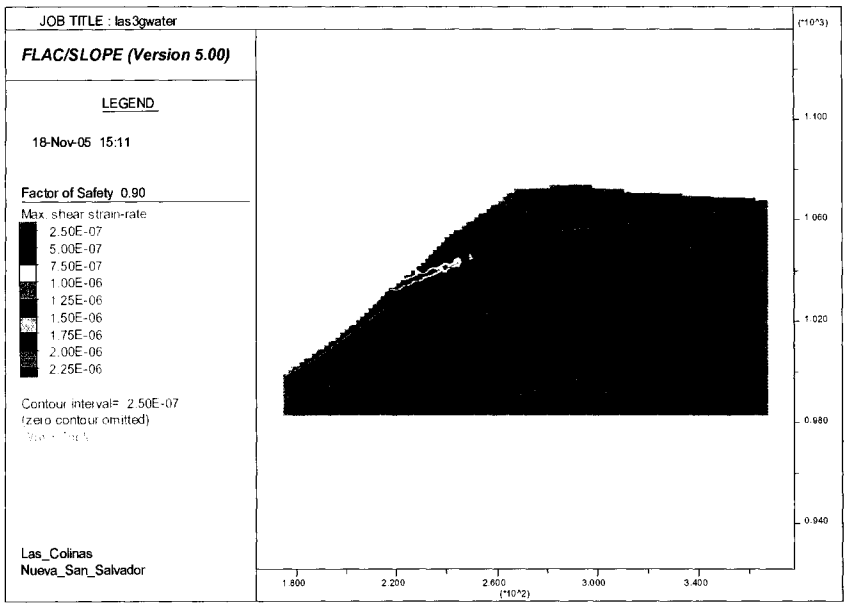

Figure 5.15 The most critical slip surface, with the conditions as in Figure 5.14 except for the groundwater level. When the groundwater level rose to above the sliding surface, the factor of safety dropped to 0.90.

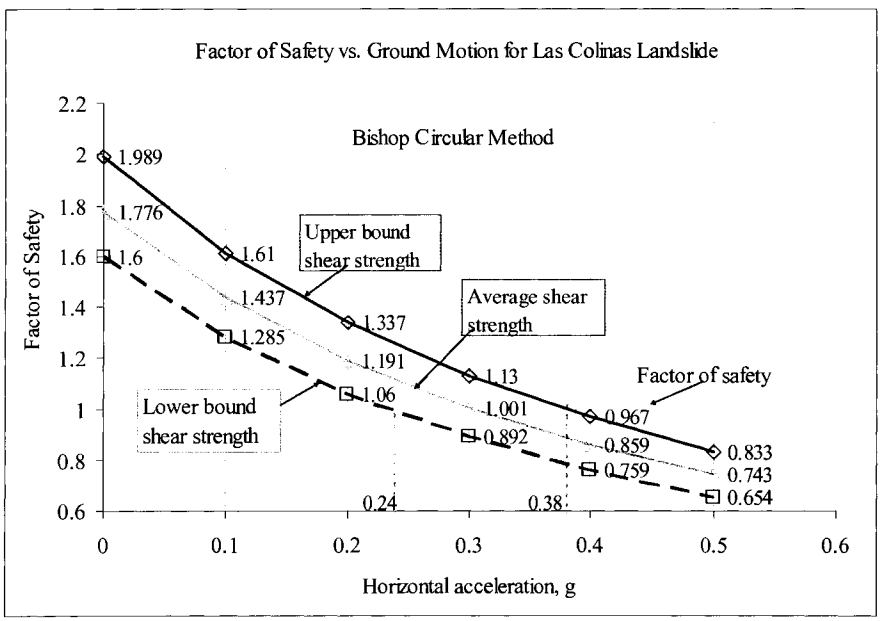

Figure 5.16 Sensitivity analysis of the effect of horizontal earthquake acceleration on the slope stability using the pseudo-static analysis method with the upper bound, average, and lower bound shear strength value of the soil mass (Table 4.5). The groundwater table is similar to Figure 5.15.

Chapter 6 Regional Earthquake-Induced Landslide Hazard Zonation: Block Sliding Model

6.1 Introduction

Seismic-induced landslide hazard maps indicate the susceptibility of slope failure under potential earthquake shaking. Accordingly, hazard zonation maps should display the location of actual and potential slope failures and provide information on the time or probability of their future occurrences (i.e., the return period). The method developed in this research could be used to generate landslide hazard maps over a large area and to identify zones with different priorities for engineering and land use planning. In geotechnical engineering, the pseudo-static seismic method is commonly used in the evaluation of slope stability. Also, in many cases, the dynamic displacement model developed by Newmark (1965) has been used in earthquake-induced landslide assessment (Jibson, 1987, Jibson et al., 1998). Both the pseudo-static and Newmark models have been used not only to assess the stability of an individual slope but also to assess stability over a large area, especially in GIS-based earthquake-induced landslide hazard zonation.

The most common method used to determine seismic-induced slope stability is to calculate the pseudo-static factor of safety (FS), critical horizontal acceleration (a_y), and Newmark displacement (u) based on deterministic methods. Landslides, in which a planar slip surface is approximately parallel to the ground surface, can be analyzed effectively using the infinite slope analysis method (Skempton and Delory, 1957). In the infinite slope model, the soil is assumed to slide on a planar slip surface, and the slope is assumed to be infinite in extent at an inclination, α, to the horizontal.

The infinite slope model has been adopted by many researchers to perform the slope stability analysis in GIS-based landslide hazard zonation. It is the preferred model mainly because geotechnical parameters and the geometry of landslides cannot be well defined in a study area. However, in most cases, the sliding surfaces are not parallel to the slope surfaces; this is especially true for the deep circular failure mode in

homogenous slope materials. The depth of the potential sliding mass is not constant. In this case, the block sliding model developed in this study can be used to better assess slope stability.

Another method described in this chapter is probabilistic analysis considering the uncertainties of geotechnical parameters. The Monte-Carlo method is applied to simulate the probabilistic distribution of geotechnical, seismic, and hydrogeological parameters.

In GIS-based raster data analysis, a grid square (or a cell, or a pixel) represents a 1D infinite slope element or a sliding block with the same size as the grid unit. Therefore, the slope can be viewed as a combination of number of sliding blocks. Slope stability analysis can then be performed based on each block. The output maps include the pseudo-static factor of safety, Newmark displacement, or critical acceleration, and failure probability of grids, indicating the landslide susceptibility of a study area.

6.2 Infinite Slope Model

The infinite slope model is a one-dimensional model describing the stability of slopes with an infinitely long failure plane. Failure is assumed to occur by sliding of a slab of soil on a planar slip surface which is parallel to the ground surface. It is only applicable to the calculation of shallow translational slides (Figure 6.1).

Considering individual block sliding, the formula to calculate the static safety factor is as follows (Skempton and Delory, 1957):

$$FS = \frac{c' + (\gamma - m\gamma_w) H \cos^2 \alpha \tan \phi'}{\gamma H \sin \alpha \cos \alpha} \tag{6.1}$$

Taking into account the horizontal earthquake inertial force, kW, proportional to the weight of the body, W, by a critical horizontal acceleration k, the factor of safety becomes (Van Westen, 1996, Luzi et al., 2000):

$$FS = \frac{c' + (\gamma H \cos^2 \alpha - \gamma H k \cos \alpha \sin \alpha - \gamma_w h_w \cos^2 \alpha) \tan \phi'}{\gamma H \sin \alpha \cos \alpha + \gamma H k \cos^2 \alpha} \tag{6.2}$$

where: ϕ' is effective friction angle (°); c' is effective cohesion (kPa); γ is unit weight of sliding mass (kN/m^3); γ_w is unit weight of water (kN/m^3); H is depth of failure surface below the ground surface (m); h_w is height of water table above sliding surface (m); α is slope surface angle (°); k is seismic coefficient. The h_w can be replaced with $m \cdot h$, as $m = h_w/H$; m can be considered as a groundwater saturation ratio.

If one also considers the vegetation root strength c_r and tree surcharge q_0, the value of root strength will be added to the cohesion, and the soil weight will include additional tree surcharge.

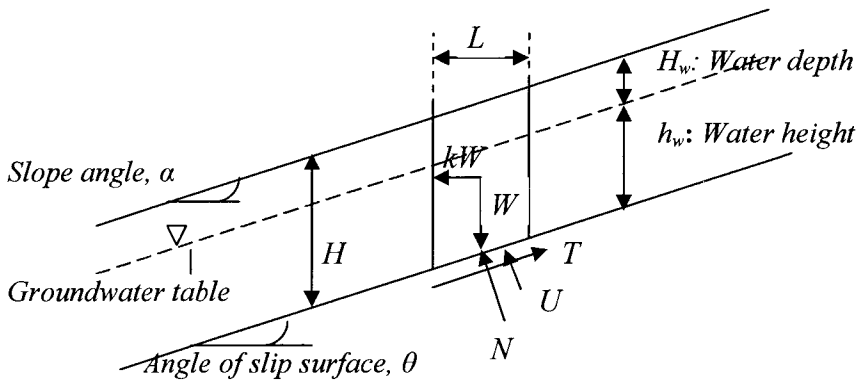

Figure 6.1 Infinite slope model: slice of an infinite slope (T is shear strength; N is normal force of the slice; U is water force; L is width of a slice, H_w is depth of groundwater table, and θ is dip angle of slip surface)

6.3 Block Sliding Model

An individual block, a grid in GIS raster dataset, is shown in Figure 6.2. According to the limit equilibrium principle, the formula to calculate the static safety factor of this block along the sliding direction is as follows:

$$FS_{static} = \frac{c'A + (W\cos\theta - U)\tan\phi'}{W\sin\theta} \qquad (6.3)$$

where: θ is slip surface dip angle along sliding direction.

Taking into account the earthquake horizontal acceleration, the pseudo-static factor of safety of the block is:

$$FS_{pseudo} = \frac{c'A + (W\cos\theta - kW\sin\theta - U)\tan\phi'}{W(\sin\theta + k\cos\theta)} \tag{6.4}$$

where: A is area of sliding surface, m^2; U is water force, kN. The other means of notation are the same as those of Equation 6.2. A can be calculated as:

$$A = L^2 / \cos\theta \tag{6.5}$$

where: L is the width of a block, m.

The U can be calculated as:

$$U = \gamma_w h_w A \tag{6.6}$$

where h_w is the average height of the water column as shown in Figure 6.2.

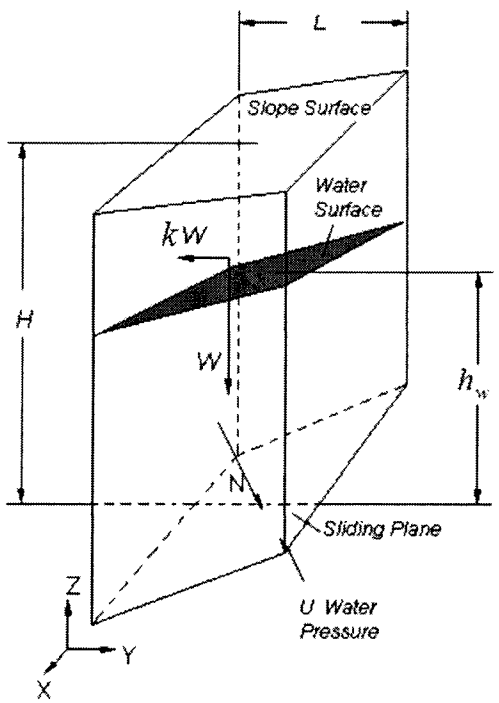

Figure 6.2 A sliding block in the 1D slope analysis model (H: height of the block; L: width of the block; h_w: groundwater height from sliding surface; U: water force; W: weight of the block; and N: normal force acting on the sliding surface)

If the thickness of the sliding block is assumed to be uniform and the dip angle of the slip surface equals the slope surface angle, the block sliding model becomes the infinite slope model. Hence, the infinite slope model can be considered as a special case of the block sliding model.

6.4 Newmark Displacement of Block Sliding

Newmark (1965) defined the following relationship to calculate the critical acceleration (yield acceleration) in the case of planar slip:

$$a_y = (FS_{static} - 1)\sin\alpha \tag{6.7}$$

where FS_{static} is the static factor of safety of a slope and α is the thrust angle of the landslide block, which can be approximated by the slope angle for an infinite slope model or the angle of the sliding surface for a block sliding model.

The critical horizontal acceleration also can be directly derived from the slope stability equation. For infinite slope, setting FS equal to unity in Equation 6.2, the corresponding critical acceleration (k value when static FS=1) can be calculated as:

$$a_y = \frac{c'/\cos^2\alpha + (\gamma - m\gamma_w)H\tan\phi' - \gamma H\tan\alpha}{\gamma H + \gamma H\tan\alpha\tan\phi'} \tag{6.8}$$

For the block sliding model (Equation 6.4), the critical acceleration is:

$$a_y = \frac{cA - W\sin\theta + (W\cos\theta - U)\tan\phi}{W(\cos\theta + \sin\theta\tan\phi)} \tag{6.9}$$

The Newmark displacement analysis requires a prior knowledge of the static factor of safety, slope angle, and earthquake strong-motion record. Many different regression equations have been developed utilizing the basic Newmark (1965) methods. Ambraseys and Menu (1988) developed a simple displacement prediction equation based on peak and yield acceleration:

$$\log u = 0.90 + \log\left[\left(1 - \frac{a_y}{a_{\max}}\right)^{2.53}\left(\frac{a_y}{a_{\max}}\right)^{-1.09}\right] \qquad (6.10)$$

Where u is the estimated down slope permanent displacement caused by an earthquake, cm; a_y is yield acceleration, g; and $a_{\max}$ is peak ground acceleration (PGA) of the design earthquake, g.

Equation 6.10 is valid for $0.1 \leq a_y/a_{max} \leq 0.9$, and a_y is computed using the residual strength of the soil. Based on the Newmark (1965) method, Equation 6.7 is valid only for those cases where the pseudo-static factor of safety is less than 1.0. In essence, the peak ground acceleration $a_{\max}$ must be greater than the horizontal yield acceleration a_y (Day, 2002).

Jibson (1993) used a regression equation to estimate Newmark displacement as a function of Arias Intensity and critical acceleration:

$$\log u = 1.46 \log I_a - 6.642 a_y + 1.546 \qquad (6.11)$$

where u is the displacement, cm; I_a is Arias Intensity, m/sec; and a_y is yield acceleration, g. The model's standard deviation is 0.409.

Jibson et al. (1998) modified Equation 6.11, and used a much larger group of strong-motion records from 13 earthquakes in California with 280 recording stations to develop a new equation:

$$\log u = 1.521 \log I_a - 1.993 a_y + 1.546 \qquad (6.12)$$

The model's standard deviation is 0.375. The Newmark displacement again can be estimated as a function of Arias Intensity and critical acceleration.

Yegian et al. (1991) developed an expression to calculate the median normalized Newmark displacement (u_n) considering earthquake frequency and duration. Newmark displacements were calculated for the regression analysis by double-integrating 348 time histories of actual earthquakes, which were compiled by Franklin and Chang (1977).

$$\log\left(\frac{u_n g}{a_{\max} N_{eq} T^2}\right) = 0.22 - 10.12\frac{a_y}{a_{\max}} + 16.38\left(\frac{a_y}{a_{\max}}\right)^2 - 11.48\left(\frac{a_y}{a_{\max}}\right)^3 \qquad (6.13)$$

The model's standard deviation, $\sigma_{\log u_n}$, is 0.45. In the above equation, u_n is normalized Newmark displacement, cm; N_{eq} is an equivalent number of cycles, and T is the predominant period of the input motion, sec. To employ this model, values for two parameters, N_{eq} and T, need to be selected. The mean number of equivalent cycles for an M=7 earthquake is approximately 8 according to Seed et al. (1975). Based on Seed et al., (1969), the predominant period is approximately 0.30 s at rock outcrops for distances less than 40 km.

The *PGA* is the most commonly used ground motion parameter in seismic hazard assessment and Newmark displacement calculation. A number of regression equations of attenuation relationships for different geographic and tectonic environments have been developed. For earthquakes in a subduction zone, peak ground acceleration can be predicted by Atkinson and Boore's model (Atkinson and Boore, 2003, Cepeda et al., 2004), which was mentioned in Chapter 5.

The different permanent displacement approaches were compared for seismic slope stability analysis by Miles and Keefer (1999) based on a case study of the Oakland East Quadrangle in California. A summary of the statistics of Newmark displacement and standard deviation is provided in Table 6.1. The displacements obtained using these three methods lead to strikingly different results. The method used by Yegian et al. (1991) obtained the highest value, while method by Jibson et al. (1998) had a smaller value. The displacement calculated by Ambraseys and Menu's (1988) method is between the results obtained by the Yegian et al. and Jibson et al. methods.

For landslide hazard zonation, a proper threshold value is required for grouping hazard zones. As mentioned in Chapter 2, Wieczorek et al. (1985) used 5 cm as the critical displacement for ground cracking and slope failures assessment in San Mateo County, California. Keefer and Wilson (1989) used 10 cm as the critical displacement for coherent landslides in southern California, and Jibson and Keefer (1993) used a 5~10 cm range as the critical displacement for landslides in the Mississippi Valley. The above threshold values can be used for displacement-based landslide hazard zonation.

Table 6.1 Summary of the statistics of Newmark displacement and standard deviation for dry and saturated conditions (Miles and Keefer, 1999)

Approaches		Mean (cm)	Min(cm)	Max (cm)	σ (cm)
Ambraseys and Menu (1988)	Dry	2.22	0.08	308.35	8.66
	Saturated	13.17	0.10	520.97	45.15
Yegian et al (1991)	Dry	6.89	0.00	1250.25	34.72
	Saturated	44.74	0.00	1607.57	170.63
Jibson et al (1998)	Dry	1.42	0.09	311.35	5.59
	Saturated	10.72	0.12	598.93	44.35

6.5 Probability and Reliability Analysis of Slope Stability

6.5.1 Uncertainty, Reliability and Probability

Most observed phenomena contain a certain degree of uncertainty. Slope stability analysis deals with the uncertainty of geotechnical parameters and environments. Geological conditions, the spatial variability of soil/rock properties, and the presence of ground water, the inadequacy of test data, simplification of the analysis model, seismic events, and rainfall events are all factors with uncertainty. Conventional deterministic slope stability analysis does not account for the above uncertainties in an explicit manner and usually relies on a conservative approach to deal with the problem of uncertainty. Probabilistic methods, which complement conventional analysis, provide the means for quantifying such uncertainty.

Reliability analysis deals with the relationship between the load a system must carry and its ability to carry this load. Because the load and the resistance may be uncertain, the result is also uncertain. It is common to express reliability in the form of a reliability index, which can be related to probability of failure. In reliability analysis, safety is determined by comparing the resistance to the applied load.

In the case of slope stability analysis, if R is the resisting force and S is the sliding force, both R and S are random in nature and are statistically independent. Their

randomness is characterized by mean, standard deviation, and corresponding probability functions. When R is less than S, a shear failure occurs. Figure 6.3 shows the distributions of R and S and the definition of failure probability. The area of overlap between the two curves (the shaded region) where the R is less than S provides a qualitative measure of the failure probability (Haldar and Mahadevan, 2000). This area of overlap depends on three factors: the relative positions of the two curves, which are represented by the means (μ_R, μ_S); the dispersions of the two curves, which are characterized by the standard deviations (σ_R, σ_S), and the shapes of the two curves, which are represented by the probability density functions, $f_R(r)$ and $f_S(s)$.

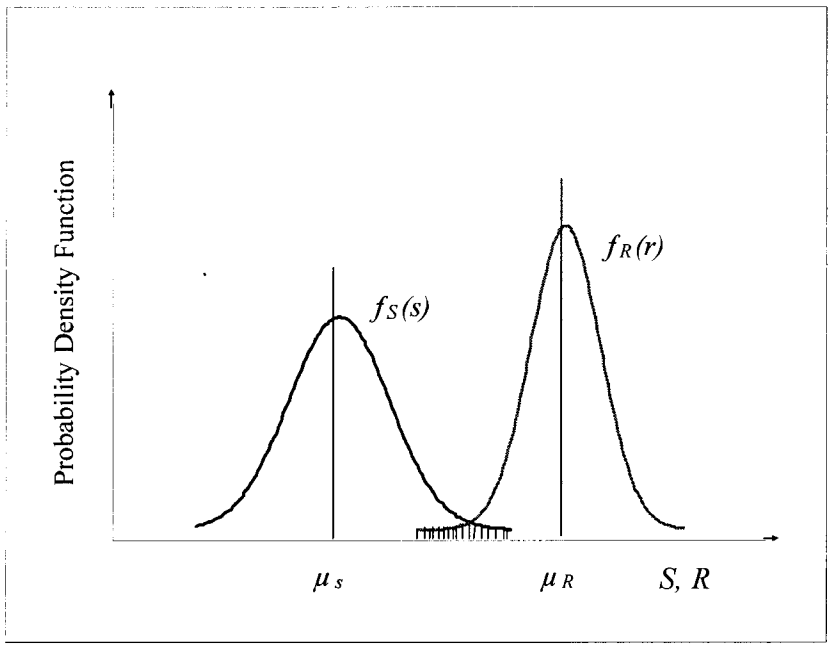

Figure 6.3 Definition of failure probability and the distribution of S and R. The area of overlap between the two curves (the shaded region) provides a qualitative measure of failure probability (Haldar and Mahadevan, 2000).

From Figure 6.3, failure probability (or risk) can be expressed as (Haldar and Mahadevan, 2000):

$$
\begin{aligned}
P_f &= P(failure) = P(R < S) \\
&= \int_0^{\infty} [\int_0^{S} f_R(r)dr] f_S(s)ds \\
&= \int_0^{\infty} F_R(s) f_S(s)ds
\end{aligned}
\qquad (6.14)
$$

where $F_R(s)$ is the cumulative distribution function (CDF) of R evaluated at s. Equation 6.14 can be considered the basic equation of the risk-based design concept.

The margin of safety, M, is the difference between the resistance and the sliding forces:

$$M = R - S \qquad (6.15)$$

If R and S are normal variables (i.e. $N(\mu_R, \ _R)$ and $N(\mu_S, \ _S)$), we can infer that M is also a normal random variable (i.e., $N(\mu_R - \mu_S, \sqrt{\sigma_R^2 + \sigma_S^2})$). Equation 6.14 can, then, be used to define the probability of failure as

$$
\begin{aligned}
& P_f = P(M < 0) \\
or \quad & P_f = \Phi\left[\frac{0 - (\mu_R - \mu_S)}{\sqrt{\sigma_R^2 + \sigma_S^2}}\right] \\
or \quad & P_f = 1 - \Phi\left[\frac{\mu_R - \mu_S}{\sqrt{\sigma_R^2 + \sigma_S^2}}\right] \\
or \quad & P_f = 1 - \Phi(\beta)
\end{aligned}
\qquad (6.16)
$$

where: Φ is the cumulative distribution function (CDF) of the standard normal variate, β is the reliability index or safety index, defined as a ratio between the mean value of M and its standard deviation in first-order reliability method:

$$\beta = \frac{\mu_M}{\sigma_M} = \frac{\mu_R - \mu_S}{\sqrt{\sigma_R^2 + \sigma_S^2}} \qquad (6.17)$$

Geotechnical engineers are usually more accustomed to dealing with the factor of safety, *FS*. The factor of safety is:

$$FS = \frac{R}{S} \qquad (6.18)$$

Failure occurs as the factor of safety drops below $FS = 1$, and the probability of slope failure, P_f, is given by:

$$P_f = P_f(FS < 1.0) \qquad (6.19)$$

However, R and S depend on other variables as well. For example, R depends on in-situ soil properties and geometric parameters. The resisting forces have uncertainty due to the inherent spatial variability of soil properties.

The reliability index, β, is a convenient measure for evaluating the stability of a slope. In terms of the mean or expected value, $E[FS]$, and the standard deviation, σ_{FS}, of the factor of safety, the reliability index is defined by:

$$\beta = \frac{E[FS] - 1}{\sigma_{FS}} \qquad (6.20)$$

Calculation of reliability is more difficult when it is expressed in terms of the factor of safety because FS is the ratio between two uncertain parameters, R and S.

The procedure for reliability analysis includes: establishing an analytical model, estimating descriptions of the parameters, calculating the statistical moments of the performance function, calculating the reliability index, and computing the failure probability.

The commonly used methods for reliability analysis in slope engineering include the first order reliability method or the Hasofer-Lind approach (FORM), the first-order second moment (FOSM) method, point estimate methods, and the Monte-Carlo simulation method (Baecher and Christian, 2003). In this research, the Monte-Carlo simulation was used.

6.5.2 The Uncertainty of Geotechnical Parameters

The uncertainty of geotechnical parameters is caused by limited material test results and the spatial variation of geological conditions. Usually, the probabilistic distribution of shear strength and unit weight can be obtained by statistical analysis of test data.

In probability analysis, the geotechnical or other parameters can be described as random variables. If x is a random variable and n observations of x are available, the mean or expected value of x, denoted as μ_x or $E(x)$, can be calculated for n observations as:

$$E(x) = \mu_x = \frac{1}{n}\sum_{i=1}^{n} x_i \qquad (6.21)$$

where $E(x)$ is a measure of central tendency in a dataset, also known as the first central moment.

The variance of x, a measure of spread in data about the mean, also known as the second central moment, denoted as $Var(x)$, can be estimated as

$$Var(x) = \frac{1}{n-1}\sum_{i=1}^{n}(x_i - \mu_x)^2 \qquad (6.22)$$

The standard deviation of a set of data x, denoted as σ_x, is

$$\sigma_x = \sqrt{Var(x)} = \sqrt{\frac{\sum_{i=1}^{n}(x_i - \mu_x)^2}{n-1}} \qquad (6.23)$$

The skewness, also known as the third central moment, is

$$Skewness = \frac{1}{n}\sum_{i=1}^{n}(x_i - \mu_x)^3 \qquad (6.24)$$

The range of a dataset denoted as r_x is the difference between the largest and smallest values of x,

$$r_x = \left|x_{\max} - x_{\min}\right| \qquad (6.25)$$

Like the standard deviation, the range is a measure of dispersion in a dataset. Range has poor statistical properties in that it is sensitive to extreme values in a data set; however, it is easily evaluated where there are insufficient observations of x and is therefore used often. However, the relationship between the standard deviation and range depends on how many observations of x are made. Assuming that the dataset has a normal distribution, the standard deviation can be estimated as follows

$$\sigma_x = (x_{\max} - x_{\min}) \cdot N_n \qquad (6.26)$$

where N_n is a multiplier (i.e., correction factor) depending on sample size. The value of N_n can be found in Table 6.2 (Baecher and Christian, 2003).

The groundwater table is affected by rainfall, drainage networks, regional hydrogeologic conditions, and slope material properties. The basic hydrogeologic method for determining the depth of the water table is field investigation, which gathers information on spring occurrence, and the depth of the water table in local wells and monitoring wells. This information can be found in regional hydrogeologic maps. However, the water table varies with climatic changes and with the seasons, and its distribution involves uncertainties which should be considered in slope stability analysis.

Table 6.2 Multipliers for estimating standard deviation for a range of a normally distributed variables (Burington and May, 1970, Snedecor and Cochran, 1989, Baecher and Christian, 2003)

n	N_n	n	N_n	n	N_n
2	0.866	11	0.315	20	0.286
3	0.510	12	0.307	30	0.244
4	0.486	13	0.300	50	0.222
5	0.430	14	0.294	75	0.208
6	0.395	15	0.288	100	0.199
7	0.370	16	0.283	150	0.190
8	0.351	17	0.279	200	0.180
9	0.337	18	0.275		
10	0.325	19	0.271		

Note: n is observations of a random variable; N_n is correct factor, see Equation 6.26.

Equations 6.21 to 6.25 can be used for statistical analysis of geotechnical parameters. For shear strength, unit weight, or groundwater, the mean, standard deviation, and best-fitting probability density function can be determined by material testing and groundwater monitoring. For the distribution of geotechnical parameters, the normal distribution is frequently used. It is symmetrical, continuous, and can be described by the following probability density function, $f(x)$:

$$f(x) = \frac{1}{\sigma_x \sqrt{2\pi}} e^{-\frac{1}{2}\left(\frac{x-\mu_x}{\sigma_x}\right)^2} \qquad (6.27)$$

where $f(x)$ = probability density function; x = samples of a population ($-\infty \leq x \leq 0$); σ_x = standard deviation of x; and μ_x= mean of x.

The mean, μ_x, and standard deviation, σ_x, are two parameters of the distribution that are usually estimated applying Equations 6.21 and 6.23 to the available data. The corresponding CDF can be expressed as:

$$F_X(x) = \int_{-\infty}^{x} \frac{1}{\sigma_x \sqrt{2\pi}} e^{-\frac{1}{2}\left(\frac{x-\mu_x}{\sigma_x}\right)^2} dx \qquad (6.28)$$

The normal distribution function is widely used in probabilistic analysis of slope engineering, and is denoted as $N(\mu_x, \sigma_x)$.

6.5.3 The Monte-Carlo Simulation

To simulate the uncertainties of geotechnical parameters, the simplest form of the basic simulation of a problem is to sample each random variable several times in order to represent its real distribution according to its probabilistic distribution. The method most commonly used for this purpose is the Monte-Carlo simulation.

The generation of random numbers for variables according to their distribution is the heart of Monte-Carlo simulation (Haldar and Mahadevan, 2000). In general, all modern computers have the capacity to generate uniformly distributed random numbers between 0 and 1. Such uniform random numbers, then, can be transformed to random numbers with appropriate characteristics. A simple example is the transformation of a uniform random number, u_i, between 0 and 1 to another uniform random number, x_i, between a and b. The transformation can be performed by using the following equations (Haldar and Mahadevan, 2000):

$$u_i = \frac{x_i - a}{b - a} \qquad (6.29)$$

or

$$x_i = a + (b - a)u_i \tag{6.30}$$

where u_i is uniform random number in [0, 1]; x_i is uniform random number in [a, b].

If X satisfies the assumption of normal distribution, N(μ_x, σ_x), then $S = \frac{X - \mu_x}{\sigma_x}$ is a standard normal variate, N(0, 1). For normal distributions, the random number can be generated as:

$$u_i = \Phi(s_i) = \Phi(\frac{x_i - \mu_x}{\sigma_x}) \tag{6.31}$$

$$s_i = \frac{x_i - \mu_x}{\sigma_x} \tag{6.32}$$

$$x_i = \mu_x + \sigma_x s_i = \mu_x + \sigma_x \Phi^{-1}(u_i) \tag{6.33}$$

Φ^{-1} is the inverse of the CDF of a standard normal variable. According to Equation 6.31, in order to generate a random number of normal distributions, the u_i values first need to be transformed to s_i, i.e., $s_i = \Phi^{-1}(u_i)$.

A computer program can be written to generate random numbers according to any distribution. There are many ways to transform an input of one set of randomly distributed variables to an output with a different distribution function. Probably the most important of these transformation functions is known as the Box-Muller (1958) transformation. It allows us to transform uniformly distributed random variables into a new set of random variables with a normal (or Gaussian) distribution.

If x_1 and x_2 are uniformly and independently distributed between 0 and 1, then u_1 and u_2 as defined below have a standard normal distribution N(0,1).

$$\begin{aligned} u_1 &= \sqrt{-2\ln x_1}\cos(2\pi x_2) \\ u_2 &= \sqrt{-2\ln x_1}\sin(2\pi x_2) \end{aligned} \tag{6.34}$$

In slope stability analysis, parameters with higher degrees of uncertainty are randomly simulated. Those parameters include friction angle, cohesion, unit weight of sliding mass, and groundwater level. The distribution of random parameters is assumed to be normal. Figure 6.4 shows the histograms of 1000 randomly generated normal distribution numbers for soil friction angle and cohesion for TB formation, respectively.

In this technique, a large number of soil variables are sampled from their known probability distribution. For each input set of random parameters, the corresponding value of the factor of safety is calculated using the infinite slope or block sliding model. In the Monte-Carlo simulation, a large number of factor of safety values is generated (for example 2000 values) by repeatedly inputting the random variable values. The final simulation output is a set of 2000 possible factors of safety which can be displayed as a histogram. The histogram can then be used to determine the distribution of factors of safety. The mean value $E[FS]$ (or μ_{FS}) and the standard deviation σ_{FS} can be determined from the simulation results using Equations 6.21 and 6.23, respectively. The probability of slope failure is the number of factors of safety, which is less than 1 over the total number of factors of safety. The reliability index β can be evaluated by Equation 6.20.

The GIS grid-based method allows calculation of the failure probability of each grid. Landslide hazard zonation can be determined by the failure probability of the grids.

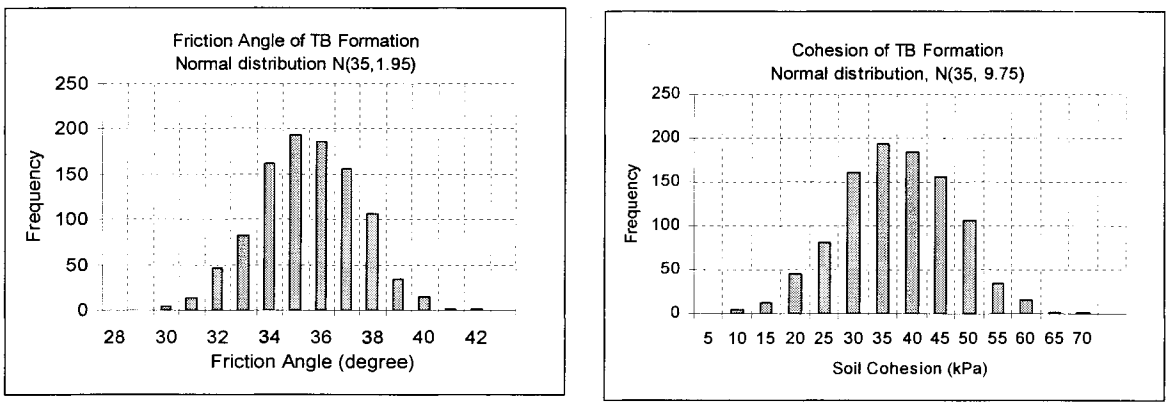

(a) (b)

Figure 6.4 Normally distributed random numbers for soil friction angle and cohesion for TB formation generated by Monte-Carlo simulation.

6.6 GIS Process

Figure 6.5 illustrates schematically the method used to evaluate slope stability and landslide hazard zonation.

The data layers needed for slope stability analysis are summarized in Table 6.3. The grid size used for the regional landslide hazard zonation is 30 m×30 m. All data sets needed for the analysis can be rasterized. The basic data format for stability analysis inside the GIS environment using ArcObjects (Burke, 2003) is the ESRI grid. For deterministic analysis of the factor of safety, Newmark displacement, and critical acceleration, the numerical operation can be performed by using ArcObjects Macro VBA (Visual Basic Application) programming. The ArcMap tools can be customized using ArcObjects with VBA programming.

For the Monte-Carlo simulation, an easier way is to export the data into the external slope stability analysis model before performing the analysis. The ESRI grid files in Table 6.3 can be transformed into point feature files. All the point data in the attribute table can be exported to text files. A VB (Visual Basic) program can easily deal with the text data files and perform the Monte-Carlo simulation. The analysis results, mean factor of safety, failure probability, and reliability index then can be imported to the GIS platform to display the result maps and perform landslide hazard zonation.

Table 6.3 Necessary data layers for slope stability analysis (block sliding model)

Data layers		Data Format	Notes
1	Slope surface angle (α)	Raster (ESRI Grid)	For Monte-Carlo simulation, the point feature data sets and deviation of random parameters (σ_m, σ_c, σ_γ, and σ_ϕ) are needed.
2	Slip surface angle (θ)	Raster (ESRI Grid)	
3	Soil friction angle and standard deviation (ϕ and σ_ϕ)	Raster (ESRI Grid)	
4	Soil cohesion and standard deviation (c and σ_c)	Raster (ESRI Grid)	
5	Soil unit weight and standard deviation (γ and σ_γ)	Raster (ESRI Grid)	
6	Soil depth (H)	Raster (ESRI Grid)	
7	Horizontal acceleration (k or PGA)	Raster (ESRI Grid)	
8	Soil saturation ratio and standard deviation (m and σ_m)	Raster (ESRI Grid)	
9	Vegetation root strength (c_r)	Raster (ESRI Grid)	

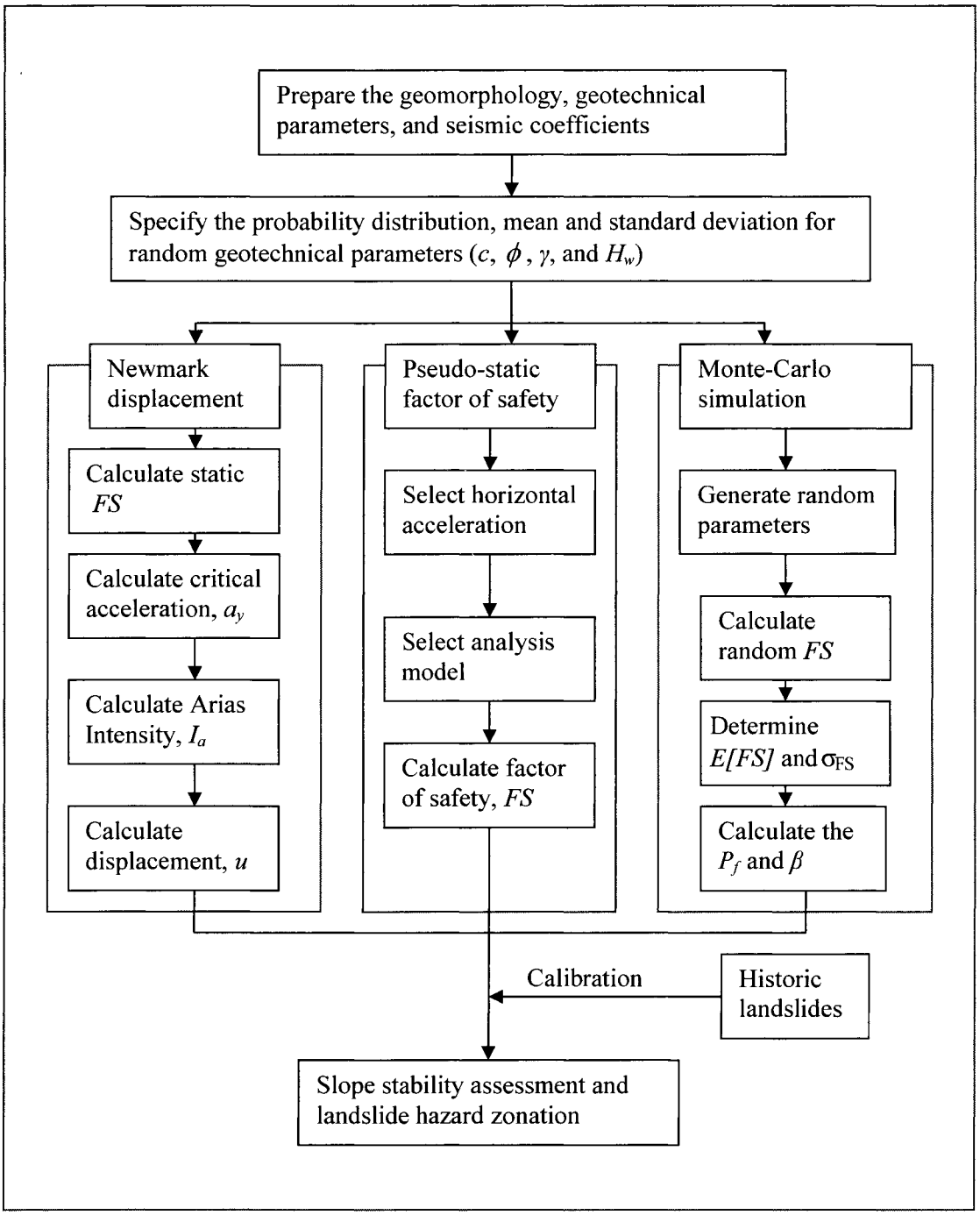

Figure 6.5 Flowchart of the 1D infinite and block sliding model for evaluating slope stability and landslide hazard zonation

6.7 Regional Landslide Hazard Zonation of Nueva San Salvador

6.7.1 General Description

Earthquake-induced landslide susceptibility maps are essential in highly earthquake prone and landslide prone regions for loss-reduction land use planning. The GIS-based infinite slope and block sliding models were applied to the test site in Nueva San Salvador. The GIS source data for analysis were processed using ArcGIS 9.1. The analysis models including pseudo-static analysis, the Newmark displacement model, and the probabilistic model (Monte-Carlo simulation) were used in regional landslide hazard zonation. The major aim of the analysis was to locate the landslide susceptible zones, assess their hazard levels, and produce landslide susceptibility maps to aid in planning for future earthquakes. Several groups of input data were used for comparison and sensitivity analysis.

6.7.2 Selection of Geotechnical Parameters

The selection of geotechnical parameters is a critical step for slope stability analysis. Field investigation and laboratory and in-situ tests are necessary for the determination of geotechnical parameters. In this study, geotechnical parameters were obtained from the published literature and geotechnical reports by Lotti C. & Association (2001). Most of the samples taken for testing were from the TB formation. The shear strengths of San Salvador, Cuscatlan, and Balsamo formations are believed to be higher than those of the TB formation. The selection of lithologic units (shown on a 30 m grid size) was based on geologic mapping of the region (Figure 3.6 in Chapter 3). For shallow landslide susceptibility analysis, the sliding formation was confined to the shallow material, which is usually weathered and has a low shear strength. For the TB formation, the friction angle according to the direct shear test is between 30° and 39°, and the cohesion varies between 6 and 90 kPa. For the unweathered bedrock, cohesion can

exceed 180 kPa but the friction angle remains about 40°. The dry unit weight of volcanic soil is very low and varies between 11 and 18 kN/m^3. Table 6.4 shows the mean and standard deviation of selected geotechnical parameters calculated using Equation 6.26 based on the average value and range of geotechnical parameters listed in Table 4.7. The N_n value in Equation 6.26 is assumed to be 0.325 for S4 formations because more tests were performed on TB soil. For other formations, the soil testing was very limited, and hence the N_n value is assumed to be 0.486.

Table 6.4 Shear strength parameters applied in landslide hazard zonation of Nueva San Salvador

Formation	Units	Friction (ϕ°)		Cohesion, c (kPa)		Unit Weight, γ (kN/m^3)	
		Mean	$\sigma_{tan\phi}$	Mean	σ_c	Mean	σ_γ
San Salvador	S5	39	3.888	75	14.58	15	1.944
	S4	35	1.95	35	9.75	12	0.65
	S3	36	2.916	50	9.72	13	1.944
	S2	38	2.916	65	14.58	13	0.972
Cuscatlan	C3	39	3.888	80	19.44	15	1.944
	C1	40	3.888	85	19.44	15	1.944
Balsamo	B3	41	4.86	110	19.44	17	1.944
	B1	42	4.86	120	29.16	17	1.944

Because of Nueva San Salvador's tropical weather, most of the land in the study area is covered by orchard/plantation, coffee trees, and dense bushes. The root strength thus increases slope stability. The general root strength varies from 3.7 to 12.6 kPa (Wu, 1984). For simplicity, the root strength is added to soil cohesion. The surcharge of vegetation is ignored because it has no significant influence on the slope stability based on the block sliding method. By using Landsat satellite images and professional judgment the vegetation can be divided into 4 classes. The root strength of each of these classes is listed in Table 6.5.

Table 6.5 Root strength of vegetation

Vegetation Class	Vegetation	Type	Root strength (kPa)
1	Heavy vegetation area	Orchard/coffee plantation	10
2	Moderate vegetation area	Orchard	5.7
3	Scattered tree area	Tree	3.0
4	Grass and bared land	Tropical grass	0

6.7.3 Peak Ground Acceleration

Pseudo-static slope stability analysis requires a properly selected seismic coefficient. The general method for determination of PGA is listed in Table 2.5 (Chapter 2). Generally, for slope, dam, and embankment stability analysis, the selected horizontal seismic coefficients are 0.15 to $0.5a_{max}/g$.

The seismic hazard maps of El Salvador (with 475-year return period accelerations) proposed in different studies are shown in Figure 5.3 (Chapter 5). In Figure 5.3, four authors give different peak ground accelerations, namely 0.45~0.5 g, 0.8 g, 0.31 g, and 1.0 g. According to the slope stability study of the Las Colinas landslide using the pseudo-static analysis (Luo et al., 2004), the yield acceleration of the Las Colinas landslide was 0.3 g under unsaturated soil conditions. The January 13, 2001 earthquake was probably the largest earthquake encountered in the region. Thus, the PGA of that earthquake was selected as a_{max} for regional landslide hazard zonation. In this regional landslide hazard zonation, the amplification of ground motion was ignored. The upper bound seismic coefficient value of $0.5a_{max}/g$ was selected for pseudo-static analysis. Based on the January 13, 2001 earthquake records, the horizontal acceleration in the study area predicted using geostatistic method (ordinary kriging) was about 0.4~0.8 g. Hence, the actual seismic coefficients, k, applied in the slope stability analysis were 0.2 to 0.4.

6.7.4 Landslide Depth and Groundwater Conditions

The slope failures triggered by earthquakes in El Salvador have been relatively shallow. From the statistics of 144 earthquake triggered historic landslides, 76% of the landslides had a depth of 2~6 m and 15% of the landslides had failure depth over 20 m. The infinite slope model is suitable for shallow mass sliding. Table 6.6 shows the soil depths used in the regional hazard assessments by different authors. The general failure depth applied in these analyses was 2 to 8 m.

Table 6.6 Soil depth used in application of regional landslide hazard assessment by different authors

Authors	Approach	Soil Depth in Analysis	Lithology Types
Luzi et al., 2000	Infinite slope model	4~8 m	Debris, sandstone, marble, igneous etc.
Jibson et al., 1998	Infinite slope, Newmark displacement	2.4 m	Sandstone, silt, clay, shale, Quaternary deposits, etc
Van Westen and Terlien, 1996	Infinite slope model	1~10 m	Volcanic ash and filling materials
Khazai and Sitar, 2002	Infinite slope model	0.5~2 m	Sandstone and clayey rock, etc.

The groundwater conditions in the study area are not exactly known. During the dry summers, geologist at SNET observed a layer of soil 7 m thick composed of almost dry, median to coarse grains in the Las Colinas area. The rest of the geological layer overlaying the welded ignimbrite (call TB in the profile), is predominantly fine grains, and median and coarse material which has capillary water but is not under a saturation condition. Even in the dry season, there are springs in the Las Colinas landslide zone coming out along the fractures in the ignimbrite or in the contact zone between the top of the ignimbrites and the ashes. During the rainy season, there are some narrow zones where the layers might be saturated and associated with paleo topographic depressions. This water could feed the fractures in the ignimbrites (TB). These zones are more susceptible to landslides triggered by earthquakes or heavy rainfalls (Hernandez, 2005).

In this research, the geologist at SNET suggested using 7m thickness for shallow landslide analysis. The groundwater table is changeable, so an assumption of a watertable 5m deep (m=0.3) was used to generate landslide hazard zonation. Dry and fully saturated conditions were also considered for comparison. The fully saturated condition represents a scenario with water table coinciding the ground surface. The dry condition represents a scenario with the water level at a depth greater than the depth of sliding surface.

6.7.5 Model Validation

Validation is a vital procedure for landslide hazard assessment. Once the results of landslide susceptibility have been assessed using the analysis model, the model or input data used in the analysis should be checked for accuracy and reliability.

To validate and fine tune the analysis model, field investigation, satellite images, and past landslide information are used. This validation is a necessary step to decide whether the calculated factors of safety and displacement are acceptable, and whether analyzed high landslide susceptibility areas are consistent with the past slope failure areas. If the calculated static factor of safety is less than 1.0 in a stable area, one can infer that the selected geotechnical parameters might be lower than the actual parameters or that the selected groundwater level is higher than the actual conditions. Considering the uncertainty of these parameters, back analysis to determine well-suited geotechnical parameters is required.

El Salvador was hit by at least 14 destructive earthquakes with intensity up to X from 1915 to 2001. The information on triggered landslides is available for the most recent events. The January 13, 2001 earthquake was use to validate the analysis model.

6.7.6 Results

The calculated cases of regional landslide hazard zonation of Nueva San Salvador are listed in Table 6.7. These analyses considered the seismic coefficient k=0.5a_{max}/g, dry and partially saturated soil conditions (m=0.3, depth of the groundwater table H_w=5 m), and interpolated soil depth. The final maps are represented by the critical acceleration, Newmark displacement, factor of safety, failure probability, and reliability index, which are then used to classify the study area into five landslide susceptibility zones.

Table 6.7 The conditions used in regional earthquake-induced landslide hazard zonation

Cases	Evaluation Parameters	Horizontal Seismic Coefficient, k_h	Groundwater	Soil Depth H	Method
1	Yield acceleration	N/A	Dry	Interpolated	Pseudo-static
2	Displacement	a_{max} of Jan 13, 2001	Dry	Interpolated	Newmark
3	Factor of safety	$0.5a_{max}/g$	Dry	Interpolated	Pseudo-static
4	Factor of safety	$0.5a_{max}/g$	m=0.3	Interpolated	Pseudo-static
5	Failure probability Reliability index	$0.5a_{max}/g$	m=0.3	Interpolated	Monte-Carlo

From a geotechnical engineering point of view, a factor of safety FS<1.0 indicates an unstable slope, while if FS=1.0~1.15, the slope is marginally stable. For pseudo-static slope stability analysis, an acceptable factor of safety is 1.15 or greater. A factor of safety of 1.5 is typically an acceptable condition for a stable slope. For Newmark displacement, a slope will be considered critical if its displacement value is 5~10 cm. The acceptable displacement should be less than 5 cm. Therefore, landslide susceptibility can be evaluated using the slope stability index. Following general practice, the degrees of landslide hazard were grouped into five susceptibility zones (see Table 6.8).

As expected, most unstable slopes with lower critical acceleration and factors of safety and with higher displacement and failure probability are associated with steep slope angles and lower shear strength areas.

Table 6.8 The landslide susceptibility zones, evaluation parameters, and ranges for each landslide susceptibility zone

Zones	Landslide susceptibility	a_y (g)	u (cm)	*FS*	*FP*	*RI*
1	Very high landslide susceptibility zone, landslides are expected.	0~0.2	>10	<1	>0.5	<0
2	High landslide susceptibility zone, landslides are likely to occur.	0.2~0.3	5~10	1~1.15	0.5~0.1	0~1.0
3	Moderate landslide susceptibility zone, moderate levels of landslide hazard exist.	0.3~0.6	2~5	1.15~1.3	0.1~0.05	1~2
4	Low landslide susceptibility zone, landslides are not likely to occur	0.6~0.8	0~2	1.3~1.5	0.005	2~3.0
5	Very low landslide susceptibility zone, safe slopes.	>0.8	0	>1.5	<0.005	>3.0

Notes: a_y = yield acceleration or critical acceleration; u=Newmark displacement, *FS*=factor of safety; *FP*=failure probability; *RI*=reliability index

Figures 6.6 and 6.7 show the yield acceleration and Newmark displacement obtained from the block sliding model assuming dry soil conditions. The values of yield acceleration and displacement were grouped into five ranges to illustrate the relative landslide susceptibility in the maps.

The areas with very high landslide susceptibility (those where the computed yield acceleration is less than 0.2 g or the displacement is greater than 10 cm) are distributed in the Balsamo Ridge area (south of Nueva San Salvador), the Pan-American Highway area (west of Nueva San Salvador), and the San Salvador volcano crater. Many unstable slopes are also located in the south part of the study area because of its steep geomorphologic features.

The Balsamo Ridge area, especially in the area of the Las Colinas landslide, is a critical area because of its proximity to a community with a high population. The shear strength of soil is relatively low and the slope is steep. The January 13, 2001 earthquake triggered a large landslide (the Las Colinas landslide) and caused a disaster to the neighborhood. Slope mitigation is needed for the ridge area.

The Pan-American Highway was built along a drainage valley. Some of the slopes on the northern side of highway were steeply cut with slope angles over 70°. It is a dangerous area prone to rock falls and block sliding, which actually occurred during the 2001 earthquakes.

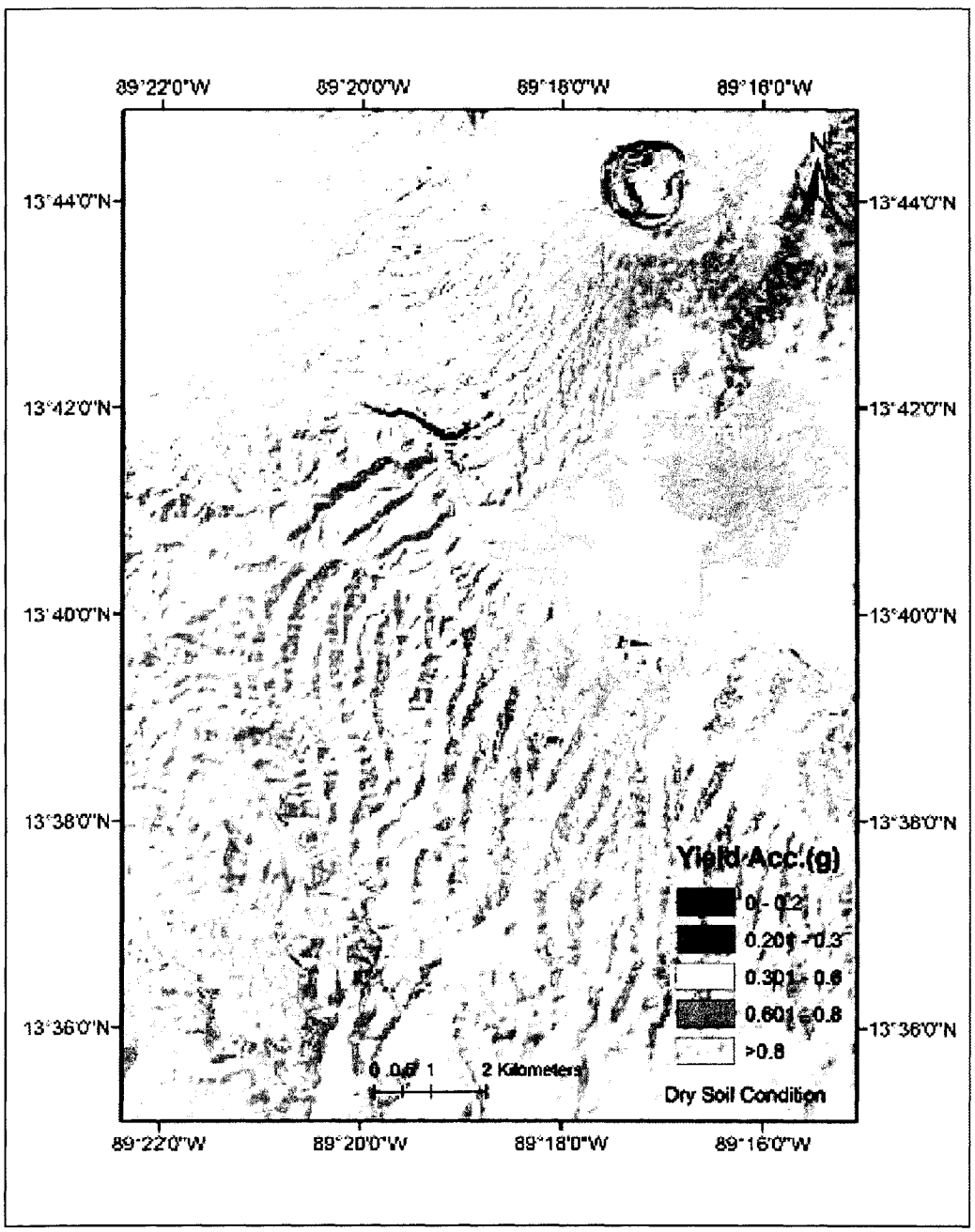

Figure 6.6 Map of the horizontal yield (critical) acceleration calculated using the block sliding model (dry soil condition).

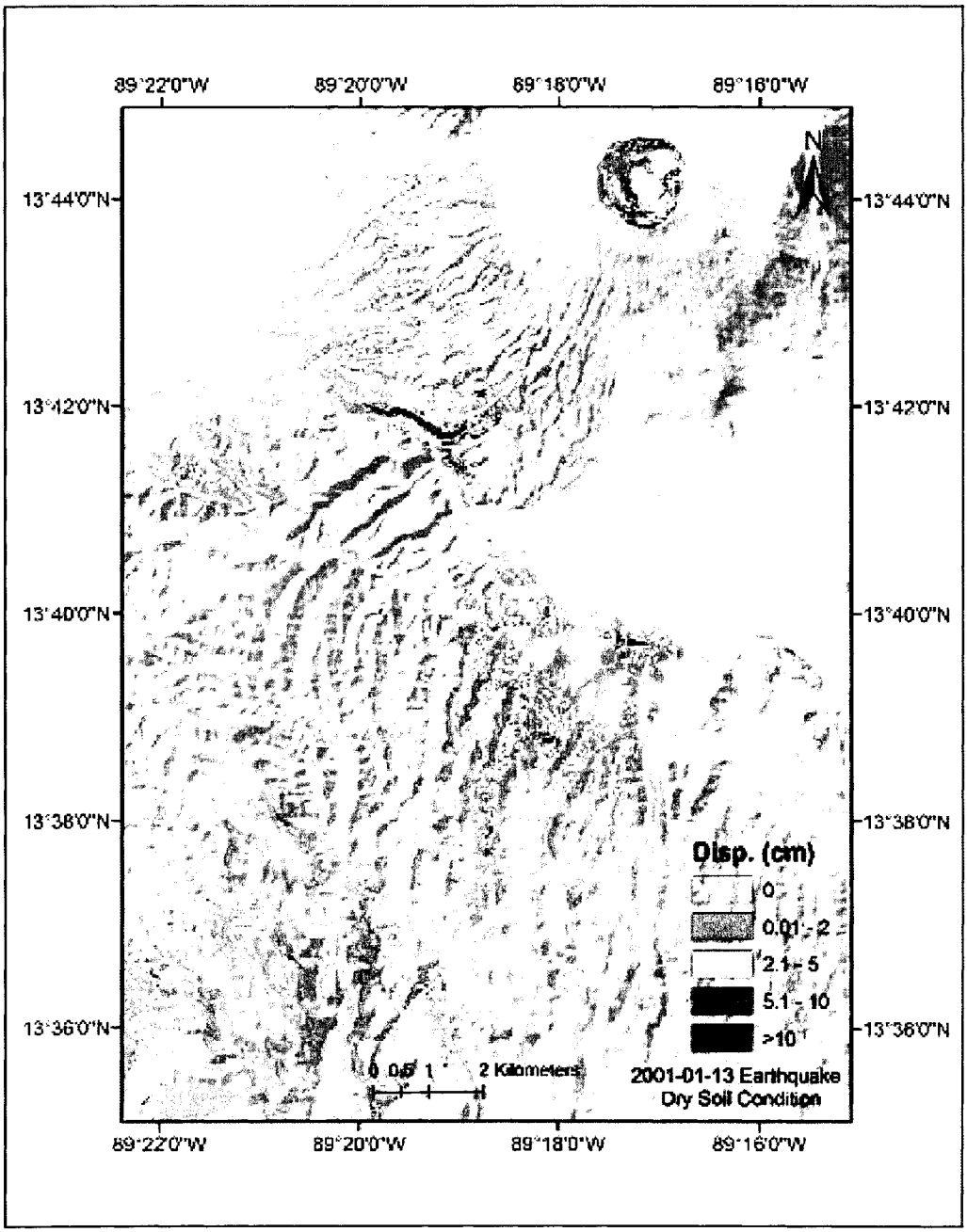

Figure 6.7 Map of the Newmark displacement calculated using the block sliding model and the empirical equation (dry soil condition, 2001 earthquake)

The volcanic crater area is also a high landslide susceptibility zone due to steep slopes. Some residential and hospitality facilities have been developed around the crater. A landslide damage analysis should be conducted in order to reduce the landslide risk.

Figure 6.8 shows a landslide susceptibility map representing factors of safety at dry soil condition and $k=0.5a_{max}/g$. The locations of very high landslide susceptibility areas (FS<1) are similar to those on the displacement map with (u>10 cm).

Groundwater conditions during earthquake shaking are poorly understood, but they need to be considered in landslide hazard zonation. Several sensitivity analyses were performed in response to changes of groundwater level. The degree of soil saturation has a significant impact on the landslide susceptibility. Figure 6.9 shows the factor of safety at groundwater saturation ratio m=0.3 (groundwater depth H_w=5 m). The area of very high susceptibility (FS<1) in saturated soil conditions is more than ten times the area of high susceptibility in dry soil conditions.

Figure 6.10 shows the percentage (%) and area (km^2) of each landslide susceptibility zone. In dry soil condition in the study area, the percentage and area of very high landslide susceptibility are 0.12% and 0.29 km^2, respectively. In contrast, when groundwater saturation ratio m=0.3, the percentage and area of very high landslide susceptibility are 1.08% and 2.36 km^2, respectively.

The corresponding landslide susceptibility maps presented by failure probability and the reliability index are shown in Figures 6.11 and 6.12. In probabilistic analysis, the factor of safety is related only to the mean value of the parameters. However, failure probability and the reliability index are related to both mean value and standard deviation. Figures 6.9, 6.11, and 6.12 show the same very high landslide susceptibility zones (the areas with factor of safety<1, failure probability >0.5, or reliability index >0).

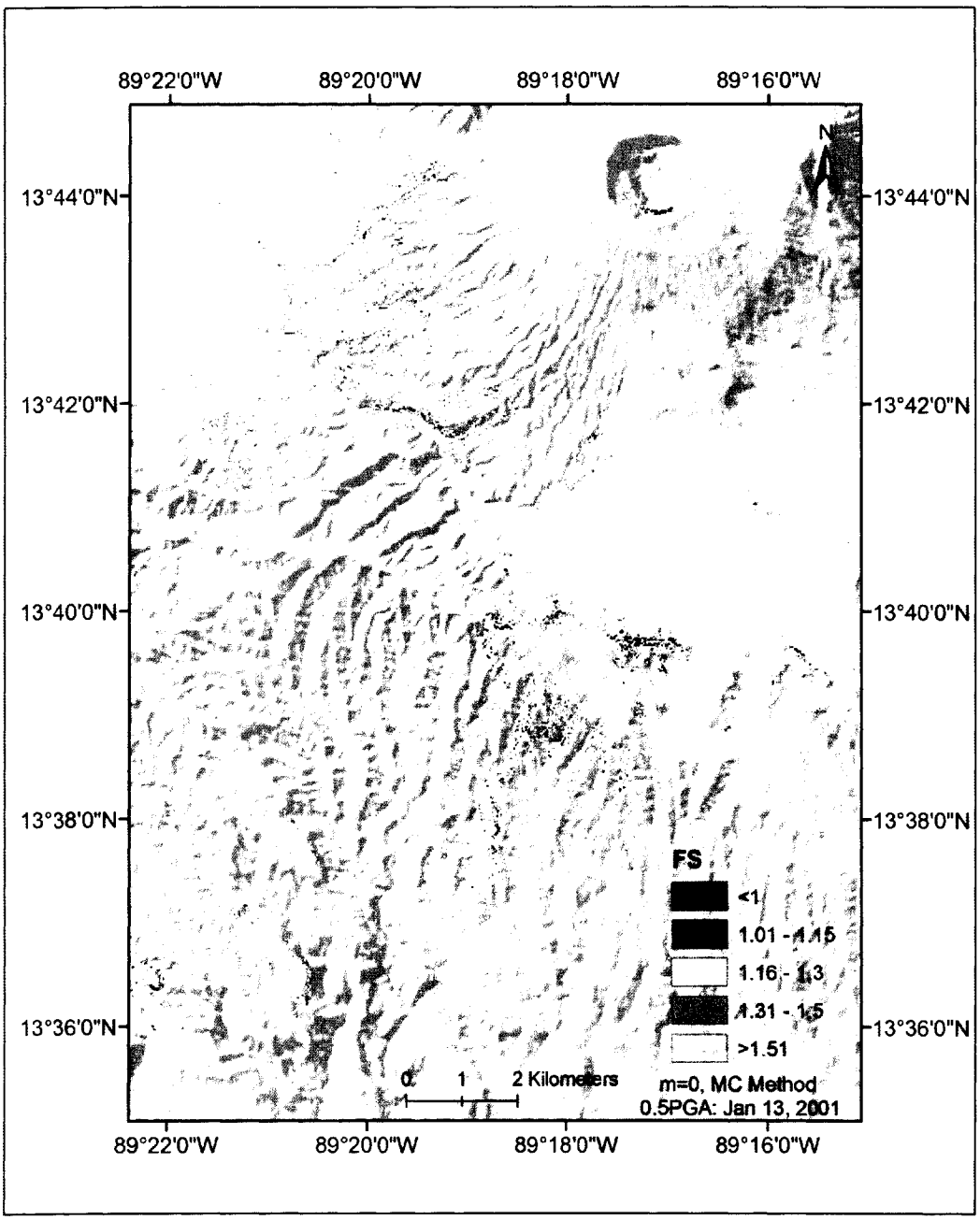

Figure 6.8 Map of the factor of safety calculated using the Monte-Carlo simulation with the block sliding model (dry soil condition, horizontal seismic coefficient k=0.5a_{max}/g of 2001 earthquake)

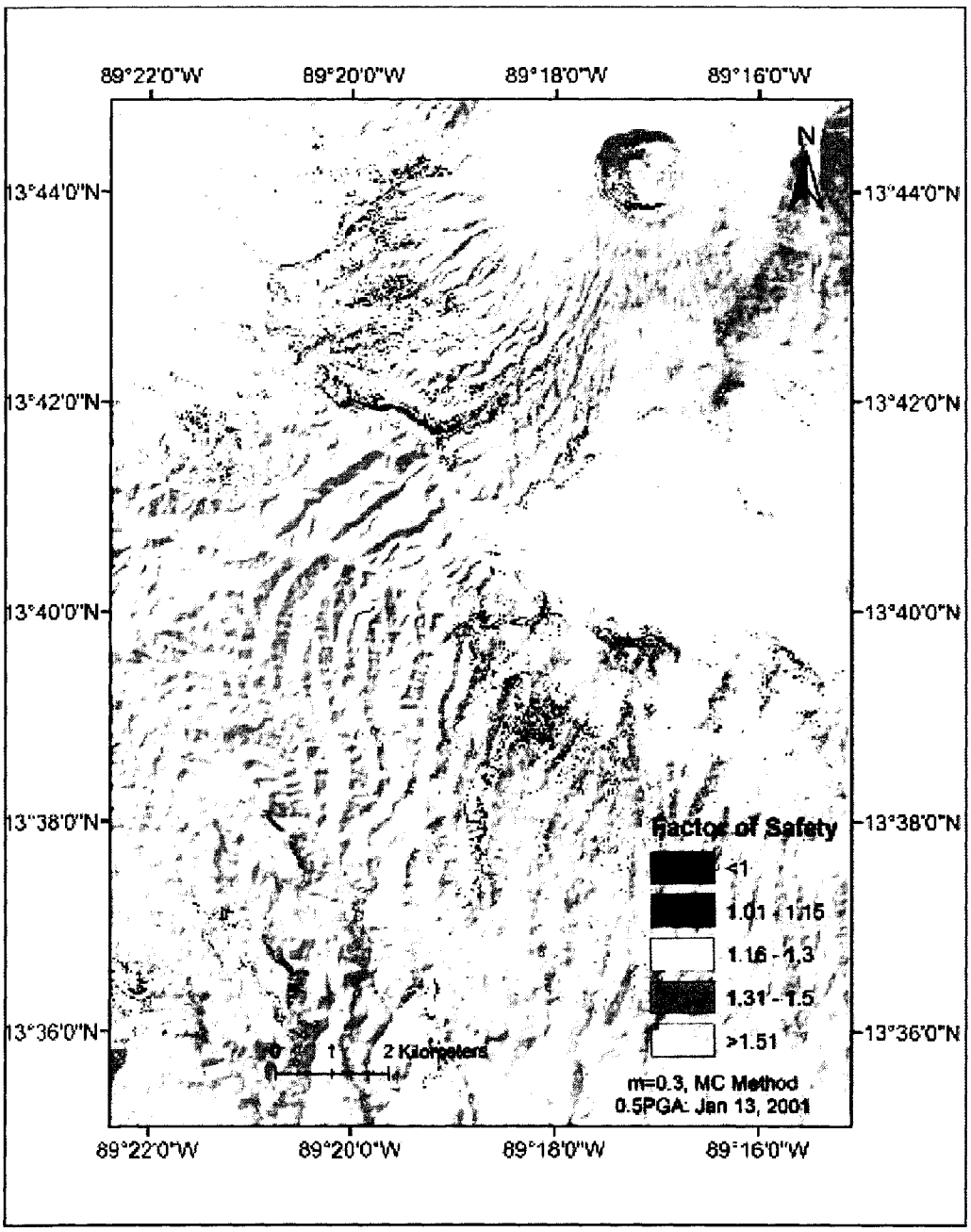

Figure 6.9 Map of the factor of safety calculated using the Monte-Carlo simulation with the block sliding model (soil saturation ratio m=0.3, horizontal seismic coefficient k=0.5a_{max}/g of 2001 earthquake)

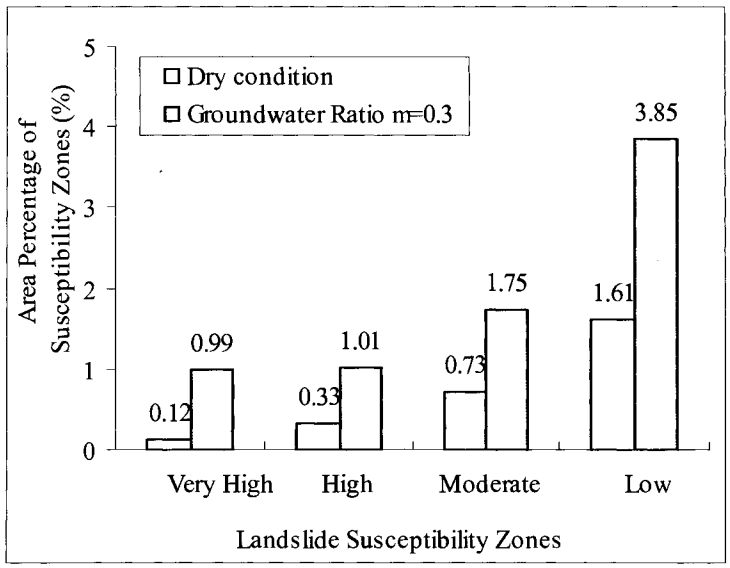

(a) Area percentage (%) of each landslide susceptibility zone

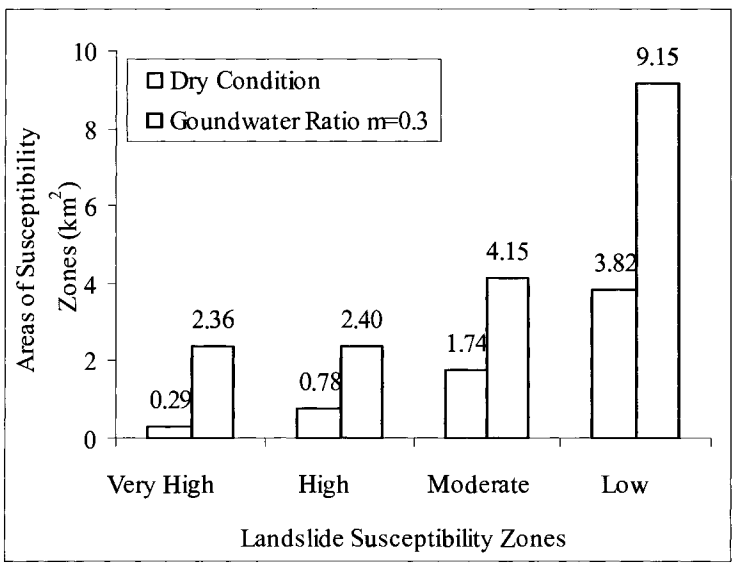

(b) Areas (km^2) of each landslide susceptibility zone

Figure 6.10 Graph shows the percentage (%) and area (km^2) of each landslide susceptibility zone in the study area. The percentage and area of the very high landslide susceptibility zone are 0.12% and 0.29km^2, respectively in dry soil conditions. The percentage and areas of very high landslide susceptibility are 0.99% and 2.36km^2, respectively for conditions of m=0.3. The percentages of very low landslide susceptibility area for both cases are 97.21% and 92.39%, respectively.

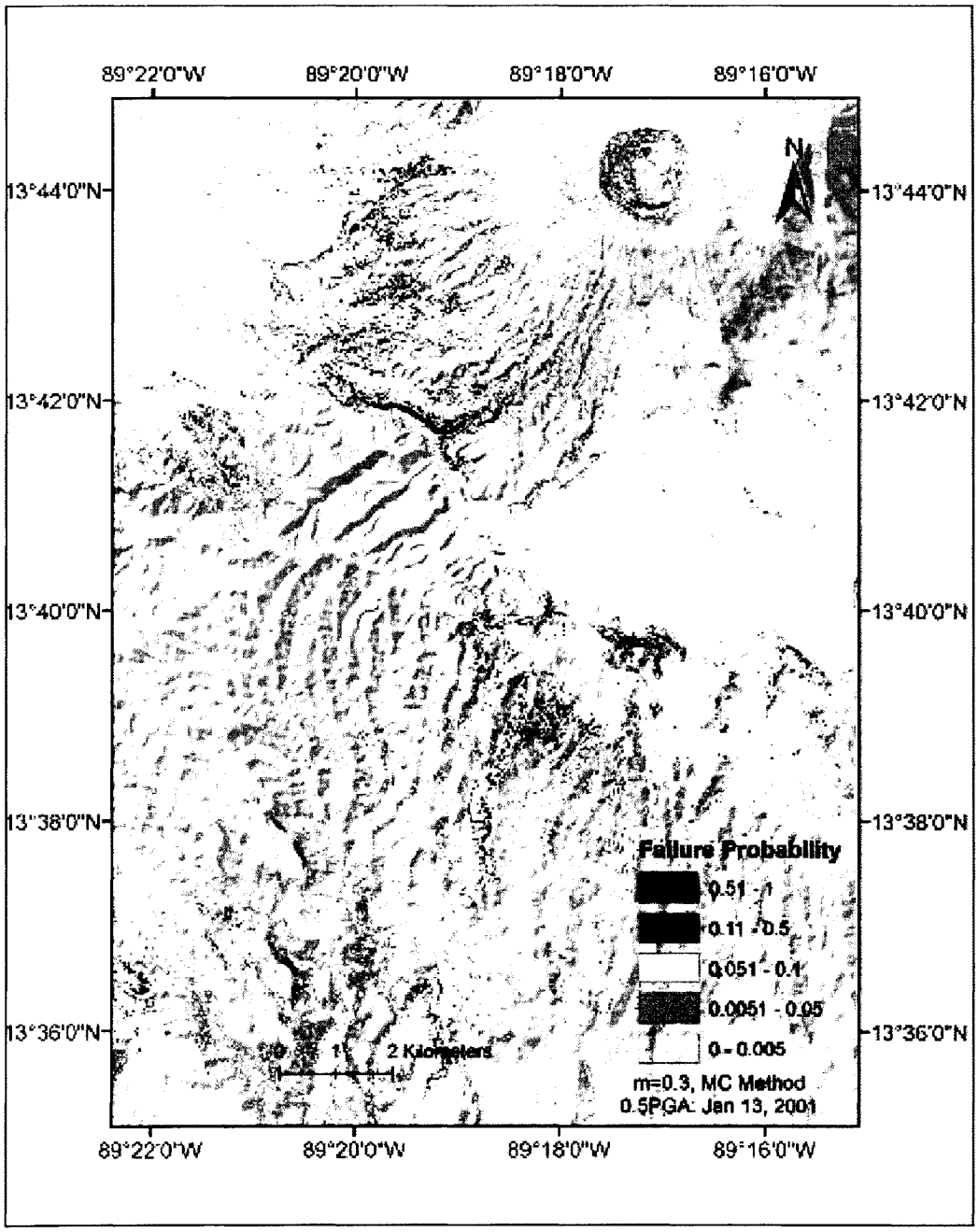

Figure 6.11 Map of the failure probability calculated using the Monte-Carlo simulation with the block sliding model (soil saturation ratio m=0.3, horizontal seismic coefficient $k=0.5a_{max}/g$ of 2001 earthquake)

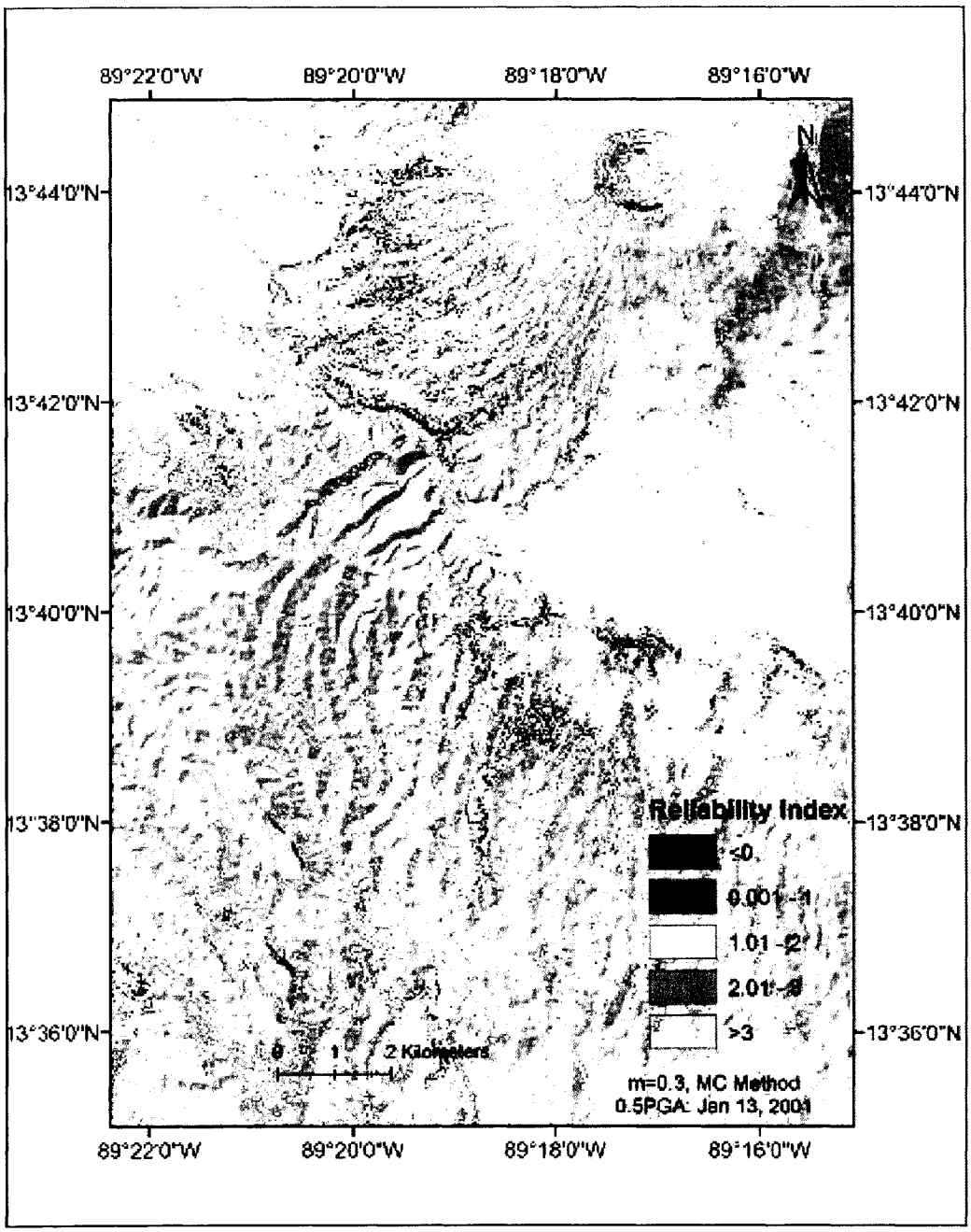

Figure 6.12 Map of the reliability index calculated using the Monte-Carlo simulation with the block sliding model (soil saturation ratio m=0.3, horizontal seismic coefficient $k=0.5a_{max}/g$ of 2001 earthquake)

6.8 Discussion

The regional earthquake-induced landslide susceptibility maps provide valuable information on the slope stability over a large area, which is of great interest in land use, infrastructure planning, engineering and hazard mitigation design.

Figures 6.8 and 6.9 show earthquake-induced landslide susceptibility during the dry and rainy seasons, respectively. The conditions of seismic shaking used in the analysis are similar to those of the January 13, 2001, earthquake. The decision makers for land use and city planning need to take necessary precautions in planning and permitting for residential or infrastructure development. Some mitigation to avoid future slope failure is required in the area of very high landslide susceptibility.

The block sliding model developed in this study is an appropriate method for regional landslide susceptibility assessment. However, the reliability of the analysis relies heavily on the spatial data used as input, and in particular on the geotechnical parameters and groundwater conditions. This model will give unreliable results if the input data do not correctly represent the actual geological conditions. For rock slopes, geological discontinuities have a significant influence on the slope stability, which is not included in the block sliding or infinite slope model. Due to the lack of detailed data on material properties, only general conclusions can be drawn from the resulting susceptibility maps. The failure probability map which considered uncertainties of geotechnical parameters is a better method for landslide hazard zonation.

Moreover, the landslide hazard zonation produced using this method considered only the occurrence of translational slides. The landslides triggered by earthquakes may be not translational slides, and perhaps they cannot be modeled correctly using a slope analysis model with uniform sliding depth. Therefore, the resulting factor of safety or failure probability should not be used as absolute values. For the inclusion of other landslide types and failure mechanisms, the infinite or block sliding model should be combined with other methods.

Chapter 7 Site-Specific Earthquake-Induced Landslide Hazard Zonation: 2D Model

7.1 Introduction

A GIS-based two-dimensional (2D) deterministic approach to analyze seismic slope stability was developed in this study. Unlike the infinite slope model and the block sliding model, which rely on individual block analysis, the 2D approach is based on the stability of overall blocks within pre-defined slope profiles. Consequently, the conventional 2D slope stability analysis method and probabilistic approach are applied to the GIS-based slope stability analysis. The factor of safety, critical horizontal acceleration, and earthquake-induced Newmark displacement of the slope profiles are calculated using a customized program that was written for this research. The program combines VBA with GIS grid-based spatial analysis. Slope stability and landslide hazard are mapped in terms of factor of safety or failure probability. The Balsamo Ridge area in Nueva San Salvador was selected for the site-specific hazard zonation.

7.2 GIS-based 2D Slope Stability Analysis Model

7.2.1 General Description

As mentioned in Chapter 6, a common GIS-based method, which is often applied to translational slides, is the infinite slope model. It is a popular slope stability analysis tool because it is both simple and applicable to many shallow landslides. In GIS-based slope stability analysis, the infinite slope model uses grids (cells or pixels) in raster datasets as mapping units. The factor of safety or displacement in each grid is derived from a combination of GIS datasets. This method is appropriate for failure analysis of a soil mass that overlies a sloping drainage barrier that may be bedrock or a less permeable and well compacted soil layer (Hammond el al. 1992). However, the infinite slope model does not adequately predict deep-seated, rotational failure. In this study, a GIS-based 2D

slope stability model was developed to analyze the earthquake-induced landslide hazard. The slope profile (or cross section for slope stability analysis) was used as the analysis profile and the mapping unit for 2D slope stability analysis. The slope stability of the study area was determined by combining the stability of a number of slope profiles. From the point of view of the raster data process, a slope profile consists of a number of grid cells. Each grid cell is assigned a value for each factor (terrain parameters, geotechnical properties, land use, etc.). The dataset needed for slope stability analysis for each profile can be obtained from a stack of raster map layers using GIS data processing. After that, slope stability can be analyzed using 2D slope stability methods. This study uses the ordinary method of slices and the Bishop simplified method to perform the slope stability analysis. In order to simplify the GIS-based process, a simple method, called the block sliding method, is introduced for 2D analysis.

7.2.2 Ordinary Method of Slices

For the ordinary method of slices, the factor of safety is obtained directly. This method assumes that the inter-slice forces are parallel to the base of each slice, and that thus they can therefore be neglected.

In general, earthquake acceleration increases the overturning moment, assuming that the potential sliding surface is circular with radius R_0 (Figure 7.1). The mass above the sliding surface is divided into a number of vertical slices. Under the action of earthquake inertia force, the overturning moment (driving moment) for all slices is given by:

$$M_o = R_o \cdot \sum_{i=1}^{n} (W_i \sin\alpha_i + kW_i \cos\alpha_i) \qquad (7.1)$$

where: M_o = overturning moment for all soil slices, kN·m

R_o = radius of potential circular surface, m

W_i = weight of soil slice, kN

k = seismic coefficient

α_i = dip angle of shearing surface (dip angle of sliding plane), °.

n = total number of soil slices

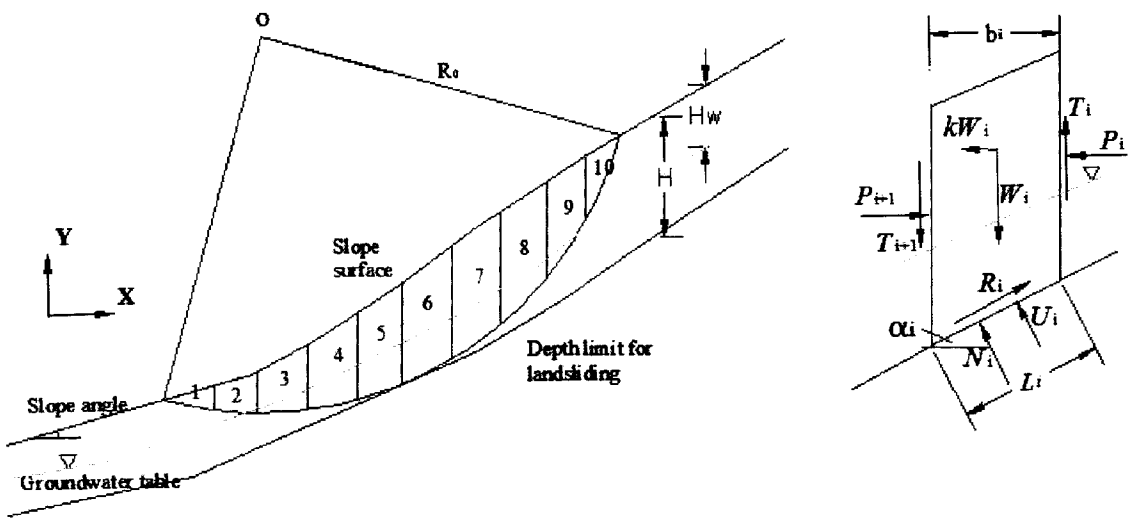

Figure 7.1 Stability analysis of a slope using the ordinary method of slices and the Bishop simplified method. The left graph shows a circular sliding surface with radius of R_o and the right graph shows the force acting on a slice (T_i is a shear force on vertical side, P_i is ta normal lateral force, N_i is a normal reacting force, U_i is a water force, and R_i is a shear force along a slip surface)

The resisting moment can be expressed as:

$$M_r = R_o \cdot \sum_{i=1}^{n} [c_i L_i + (W_i \cos\alpha_i - kW_i \sin\alpha_i - U_i)\tan\phi_i] \qquad (7.2)$$

where: M_r = resisting moment for all soil slices, kN·m

c_i = cohesion of slip surface, kPa

ϕ_i = effective friction angle of shearing surface, degree

U_i = water force acting on the slip surface, kN

L_i = length of slip surface, m

Under conditions of equilibrium, the moment of the driving force about the center of the sliding circle equals the moment of the resisting force. The factor of safety in ordinary method of slices is:

$$FS = \frac{\sum_{i=1}^{n}[c_i L_i + (W_i \cos\alpha_i - kW_i \sin\alpha_i - U_i)\tan\phi_i]}{\sum_{i=1}^{n} W_i(\sin\alpha_i + kW_i \cos\alpha_i)} \qquad (7.3)$$

The critical horizontal acceleration (yield acceleration, a_y), also known as the minimum acceleration (that is, the acceleration required to reduce the factor of safety to unity) can be calculated using Equation 7.3:

$$a_y = \frac{\sum_{i=1}^{n}[c_i L_i + (W_i \cos\alpha_i - U_i)\tan\phi_i - W_i \sin\alpha_i]}{\sum_{i=1}^{n} W_i(\cos\alpha_i + W_i \sin\alpha_i \tan\phi_i)} \qquad (7.4)$$

The ordinary method of slices, in general, gives a conservative factor of safety. Therefore, it can be assumed that the ordinary method of slices gives a lower yield acceleration value than the actual value (Kim and Sitar, 2004).

7.2.3 Bishop Simplified Method

In the Bishop simplified method, slope failure is assumed to occur because of the rotation of a block of soil on a circular slip surface centered on point O (Figure 7.1). By examining the overall moment equilibrium about the rotation center, the factor of safety can be calculated. Also, it is also assumed that the interslice forces are horizontal. Ignoring the interslice shear forces (i.e, $\Delta T = T_{i+1} - T_i = 0$ in Figure 7.1) and considering the water force and the earthquake force, the original formulation by Bishop (1955) for pseudo-static factor of safety calculation can be rewritten as the following equation:

$$\begin{cases} FS = \dfrac{\sum_{i=1}^{n}[cb_i + (W_i - kW_i \sin\alpha_i - u_i b_i)\tan\phi_i]\dfrac{1}{m_{\alpha i}}}{\sum_{i=1}^{n} W_i(\sin\alpha_i + k\cos\alpha_i)} \\ m_{\alpha i} = \cos\alpha_i + \dfrac{\tan\phi_i \sin\alpha_i}{FS} \end{cases} \qquad (7.5)$$

where: $u_i = \gamma_w H_w$, b_i is the width of slice. Note that the factor of safety, *FS*, is presented on both sides of the Equation 7.5. Hence, a trial-and-error or iterative procedure is needed to find the value of *FS*, and a number of failure surfaces must be investigated to find the critical sliding surface that produces the minimum factor of safety.

Equation 7.5 can be rearranged in terms of yield acceleration as follows:

$$\begin{cases} a_y = \dfrac{\sum_{i=1}^{n}[c_i b_i + (W_i - u_i b_i)\tan\phi_i]\dfrac{1}{m_{\alpha i}} - \sum_{i=1}^{n} W_i \sin\alpha_i}{\sum_{i=1}^{n} W_i(\sin\alpha_i \tan\phi_i \dfrac{1}{m_{\alpha i}} + \cos\alpha_i)} \\ m_{\alpha i} = \cos\alpha_i + \tan\phi_i \sin\alpha_i \end{cases} \tag{7.6}$$

Equation 7.6 can be used to directly compute the yield horizontal earthquake acceleration.

7.2.4 Block Sliding Model

The factor of safety of a non-circular slope profile can be calculated on the basis of the overall force equilibrium of blocks within the profile such as the one in Figure 7.2. Generally, the factor of safety calculation for multiple sliding blocks also requires consideration for the overall moment equilibrium about an assumed center of rotation (R_o is not constant). In order to simplify the GIS-based calculation, it has to be assumed that the inter-block shear forces $\Delta T = T_{i+1} - T_i = 0$ and normal forces $\Delta T = P_{i+1} - P_i = 0$. The total resisting force and sliding force along the failure surface are the sum of resisting force and sliding force of each block in the slope profile (in 2D, a block is also a slice). Considering force equilibrium, an approximate value for the factor of safety of such a profile can be obtained by dividing the total resisting force by the total sliding force:

$$FS = \frac{\sum_{i=1}^{n} R_i}{\sum_{i=1}^{n} T_i} = \frac{\sum_{i=1}^{n}[c_i A_i + (W_i \cos\alpha_i - kW_i \sin\alpha_i - U_i)\tan\phi_i]}{\sum_{i=1}^{n}[W_i(\sin\alpha_i + k\cos\alpha_i)]} \tag{7.7}$$

Where: R_i = resisting force of ith soil block, kN

T_i = Sliding force of ith soil block, kN

A_i = area of a slip surface, m^2

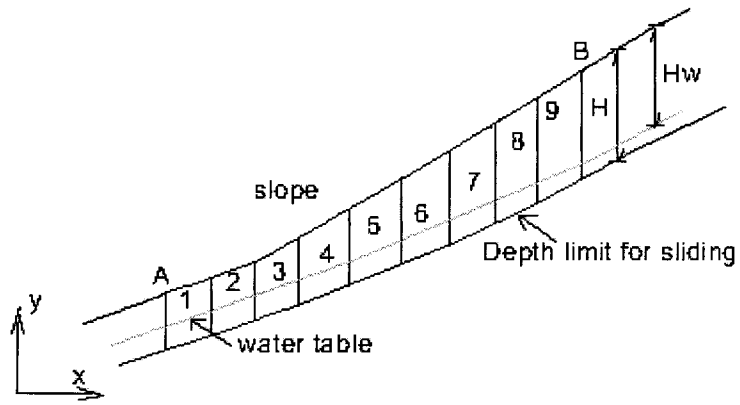

Figure 7.2 A slope profile and its blocks in the 2D block sliding model. Assuming that the blocks (blocks 1 to 9 in this case) will slide along a slip surface, slope stability is calculated according to the total resisting and sliding forces of the blocks.

The Equation 7.7 can produce errors because it ignores the influence of force direction, inter-block forces, and moment equilibrium. However, if the variation of the angle of the sliding surface is less than 10° within the profile, the error in the factor of safety in the profile could be less than 10%.

The difference between this method and the ordinary method of slices is that the sliding surface is not necessarily circular in the block sliding model. Thus, the factor of safety in the block sliding model might be less than the factor of safety calculated with the circular slices method. This is a simplified method to calculate 2D slope stability using GIS-based analysis. In the GIS process, such blocks can be viewed as a grid in a raster dataset. The force of each grid on a slope profile can be calculated according to the input datasets.

7.2.5 Probability and Reliability Analysis

Since the factor of safety calculated under the limit equilibrium method cannot reflect the uncertainty of geotechnical parameters, the Monte-Carlo simulation and the first order reliability method (FORM) (also known as Hasofer-Lind approach (Hasofer and Lind, 1974)), was explored for probabilistic analysis. The Monte-Carlo simulation was discussed in Chapter 6. The Hasofer-Lind method is briefly introduced next.

The first order reliability method developed by Hasofer and Lind gives a measure of the structural reliability in terms of the reliability or safety index, β, which is defined as the shortest distance between the origin of the reduced coordinate system and the failure surface defined by the limit state ($g(X) = 0$) as shown in Figure 7.3.

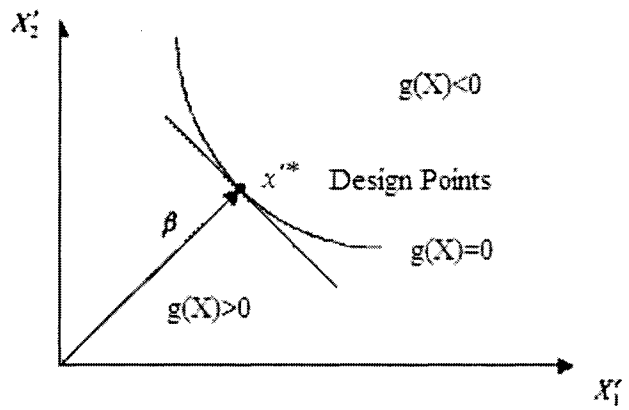

Figure 7.3 Hasofer-Lind reliability index: nonlinear performance function

The point on the failure surface corresponding to β is called the design point or the most probable failure point (MPP) with coordinates defined as:

$$x_i'^* = -\alpha_i^* \beta \tag{7.8}$$

and direction cosines (unit vectors) defined as:

$$\alpha_i = \frac{\left(\frac{\partial g}{\partial x_i'}\right)}{\sqrt{\sum\left(\frac{\partial g}{\partial x_i'}\right)^2}} \tag{7.9}$$

where x_i' corresponds to x_i in reduced coordinate system. When limit-state function is nonlinear, as is the case here, β is determined through an iterative procedure based on an initial estimate for the coordinates of MPP.

The probability of failure is directly related to β according to the following relationship:

$$P_f = \Phi(-\beta) \tag{7.10}$$

where Φ is the cumulative distribution function (CDF) of the standard normal variate.

The limit state function for slope stability analysis is formulated as:

$$g(X) = R - S \tag{7.11}$$

R is the resisting force and S is the sliding force, and both R and S are random in nature and statistically independent. For the ordinary method of slices, according to Equation 7.3, $g(X)$ can be expressed as:

$$\begin{aligned} g(X) &= \sum[cL + (W\cos\alpha - kW\sin\alpha - U)\tan\phi] \\ &\quad - \sum(W\sin\alpha + kW\cos\alpha) \\ &= \sum[cL + \gamma\cdot\tan\phi(h\cdot b\cdot\cos\alpha - k\cdot h\cdot b\cdot\sin\alpha) - \gamma_w\cdot m\cdot h\cdot L\cdot\tan\phi \\ &\quad - \gamma\cdot(h\cdot b\cdot\sin\alpha + k\cdot h\cdot b\cdot\cos\alpha)] \end{aligned} \tag{7.12}$$

where X is the vector of random variables. So, the failure criterion is g(X)=0. In Equation 7.12, $g(X) < 0$ means failure, $g(X) > 0$ indicates safe, and $g(X) = 0$ represents the limit state (boundary separating the failure and safe regions).

In this case, g is a function of four random variables (friction coefficient, $\tan\phi°$, cohesion, c; soil unit weight, γ; and groundwater ratio, m). Each random variable is assumed to be normally distributed. To simplify the expression, Equation 7.12 can be rewritten as:

$$g(X) = \sum (cL + A_1 \cdot \gamma \cdot \tan\phi - A_2 \cdot m \cdot \tan\phi - A_3 \cdot \gamma) \tag{7.13}$$

Where:

$$A_1 = h \cdot b \cdot \cos\alpha - k \cdot h \cdot b \cdot \sin\alpha \tag{7.14}$$

$$A_2 = \gamma_w \cdot h \cdot L \tag{7.15}$$

$$A_3 = h \cdot b \cdot \sin\alpha + k \cdot h \cdot b \cdot \cos\alpha \tag{7.16}$$

Then

$$\frac{\partial g}{\partial c} = \sum L \qquad \frac{\partial g}{\partial c'} = \sum L\sigma_c \tag{7.17}$$

$$\frac{\partial g}{\partial \gamma} = \sum A_1 \tan\phi - A_3 \qquad \frac{\partial g}{\partial \gamma'} = \sum (A_1 \tan\phi - A_3)\sigma_r \tag{7.18}$$

$$\frac{\partial g}{\partial \tan\phi} = \sum A_1\gamma - A_2 m \qquad \frac{\partial g}{\partial \tan'\phi} = \sum (A_1\gamma - A_2 m)\sigma_{\tan\phi} \tag{7.19}$$

$$\frac{\partial g}{\partial m} = \sum -A_2 \tan\phi \qquad \frac{\partial g}{\partial m'} = \sum (-A_2 \tan\phi\sigma_m) \tag{7.20}$$

The procedure for calculation of the reliability index β is described as follows:

(1) Assume an initial value for the design point x_i^*. It is common to start with the mean values of the basic random variables.

(2) Evaluate the directional cosines at the failure point α_i. The partial derivatives that are needed for computing α_i can be obtained using Equations 7.17 to 7.20.

(3) Solve the following equation for the root β :

$$g[(\mu_c - \alpha_c\sigma_c\beta),(\mu_\gamma - \alpha_\gamma\sigma_\gamma\beta),(\mu_{\tan\phi} - \alpha_{\tan\phi}\sigma_{\tan\phi}\beta),(\mu_m - \alpha_m\sigma_m\beta)] = 0 \tag{7.21}$$

(4) Using β obtained in step (3), evaluate a new design point using the following equation

$$x_i^* = \mu_{xi} - \alpha_i\beta \tag{7.22}$$

(5) Repeat steps (1) to (4) until convergence of β is obtained.

The advantage of estimating reliability with the Hasofer-Lind approach is that it only depends upon the mean and variance (first and second moment properties) of individual random variables and not their distribution type. The disadvantage is that, for non-normal random variables, accuracy is sacrificed.

7.3 Critical Slip Surface for 2D Slope Analysis

A slope may fail along a number of potential slip surfaces. In this study, a number of circular slip surfaces were generated for each corresponding slope profile, within the depth and the dimension of the potential sliding mass. The slip surface with a minimum factor of safety is considered to be critical. The depth and the dimension of the potential sliding mass were determined through statistical analysis of the dimensions of historic landslides occurred in the study area and its vicinity.

7.4 Definition of Slope Profiles

An important step for the GIS-based 2D slope stability analysis is to define the slope profiles. From a geomorphologic point of view, a slope profile is a line across the ground surface largely or entirely following the direction of the true slope (Young, 1972). Most slope profiles extend from drainage divide to talweg. In selecting representative profiles, one has to consider the general landslide dimension, the slope shape, and the geological conditions. These profiles are usually confined to slopes that are straight in plan view (which might be only a portion of entire slope profiles). Accurate topographic map or DEM (digital elevation model) would, in theory, provide the necessary information to construct the slope profiles.

A fully automatic method for slope profile definition is yet not available. Hence, the final profile determination is done semi-automatically and is based on slope shape and personal experience. The length of the slope profiles can be approximated by looking to historical landslide dimension data. DEM data in the study area is essential for a drainage network and catchment boundary analysis. A typical basin can be partitioned

using the first-order drainage line into three or four elementary slope units: a valley-head slope, two lateral-slopes (or called valley-side slope), and a spur-end slope, as represented in Figure 7.4. A slope profile can be within an elementary slope unit. The rules to define the slope profiles for the slope stability analysis can be described as follows:

(1) the profiles should be parallel to the flow direction (or steepest path) of a slope surface;

(2) in most cases, the profiles should be in between ridge line and valley line;

(3) the length of the profile should be determined through statistical analysis of the length of historic landslides;

(4) the density of slope profiles can be determined according to the degree of accuracy required for the landslide hazard zonation;

(5) the features of slope shape and topographic and geological conditions may be used to select slope profiles.

Figure 7.4 shows a catchment boundary and drainage line obtained by terrain analysis using Arc Hydro (Maidment, 2002) tools in ArcGIS (Ormsby et al., 2004). It also shows the slope profiles for 2D slope stability analysis.

7.5 GIS Data Process and Landslide Hazard Zonation

7.5.1 GIS Data Process

For GIS-based slope stability analysis, the geotechnical engineering datasets have been created on the basis of terrain, geology, and ground motion parameters. All of the datasets used in conducting a detailed seismic-induced landslide hazard zonation were digitized or rasterized in a 10 m grid spacing using GIS platform, and are listed in Table 7.1.

Figure 7.5 is a flowchart showing the sequential steps involved in the landslide hazard mapping procedure.

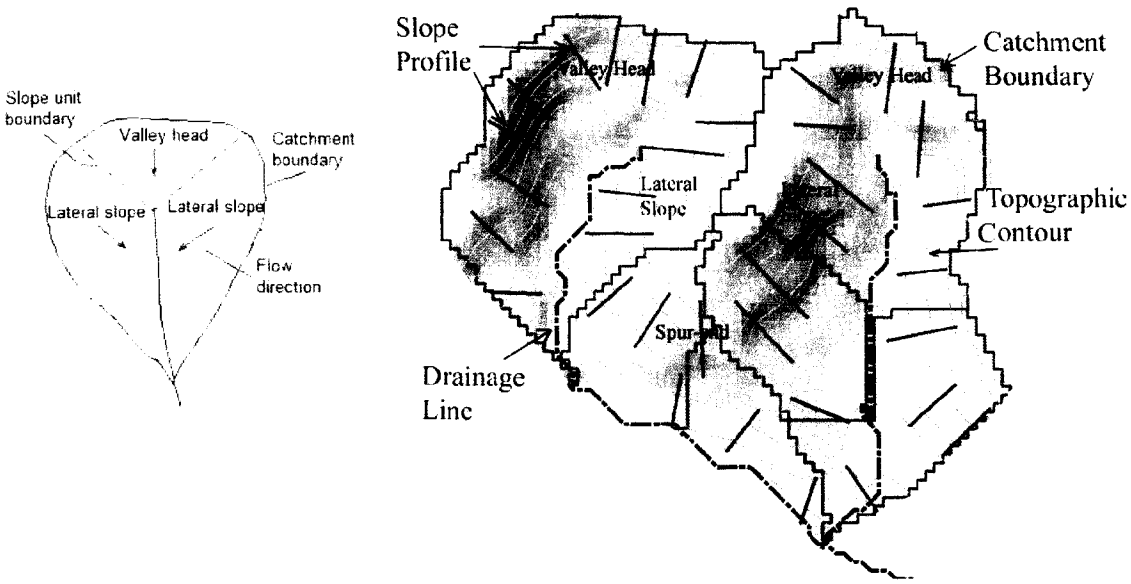

Figure 7.4 Definition of the elementary slope units in a basin (left) and the slope profiles for 2D slope stability analysis (right) in the catchments. A typical basin can be partitioned using the first-order drainage line into three or four elementary slope units: a valley-head slope, two lateral-slopes (or called valley-side slopes), and a spur-end slope. A slope profile can fall within an elementary slope unit.

Table 7.1 Necessary data layers for 2D slope stability analysis

Data Layers		Data Format	Notes
1	Slope surface angle (α)	Grid and Point	For Monte-Carlo simulation, the point feature datasets and deviation of random parameters (σ_m, σ_c, σ_γ, and σ_ϕ) are required.
2	Slip surface angle (θ)	Grid and Point	
3	Soil friction angle (ϕ and σ_ϕ)	Grid and Point	
4	Soil cohesion (c and σ_c)	Grid and Point	
5	Soil unit weight (γ and σ_γ)	Grid and Point	
6	Soil depth (H)	Grid and Point	
7	Horizontal acceleration (k or PGA)	Grid and Point	
8	Slope Profiles	Line and Point	
9	DEM (X, Y, and Z Value)	Point or Text	

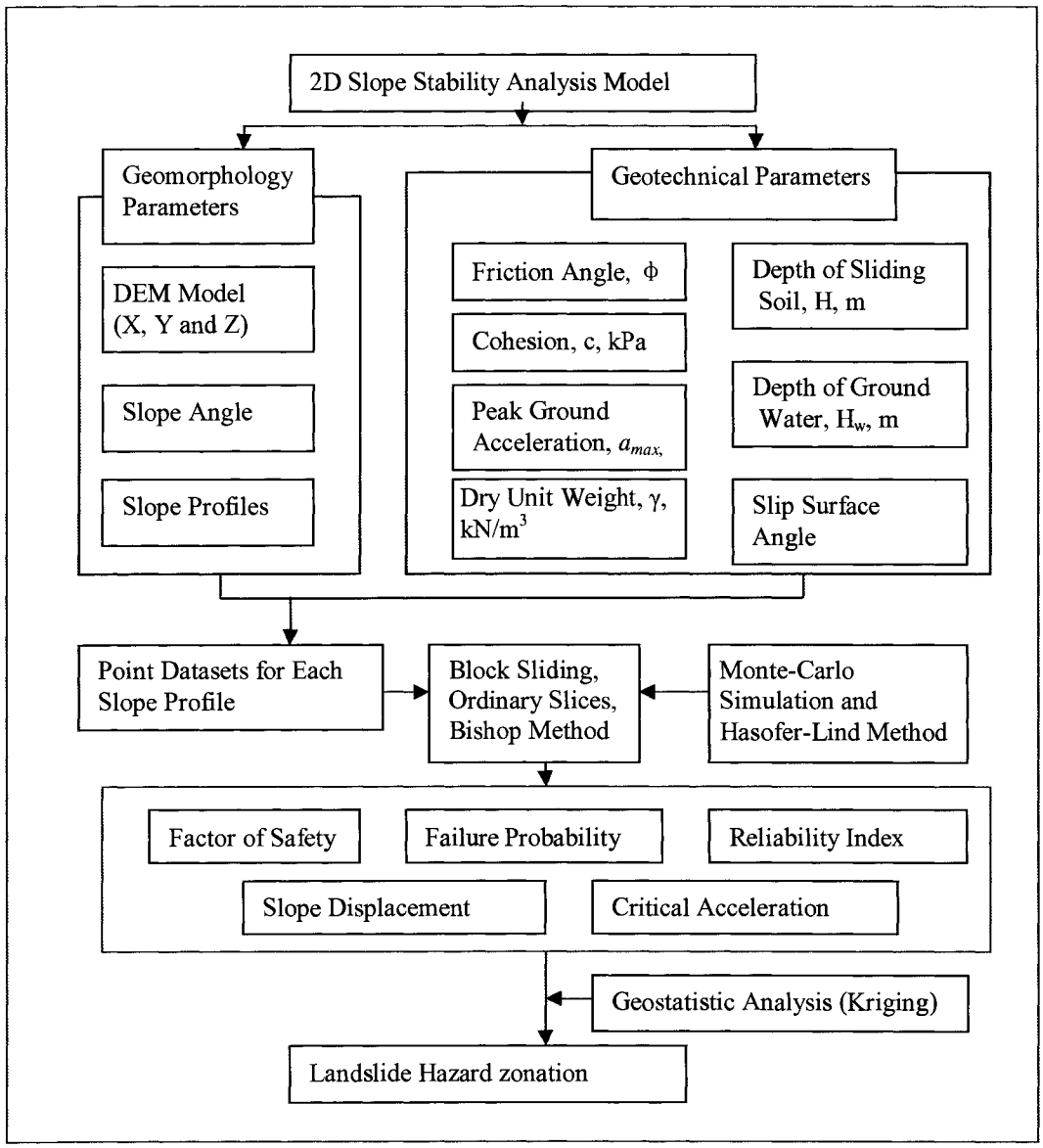

Figure 7.5 Flowchart of 2D slope stability and landslide hazard zonation

The slope stability analysis can be completed inside the GIS platform using ArcObjects (Bruke, 2003) or outside the GIS environment using any computer program. For analysis outside of GIS, all the datasets of geomorphology and geotechnical parameters in the study area are transformed into point feature from grid datasets

including point coordinates (x, y, z), slope angle, profile ID, friction angle, cohesion, unit weight, earthquake acceleration, predicted depth of potential sliding mass, groundwater depth, and/or predicted slip surface by employing ArcGIS. In the next step, attribute tables of those point map layers are converted into text files. Some effort is needed to code a computer program such as VB to identify and extract the data of the points within each slope profile by their profile numbers. With the datasets of slope profiles, the factor of safety can be easily obtained using the 2D slope stability analysis methods mentioned above. Finally, by importing calculated factor of safety data into GIS platform, the factor of safety of each slope profile can be displayed and the landslide susceptibility hazard zonation can be made by classification, or geostatistic analysis based on the slope stability index (factor of safety, critical acceleration, failure probability, etc.). A VB code was developed in this research in order to complete the analysis including data extraction for each profile, 2D factor of safety calculation, and critical slip surface searching.

7.5.2 Slope Stability Interpolation

In 2D slope stability analysis, slope stability is represented by a number of selected slope profiles. The slope stability of an area other than the selected profiles can be estimated from the data and spatial distribution of the stability index. Mathematically, this problem can be treated as an interpolation problem. The estimation can be performed using a deterministic method such as inverse distance weighted interpolation or a geostatistical method such as the kriging method.

Kriging provides a method for interpolating values for the points not physically sampled based on a continuous model of stochastic variation. It makes the best use of existing knowledge by taking into account the way that a property varies in space through the variogram model.

There are several varieties of kriging methods. Ordinary kriging is by far the most common type of kriging in use. It estimates the value of regionalized variables at unsampled places. The ordinary kriging model is described by (Johnston et al., 2003):

$$Z(\mathbf{s}) = \mu + \varepsilon(\mathbf{s}) \qquad (7.23)$$

where $\mathbf{s}$ is coordinates (X, Y) of a location, and $Z(\mathbf{s})$ is the value at that location. The model is based on constant mean, μ, and random error, $\varepsilon(\mathbf{s})$, with spatial dependence.

Assuming that the mean is unknown, the predictor is the weighted sum of the data:

$$\hat{Z}(s_0) = \sum_{i=1}^{N} \lambda_i Z(s_i) \qquad (7.24)$$

where: $Z(s_i)$ is the sampled value at the ith location; λ_i is an unknown weight at the ith location; s_0 is a prediction location; and N is the total number of sampled values.

In ordinary kriging, the weight, λ_i, depends on the semivariogram, the distance to the prediction location, and the spatial relationships along the sampled values around the prediction location. Ordinary kriging tries to find the optimal weight, λ_i.

Another more complicated method for estimation is disjunctive kriging. In general, disjunctive kriging tries to do more than ordinary kriging does. For instance, we may want to know, for the given data, the likelihood or probability that the true values at the target points exceed some threshold. To estimate these values, more elaborate techniques which depend on the statistical distribution of the variables at the target points are needed. Disjunctive kriging is one of the methods dealing with this kind of estimation. A complete description of kriging can be found in reference books such as Cressie (1993) and Chiles and Delfiner (1999).

The Geostatistical Analyst component of ArcGIS is employed in the landslide hazard zonation. Inverse distance weighted interpolation, ordinary, and disjunctive kriging methods are used for the spatial estimation based on the results of the slope stability analysis. The factor of safety or reliability index of each profile and its geographical location (the center of each profile) are imported to ArcGIS for kriging. The predicted map of slope stability can be displayed as grid or contour map showing ranked zones of landslide susceptibility.

7.6 Landslide Hazard Zonation at the Balsamo Ridge, Nueva San Salvador

7.6.1 General Description

The Balsamo Ridge area of Nueva San Salvador was selected as the study area for the 2D GIS-based analysis model. The Balsamo Ridge is located south of Nueva San Salvador. The January 13, 2001 earthquake triggered many landslides, leaving tensile cracks along the Ridge. Since the northern slope of the Ridge is much steeper than its southern side, slope failure and cracks were found on its northern slopes. The width of the landslides was 10 m to 40 m (except the Las Colinas landslide). The landslide height was 15 m to 40 m (JSCE, 2001). Figure 7.6 shows the triggered landslides, landslide crowns, cracks, and scarps in the east part of the Balsamo Ridge area during the 2001 earthquakes.

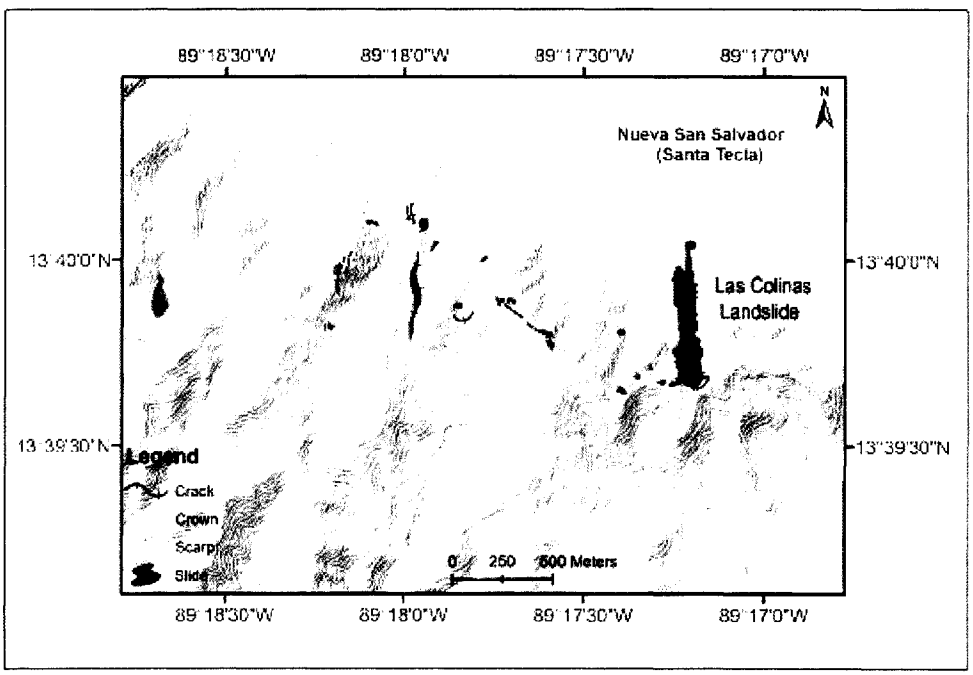

Figure 7.6 Slope failures along the Balsamo Ridge area, Nueva San Salvador (after Lotti C. & Association, 2001)

The extensive cracks remaining along Balsamo Ridge create a serious threat of further landslides. Immediate slope mitigation and the relocation of the residents who lived in the range of potential sliding area were organized by the city government. The public is concerned about the potential landslides that could be triggered by future large earthquakes. The site-specific landslide hazard zonation can provide the detailed and quantitative information necessary for hazard reduction in such an area.

The analysis models, including pseudo-static analysis and the probabilistic model (Monte-Carlo simulation and Hasofer-Lind method), were tested in the study area.

The selection of geotechnical parameters was described in Chapter 6. The determination of peak ground acceleration and the selection of the horizontal seismic coefficient are complex procedures. According to Table 2.5 (in Chapter 2), the minimum seismic coefficient for pseudo-static analysis is about 0.10, and usually k is 0.15 to $0.5a_{max}/g$. In this 2D slope stability analysis, in order to compare the results for different ground motion levels, seismic coefficients of k=0, 0.3, and 0.6 were used. k=0.3 corresponds to peak ground acceleration of 0.6g, assuming $k=0.5a_{max}/g$.

Considering the topographic amplification in the study area, the actual peak ground acceleration at the top of Balsamo Ridge during the January 13, 2001 earthquake might have exceeded 0.6 g and possibly reached 1.56 g according to the seismic response analysis in Chapter 5. The slope stability at k=0.6 was also calculated. The a_{max} of the January 13, 2001 earthquake shaking was used for displacement analysis to calibrate the analysis model.

In the 2D analysis model, a deeper sliding mass than that used in the infinite slope model was considered because Balsamo Ridge is covered by thick TB formation. One piece of evidence for the deeper sliding mass in this area is that the Las Colinas landslide had a sliding mass more than 35 m thick. A 15m thick potential sliding mass was selected for the general 2D slope stability analysis. For comparison, the distribution of predicted sliding depth based on historic landslides using the geostatistic method (kriging) was also used in the stability analysis. This prediction data indicates a varying depth of sliding mass associated with slope location. Figure 7.7 shows the slope profiles for 2D slope

stability analysis. A total of 459 profiles were selected for the 2D analysis that cover 4.91 km^2.

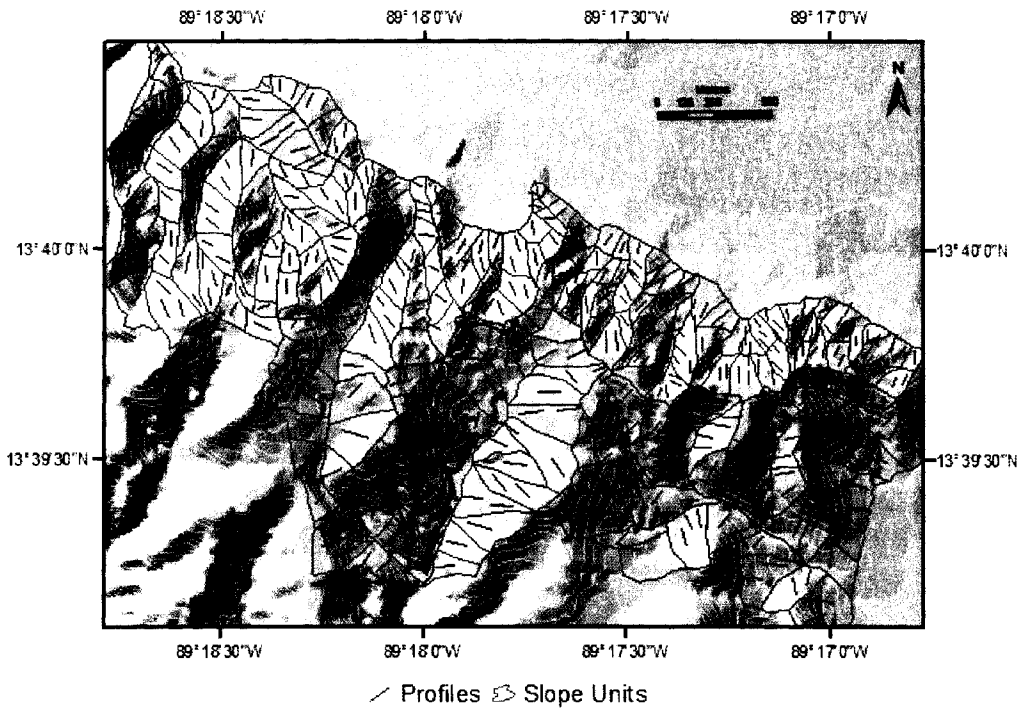

Figure 7.7 Slope profiles (459 profiles in total) for 2D slope stability analysis overlaid on image of the Balsamo Ridge area

7.6.2 Result Comparison

Figure 7.8 shows the factor of safety distribution in the Balsamo Ridge area, which was obtained from the statistics of 459 profiles calculated using the Bishop method under different *k* values but the same groundwater conditions (depth of groundwater table H_w=7 m). From these curves, at static conditions (no earthquake), all of the factors of safety are greater than 1. If seismic coefficient k is 0.3, 20 profiles have FS less than 1.0. At the condition of k=0.6, the slope stability decreased steeply and 41% of the profiles fail or are at the critical condition.

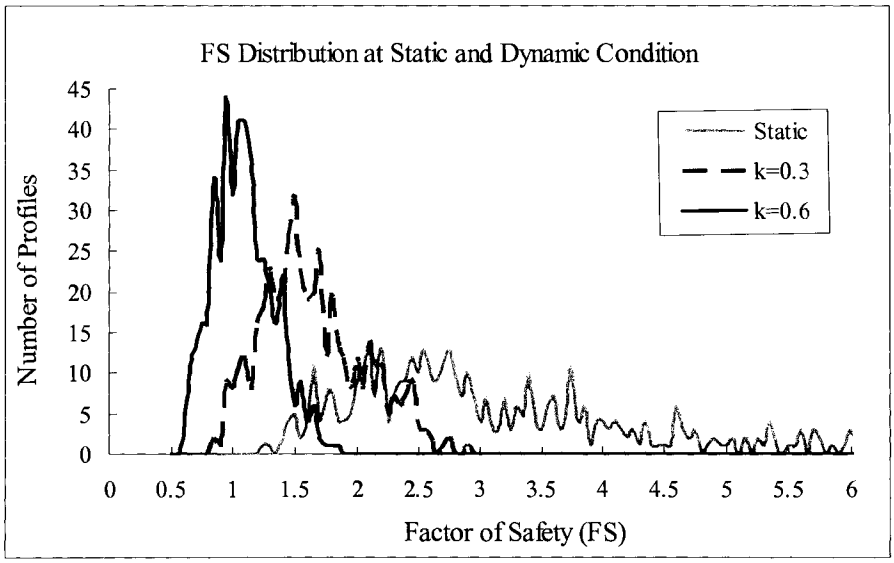

Figure 7.8 Factor of safety distribution at different acceleration conditions (Static, k=0.3, and k=0.6, H_w=7 m). If seismic coefficient k is 0.3, 20 profiles have FS less than 1.0.

The difference in the factor of safety calculated using ordinary method of slices, the Bishop simplified method, and block sliding method and the comparison and trendlines of factor of safety between the Bishop and ordinary method or block sliding model are shown in Figures 7.9 and 7.10. The correlation coefficient for both linear trendlines is greater than 0.90, which shows strong linear correlation. On average, from the results of 459 profiles, the factor of safety calculated using the Bishop simplified method is 6% greater than that using ordinary method of slices and 16% greater than that using block sliding model. The factor of safety calculated using ordinary method of slices is 10% greater than that using block sliding model. These results show that both the block sliding model and the ordinary method of slices are conservative. The Bishop simplified method is the most widely used method in slope engineering. Once the factor of safety under the ordinary method of slices or block sliding model is obtained, the factor of safety under the Bishop simplified method can be estimated according to their relationship.

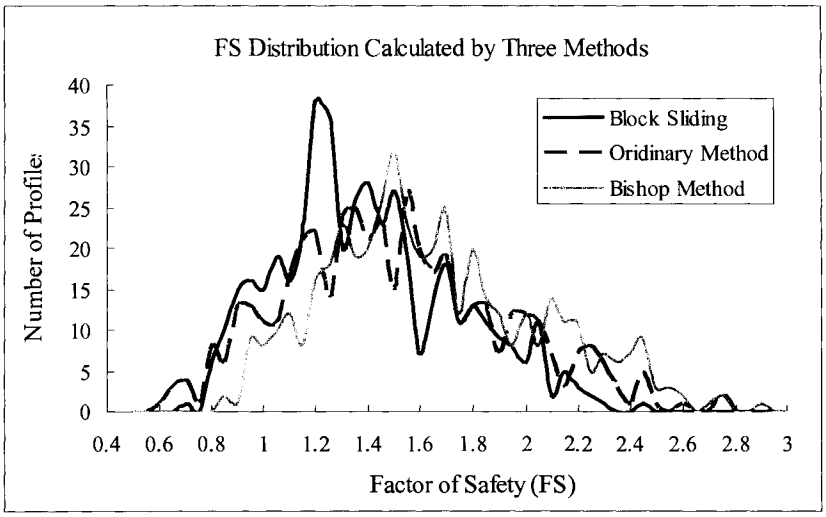

Figure 7.9 The results of a comparison of the factor of safety of 459 profiles using different methods under the same conditions (k=0.3 and H_w=7 m). Generally, the Bishop simplified method of slices obtained higher factor of safety than the ordinary method of slices. The block sliding model obtained the lowest factors of safety.

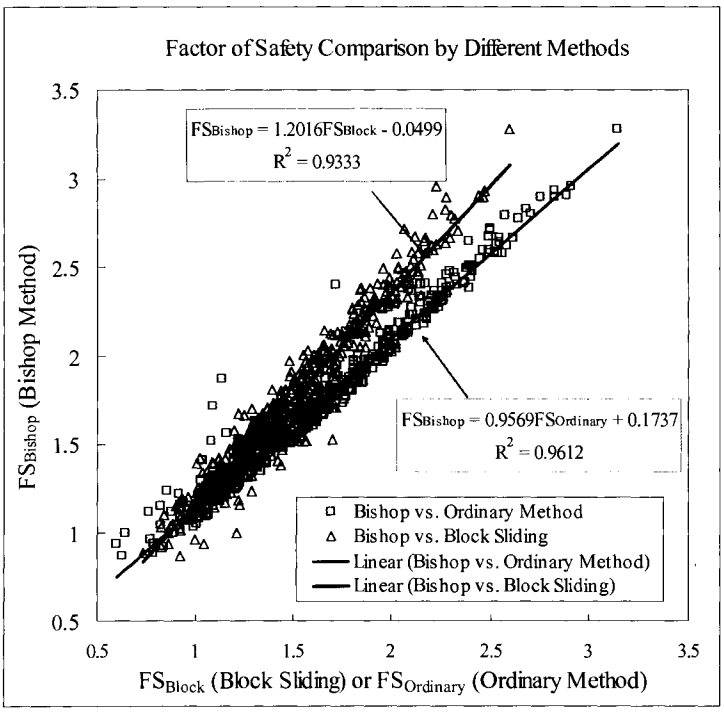

Figure 7.10 The comparison of the factor of safety of 459 profiles using the Bishop simplified method, the ordinary method of slices, and the block sliding model (k=0.3 and H_w=7 m).

Figures 7.11 to 7.12 show the relationships among mean factor of safety, failure probability, and the reliability index calculated using the Monte-Carlo simulation from the results of 459 profiles under conditions of k=0.3 and H_w=7 m. Theoretically, the factor of safety is only related to the mean value of input geotechnical parameters. Failure probability and the reliability index are not only related to mean value, but also to the standard deviation of each of the input parameters. However, failure probability has a fixed relationship with the reliability index, as presented in Equation 7.10. For any profile, it is apparent that when the factor of safety equals 1.0, the failure probability is 0.5 and reliability index is 0. Beyond this point, the relationship is related to the standard deviation of input parameters.

Figure 7.13 is a graph of critical acceleration compared against the static factor of safety calculated using ordinary method of slices. The following exponential regressive equation describes the relationships between critical acceleration and the static factor of safety:

$$a_y = 1.081\exp(-0.005419FS) - 1.714\exp(-0.4869FS) \qquad (7.25)$$

where: FS_{Static} is static factor of safety. R-square is 0.9604.

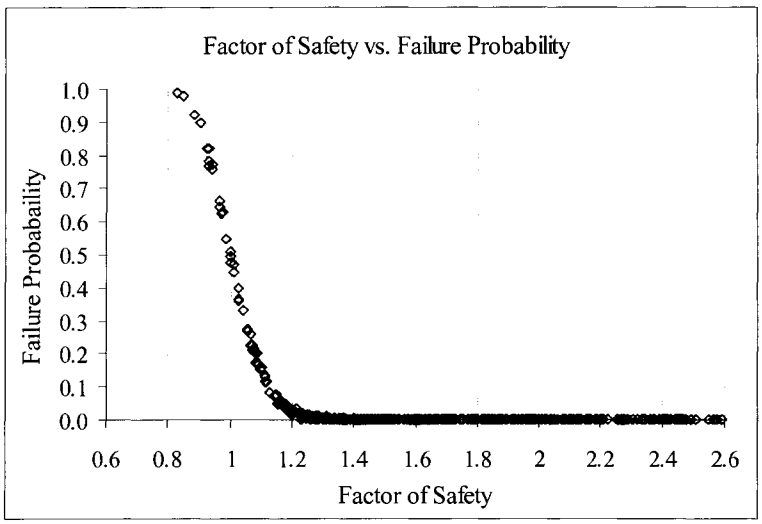

Figure 7.11 Failure probability vs. mean factor of safety of 459 slope profiles obtained using the Monte-Carlo simulation. Normal distribution is assumed for geotechnical parameters.

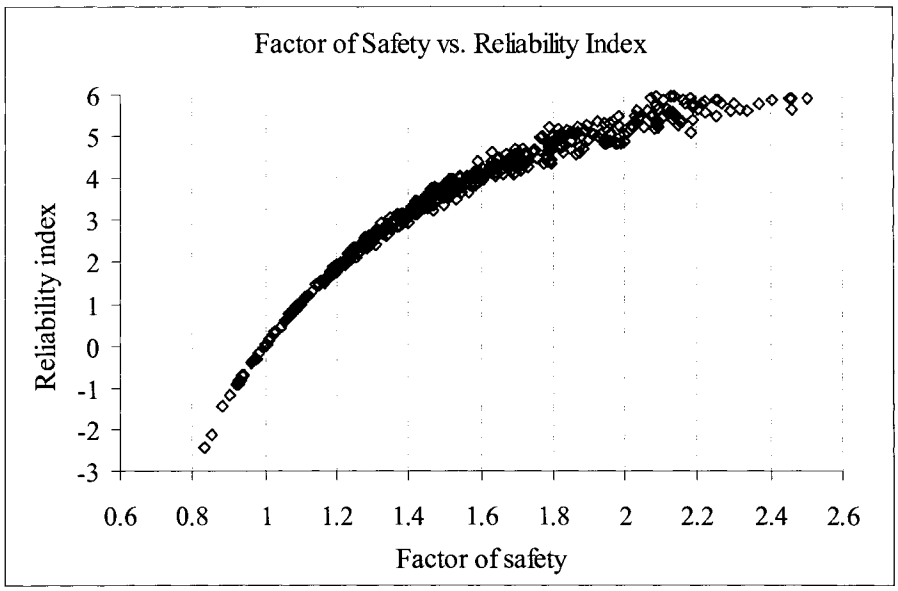

Figure 7.12 Reliability index vs. mean factor of safety of 459 slope profiles obtained using the Monte-Carlo simulation. Normal distribution is assumed for geotechnical parameters.

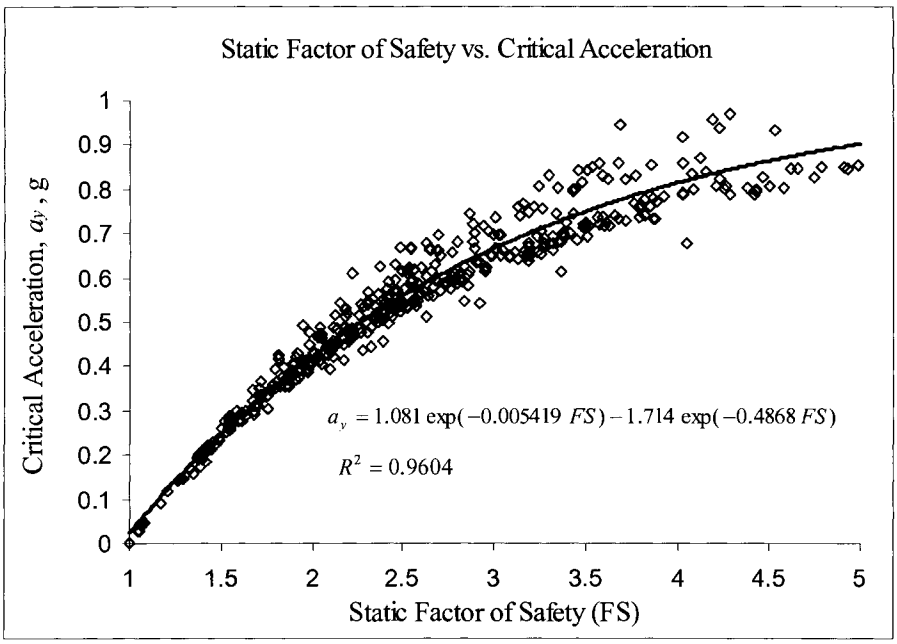

Figure 7.13 Yield horizontal acceleration against the static factor of safety calculated using the ordinary method of slices. When the static factor of safety equals 1.5, the critical acceleration is around 0.22 g.

Figure 7.14 is a graph of critical acceleration against the pseudo-static factor of safety (k=0.3 and H_w=7 m) calculated using the ordinary method of slices. In this figure, when the factor of safety equals 1.0, the critical acceleration is around 0.3 g.

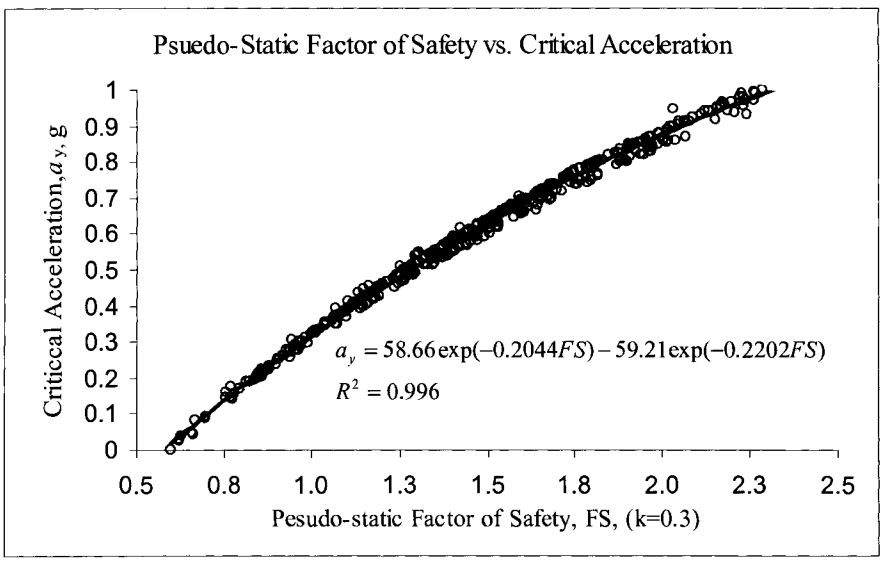

Figure 7.14 Yield horizontal acceleration against the pseudo-static factor of safety calculated using ordinary method of slices (k=0.3, H_w=7 m). When the factor of safety equals 1, the critical acceleration is around 0.3 g.

Figure 7.15 shows the Newmark displacement graphed against yield horizontal acceleration calculated using the Ambraseys and Menu Equation and the equations of Jibson et al. In the displacement analysis, the *PGA* (or a_{max}) and I_a values were generated using the ordinary kriging based on data from the ground motion records of the January 13, 2001, earthquake. Figure 7.15 also illustrates that the Ambraseys and Menu's equation has a larger displacement than Jibson et al.'s equation. In the valid range for $0.1 \leq a_y/a_{max} \leq 0.9$, the maximum displacement calculated by the Ambraseys and Menu's Equation is 120 cm, and the corresponding displacement is 45 cm using the Jibson et al.'s Equation.

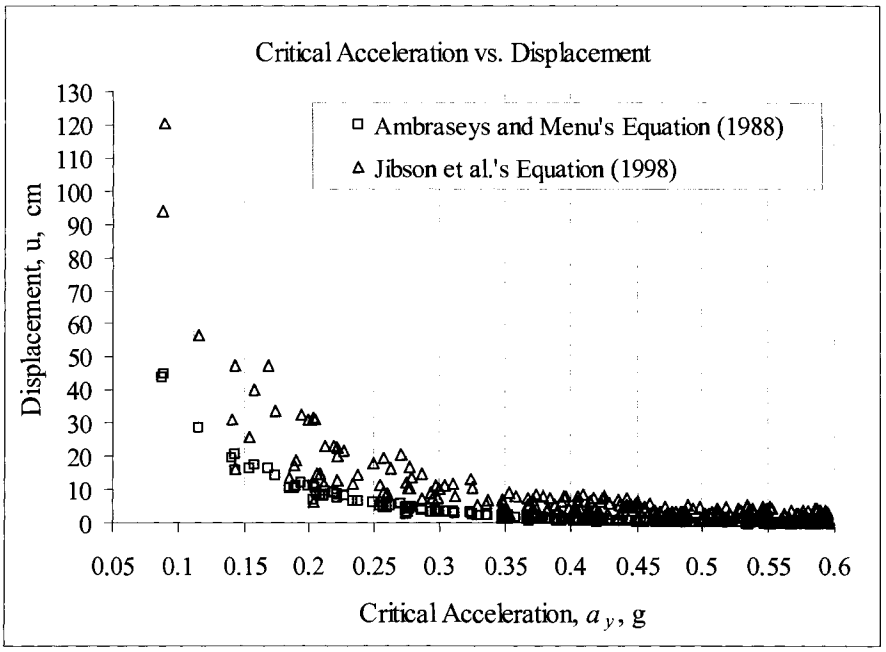

Figure 7.15 Yield horizontal acceleration graphed against the Newmark displacement calculated using Ambraseys and Menu's Equation and Jibson et al.'s equation. In this case, the Jibson et al. equation obtained a larger displacement than Ambraseys and Menu's equation.

7.6.3 Landslide Hazard Zonation

Earthquake-induced landslide susceptibility can be assessed and grouped, using one of the slope stability indices, into five categories: very high, high, moderate, low, and very low landslide susceptibility zones. The recommended ranges of Newmark displacement and the factor of safety for each landslide susceptibility zone are listed in Table 7.2. Like 1D analysis, the landslide susceptibility in the study area also can be classified by critical acceleration, failure probability, or the reliability index. The relationships among mean factor of safety, failure probability, and the reliability index displacement, and critical acceleration are shown in Figures 7.11, 7.12, 7.14, and 7.15.

Table 7.2 Landslide susceptibility zones and evaluation parameters

Zones	Landslide Susceptibility	Displacement, *u (cm)*	Factor of Safety, *FS*
1	Very high landslide susceptibility zone, landslides are expected	>10	<1
2	High landslide susceptibility zone, landslides are likely to occur	5~10	1~1.15
3	Moderate landslide susceptibility zone, moderate level of landslide hazard exists	2~5	1.15~1.3
4	Low landslide susceptibility zone, landslides are not likely to occur	0.1~2	1.3~1.5
5	Very low landslide susceptibility zone, safe slopes	0	>1.5

As expected, most unstable slopes are associated with areas of steep slope angle and lower shear strength. In the 2D study, the unstable slope profiles in the Balsamo Ridge area mainly occurred at the northern slope. Figure 7.16 shows the yield (critical) horizontal acceleration calculated using ordinary method of slices. The very high landslide susceptibility area, where the horizontal yield acceleration is less than 0.3 g, is close to the slope crown area of the northern side of the ridge. The southern side of the ridge belongs to low to the moderate landslide susceptibility zone because of its low slope angle.

Figure 7.17 shows the factor of safety map obtained using the Bishop simplified method. The crown area of the ridge has a lower factor of safety. Comparing the results calculated using the ordinary method of slices (Figure 7.18), the factor of safety distribution has some differences. Because the ordinary method of slices is conservative, the Bishop simplified method is a recommended method for factor of safety calculation in landslide hazard zonation. Figure 7.19 shows the classified reliability index of slope profiles at the study area calculated using the ordinary method of slices and the Hasofer-Lind method (k=0.3, H_w=7 m). In Figures 7.18 and 7.19, the result of landslide susceptibility classification according to the reliability index is very similar to that according to the factor of safety, since both calculations are based on the ordinary method of slices.

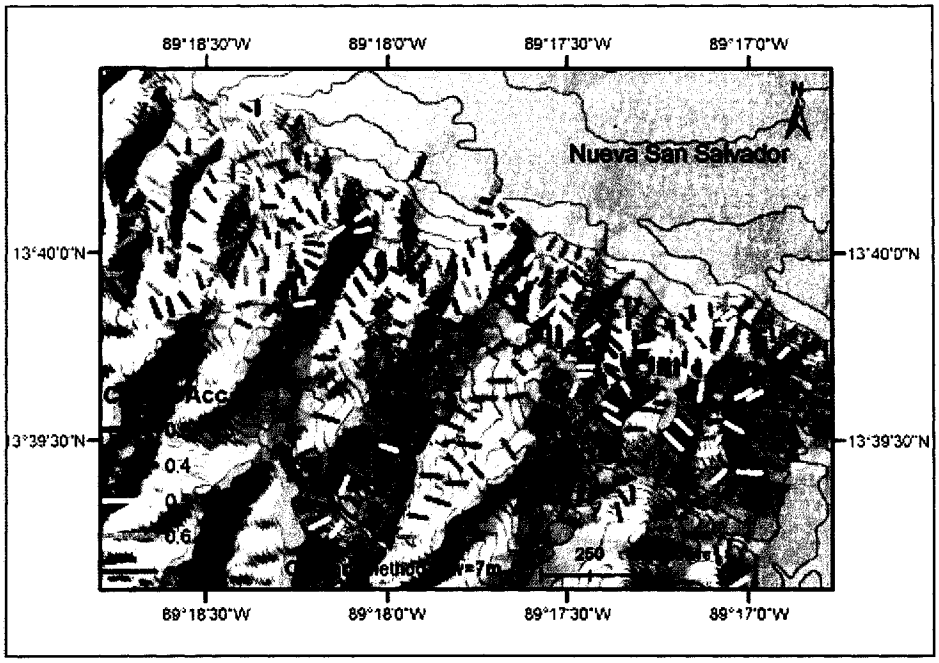

Figure 7.16 Critical (yield) horizontal acceleration of the slope profiles in the study area calculated using the ordinary method of slices (k=0.3, H_w=7 m)

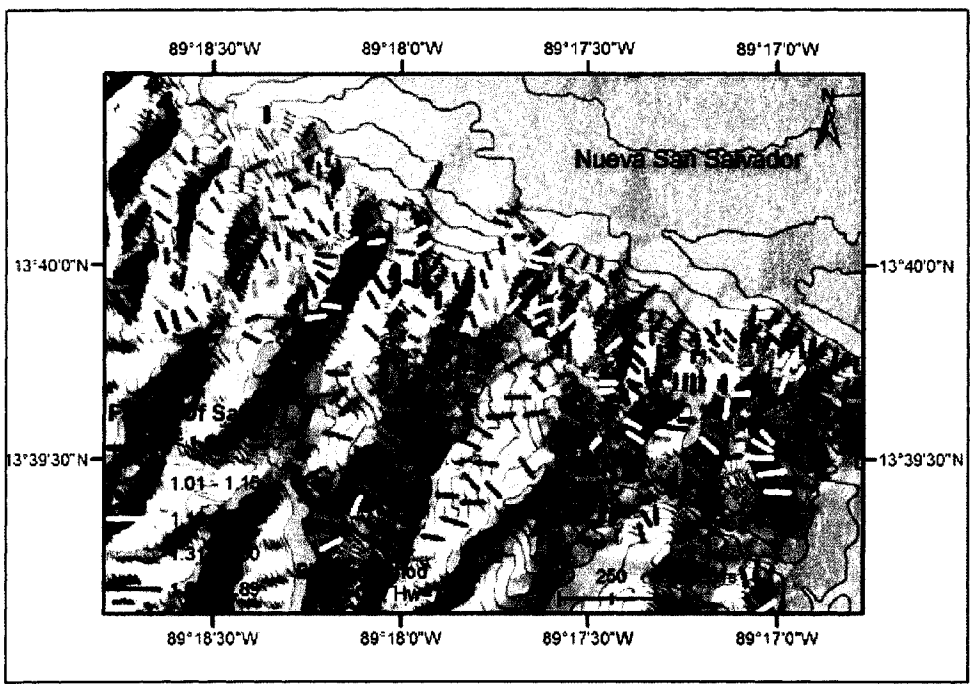

Figure 7.17 Factor of safety of the slope profiles in the study area calculated using the Bishop simplified method (k=0.3, H_w=7 m)

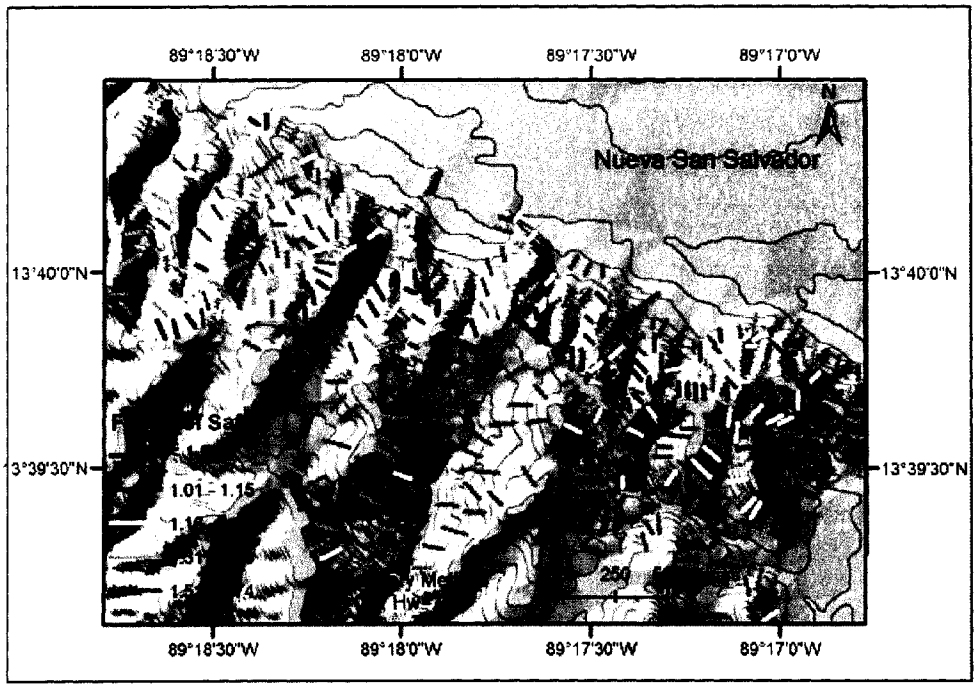

Figure 7.18 Factor of safety of the slope profiles in the study area calculated using the ordinary method of slices (k=0.3, H_w=7 m)

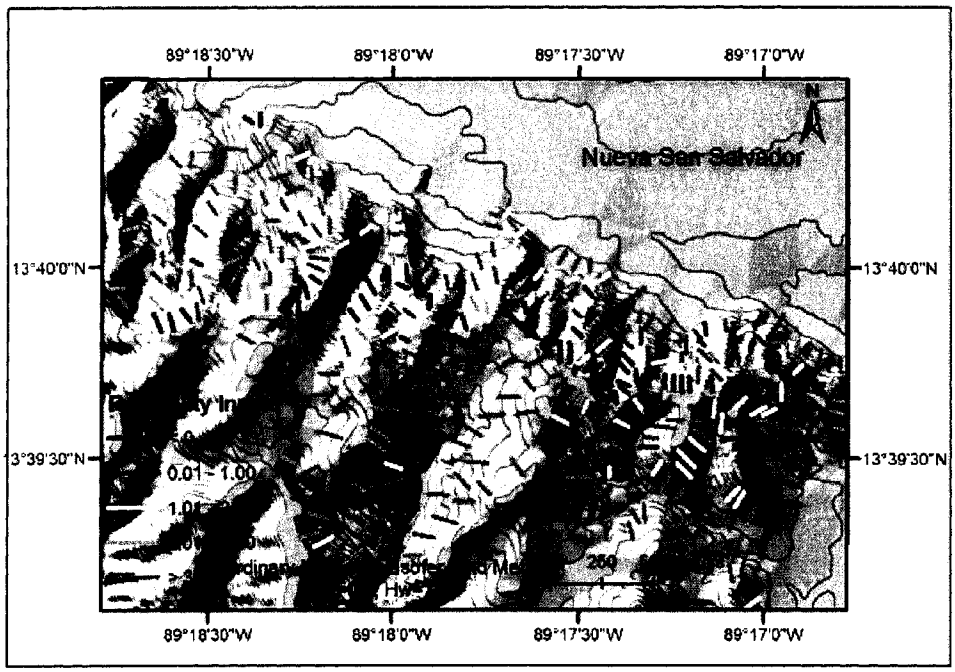

Figure 7.19 Reliability index of the slope profiles in the study area calculated using the ordinary method of slices and the Hasofer-Lind method (k=0.3, H_w=7 m)

Figure 7.20 shows a slope stability comparison in static and earthquake conditions with H_w=7 m. In the static condition (Figure 7.20a), all slope profiles are stable. Figure 7.20b shows the Newmark displacement during the January 13, 2001 earthquake. The slope profiles with displacement greater than 10cm have the high landslide susceptibility. Figures 7.20c and 7.20d show failure probability and the reliability index calculated using the Bishop simplified method with the Monte-Carlo simulation (k=0.3, H_w=7 m).

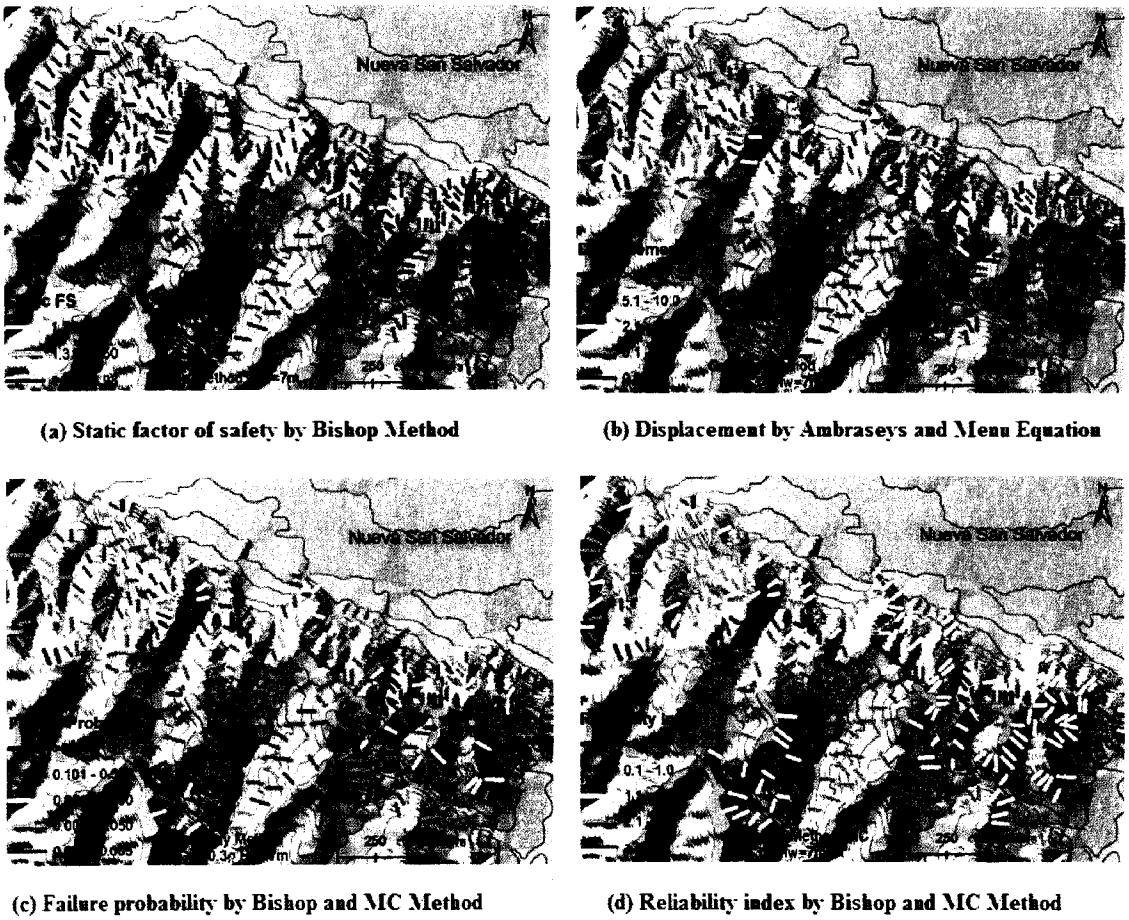

(a) Static factor of safety by Bishop Method

(b) Displacement by Ambraseys and Menu Equation

(c) Failure probability by Bishop and MC Method

(d) Reliability index by Bishop and MC Method

Figure 7.20 Slope stability comparison in the static and earthquake conditions (H_w=7 m): (a) static factor of safety using the Bishop simplified method; (b) Newmark displacement during the January 13, 2001 earthquake; (c) failure probability at k=0.3 calculated using the Bishop simplified method with the Monte-Carlo (MC) simulation; and (d) reliability index at k=0.3 calculated using the ordinary method of slices with the Monte-Carlo (MC) simulation.

Figures 7.21 and 7.22 show the landslide susceptibility map predicted by the ordinary kriging method based on the pseudo-static factor of safety and the reliability index of slope profiles. The map shows that the high landslide susceptibility zone (FS<1, or reliability index<0) is distributed in the crown area of the northern slope of the ridge. In this zone, potential landslides are expected under strong earthquake shaking similar to the January 13, 2001 earthquake. For validation of the analysis model, the triggered slope failures (cracks, slides, scarps, and crowns) during the January 13, 2001 earthquake are overlapped with the slope stability map. Comparing the analysis results of the triggered landslides, most of the landslides and cracks occurred in the high landslide susceptibility zones. Slope mitigation is necessary in this area in order to avoid slope failure during a future earthquake event. Some slope stabilization works had been completed around this area by the local government with the help of an engineering consulting company.

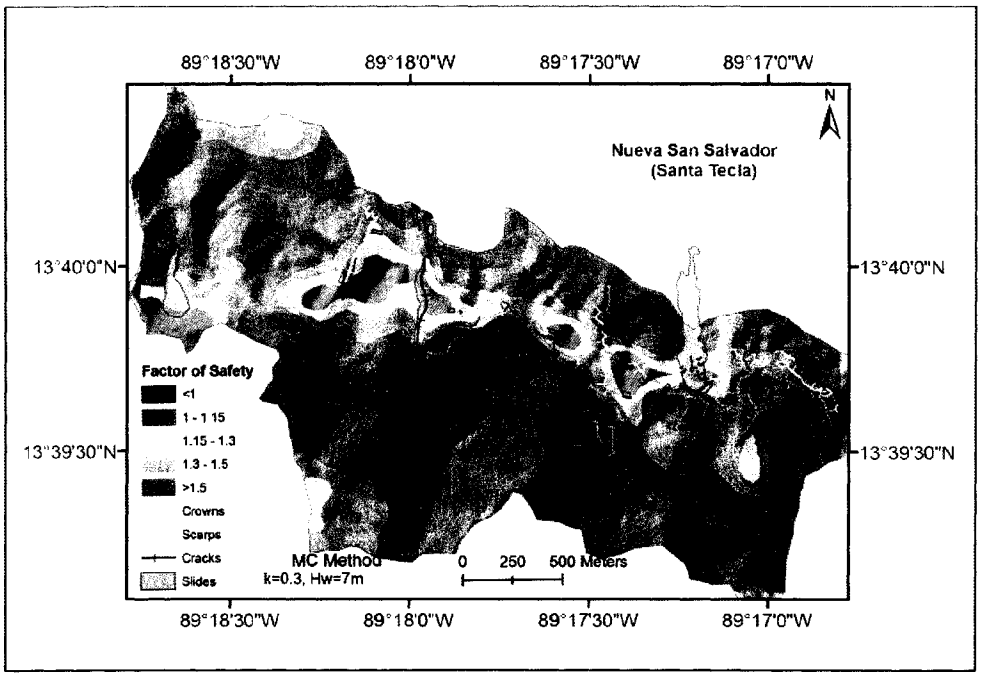

Figure 7.21 Landslide susceptibility map interpolated using the ordinary kriging method (factor of safety was calculated using the Bishop simplified method under the conditions of k=0.3, H_w=7 m).

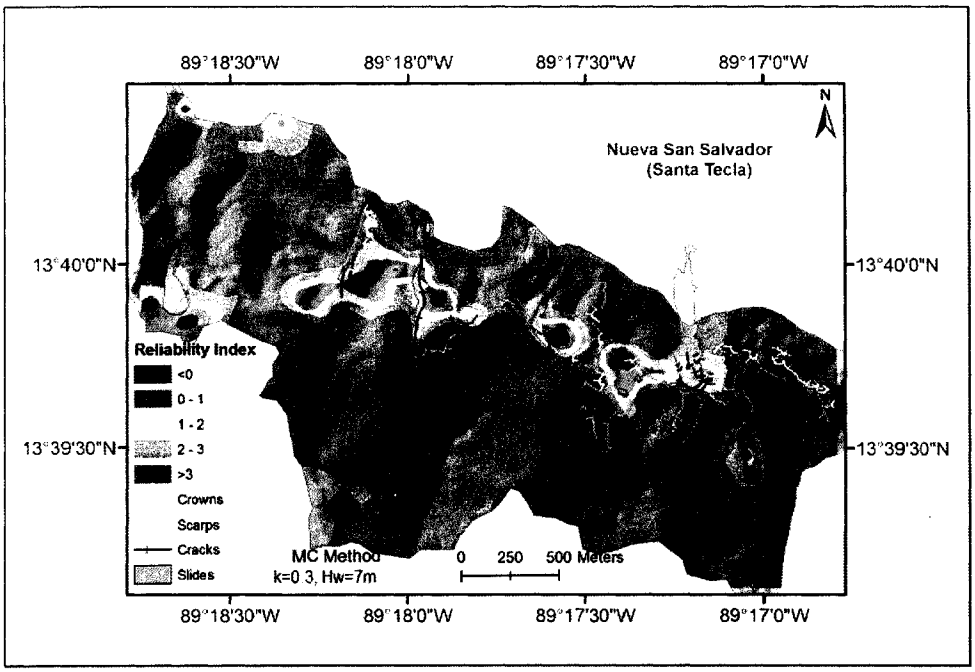

Figure 7.22 Landslide susceptibility map interpolated using the ordinary kriging method (reliability index was calculated using the Monte-Carlo simulation under the conditions of k=0.3, H_w=7 m)

7.7 Discussion

The accuracy of slope stability calculation was improved by using the GIS-based 2D slope stability analysis, which involves deterministic and probabilistic methods and slope profile definition. This method can be used to analyze the slope stability of a large number of slope profiles which are consistent with the slope stability analysis in geotechnical engineering design. A study of earthquake-induced slope stability demonstrates the applicability of GIS to data processing and slope stability calculation. Such 2D analysis methods are most suited for the site-specific landslide hazard zonation.

In order to consider the spatial variability of the soil properties and the uncertainty of geotechnical parameters, the probabilistic analysis may increase the accuracy of slope stability analysis and landslide hazard assessment in a study area.

The proposed geomorphologic and geotechnical data processing procedure via GIS is available through spatial data analysis. A slope stability analysis model outside the GIS environment can be implemented with minor effort by using the VB program. Such a 2D method is beneficial to landslide hazard assessment and slope engineering practice. A map of factor of safety with a level of accuracy achieved using the 2D method can be used for engineering design and decision-making in land use development.

In this study, we have adopted three methods, namely the ordinary method of slices, the Bishop simplified method, and the block sliding model, for earthquake-induced slope stability analysis. The Monte-Carlo simulation has also been used for probabilistic analysis. It is observed that the three slope stability methods all obtained very useful results for landslide hazard assessment. The results of the three methods show a strong linear correlation among them. On average, based on the results of 459 profiles, the factor of safety calculated using the Bishop simplified method is 6% greater than that using the ordinary method of slices and 16% greater than that using the block sliding model. The factor of safety calculated using the ordinary method of slices is 10% greater than that using the block sliding model.

Comparing the results obtained using the infinite slope model and the 2D method at the same horizontal acceleration (k=0.3) and groundwater conditions (groundwater depth is 7m), the trend of slope stability and the high landslide susceptibility zones are consistent. Figure 7.23 illustrates the 1D factor of safety calculated using the infinite slope model in the Balsamo Ridge area. For the shallow potential landslides, the very high landslide susceptibility grids (factor of safety less than 1) are distributed in the slope crown area and are strongly related to slope angle. This figure also shows that most of the very high landslide susceptibility grids occur in the region of earthquake-triggered landslide, which is also the region where crack occurred during the 2001 earthquakes.

Figure 7.24 shows the comparison of factor of safety distributions calculated using the 1D infinite slope model and the 2D Bishop simplified method at k=0.3, H_w=7m condition. The 1D result is overlaid on the 2D landslide susceptibility map. At the crown area, both methods obtained similar results.

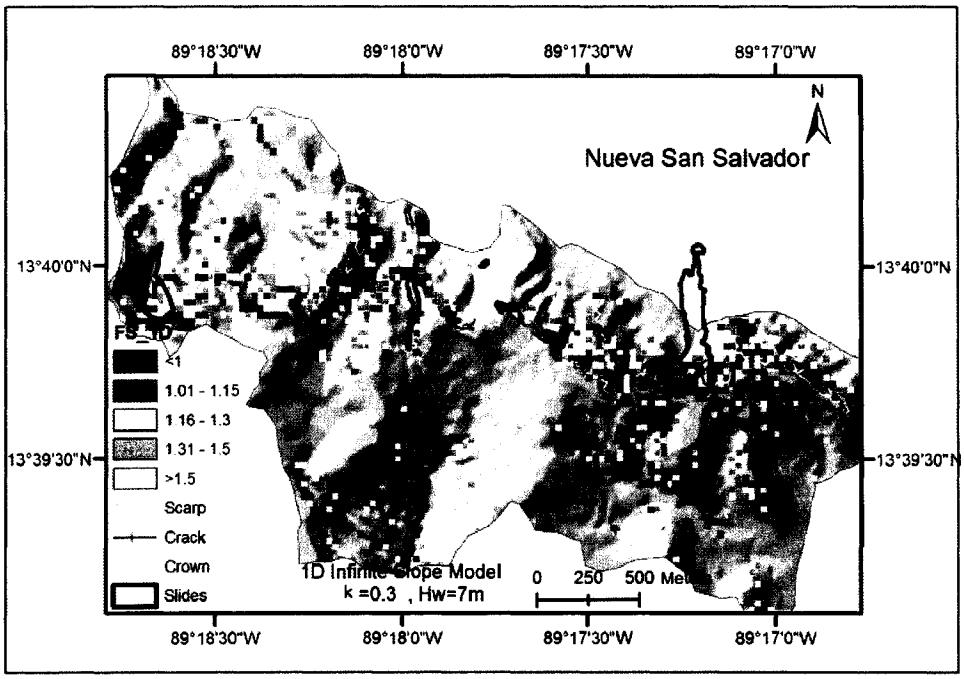

Figure 7.23 The factor of safety distribution map for the Balsamo Ridge area calculated using the infinite slope model under the conditions of k=0.3, H_w=7 m.

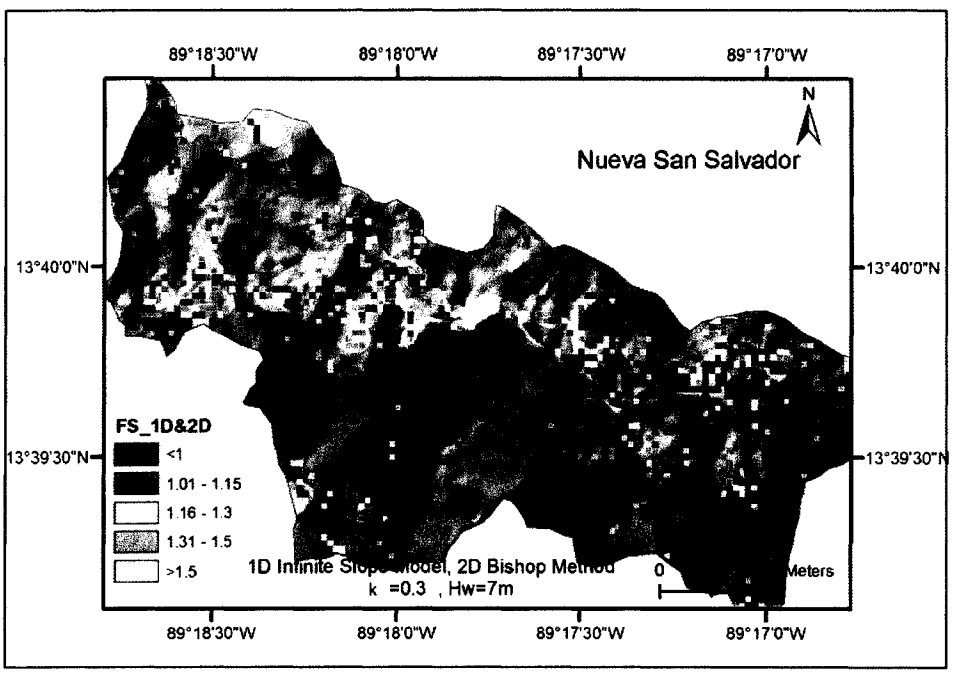

Figure 7.24 The factor of safety distribution map for the Balsamo Ridge area calculated using the infinite slope model (shown as dots) and the 2D Bishop simplified method (filled contour map) under the conditions of k=0.3, H_w=7 m .

Result comparison of landslide hazard zonation based on the slope stability index using the geostatistical method (kriging), shows that the 2D model is a feasible and cost-effective approach to slope stability analysis and seismic-induced landslide hazard zonation.

It is important to note that such a GIS-based slope stability analysis can yield erroneous results if the input data, especially the geotechnical properties and groundwater conditions are not correctly determined. The most common drawback of the 2D deterministic model is that data processing for this analysis is time consuming, which is true for any GIS-based approach. The necessary data processing requires frequent data format conversion, such as from raster grids to feature points. The coordination system, map projection, and size of each map layer must exactly match. There is also a need to develop an automatic slope profile definition program.

Chapter 8 Site-Specific Earthquake-Induced Landslide Hazard Zonation: 3D Model

8.1 Introduction

Slope failures in natural terrain and road cuts are three-dimensional (3D) with spatial variations in geological characteristics. However, in geotechnical engineering, slope stability has usually been analyzed using 2D methods. Since the late 1960s, more attention has been paid to the development and application of 3D slope stability analysis. A large number of studies of 3D slope stability problems have been done in the last two decades (Duncan, 1996). Most 3D approaches are extensions of the 2D slice methods. Along them, Hovland's analysis (Hovland, 1977) was based on an extension of the ordinary method of slices, which assumed zero normal stresses on vertical surfaces. The Hungr's method (Hungr, 1987) was an extension of the Bishop simplified method. Lam and Fredland (1993) presented a generalized model which is an extension of the 2D general limit equilibrium formulation.

By summarizing studies of the 3D slope stability, Duncan (1996) concluded that the 3D safety factor is greater than the 2D factor of safety and that the percentage difference between the 2D and 3D analysis can be as large as 30%. Some authors generalized this observation and concluded that the difference ranges between 3% and 30% and that the average is 13.9% (Gens et al., 1988). A 3D slope stability analysis could be conducted to supplement a 2D analysis.

In some cases, the 1D and 2D slope stability analyses and landslide hazard zonation produced in GIS applications yield acceptable results. However, the results appear to give a conservative estimate for slope stability due to the fact that they ignore the influence of lateral forces. Therefore, for a more accurate and realistic stability analysis it is necessary to use the 3D methods to analyze slope stability, even though the 3D analysis is more difficult to perform than the 1D infinite slope model. A few attempts to use a 3D model have recently been made (Xie et al., 2003, 2005).

Among the 3D methods, the general limit equilibrium method of columns is the most popular and is considered as the most feasible method for practical engineering applications. The overall slip surface can be assumed as a sphere or ellipsoid. The potential failure mass is separated into discrete columns. Such discrete soil/rock columns in 3D analysis can be described using grid-based raster data sets in GIS. The slope geometry and geotechnical parameters of each column can be presented in several map layers. The grid can be generated so as to be compatible with the columns in the 3D slope stability analysis. GIS spatial analysis tools can easily process multiple datasets. Thus the column-based 3D models can be used for the stability calculation in GIS. The factor of safety of a slope area can be obtained by running an analysis program inside the GIS environment or by exporting it to an external analysis module for calculation.

The Balsamo Ridge area in Nueva San Salvador was selected for this site-specific hazard zonation. The area experienced strong seismic shaking which triggered destructive landslides, cracks, and other surface damage during the 2001 earthquakes. The horizontal earthquake acceleration at the top of the ridge was estimated to be over 0.6g (Jibson et al., 2004).

8.2 Slope Stability Analysis Model: 3D Column Method

8.2.1 General Description

In GIS-based 3D landslide hazard assessment, the slope unit was selected as a mapping unit. Terrain or hydrology analysis methods can be used to identify such slope units from the DEM (Digital Elevation Model) dataset. All original datasets for stability analysis are available with respect to each grid cell. After partitioning the study area into a number of slope units, the slope unit data can be exported to an external computer program. A 3D slope stability program extracts data of each grid within the boundary of pre-defined slope units. By inputting data for each slope unit into the 3D slope stability analysis model, the factor of safety can be obtained.

In this study, a GIS-based 3D approach was developed based on the block (columns) analysis within pre-defined slope units. The conventional 3D slope stability analysis method can be applied in the GIS-based slope stability analysis. The Hovland's (1977) 3D slope stability analysis method was used to calculate the factor of safety. A relatively simple 3D block sliding method was also explored. In the 3D models, the calculation was performed outside the GIS platform with an external slope stability program. The GIS data were exported to an external computer program of slope stability analysis. The results calculated by the program were imported to the GIS platform. And then, the slope stability and landslide hazard zonation were performed in a GIS platform based on the 3D factor of safety. A VB program was developed to implement the 3D slope stability analysis.

8.2.2 Hovland's 3D Column Method

The geometry of a potential 3D slope failure mass is illustrated in Figure 8.1. The failure mass is divided into a number of columns with vertical interfaces. The potential overall slip surface postulates as a spherical or ellipsoid surface. A 3D view of individual columns, analogous to a slice in a 2D analysis, is shown in Figure 8.2. In Figure 8.2, H is height of the column; L is width of the column; H_w is height of groundwater; E_L, E_R, P_L, P_R are intercolumn normal force; T_L, T_R, S_L, S_R are intercolumn shear force; N, U, T are normal forces, water pressure, and shear forces acting on the slip surface, respectively; and α is dip angle of the slip surface.

Hovland's method (Hovland, 1977) is an extension of ordinary method of slices. The analysis assumes that the soil column is selected small enough so that all faces can be described by planes. The depth of the column, H, is simply computed approximately from the center of the top surface to the center of the slip surface (bottom). In order to avoid complicated coordination transformation, the global coordination system and vector method are applied in the geometric description and force analysis for each column, as will be described in this section.

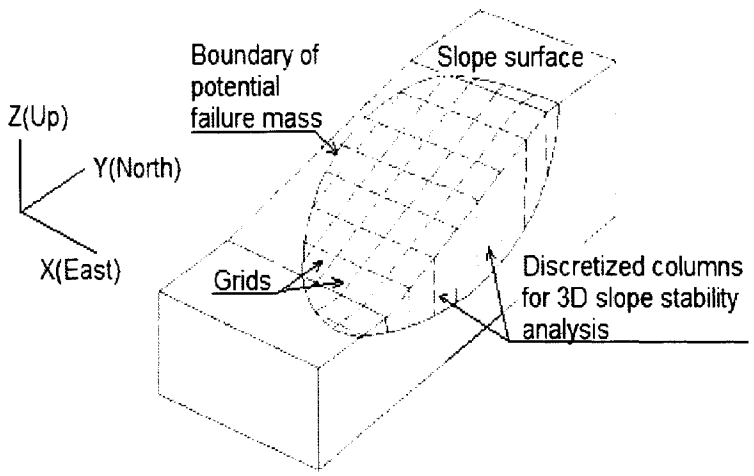

Figure 8.1 Schematic view of a 3D potential failure mass. The potential overall slip surface is postulated to be a spherical or ellipsoid surface. Each GIS grid represents a soil block or soil column.

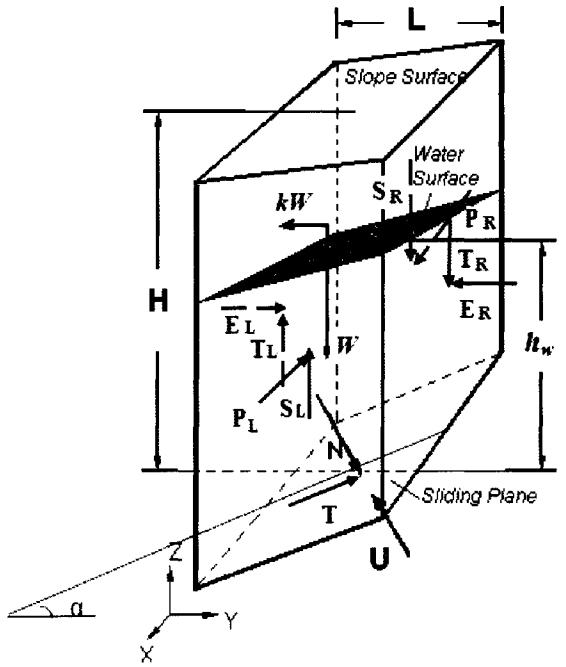

Figure 8.2 A 3D view of an individual column. H is the height of the column; L is width of column; H_w the height of groundwater; E_L, E_R, P_L, P_R are intercolumn normal forces; T_L, T_R, S_L, S_R are intercolumn shear forces; N, U, T are normal force, water pressure, and shear force acting on the slip surface, respectively; and α is the dip angle of the slip surface.

The formula of the factor of safety can be derived in a manner similar to that used for the 2D ordinary method of slices. Like the 2D method, the 3D method also ignores the intercolumn forces. The 3D static factor of safety can be expressed as:

$$FS_{3D} = \frac{\sum_{i=1}^{n}[c_i A_i + (W_i \cos\alpha_i - \gamma_w h_{w_i} A_i)\tan\phi_i]}{\sum_{i=1}^{n} W_i \sin\alpha_i} \qquad (8.1)$$

where: ϕ_i is effective friction angle of sliding surface; c_i is cohesion of sliding surface; α_i is dip angle of sliding surface (plane); A_i is area of slip surface; W_i is weight of soil column; γ_w is unit weight of water; h_w is water column height from the center of slip surface to groundwater table; and n is total number of columns.

Considering the horizontal earthquake force, kW, the 3D pseudo-static factor of safety can be calculated as:

$$FS_{3D} = \frac{\sum_{i=1}^{n}[c_i A_i + (W_i \cos\alpha_i - kW_i \sin\alpha_i - \gamma_w h_{wi} A_i)\tan\phi_i]}{\sum_{i=1}^{n}[W_i(\sin\alpha_i + k\cos\alpha_i)]} \qquad (8.2)$$

where: k is the seismic coefficient.

This method may be inaccurate because it assumes a zero normal stress on the vertical surface. However, for GIS-based slope stability and landslide hazard zonation, such deviations may be considered acceptable for site specific landslide hazard assessment.

One of the important steps in the 3D column method is determining the spherical or ellipsoid slip surface for each slope unit. This 3D surface will intersect with each soil column and form a potential sliding surface. The overall slip surface consists of the individual slip surfaces of all columns, and is assumed to be planar with a dip angle and dip direction. In the force analysis, all forces will be decomposed at each slip surface. In order to simplify the coordinate transformation, all slip surfaces and forces should be described in a same coordinate system. Therefore, the vector analysis method is used to perform the geometry and force analysis in the 3D model.

8.2.3 Geometric Description of Columns

In the 3D model, the vector analysis method is employed to describe the geometry of sliding blocks (or soil columns) and the accompanying forces (Goodman and Shi, 1985). Based on the rigid limit equilibrium concept of stability analysis, the principal assumptions are: (1) the sliding surface of each column is assumed to be perfectly planar (which is acceptable if the width of columns is small enough); (2) sliding blocks are assumed to be rigid; (3) the failure mode of multiple blocks is planar failure (sliding along one sliding surface); (4) at the critical condition, the factor of safety of all individual columns is the same; (5) the overall factor of safety is calculated based on the force or moment equilibrium of the entire column system.

Defining the coordinate system as x being east, y being north and z being up, the slope surface and sliding surface of a column is represented by a plane with dip angle (α) and dip direction (β). The equation of the plane through point (x_0, y_0, z_0) with normal vector (l, m, n) is:

$$l(x-x_0)+m(y-y_0)+n(z-z_0)=0 \tag{8.3}$$

The values of normal vector coordinates of the sliding plane or joint are:

$$\begin{cases} l=\sin\alpha\sin\beta \\ m=\sin\alpha\cos\beta \\ n=\cos\alpha \end{cases} \tag{8.4}$$

where: α = dip angle of a plane; β = dip direction of a plane; and (x_0, y_0, z_0) are the coordinates of a point on the plane as shown in Figure 8.3.

The 3D geometric analysis can be used to determine the normal vectors of planes, coordinates of corners, the areas of slip surface of each column, sliding direction, and the volume of each column.

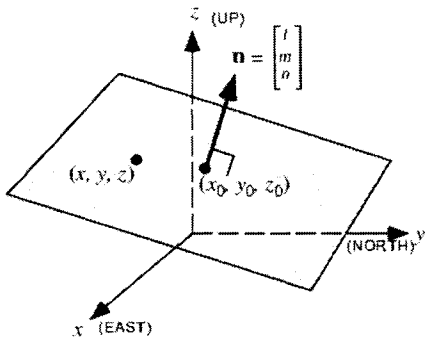

Figure 8.3 A plane and its normal vector (**n**). The coordinate system is x being east, y being north and z being up. Plane equation can be determined by its normal vector and a point on the plane.

8.2.4 Force Description by Vector Analysis

If the magnitude and direction of a force is represented by $\vec{F}$, then the components of the force are the coordinate values:

$$\vec{F} = (X, Y, Z) \tag{8.5}$$

The magnitude of the force is:

$$\left|\vec{F}\right| = \sqrt{X^2 + Y^2 + Z^2} \tag{8.6}$$

The direction of $\vec{F}$ is given by:

$$\vec{f} = \left(\frac{X}{\left|\vec{F}\right|}, \frac{Y}{\left|\vec{F}\right|}, \frac{Z}{\left|\vec{F}\right|} \right) \tag{8.7}$$

For example, the direction $\vec{n}$ of a normal force on a plane P is:

$$\vec{n} = (l, m, n) \tag{8.8}$$

If the magnitude of a normal force is N, then the components of N at X, Y and Z direction will be:

$$\vec{N} = (lN, mN, nN) \tag{8.9}$$

For horizontal earthquake force:

$$\left|\vec{F}_q\right| = kW \tag{8.10}$$

$$\vec{F}_q = kW(\sin\beta_e,\ \cos\beta_e,\ 0) \qquad (8.11)$$

where: k=seismic coefficient

W = the weight of rock block, kN

β_e = direction of horizontal acceleration

The resultant force, $\vec{R}$, of a series of intersecting forces $F_1, F_2, \ldots, F_n$ is:

$$\vec{R} = \sum_{i=1}^{n} F_i = (\sum_{i=1}^{n} X_i, \sum_{i=1}^{n} Y_i, \sum_{i=1}^{n} Z_i) \qquad (8.12)$$

8.2.5 Defining the Overall Slip Surface

The overall slip surface can be assumed to be a spherical or ellipsoid surface. For a spherical surface, if the coordinates of 4 points are given in 3 dimensions, then the equation of the slip sphere containing those points on the surface can be found by solving the following determinant.

$$\begin{vmatrix} x^2+y^2+z^2 & x & y & z & 1 \\ x_1^2+y_1^2+z_1^2 & x_1 & y_1 & z_1 & 1 \\ x_2^2+y_2^2+z_2^2 & x_2 & y_2 & z_2 & 1 \\ x_3^2+y_3^2+z_3^2 & x_3 & y_3 & z_3 & 1 \\ x_4^2+y_4^2+z_4^2 & x_4 & y_4 & z_4 & 1 \end{vmatrix} = 0 \qquad (8.13)$$

The conditions on the 4 points are: no three combinations of the 4 points can be collinear and all 4 points cannot lie on the same plane (coplanar). Figure 8.4 shows a spherical slip surface defined for 3D slope stability analysis.

If the determinant is found using the expansion by minors with the top row, the equation of the sphere can be written simply in term of the minors M_{1j}:

$$(x^2+y^2+z^2)M_{11} - xM_{12} + yM_{13} - zM_{14} + M_{15} = 0 \qquad (8.14)$$

The general equation of a sphere with radius, R_0, centered at (x_0, y_0, z_0) is:

$$(x-x_0)^2+(y-y_0)^2+(z-z_0)^2=R_0^{\ 2} \tag{8.15}$$

The center, (x_0, y_0, z_0), and radius, R_0, of the sphere can be solved based on Equations 8.14 and 8.15:

$$\begin{aligned} x_0 &= \frac{1}{2}M_{12}/M_{11} \\ y_0 &= -\frac{1}{2}M_{13}/M_{11} \\ z_0 &= \frac{1}{2}M_{14}/M_{11} \\ R_0^{\ 2} &= x_0^2+y_0^2+z_0^2-M_{15}/M_{11} \end{aligned} \tag{8.16}$$

If either the four points are coplanar or three are collinear, the M_{11} will equal zero.

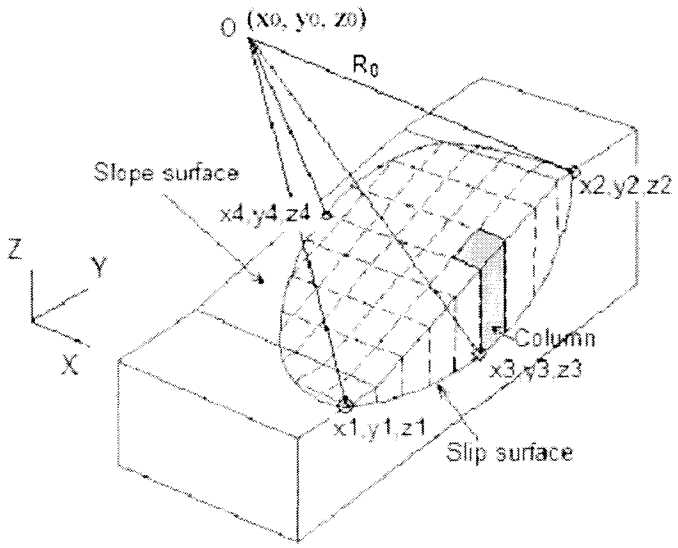

Figure 8.4 Spherical slip surface definition for the 3D slope stability analysis. A spherical slip surface can be determined by 4 space points. The conditions on the 4 points are: no any three points can be collinear and all 4 points cannot lie on the same plane (coplanar)

8.2.6 Critical Slip Surface for 3D Slope Stability Analysis

The slope may fail along a number of potential slip surfaces. In this study, a number of spherical slip surfaces were generated for each slope unit within a pre-defined depth and dimension of potential sliding mass. The slip surface with the minimum factor of safety will be considered to be the critical surface. The depth and dimension of the potential sliding mass was determined by statistical analysis of the dimensions of historical landslides in the study area and its vicinity.

8.3 Block Sliding Model

The GIS-based 3D block sliding model is an extension of the 2D block sliding model. The area for the 3D block sliding model is the entire slope unit, which is shown in Figure 8.5.

This approach is based on force equilibrium of columns of potential sliding mass in a slope unit. Ignoring the lateral forces acting on the vertical sides of each column, the total resisting forces and sliding forces are the sums of resisting forces and sliding forces of all columns within an entire slope unit, respectively. The 3D pseudo-static factor of safety can be calculated by dividing the total resisting force by the total sliding force:

$$FS_{3D} = \frac{\sum_{i=1}^{n} R_i}{\sum_{i=1}^{n} T_i} = \frac{\sum_{i=1}^{n} [c_i A_i + (W_i \cos\alpha_i - kW_i \sin\alpha_i - U_i)\tan\phi_i]}{\sum_{i=1}^{n} [W_i(\sin\alpha_i + k\cos\alpha_i)]} \qquad (8.17)$$

where FS_{3D} is the 3D pseudo-static factor of safety. Other elements in Equation 8.17 are same as those in Equation 8.1. This method ignores all of the intercolumn forces acting on the sides of the columns. The magnitudes of resisting force and sliding force mainly depend on the slope surface inclination and the area of pre-defined slope units.

Equation 8.17 can produce error due to ignoring the influence of force direction, inter-coloum forces, and moment equilibrium. However, if the variation of angle of sliding surface is less than 10° within a profile, as in the 2D block sliding method, the error in the factor of safety of slope unit may be less than 10%.

This is a simplified GIS-based method for the 3D slope stability analysis. The results may be conservative due to the fact that the entire area of a slope unit was used. Actually, landslides rarely happen in such a large area. Therefore, caution should be exercised when interpreting the results. However, this method can speed up GIS-based analysis because there are fewer complications in computation.

In order to improve the accuracy of the 3D block sliding model, the boundary of slope units can be buffered to a certain distance. The buffered boundary area will not be considered as the area of the slope unit, which will reduce some distortions near valley baselines and the dividing line in a drainage basin, because the areas near the valley line and dividing lines usually have smaller slope angle.

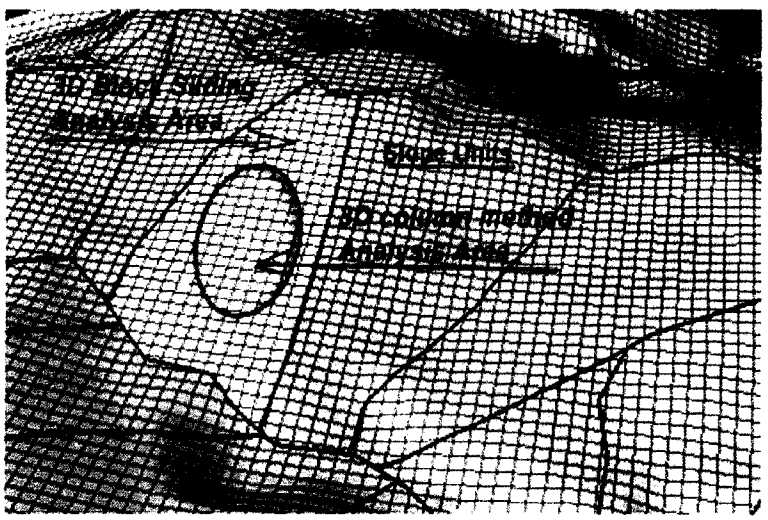

Figure 8.5 The analysis area for the 3D block sliding model and the Hovland's column method. The analysis area for the 3D block sliding model is the entire slope unit, and the analysis area for the Hovland's model is the area of a spherical slip surface within the slope unit.

8.4 The Definition of Slope Units

The GIS-based 3D slope stability and landslide hazard zonation requires selecting suitable mapping units. A mapping unit is a portion of the land surface which contains a set of ground conditions different from the adjacent units across definable boundaries (Hansen, 1984). Division of landscapes into identifiable sections is based primarily on soil-forming processes, or landforms and landscape elements, or combination of both. The general mapping units in landslide hazard zonation include grid cells, unique-condition units, slope units, and geomorphic units. For the 3D slope stability analysis, the slope unit was selected as mapping unit for this study area. Since a physical relationship exists between landsliding and the fundamental morphological elements in a mountain area, the slope unit seems most appropriate for landslide hazard assessment (Carrara et al., 1995).

The slope unit can be considered to be the left or right side of a sub-basin of any order into which a watershed can be partitioned. Therefore, it can be delimited by a ridge line and a valley line. The slope unit partition is based partly on plan forms and partly on the position of slope in relation to drainage lines. The basin can be partitioned into three units using catchment boundaries and first-order drainage lines: the valley head and the two lateral slopes as illustrated in Figures 8.6. Slope units can be resized according to the prevailing slope failure mode and size, partitioning a river basin into nested subdivisions, coarser for larger landslides and finer for smaller slope failures (Montgomery and Dietrich, 1994). Slope units can be further subdivided into geomorphic units. Ruhe and Walker (1968) further identified geomorphic units of headslope, noseslope, and sideslope, which are divergent, convergent, and linear possibilities for flow lines, corresponding to curvature in planimetirc view (Figure 8.6).

Due to the difficulties in manually identifying sub-basin boundaries, an automated procedure is required. Many techniques for automatically generating drainage-divide networks are available, for example, ArcHydro (Maidment, 2002) and ArcGIS Hydrology tools. Information about the drainage network can be obtained from the DEM

or ESRI grid. ArcHydro tools in ArcGIS can be used to draw dividing lines to form slope units using the ridge lines and valley lines as boundaries. However, this method requires a high resolution DEM data. Low resolution DEM data may not be sufficient for detailed slope unit classification. As a result, low resolution DEM data cannot provide reliable and accurate results for the 3D slope stability analysis. The final slope unit classification is performed according to the drainage network, catchment boundaries, and slope types with manually adjustments. Experience in terrain analysis is necessary to carry out such a slope unit classification.

The effective size of slope units for slope stability analysis depends on the scale of the topographic map. A larger scale topographic map can serve to form finer slope units. Therefore, large scale topographic maps are suggested for more accurate slope stability analysis. However, the appropriate size of the slope unit should relate to the average size of the historic landslides occurred in the study area as well.

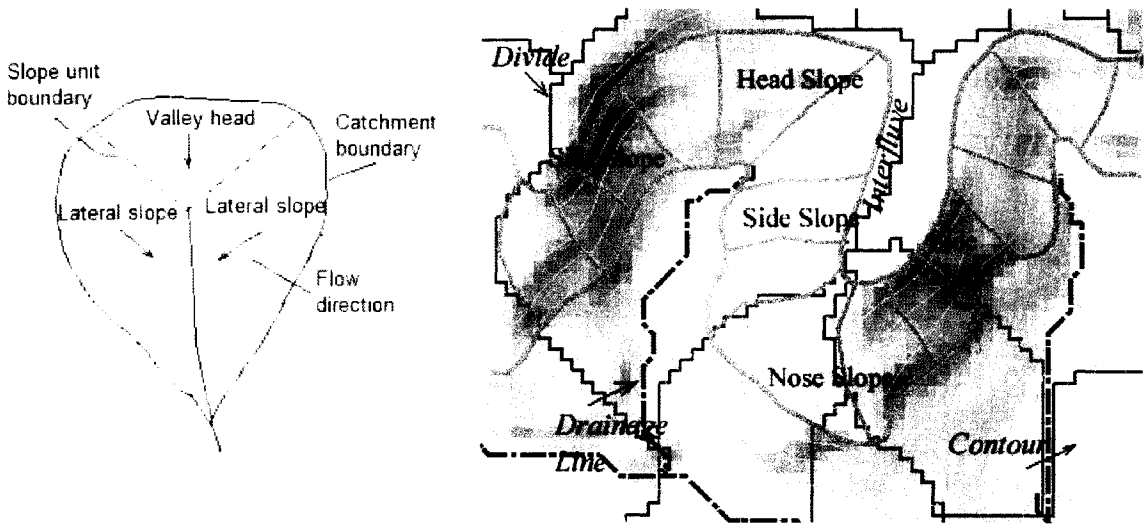

Figure 8.6 Definition of slope units (left) and geomorphic units (right) in a basin as used to determine mapping units in the 3D slope stability analysis. Slope units can be partitioned by ridge lines and valley lines and elementary slope can be defined as valley head (or head slope), lateral slope (or side slope), spur-end (or nose slope).

8.5 GIS Data Process and Landslide Hazard Zonation

The GIS procedure for data processing for the 3D analysis is similar to that for the 2D analysis. The factor of safety of the slope units is calculated using a VB program developed for this study. The slope stability and landslide susceptibility are mapped based on the 3D factor of safety.

All of the data sets needed to conduct a detailed seismic-induced landslide hazard zonation were digitized and rasterized at a 10m grid spacing in ArcGIS platform. The data layers needed for 3D analysis are listed in Table 8.1.

Table 8.1 Data layers for the 3D slope stability analysis

Data Layers		Data Format
1	Slope surface angle (α)	Grid and Point
2	Slip surface angle (θ)	Grid and Point
3	Soil friction angle (ϕ)	Grid and Point
4	Soil cohesion (c)	Grid and Point
5	Soil unit weight (γ)	Grid and Point
6	Soil depth (H)	Grid and Point
7	Horizontal acceleration (k or PGA)	Grid and Point
8	Slope units	Polygon and Point
9	DEM model (X, Y, and Z value)	Point or Text

Figure 8.7 is a flow chart showing the sequential steps involved in hazard mapping.

The earthquake-induced landslide susceptibility zone can be estimated using the value of the factor of safety listed in Table 8.2.

In the 3D columns method, the factor of safety of a spherical sliding mass represents the factor of safety of a slope unit. In fact, the analyzed spherical sliding mass is only a part of a slope unit because the length of a sliding mass is inside the boundary of a slope unit. Considering the analyzed spherical sliding mass as a sampled point, the

factor of safety of the unsampled region can be estimated by interpolation techniques using geostatistical analysis. As in the 2D analysis, the inverse distance method or the ordinary kriging method is used for the 3D landslide hazard zonation.

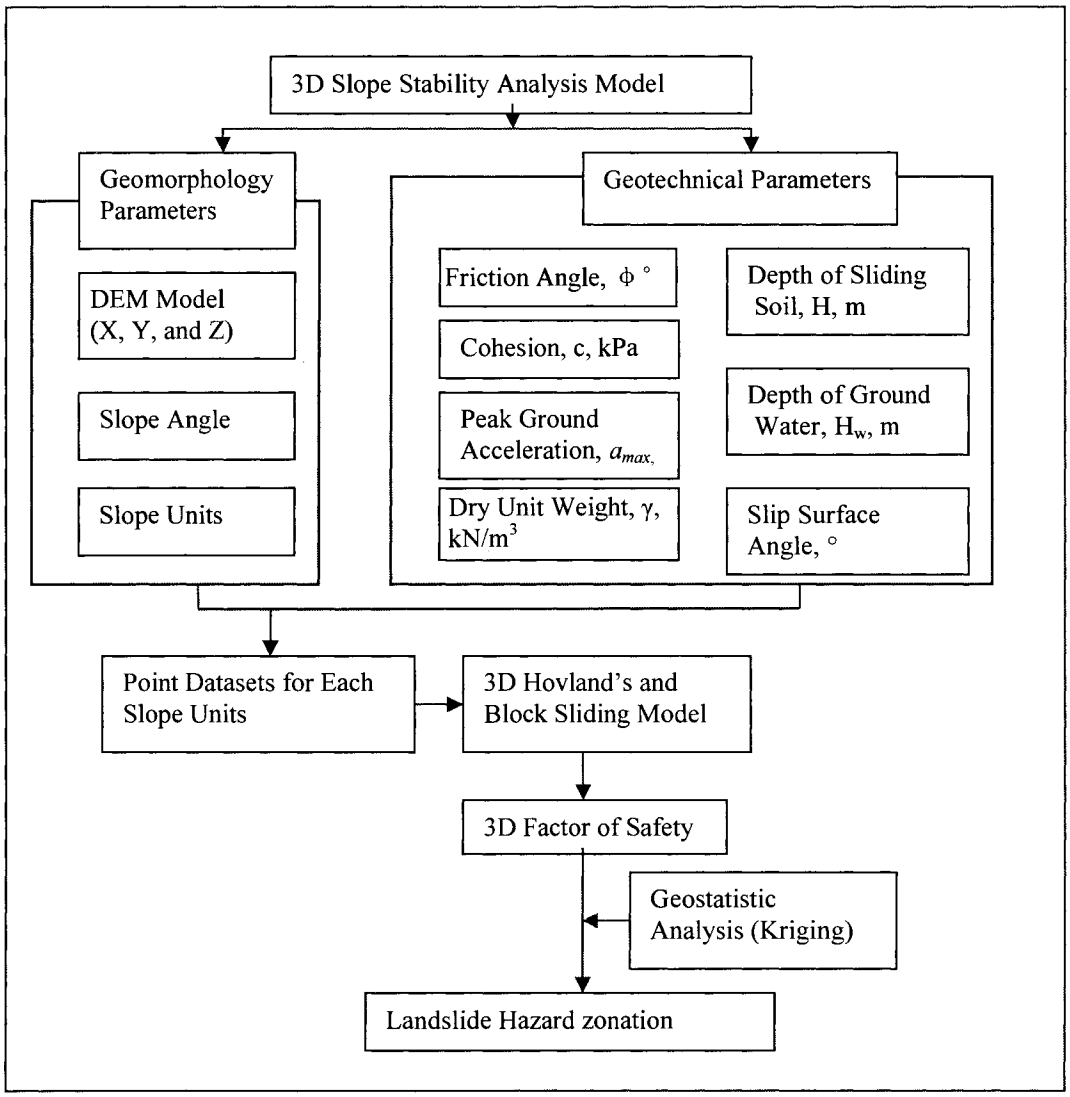

Figure 8.7 Flowchart of the 3D slope stability analysis and landslide hazard zonation.

Table 8.2 The landslide susceptibility zones and ranges of factor of safety for each landslide susceptibility zone

Zones	Landslide Susceptibility	Pseudo-static *FS*
1	Very high landslide susceptibility zone, landslides are expected	<1
2	High landslide susceptibility zone, landslides are likely to occur	1~1.15
3	Moderate landslide susceptibility zone, moderate levels of landslide hazard exists	1.15~1.3
4	Low landslide susceptibility zone, landslides are not likely to occur	1.3~1.5
5	Very low landslide susceptibility zone, safe slopes	>1.5

8.6 Landslide Hazard Zonation of Balsamo Ridge, Nueva San Salvador

8.6.1 General Description

The 3D slope analysis model was tested in the Balsamo Ridge area of Nueva San Salvador. The analysis models include Hovland's column method and block sliding method. The geotechnical parameters are same as those in the 2D analysis.

According to statistical data of historic landslides, the length of half of the documented landslides is between 25 and 100 m. Therefore, for Hovland's method, the length of potential landslides is considered to be between 25 and 100 m. The maximum depth of the sliding mass is 15 m. In the analysis, the slope stability analysis program searches for the slip surface with the minimum factor of safety.

The study area in Balsamo Ridge area is divided into 262 slope units. The total area of the study region is 4.91 km^2, and the average surface area of slope units is 18,745 m^2. Figure 8.8 shows the slope units used in the 3D slope stability analysis. In Figure 8.8, the slope units are overlaid onto a contour map and a hillshed image of the Balsamo Ridge area.

8.6.2 Result Comparison

The main testing scenarios of the 3D analysis are listed in Table 8.3. Static (no earthquake) and dynamic loading (seismic coefficients k=0.3 and k=0.6) with dry and partially saturated conditions are considered in the calculation. Both the Hovland's column method and the block sliding model were used to analyze the 3D slope stability.

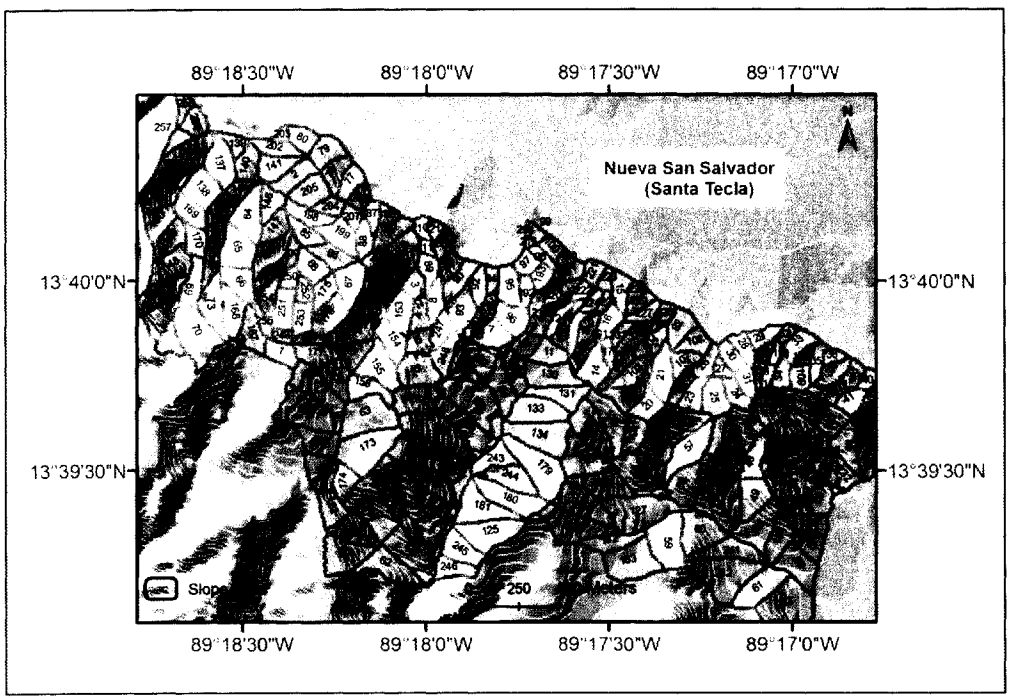

Figure 8.8 Slope units and their ID numbers for the 3D slope stability analysis in the study area

Table 8.3 The calculating conditions in the 3D slope stability analysis

3D Hovland's Method and Block Sliding Model			
Cases	k	Ground Water Condition	Max. Soil Depth
1	No earthquake	Dry	15m
2	0.3	Dry	15 m
3	0.3	7m	15 m
4	0.6	7 m	15 m

Figure 8.9 shows the 3D factor of safety distribution under different peak ground accelerations with the same groundwater conditions (depth of groundwater table H_w=7m), which was obtained using the statistics from 262 factors of safety calculated using Hovland's model. From these curves, under static condition, the factors of safety of all slope units are greater than 1.2, which indicates that the entire area is stable. If k is 0.3, the factors of safety of the three slope units are less than 1.0, and 32 of slope units' factors of safety are between 1 and 1.15. At the condition of k=0.6, the slope stability decreases rapidly, and 125 slope units fail or are at the critical condition.

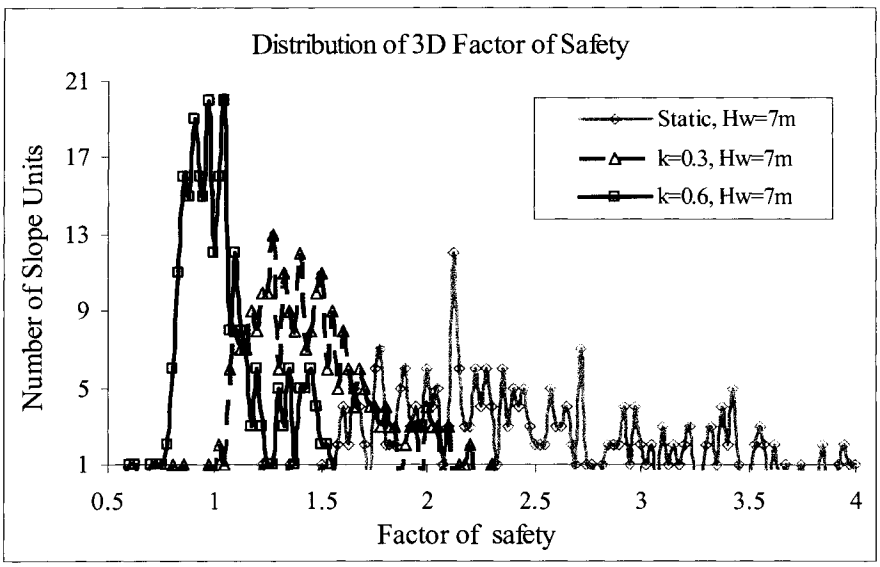

Figure 8.9 Factor of safety distribution (3D) under the conditions of 7m depth of ground water and different peak ground accelerations (statistical histogram curves of 262 factors of safety calculated using the Hovland's column method)

Figure 8.10 shows the comparison of factor of safety using the Hovland's method and the block sliding method. The correlation coefficient, R, is 0.61. The correlation of the two factors of safety is not perfect, but they do have a significant relationship.

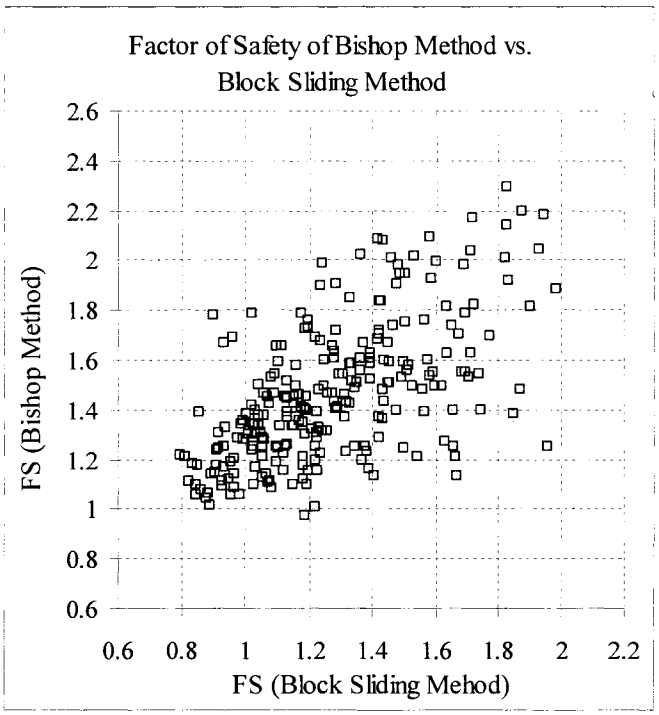

Figure 8.10 Comparison of factor of safety using the Hovland's method and the block sliding method (k=0.3 and H_w=7 m)

8.6.3 Landslide Hazard Zonation

The value of the factor of safety was ranked to illustrate relative landslide susceptibility. The ranges of factor of safety for each susceptibility zone are listed in Table 8.2.

The maps (Figures 8.11 and 8.12) show the distribution of the factors of safety obtained from the 3D Hovland's model under static (k=0) and dynamic conditions (k=0.3). Under static conditions, the slope units within entire area are stable. At k=0.3, three slope units in the northwest part of the area fail and thirty-two slope units on the northern slope are marginal (FS=1.01 to 1.15). Consistent with the 2D result, the high and moderate landslide susceptibility areas (lower factor of safety areas) are distributed along the northern side of the ridge. Some of the triggered landslides and cracks during the 2001 earthquakes occurred in these areas. This result is consistent with the instability and the slope failure areas during 2001 earthquakes.

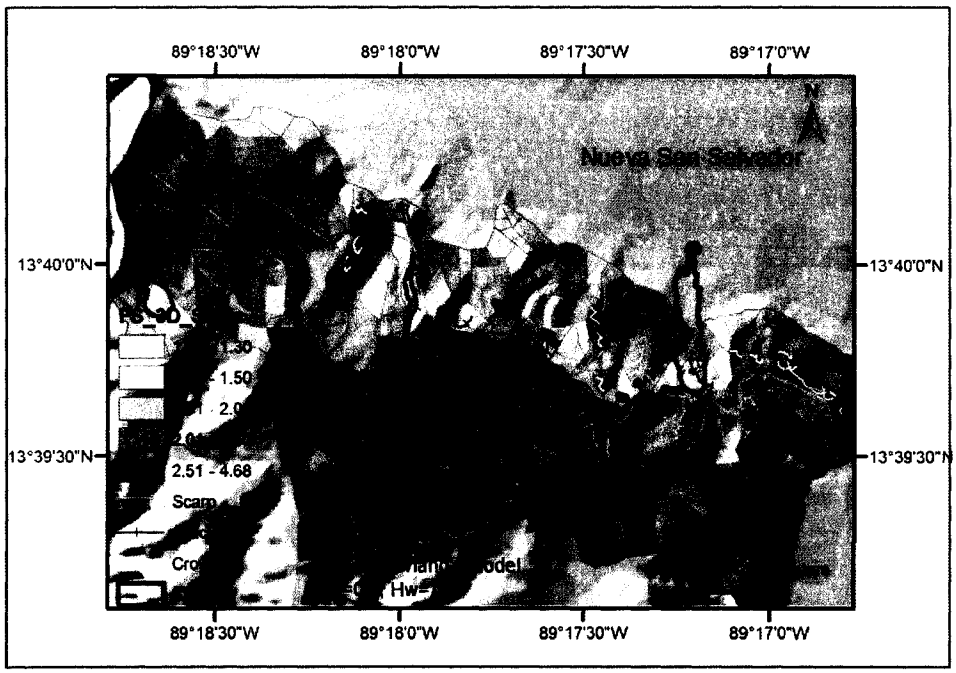

Figure 8.11 The 3D factor of safety calculated using the Hovland's model (no earthquake, H_w=7 m) and locations where slope failures occurred during 2001 earthquakes.

Figure 8.12 The 3D factor of safety calculated using the Hovland's model (k=0.3, H_w=7m) and locations where slope failures occurred during 2001 earthquakes

For comparison purposes, the slope stability calculated using the block sliding model is shown in Figure 8.13. The factor of safety calculated using the block sliding model has the same trends as that calculated using the Hovland's model. Comparing the results calculated using both models, Hovland's model yields higher factors of safety. The 3D results show that most of the historic landslides and cracks occurred in the high landslide susceptibility zones.

Figures 8.14 and 8.15 show the landslide hazard zonation map predicted using the ordinary kriging method based on factor of safety calculated using the Hovland's and the block sliding model. The map generated by the block sliding model appears to have slightly overestimated the very high landslide susceptibility area (Figure 8.15). The map generated by Hovland's model slightly underestimated the very high landslide susceptibly zones. Overlaying the historic slope movement, the landslides, scarps, and cracks appear in the very high and high landslide susceptibility zones. These results indicate that the 3D analysis model is valid for landslide hazard zonation. To avoid potential slope failure in the future earthquakes, slope mitigation is necessary in this area.

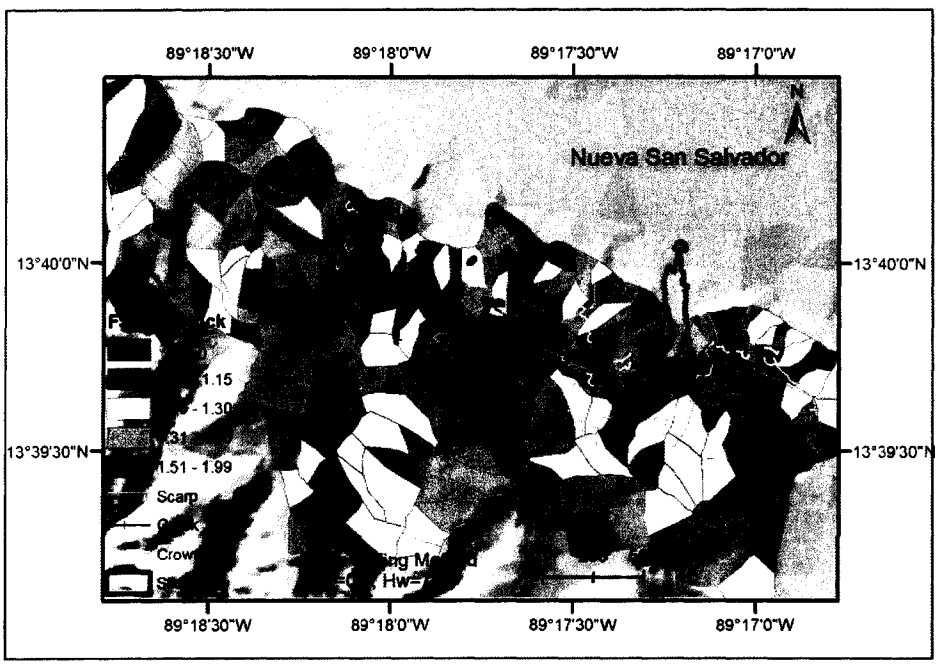

Figure 8.13 The 3D factor of safety calculated using the block sliding model (k=0.3).

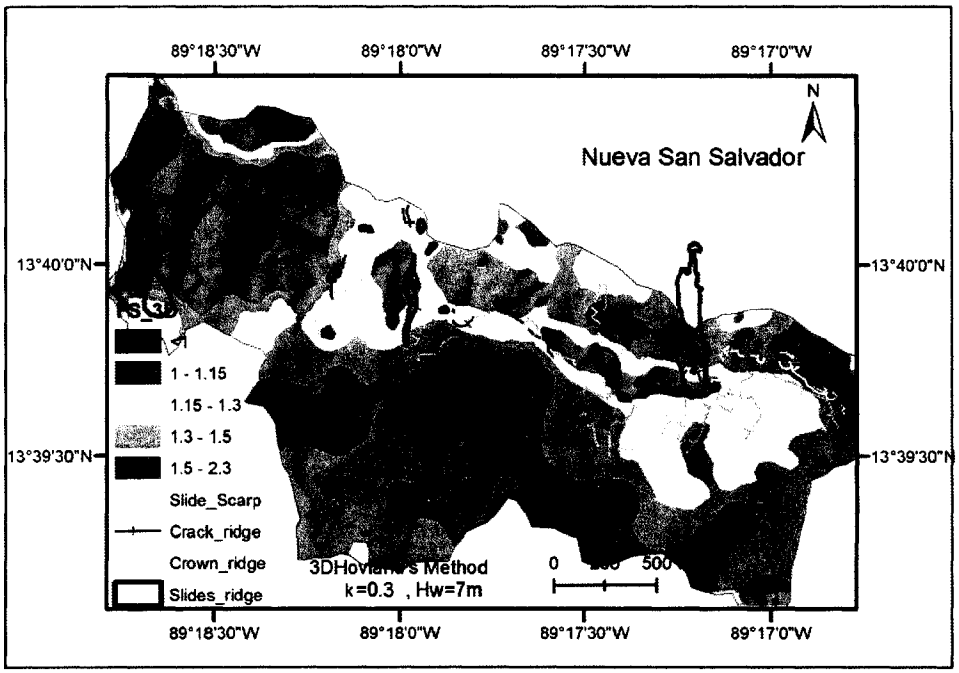

Figure 8.14 The landslide susceptibility map predicted by the 3D factor of safety (Hovland's method, k=0.3) using geostatistical analysis

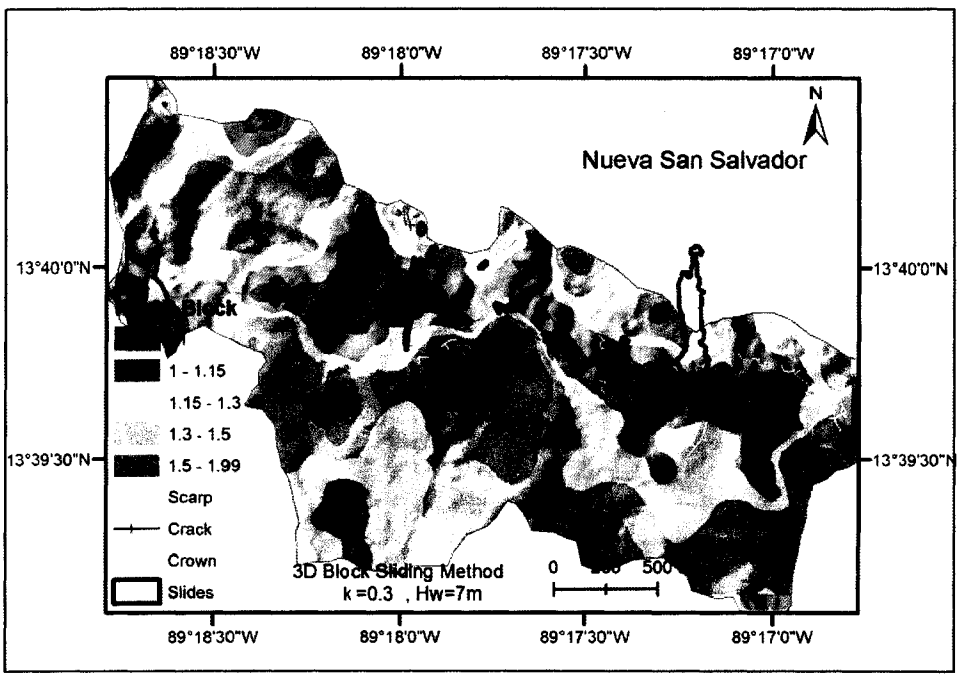

Figure 8.15 The landslide susceptibility map predicted by the 3D factor of safety (block sliding model, k=0.3) using geostatistical analysis

8.7 Discussion

The GIS-based 3D model presented in this chapter is designed for slope stability analysis and potential landslide hazard assessment. This GIS-based 3D method for earthquake-induced landslide hazard assessment was applied for the first time in the study area in Nueva San Salvador, El Salvador. The GIS-based 3D slope stability analysis model provides hazard mitigation and preparation guidance to engineers and planners by supplying more detailed information concerning landslide susceptibility. The method can be used to analyze the slope stability of a large number of slope units.

Generally speaking, there are some differences between the 3D factor of safety and the 2D factor of safety. The 3D factor of safety is generally higher than the 2D factor of safety with a few exceptional situations where the 3D factor of safety less than the 2D factor of safety.

According to the case study, the 3D factor of safety is related to the dimension of the computed potential failure mass, the number of columns (and the size of columns), groundwater conditions, and earthquake intensity. The input parameters are critical in order to obtain precise results.

The precision of slope geometry depends on the scale of digital topographic maps. If a high precision DEM is available, high accuracy slope units could be determined using terrain analysis software. That would lead to more accurate results in the 3D slope stability and landslide hazard zonation. If the resolution of DEM data is sufficient (such as 1 to 5 m), the GIS-based 3D slope stability analysis can be used by geotechnical engineers to analyze slope stability for design and mitigation purposes.

Hovland's method is a simple 3D model for slope stability analysis. The result of landslide hazard zonation based on the Hovland's 3D factor of safety is acceptable. Future work should focus both on developing a 3D model which will take into account inter-column forces, and on developing a GIS-based groundwater model which can be coupled with the slope stability analysis.

Figure 8.16 shows the comparison of the 2D and 3D factor of safety distributions. The 2D and 3D results have some differences: the 3D factors of safety usually are 15~30% greater than the 2D factors of safety. That means 2D models yielded larger very high and high landslide susceptibility zones than did the 3D model. Figure 8.16 also shows that most of the very high landslide susceptibility profiles generated by the 2D method are in the areas of the high or moderate landslide susceptibility as determined using the 3D method.

Figure 8.16 The factor of safety distribution map calculated using the 2D Bishop simplified method (line segments) and the 3D Hovland's method (slope units) under k=0.3, Hw=7 m conditions in the Balsamo Ridge area

Chapter 9 Conclusions and Future Research

9.1 Conclusions

9.1.1 Approaches to Landslide Hazard Assessment

A new GIS-based model integrated with one-, two- and three-dimensional (1D, 2D, and 3D) deterministic approaches for analyzing slope stability and mapping landslide hazards has been developed in this research. Slope stability methods used in the GIS process include the infinite slope model, the block sliding model, the ordinary method of slices, the Bishop simplified method, and the Hovland's column method. These deterministic approaches integrate the techniques of GIS spatial analysis, geostatistical analysis, the limit equilibrium method, probability analysis, and seismic slope stability analysis. The GIS-based approaches were applied to regional and site-specific landslide hazard zonation in Nueva San Salvador, El Salvador. The pseudo-static and Newmark displacement methods, both of which are widely used in geotechnical engineering, were applied to seismic slope stability analysis. A slope stability map produced using 2D and 3D methods could be used for engineering design and land development decision making.

The slope stability analysis model simulates the uncertainties of major geotechnical parameters including shear strength of the soil (friction angle and cohesion), the unit weight of the soil, and the depth of the groundwater table. Both the Monte-Carlo simulations and the first order reliability analysis (Hasofer-Lind method) were used in conducting a probability analysis of slope stability. In conducting a risk-based analysis, a probability approach is preferable to a deterministic approach because it is more rational than deterministic approach.

This research evaluates the topographic effects of ground motion and seismic response in the Balsamo Ridge area in which a middle-class Nueva San Salvador neighborhood was devastated by an earthquake-induced landslide in 2001. Slope stability and landslide susceptibility for this area were mapped in terms of slope stability index

(factor of safety, critical acceleration, Newmark displacement, failure probability, and reliability index). The 2D and 3D models produced useful results for site-specific earthquake-induced landslide hazard zonation. The earthquake-induced landslide susceptibility maps, that were produced, identified areas prone to earthquake-induced landslides under a variety of scenarios. These maps will assist geologists and policy makers in El Salvador to make decisions on how to best choose favorable locations for various land uses, and how to produce site development schemes for public works and infrastructure planning.

9.1.2 Landslide Hazard in Nueva San Salvador

The final earthquake-induced landslide susceptibility maps produced in this study include regional landslide susceptibility maps of Nueva San Salvador, which cover about 100 km^2 and site-specific landslide susceptibility maps for the Balsamo Ridge area, which cover about 5 km^2.

Previous regional landslide hazard zonation conducted in the study area shows that the areas of very high landslide susceptibility are located in the Balsamo Ridge area (south of Nueva San Salvador), along the Pan-American Highway (west of Nueva San Salvador), and inside the San Salvador volcano crater. Many of the highly unstable slopes are in the southern part of this area, which is characterized by steep geomorphological features.

The Balsamo Ridge area, especially around the site of the Las Colinas landslide, is a critical area due to its high landslide susceptibility and its proximity to a densely populated community. The shear strength of the geomaterial is relatively low and the slope is steep. The January 13, 2001 earthquake triggered a large landslide (the Las Colinas landslide) and caused a disaster for the neighborhood. The seismic response simulation showed that the magnitude of ground vibration along the top of Basalmo Ridge was increased. The peak ground acceleration and displacements along the top of Basalmo Ridge was significantly amplified in the simulation with amplification ratios of

2.6 in the northern crest and 2.5 in the southern crests, respectively. Near the crest of the northern slope, the simulation showed horizontal displacements of up to 105 cm and vertical displacements of up to 30 cm. The results of the simulation matched both the failure area and the approximate effects of the January 13 2001 Las Colinas Landslide. The simulation indicates that the crest on the north side of the ridge is where the slope is most likely to fail in a future earthquake. Slope mitigation is therefore urgently needed in the ridge area.

Another area where slope mitigation is desperately needed is along the Pan-American Highway. The Pan-American Highway was built along a drainage valley, and the northern side of the slope was cut steeply. The angle of some slopes exceeds 70°. It is a dangerous area where rock falls and block slides caused damages during the 2001 earthquakes and will likely to cause further damage during a future earthquake.

Despite the fact that volcano craters have high landslide susceptibility, mitigation is not a priority in these areas. These areas are generally unpopulated, and the risk of landslide damage and fatality is relatively low.

For site-specific hazard zonation, the unstable slope profiles in the Balsamo Ridge area mainly occur on the northern slope which has a steep angle. The area is of particular importance since there is a community located on the slope of this ridge. The soil mass in this area has a low strength. The factors of safety for 20 profiles in this area are less than 1.0, and the Newmark displacements of those profiles are greater than 10.0 cm, indicating high landslide susceptibility. In contrast, the southern side of the ridge belongs to a low to moderate landslide susceptibility zone because it has a relatively low slope angle.

Consistent with the 2D analysis, the results of the 3D model indicate that the high and moderate landslide susceptibility areas are distributed along the northern side of the ridge. The results of slope stability analysis show that: (1) in the Balsamo Ridge area, if the horizontal seismic coefficient k=0.3 and the depth of groundwater table is 7 m, the slope on the northern side of the ridge (which faces the residential area) will have high landslide susceptibility; therefore, slopes near the Las Colinas area might fail or reach the critical condition; (2) horizontal acceleration and groundwater have a strong influence on

the slope stability; consequently, if slope soils were saturated, most of the northern slope would fail under strong earthquake shaking; (3) if the horizontal seismic coefficient k=0.6 occurs, slope failure would likely happen in most of the Balsamo Ridge area. Mitigation and slope stabilization are therefore crucial to the long-term safety of the Balsamo Ridge area.

9.2 Future Research

9.2.1 Landslide Hazard Zonation Model

To improve the performance of deterministic and probabilistic models, future research should concentrate on the following slope failure modeling problems:

(1) The model developed in this study considers each grid as having homogenous geological material throughout. The vertical variation of soil property was not considered in this study. Due to the high spatial variability of the lithology and geological parameters, future models for slope stability and hazard assessment should be able to simulate heterogeneous soil masses. This ability to model heterogeneous soil masses will significantly improve the accuracy of landslide hazard zonation.

(2) To perform fast and effective slope stability analysis, scientists need an automated process to generate mapping units (such as slope profiles and slope units) for GIS-based 2D and 3D slope stability analysis. Future research should therefore work toward developing an automated method for generating mapping units.

(3) The groundwater condition is a critical factor for slope stability analysis. However, changes in groundwater levels are affected by the hydrogeological conditions, rainfall, and land cover (e.g. vegetation). Future research should place an emphasis on groundwater data collection and groundwater modeling so that input data can more closely represent the actual groundwater condition.

(4) The currently used empirical equations for Newmark displacement were derived mainly from the earthquake database for the western United States. These

equations might not be accurate for displacement analysis in El Salvador and other regions in Central America. Therefore, development of an empirical equation for seismic-induced displacement evaluation derived from the Central America earthquake data is strongly suggested.

(5) Although the pseudo-static approach to stability analysis is straightforward in producing a factor of safety, it suffers from many limitations. For example, a constant seismic coefficient may not accurately simulate the complex dynamic effects of earthquake shaking, particularly if soil strength decreases during shaking. Hence, it is necessary to carry out a detailed investigation of the dynamic material properties.

9.2.2 Landslide Hazard Zonation of El Salvador

Detailed field investigation of historic landslides in San Salvador needs to be carried out in the future. A relational geodatabase of landslide depth, dimension, slope angle and aspect, distance from road and water drainage, distance from fault, geological formation and lithology, and shear strength of the sliding mass should be completed in order to obtain a landslide distribution and allow weighting of causative factors. Such a geodatabase could be used to present the landslide distribution and to enable future landslide hazard zonation.

Detailed geological, geotechnical, and hydrological data for the San Salvador area are critical for earthquake-induced landslide hazard zonation. Detailed data collection is essential to accurate geological hazard assessment. Subsurface investigations, field sampling, in-situ and laboratory testing of geotechnical parameters, hydrological records, and the review of available published information would be of particular help in making future hazard assessments. High resolution remote sensing products are also necessary (such as aerial photographs and IKONOS images with 1 to 4 m resolution) to identify areas of landslide occurrence, analyze vegetation distribution, and investigate land use over a large area.

It is also necessary to perform in-situ monitoring of slope movements and pore water pressures. Slope displacement data during a strong earthquake is desirable for Newmark displacement-based landslide hazard evaluation. The measured displacement would be very useful in determining a displacement threshold value.

The determination of peak ground acceleration and seismic coefficients is critical to seismic slope stability analysis using either pseudo-static or Newmark displacement methods. More accurate landslide hazard zonation requires more detailed investigations of the parameters of the seismic hazards, such as the seismic hazard prediction of El Salvador in 475 return years, the largest earthquake magnitude, and peak ground acceleration in highly landsliding prone area.

El Salvador is situated in an earthquake prone region. The whole country frequently suffers from earthquake-induced landslides. In order to minimize earthquake damage and avoid fatalities, landslide susceptibility evaluation of the entire country is strongly recommended. Earthquake-induced landslide risk analysis of highly populated areas is essential for earthquake hazard response planning and loss-reduction design.

References

Abrhamson, N. A. and Silva, W. J., 1997, Empirical Response Spectral Attenuation Relation for Shallow Crustal Earthquakes, Seismological Research Letters, 68, 94-127.

Alfaro, C. S., Kiremidjian, A. S., and White, R. A., 1990, Seismic Zoning and Ground Motion Parameters for El Salvador, Report No. 93, The John A. Blume Earthquake Engineering Center, Stanford University.

Algermissen, S. T., Hansen, S. L., and Thenhaus, P.C., 1988, Seismic Hazard Evaluation for El Salvador, Report for the US Agency for International Development, 21pp.

Amaya Bubon, C. A., and Hauem Breve, E. A., 2000, Introduccion Al Setudio De Los Suelos Parcialmente Sturados E La Caracteracion De La Tierra Blanca Del Amss, B.S. Thesis, San Salvador, Universidad Centroamericana, 366pp.

Ambraseys, N. N., Simpson, K. A., and Bommer, J. J., 1996, Prediction of Horizontal Response Spectra in Europe, Earthquake Engineering and Structure Dynamics., 25, 371-400.

Ambrasey, N. N., Menu, J. M., 1988, Earthquake-Induced Ground Displacements, Earthquake Engineering and Structure Dynamics, Vol. 16, 985-1006.

Arias, A., 1970, A Measurement of Earthquake Intensity, Ed. Hansen R. J., Seismic Design for Nuclear Power Plants, MIT Press, Cambridge, Massachusetts, 438-483.

Atkinson, G. M., and Boore, D. M., 1995, New Ground Motion Relations for Eastern North America, Bulletin of the Seismological Society of America, 85, 17-30.

Atkinson, G. M., and Boore, D. M., 1997, Some Comparison Between Recent Ground Motion Relationship, Seismological Research Letters, 68, 24-40.

Atkinson, G. M. and Boore, D. M., 2003, Empirical Ground-Motion Relations for Subduction-Zone Earthquakes and Their Application to Cascadia and Other Regions, Bulletin of the Seismological Society of America, Vol. 93, No. 4, 1703–1729

Baecher, G. B. and Christian, J. T., 2003, Reliability and Statistics in Geotechnical Engineering, John Wiley & Sons Ltd, 605pp.

Bard P. Y, Riepl-Thomas J., 1999, Wave Propagation in Complex Geological Structures and Their Effects on Strong Ground Motion, Ed. Kausel E. and Manolis G. D., Wave Motion in Earthquake Engineering, International Series Advances in Earthquake Engineering, Wit, Boston, 37–95.

Baum, R. L., Crone, A. J., Escobar, D., Harp, E. L., Major, J. J., Martinez, M.., Pullinger, C., 2001, Assessment of Landslide Hazards Resulting from the February 13, 2001, El Salvador Earthquake, A report to the Government of El Salvador and the U.S. Agency for International Development, Open-File Report 01-119, USGS, 22pp.

Baxter, S., 2001, Geologic Map of El Salvador, Hermes International Institute of Paris. 2001.

Benito B., Cepeda, J. M., and Martinez Diaz, J. J., 2004, Analysis of the Spatial and Temporal Distribution of the 2001 Earthquakes in El Salvador, Ed. Rose. W. I., et al., Geological Societyof America Special Paper 375, 339-356.

Bent, A. L., and Evans, S. G., 2004, The Mw 7.6 El Salvador Earthquake of 13 January 2001 and Implications for Seismic Hazard in El Salvador, Ed. Rose. W. I., et al., Geological Societyof America Special Paper 375, 397-404.

Berdousis, P., 2001, Engineering Characterization of a Volcanic Soil From Central America, M.S Thesis, London, Imperial College, Universityof London, 205pp.

Bishop, A. W., 1955, The use of the Slip Circle in the Stability of Slopes, Geotechnique, 5, 7-17.

Bommer, J. J., Hernández, D. A., Navarrete, J. A., and Salazar, W. M., 1996, Seismic Hazard Assessments for El Salvador, Geofísica Internacional, 35, 227–244.

Bommer, J. J., Udías, A., Cepeda, J. M., Hasbun, J. C., Salazar, W. M., Suárez, A., Ambraseys, N. N., Buforn, E., Cortina, J., Madariaga, R., Méndez, P., Mezcua, J., and Papastamatiou, D., 1997, A new digital accelerograph network for El Salvador, Seismological Research Letters, 68, 426–437.

Bommer, J., Mcqueen, C., Salazar, W., Scott, S. and Woo, G. 1998, A Case Study of the Spatial Distributionof Seismic Hazard (El Salvador), Natural Hazards 18, 145–166.

Bommer J. J., Benito, M. B., Ciudad-Real M., Lemoine A., Lopez-Menjivar M. A,Madariaga, R., Mankelow, J., Mendez De Hasbun, P., Muephy, W., Nieto-Lovo, M., Rodriguez-Pineda, C. E., and Rosa, H., 2002, The El Salvador Earthquake of January and February 2001: Context, Characteristics and Implications for Seismic Risk, Soil Dynamics and Earthquake Engineering, 22(2002), 389-418.

Boore, D. M., and Joyner, W. B., 1997, Site Amplification for Generic Rock Sites, Bulletin of the Seismological Society of America, 87, 327-341.

Box, G. E. P, and Muller, M. E., 1958; A Note On the Generation of Random Normal Deviates, Annals Math. Stat, Vol. 29, 610-611

Brabb, E. E., 1988, Innovative Approaches to Landslide Hazard Mapping, Proceedings of Int. Symp. Landslides, Toronto, 1, 307-324.

Burington, R. S. and May, D. C., 1970, Handbook of Probability and Statistics with tables, New York, Mcgraw-Hill Book Company, 462pp.

Burke, R., 2003, Getting to Know Arcobjects: Programming ArcGIS with VBA, ESRI Press, 422pp.

Burrough, P. A., 1986, Principles of Geographic Information System and Land Resource Assessment, Clarendon Press, Oxford, England, 194pp.

Burroughs, E. R., Jr., and Thomas, B. R., 1977, Declining Root Strength in Douglasfir after Felling as a Factor in Slope Stability, Research Paper, Int-190. Ogden, Ut, U. S. Department of Agriculture, Forest Service, International Forest and Range Experimental Station, 27pp.

Campbell, K. C., 2003, Eengineering Models of Strong Ground Motion, Ed. Chen W. F. and Scawthorn, C., Earthquake Engineering Handbook, CRC Press, 5, 1-44.

Capolongo, D., Refice, A. and Mankelow, J., 2002, Evalating Earthquake-Triggered Landslide Hazard at the Basin Scale Through GIS in the Upper Sele River Valley, Surveys in Geophysics, 23, 596-625

Carrara, A., 1983, Multivariate Models for Landslide Hazard Evaluation, Mathematical Geology, Vol. 15, No. 3, 403-427.

Carrrara, A. 1988, Drainage and Divide Networks Derived From High-Fidelity Digital Terrain Models, Ed. Chung C. F., et al., Quantitative Analysis of Mineral and Energy Resources, Nato-Asi Series, Reidel, Dordrecht, 581-597.

Carrara A., Cardinali M., Detti R., Guzzetti F., Pasqui V., and Reichenbach P., 1991. GIS Techniques and Statistical Models in Evaluating Landslide Hazard, Earth Surface Process and Landforms, Vol. 16, 427-445

Carrara, A., Cardinali, M., Guzzetti, F., and Reichenbach, P., 1995, GIS Technology for Mapping Landslide Hazard, Ed. A. Carrara and F. Guzzetti, Geographical Information System in Assessing Natural Hazards, Academic Publication, Dordrecht, The Netherlands, 135-175

CEN European Committee for Standardisation, 1994, Eurocode 8, Design Provisions for Earthquake Resistance of Structures—Part 5: Foundations, Retaining Structures and Geotechnical Aspects, Brussels.

Cepeda, J. M., Benito, M. B., and Burgos, E. A., 2004, Strong-Motion Characteristics of January and February 2001 Earthquakes in El Salvador, Ed. Rose. W. I., et al., Geological Society of America Special Paper 375, 405-421.

Chiles, J., and Delfmer, P., 1999, Geostatistics: Modeling Spatial Uncertainty, John Wiley & Sons, Inc. 695pp.

Chok, Y. H., Kaggwa, W. S., Jaksa, M. B., Griffiths, D. V., 2004, Modeling the Effects of Vegetation on Stability of Slopes, Proceedings of 9th Australia New Zealand Conference on Geomechanics, Auckland, 391-397.

Christian J. T. and Urzua A., 1998, Probabilistic Evolution of Earthquake-Induced Slope Failure, Journal of Geotechnical and Geoenvironmental Engineering, Vol. 124, No. 11, 1140-1143.

Chung, C. F., Fabbri, A. G., 1993, The Representation of Geoscience Information Data Integreation, Nonrenewable Resources, 2(2), 122-139.

Chung C. F., Fabbri A.G., and Van Westen C.J., 1995, Multivariate Regression Analysis for Landslide Hazard Zonation. Ed. Carrara A., and Guzzetti F., Geographical Information Systems in Assessing Natural Hazards, Kluwer, Dordrecht, The Netherlands, 107-142.

Chung, C. F., Fabbri, A. G., 1999, Prediction Models in Spatial Data Analysis, ITC, Enschede, The Netherlands. Draft, Unpublished.

CIGEM (China Geological Environmental Infonet), 2004, <www. cigem.gov.cn>

Close, U. and Mccormick, E., 1922, Where the Mountains Walked, National Geographic Magazine, Vol. 41, No. 5, 445-464.

Cornforth, D. H., 2005, Landslide in Practice: Investigation, Analysis, and Remedial/Preventative Options in Soils, John Wiley & Sons, Inc. 956pp.

Cresssie, N. A. C., 1993, Statistics for Spatial Data, John Wiley & Sons, Inc, 900pp.

Crouse, C. B., Vyas, Y. K., and Schell, B. S., 1988. Ground Motions from Subduction Zone Earthquakes, Bulletin of the Seismological Society of America, 78, 1, 1-25.

Crouse, C. B., 1991a, Ground Motion Attenuation Equations for Earthquake on the Cascadia Subdeduction Zone, Earthquake Spectra, 7, 201-235.

Crouse, C. B., 1991b, Erratum: Ground-Motion Attenuation Equations for Earthquake on the Cascadia Subdeduction Zone, Earthquake Spectra, 7, 506.

Dahle, A., Bungum, H., and Dvamme, L. G., 1990, Attenuation Models Inferred From Intraplate Earthquake Recordings, Earthquake Engineering and Structure Dynamics, 19, 1125-1141.

Day, R. W., 2002, Geotechnical Earthquake Engineering Handbook, Mcgraw-Hill, 600pp.

Del Gaudio, V., Pierri, P., and Wasowski, J., 2003, An Approach to Time-Probabilistic Evaluation of Seismically Induced Landslide Hazard, Bulletin of the Seismological Society of America, 93(2), 557-569.

Division of Mines and Geology, 1997, Guidelines for Evaluation and Mitigating Seismic Hazards in California, Special Publication 117, Department of Conservation, Division of Mines and Geology.

Dobry, R., Borcherdt, R., Crouse, C., Idriss, I., Joyner, W., Martin, G., Power, M., Rinne, E., and Seed, R., 2000, New Site Coefficient and Site Classification System Used in Recent Building Seismic Code Provisions, Earthquake Spectra, Vol. 16. 41-67.

Duncan, J. M., 1996, State of the Art: Limit Equilibrium and Finite-Element Analysis of Slopes, Journal of Geotechnical Engineering, Vol. 122, No. 7, 577-593.

El-Ramly, H., Morgenstern, N. R., and Cruden, D. M., 2002, Probability Slope Stability Analysis for Practice, Canadian Geotechnical Journal, 39, 665-683.

Evans, S. G. and Bent, A. L. 2004, The Las Colinas Landslide, Santa Tecla: A Highly Destructive Flowslide Triggered by the January 13, 2001, El Salvador Earthquake, Geological Society of America Special Paper 375, 27-37.

Fabbri A. G., Chung C. J., Cendrero, A., and Remondo J., 2003, Is Prediction of Future Landslides Possible with a GIS? Natural Hazards, 30, 487-499.

Faccioli, E., 1991, Seismic Amplification in the Presence of Geological and Topographic Irregularities, Ed. St. Louis, Missouri, S. Prakash, Proceedings of the Second International Conference on Recent Advances in Geotechnical Earthquake Engineering and Soil Dynamics, March 11-15, Universty of Missouri-Rolla, 2, 1779-1797.

Franklin, A.G. and Chang, R.K., 1977, Permanent Displacements of Earth Embankments by Newmark's Sliding Block Analysis: Report 5, Miscellaneous Paper S-71-17, U. S. Army Corps of Engineers, Waterway experiment station, Vicksburg, Mississippi.

Gens, A. Hutchison, J. N. Cavounidis, S. 1988. Three Dimensional Analysis of Slices in Cohesive Soils. Geotechnique, 38, 1-23.

Goodman, R. E., and Shi, G. H., 1985, Block Theory and Its Application to Rock Engineering, Prentice-Hall, Inc, 338pp.

Gray, D. H., Leiser, A. T., 1982, Biotechnical Slope Protection and Erosion Control, New York, Van Nostrand Reinhold. 279pp.

Greenway, D. R., 1987, Vegetation and Slope Stability, Ed. andson, M. G. and Richards, K. S., Slope Stability, New York, John Wiley and Sons, 187-230.

Grimshaw, D. J., 1994, Bringing Geographical Information Systems into Business, Longman, Harlow, 273pp.

Guzman Urbina, M. A., and Melara, E., 1996, Propiedades Ingenieriles Del Suelo Del Area, Metropolitana De San Salvador, El Salvador, Revista Asia-Associacion Salvadorena De Ingenieros Y Arquitectos, San Salvador, El Salvador, No. 122, 14-22.

Guzzetti, F., Carrara, A., Cardinali, M. and Reichenbach, P. 1999, Landslide Hazard Evaluation: A Review of Current Techniques and Their Application in a Multi-Scale Study, Central Italy, Geomorphology 31, 181–216.

Haldar, A., and Mahadevan, S., 2000, Probability, Reliability and Statistical Methods in Engineering Design, John Wiley & Sons, Inc, 304pp.

Hansen A., 1984. Landslide Hazard Analysis, Ed. Brunsden D. and Prior D.B., Slope Instability, Wiley, New York, 523-602.

Harp, E. L. and Wilson, R. C., 1995, Shaking Intensity Thresholds for Rock Falls and Slides: Evidence From the 1987 Whittier Narrows and Superstition Hills Earthquake Strong Motion Records, Bulletin of the Seismological Society of America, 85 (6), 1739-1757.

Harp, E. L., and Jibson, R. W, 1995. Inventory of Landslides Triggered by the 1994 Northridge, California Earthquake, U. S. Geological Survey Open-File Report 95-213.

Hart, R. G., 1991, An Introduction to Distinct Element Modeling for Rock Engineering, Ed. Hudson, J. A., Comprehensive Rock Engineering, MP4120 II, Handout IV, 245-261.

Hartlen, J. and Viberg, L., 1988, General Report: Evaluation of Landslide Hazard, Proceedings of 5th International Symposium on Landslides, Lausanne (Ch), 1988, Vol. 2, 1037-57.

Hasofer, A. M., and Lind, N. C., 1974, An Exact and Invariant Firstforder Reliability format, Journal of Engineering Mechanics Division, ASCE, 100(Em1), 111-121.

Hammond, C. J., Prellwitz, R. W., and Miller, S., M., 1992, Landslide Hazard Assessment Using Monte-Carlo Simulation, Ed. D. H. Bell, Proceedings of the Sixth International Symposium On Landslides, Chrischurch, New Zealand, Balkema, 959-964.

Hernandez, W., 2005, Personal Communication (Geologist, Snet, El Salvador).

Ho, Carlton L. and Miles, Scott B., 1997, Deterministic Zonation of Seismic Slope Instability: An Application of GIS, Spatial Analysis in Soil Dynamics and Earthquake Engineering, Geotechnical Special Publication, No. 67, ASCE, 87-102.

Hovland, H. J., 1977, Three-Dimensional Slope Stability Analysis Method, Journal of the Geotechnical Engineering Division, Proceedings of the American Society of Civil Engineers 103(GT9), 971– 986.

Ruhe, R. V. and Walker, P. H., 1968, Hillslope Models and Soil Formation, Open Systems, Transactions of the 9th Congress of the International Soil Science Society, Adelaide, II. 551-560.

Hungr, O., 1987, An Extension of Bishop's Simplified Method of Slope Stability Analysis to Three Dimensions, Geotechnique, 37(1), 113-117.

Hynes-Griffin, M. E. and Franklin, A. G., 1984, Rationalizing The Seismic Coefficient Method, Miscellaneous Paper, Gl-84-13, U. S. Army Crops of Engineers Waterway Experiment Station, Vicksburg, Mississippi.

International Association of Engineering Geology (Iage), 1976, Engineering Geological Maps: A Guides to Their Preparation, Unesco Press, Paris, 79pp.

Itasca, 2005, FLAC 5.0: Theory and Background, Itasca Consulting Group, Inc.

Jibson, R. W., 1987, Summary of Research on The Effects of Topographic Amplification of Earthquake Shaking on Slope Stability, U. S. Geological Survey Open-File Report 87-268, 166pp.

Jibson, R. W., 1993, Predicting Earthquake-Induced Landslide Displacements Using Newmark's Sliding Block Analysis, Transportation Research Record, No.1411, 9-17.

Jibson, R. W., and Keefer, D. K., 1993, Analysis of the Seismic origin of Landslides---Example from the New-Madrid Seismic Zone, Geological Society of America Bulletin, 105(5), 521-536.

Jibson, R. W., and Harp E. L, 1998, A Method for Producing Digital Probabilistic Seismic Landslide Hazard Maps: An Example From the Los Angeles, California, Area, U. S. Geological Survey Open-File Report 98-113.

Jibson, W., Crone, A.J., 2001: Observations and Recommendations Regarding Landslide Hazards Related to the January 13, 2001 M-7.6 El Salvador Earthquake, U.S. Geol. Survey Open File Report 01-141, 19pp.

Jibson, R. W., Crone, A. J., Harp, E. L., Baum, R. L., Major, J. J., Pullinger C. R., Escobar C. D., Martinez M., and Smith M. E., 2004, Landslides Triggered by the 13 January and 13 February 2001 Earthquakes in El Salvador, Geological Society of America Special Paper No. 375.

Johnston, K., Ver Hoef, J. M., Krivoruchko, K., and Lucas, N., 2003, ArcGIS9: Using ArcGIS Geostatistical Analyst, ESRI, 300pp.

JSCE (Japan Society of Civil Engineers), 2001, The January 13, 2001 of the Coast of El Salvador Earthquake, Earthquake Engineering Committee, JSCE.
<http://www.jsce.or.jp/report/11/01/contents.htm>

Keefer, D. K., 1984, Landslide Caused by Earthquakes, Geological Society America Bulletin 95, 406-421.

Keefer, D. K., and Wilson, R. C., 1989, Predicting Earthquake-Induced Landslides with Emphasis on Arid and Semi-Arid Environments, Ed. Sadler P. M. and Morton D. M. Landslide in a Semi-Arid Environment, Inland Geological Society, San Bernardino, CA, 118-149.

Khazai, B., 2004, GIS Approach to Seismic Slope Stability, Ph.D Dissertation, University of California, Berkeley, 291pp.

Khazai B. and Sitar N., 2000, Assessment of Seismic Slope Stability Using GIS Modeling, Geographic Information Sciences, Vol. 6, No. 2.

Khazai B. and Sitar N., 2002, Landsliding in Native Ground: A GIS Based Approach to Regional Seismic Slope Stability Assessment,
<http://www.ce.berkeley.edu/ ~khazai/research/report/index2.html>

Kim, J., and Sitar, Nicholas, N., 2004, Estimation of Yield Acceleration in Slope Stability, Journal of Geotechnical and Geoenvironmental Engineering, Vol. 130, No. 1. 111-115.

Kobayashi, Y. 1981, Causes of Fatalities in Recent Earthquakes in Japan, Journal of Disaster Sciences, 3, 15-22.

Kramer, S. L., 1996, Geotechnical Earthquake Engineering, Prentice Hall, 653pp.

Krinitzsky, E. L., Gould, J. P., and Edinger, P. H., 1993, Fundamental of Earthquake-Resistant Construction, Wiley, New York.

Lam, L. and Fredland, D. G., 1993, A General Limit Equilibrium Model for Three-Dimensional Slope Stability Analysis, Canadian Geotechnical Journal 30, 905–919.

Leschisky, D., and Huang, Ching-Chang, 1992, Generalized Three Dimensional Slope Stability Analysis, Journal of Geotechical Engineering, 118(11), 1748–1763.

Lindholm, C., Rojas, W., Bungum, H., Dahle, A., Camacho, E., Cowan, H., and Laporte, M., 1995. New Regional Seismic Zonation for Central America. Proceedings of Fifth International Conference On Seismic Zonation, Nice, 17-19 October, Vol. I, 437-444

Lopez, M., Bommer J. J., and Pinho, R., 2004, Seismic Hazard Assessments, Seismic Design, and Earthquake Engineering in El Salvador, Geological Society of America Special Paper 375, 301-320.

Loria, C. S., 2003, Numerical Assessment of the Influence of Earthquakes on Irregular Topographies--- Analysis of Colombia, 1999 and El Salvador, 2001 Earthquakes, M.S Thesis, Delft, The Netherlands, 127pp.

Lotti C. & Association, 2001, B: Informe Final, Análisis-Evaluación Modelos Numéricos: Detalle de Cálculo Del Análisis de Estabilidad y Modelación de la Expansión con la Técnica de Elementos Finitos, Anexo 2.2.1.2. – El Salvador, Technical Report, Financed by Bid, Property of Ministerio De Medio Ambiente y Recursos Naturales, 112 pp.

Low, B. K., Gilbert, R. B., and Wright, S. G., 1998, Slope Reliability Analysis Using Generalized Method of Slices, Journal of Geotechnical and Geoenvironment Engineering, Vol. 124, No. 4, 350-362

Low, B. K. and Tang, W. H., 1997, Reliability Analysis of Reinforced Embankments on Soft Ground, Canadian Geotechnical Journal, 34, 627-685.

Luo, H. Y., Zhou, W., Huang, S. L., and Chen, G., 2004, Earthquake-induced landslide stability analysis of the Las Colinas landslide in El Salvador, International Journal of Rock Mechanics and Mining Sciences, 41(3), 477-478.

Luzi, L. Pergalani F. and Terlien, M. T. J., 2000, Slope Vulnerability to Earthquakes at Subregional Scale, Using Probabilistic Techniques and Geographic Information System, Engineering Geology, 58, 313-336

Maidment, D. R., 2002, Arc Hydro: GIS for Water Resource, ESRI Press, 203pp.

Manson, M. W., Keefer, D. K. and MacKittrick, 1992, Landslides and Other Geologic Features in the Santa Cruz Mountains, California, Resulting Fron the Loma Prieta Earthquake of October 17, 1989, DMG Open-file Report 91-05, California Department of Conservation, Division of Mines and Geology.

Malkawi, A. I. H., Hassan, W. F., and Abdulla, F. A., 2000, Uncertainty and Reliability Analysis Applied to Slope Stability, Structure Safety, 22, 161-187

Marcuson, W. F., 1981, Moderator's Report for Session on Earth Dams and Safety of Slopes Under Dynamic Loads, Proceedings, International Conference on Recent Advances on Geotechnical Earthquake Engineering and Soil Dynamics, Vol.3, St. Louis, Missouri, 1175.

Mavrommati, Z. C., 2000, Seismic Behavior of Slopes in an Unsaturated Volcanic Soil, M.S Thesis, Imperial College, University of London, London, 116pp.

Meijerink, A. M. J., 1988, Data Acquisition and Data Capture Through Terrain Mapping Units, International Computer Journal, 1, 23-44.

Miles, S.B. and Keefer, D. K., 1999, Comparison of Seismic Slope-Performance Models -- Case Study of the Oakland East Quadrangle, CA, U. S. Geological Survey Open-File Report 99-137.

Molas, G. L., and Yamazaki, F, 1995, Attenuation of Earthquake Ground Motion in Japan Including Deep Focus Events, Bulletin of the Seismological Society of America, 85, 1343-1358.

Montgomery, D. R. and Dietrich, W. E., 1994, A Physically Based Model for the Topographic Contral of Shallow Landslidng, Water Redourced Research 30(4), 1153-1171.

Munfakh, G., 1998, Geotechnical Earthquake Engineering, Reference Manual / Principle Training Course in Geotechnical and Foundation Engineering: NHI Course No. 13239, Module 9, U.S. Department of Transportation.

Nash, D., 1987, A Comparative Review of Limit Equilibrium Methods of Stability Analysis, Slope Stability, Ed. anderson M. G. and Richards, K. S., John Wiley & Sons. 648pp.

Newman, E. B., Paradis, A. R., Brabb, E. E., 1978, Feasibility and Cost of Using a Computer to Prepare Landslide Susceptibility Maps of San Francisco Bay Region, California, Bulletin 1443, U. S. Geological Survey, Reston,Va, 29pp

Newmark, N. M., 1965, Effects of Earthquakes on Dams and Embankments, Geotechique, Vol. 15, No. 2, 139-160.

NRC(National Research Council), 1985, Reducing Losses From Landslides in the United States, Washington, DC, National Academy Press, 41pp.

National Research Council, 1996, Landslides: Investigation and Mitigation, Ed. Turner, A. K. and Schuster R. L., Transportation Research Board Special Report, 247, Washington, Dc, National Academy Press, 673pp.

NRC (National Research Council), 2004, Partnerships for Reducing Landslide Risk: Assessment of the National Landslide Hazards Mitigation Strategy, Committee on the Review of the National Landslide Hazards Mitigation Strategy, National Research Council.

O'Loughlin, C. L., Ziemer, R. R., 1982, the Importance of Root Strength and Deterioration Rates Upon Edaphic Stability in Steepland Forests, Carbon Uptake an Allocation in Subalpine Ecosystems as a Key to Management, Proceedings of an IUFRO Workshop, 1982 August, Corvallis, OR, Oregon State University Forest Research Laboratory, 70-78.

Pack, R. T., Tarboton, D. G. and Doodwin, C. N., 2001, Assessing Terrain Stability in a GIS Using Sinmap, Presented at the 15th Annual GIS Conference, GIS 2001, February 19-22, Vancouver, BC, Canada.

Plafker, G. and Ward, S. N., 1992, Thrust Faulting and Tectonic Uplift along the April 1922, 1991 Costa Rica Earthquake, Tectonics, 11, 709-718.

Paolucci, R., 2002, Amplification of Earthquake Ground Motion by Steep Topographic Irregularities, Earthquake Engineering Structure and Dynamics, 31, 1831–1853

Refice, A. and Capolongo, D., 2002, Probabilistic Modeling of Uncertainties in Earthquake-Induced Landslide Hazard Assessment, Computers & Geosciences, 28, 735-748.

Rojas, W., Cowan H., Lindholm, C., Dahle A. and Bungum H., 1993, Regional Seismic Zonation for Central America: A Preliminary Model. Norsar Tech. Rep. No. 2-12, 39pp.

Rolo, R., 1998, Elements of Seismic Hazard in El Salvador and Central America, Imperial College, University of London, London, 205pp.

Rolo, R., Bommer, J. J., Hougnton B. F., Vallance J. W., Berdousis P., Mavrommati, C. and Murphy, W., 2004, Geologic and Engineering Characterization of Tierra Blanca Pyroclastic Ash Deposits, Ed. Rose, W. I., et al., Natural Hazards in El Salvador, The Geological Society of America, Special Paper 375, 55-67.

Rosenfeld, C. L., 1994, The Geomorphological Dimension of Natural Disaster, Geomorphology, 10, 27-36.

Santacana N., Baeza, B., Corominas, J., Paz, A. D. and Marturia, J., 2003, A GIS-Based Multivatiate Statistical Analysis for Shallow Land Susceptibility Mapping in La Pobla De Lillet Area (Eastern Pyrenees, Spain), Natural Hazards, 30, 281-295.

Sarkar, S. and Kanungo, D. P., 2001, Landslide Identification and Mapping Using Remote Sensing and GIS, Central Building Research Institute, Roorkee, India

Sassa, K., 1999, Landslides of the World, Japan Landslide Society, Kyoto University Press, 413pp.

SCEC, 2002, Recommended Procedures for Implementation of DMG Special Publication 117, Guidelines for Analyzing and Mitigation Landslide Hazards in California. ASCE Los Angeles Section Geological Group, Published by South California Earthquake Center.

Schmidt-Thome, M. 1975, The Geology in the San Salvador Area (El Salvador, Central America), A Basis for City Development and Planning, Geologischen Jahrbuch, Vol. B13, 207-228.

Schuster, R.L., and Highland L.M., 2001, Socioeconomic and Environmental Impacts of Landslides in the Western Hemisphere, U.S. Geological Survey Open-File Report 01-0276.

Seed, H. B., 1979, Consideration in Earthquake-Resistant Design of Earth and Rockfill Dams, Geotechnique, Vol. 29, No. 3, 215-263.

Seed, H. B., Mori, K., and Chan, C.K., 1975, Influence of Seismic History on the Liquefaction Characteristics of Sands: Earthquake Engineering Research Center Report EERC 75-25, University of California at Berkeley.

Seed, H.B., Idriss, I. M., and Kiefer, F. W., 1969, Characteristics of Rock Motions During Earthquakes, Journal of Soil Mechanics and Foundations Division, American Society of Civil Engineers, No. 95, SM5, 1199-1218.

Sidle, R. C., 1984, Relative Importance of Factors Influencing Landsliding in Coastal Alaska, Proceedings of 21st Anaual Engineering Geology and Soils Engineering Symposium, 1984 April 5-6, Moscow, ID, Idaho Transportation Department and University of Idaho, 311-324.

Singh, S. K., Gutierrez, C., Arboleda, J., Andfordaz, M., 1993. Peligro Sísmico en El Salvador. Universidad Nacional Autónoma de Mexico, Mexico.

Skempton, A. W., and Delory, F. A., 1957, Stability of Natural Slopes in London Clay, Proceedings of 4th International Conference of Soil Mechanics and Foundation Engineering, London, 2, 378-381.

Snedecor, G. W. and Cochran, W. G., 1989, Statistical Method, Iowa State University Press, 503pp.

Soeters, R., and Van Westen C. J., 1999, Slope Instability Recognition, Analysis, and Zonation, Landslides: Investigation and Mitigation, Special Report 247, Transportation Research Board, National Research Council, Chapter 8, 129-177.

Spiegelhalter D. J., 1986, A Statistical View of Uncertainty in Expert Systems, Ed. Gale W. A., Artificial Intelligence and Statistics, Reading, Addison-Wesley, Massachusetts, 17–55.

Spiker, E. C. and Gori, P. L, 2000, National Landslide Hazards Mitigation Strategy, A Framework for Loss Reduction, U. S. Geological Survey, Open-File Report 00-450.

Spudich, P., Joyner, W. B., Lindh, A. G., Boore, D. M., Margaris, B. M., and Fletcher, J. B., 1999, Sea99: A Revised Ground Motion Prediction Relation for use in Extensional Tectonic Regimes, Bulletin of the Seismological Society of America, 89, 1156-1170.

Taniguchi, E., and Sasaki, Y., 1986, Back Analysis of Landslide due to Naganoken Seibu Earthquake of September 14, 1984, Proceedings of 11th ISSMFE Conference, Session.

Terzaghi, K., 1950, Mechanism of Landslides, Engineering Geology Volume, Geological Society of America.

Thenhaus, P. C. and Campbell, K. W., 2003, Seismic Hazard Analysis, Ed. Chen W. F. and Scawthorn, Earthquake Engineering Handbook, CRC Press.

Toro, G. R., Abrahamson, N. A., and Schneider, J. F., 1997, Model of Ground Motion S From Earthquakes From Central and Eastern North America: Best Estimates and Uncertainties, Seismological Research Letters, 68, 41-57.

Tsukamoto, Y., and Minematsu, H., 1987, Evaluation of the Effect of Deforestation on Slope Stability and Its Application to Watershed Management, Forest Hydrology and Watershed Management: Proceedings of a Symposium, 1987 August 9-22, Vancouver, BC, IAHS, 167. Washington DC, International Association of Hydrological Sciences. 181-189.

USGS, 2001, <http://neic.usgs.gov /neis/eq_depot/2001/eq_010213>

U.S Department of Transportation, 1996, Reinforced Slope Stability: A Microcomputer Program User's Manual, 190pp.

Van Westen, C. J., 1993, Application of Geographic Information Systems to Landslide Hazard Zonation. ITC Publication No: 15. International Institute for Aerospace and Earth Resources Survey, Enschede, The Netherlands, 245pp.

Van Westen C. J. and Terlien M. T. J., 1996, An Approach Towards Deterministic Landslide Hazard Analysis in GIS. A Case Study From Manizales (Colombia), Earth Surface Processes and Landforms, Vol. 21, 853-868.

Van Westen, C. J., Rengers, N., and Terlien, M. T. J., Soeters, R., 1997, Prediction of the Occurrence of Slope Instability Phenomena Through GIS-Based Hazard Zonation, Geol Rundsch, 86:404-414

Van Westen, C. J., 2000, The Modeling of Landslide Hazards Using GIS, Surveys in Geophysics, Kluwer Academic Publishers, 21, 241-255.

Varnes, D. J., 1984, Landslide Hazard Zonation: A View of Principles and Practices, Commission in Landslides of the IAEG, Unesco, Natural Hazards, No. 3, 61pp

Wang, Z. M., Graham G. B. and Madin I. P., 2001, Earthquake Hazard and Risk Assessment and Water-Induced Landslide Hazard in Benton County, Oregon, Final Report, Oregon Department of Geology and Mineral Industries.

Weber, H. S., and Wiesemann, Compliler, 1978, Mapa Geologico de la Republica de El Salvador, Scale: 1:100,000, Bundesanstalt fur Geowissen-Schaften und Rohstoffe, Hannover, Germany.

Wieczorek, G. F., 1984. Preparing a Detailed Landslide Inventory Map for Hazard Evaluation and Reduction. Bulletin, Association of Engineering Geologists, 21(3), 337-342.

Wieczorek, G. F., Wilson, R. C., Keefer, D. K., Harp, E. L., and Tannaci, N. D., 1985, Map Showing Ground Failures From the Greenville/Mount Diablo Earthquake Sequence of January 1980, Northern California, U.S. Geological Survey, Misc. Field Studies, Map MF 1711.

Wieczorek, G. F., 1999, Landslide Triggering Mechanisms, Landslides: Investigation and Mitigation, Special Report 247, Transportation Research Board, National Research Council, Chapter 4, 129-177.

Wilson, R. C. and Keefer, D. K. 1983, Dynamic Analysis of a slope failure from the 6 August 1979 Coyote Lake, California, earthquake, Bulletin of the Seismological Society of America, V. 73(3), 863-877.

Wilson, R. C. and Keefer, D. K. 1985, Predicting Areal Limits of Earthquake-Induced Landsliding, Evaluating Earthquake Hazards in the Los Angeles Region, Ed. Ziony, J., I., Professional Paper 1360, USGS, Resten, VA, 317-345.

Wu, T. H., 1984, Effect of Vegetation on Slope Stability, Transportation Res. Rec. 965, Washington DC, Transportation Research Board, 37-49.

Wu, T. H., Mckinnel, W. P., Swanston, D. N., 1979, Strength of Tree Roots and Landslides of Prince of Wales Island, Alaska, Canadian Geotechncial Journal, 16(1), 19-33.

Xie, M., Esaki T., Zhou, G., 2003[1], GIS-Based Probabilistic Mapping of Landslide Hazard Using a Three-Dimensional Deterministic Model, Natural Hazards 00, 1-18, 2003.

Xie M., Esaki T. Zhou, G., Mitani, Y., 2003[2], Geographic Information Systems-Based Three-Dimensional Critical Slope Stability Analysis and Landslide Hazard Assessment, Journal of Geotechnical and Geoenvironmental Enginering, Vol. 129, No. 12, 1109-1118.

Xie M. and Esaki T., 2005, GIS-Based Limit Equilibrium Approaches for 3d Slope Stability, The 40th U.S. Symposium On Rock Mechanics (USRMS), ARMA/USRMS 05-702

Yegian, M. K., Marciano, E., and Ghahraman, V. G., 1991, Earthquake-Induced Permanent Deformations: Probabilistic Approach: Journal of Geotechnical Engineering, ASCE, V. 17, No. 1, 35-50.

Yin, K. L., and Yan, T. Z., 1988, Statistical Prediction Model for Slope Instability of Metamorphosed Rocks, Ed. Bonnard, C., Proceedings of Fifth International Symposium in Landslides, Lausanne, Rotterdam, The Netherlands, Vol.2, 1269-1272.

Youd, T. L., 1978, Major Cause of Earthquake Damage is Ground Failure, Civil Engineering Magazine, ASCE, Vol.48, No.4, 47-51.

Young, A., 1972, Slopes, Geomorphology, Text 3, Oliver & Boyd, 288pp.

Youngs, R. R., Chiou, S. J., Silva, W. J., and Humphery, J. R., 1997, Strong Ground Motion Attenuation Relationship for Subdeduction Zone Earthquakes, Seismological Research Letters, 68, 58-73.

Zeizel, A.J., 1988. Foreword, Colorado Landslide Hazard Mitigation Plan, Colorado Geological Survey Bulletin 48, 3.

Zhou G., Esakia T., Y. Mitania, M. Xie, J. Mori, 2003, Spatial Probabilistic Modeling of Slope Failure Using an Integrated GIS Monte Carlo Simulation Approach, Engineering Geology, 68, 373–386